Satellite estimation of biophysical parameters for ecological models.

Prieto-Blanco, Ana

Satellite estimation of biophysical parameters for ecological models

Ana Prieto-Blanco

Department of Geography

University of Wales Swansea

Thesis submitted in fulfilment of the requirements for the degree of

Doctor of Philosophy in the University of Wales

September 2007

ProQuest LLC.
789 East Eisenhower Parkway
P.O. Box 1346
Ann Arbor, MI 48106 – 1346

Declaration

This work is the result of my own indepedent work, except where otherwise stated. Other sources are acknowledged by footnotes giving explicit references. A bibliography is appended.

Signed (candidate)

Date 6/9/07

Statement

This work has not previously been accepted for any degree and is not concurrently being submitted in candidature for any other degree.

Signed (candidate)

Date 6/9/07

Summary

Ecological models are central to understanding of hydrological and carbon cycles. These models need input from Earth Observation data to function at regional to global scales.

Requirements of these models and the satellite missions designed to fulfill them are reviewed to asses the present situation. The aim is to establish a better informed framework for the design and development of future satellite missions to meet the needs of ecological modellers.

Key land surface parameters that can potentially be derived by remote sensing are analysed - leaf area index, leaf chlorophyll content, the fraction of photosynthetically-active radiation absorbed by the canopy and the fractional cover - as well as the aerosol optical thickness.

Three coupled models - PROSPECT, FLIGHT and 6S - are used to simulate top of the atmosphere reflectances observed in a number of viewing directions and spectral wavebands within the visible and near-infrared domains.

A preliminary study provides a sensitivity analysis of the top of the atmosphere reflectances to the input parameters and to the viewing angles.

Finally, a methodology that links ecological model requirements to satellite instrument capabilities is presented. The three coupled models - PROSPECT, FLIGHT and 6S - are inverted using a simple technique based on look-up tables (LUTs). The LUT is used to estimate canopy biophysical variables from remotely-sensed data observed at the top of the atmosphere with different directional and spectral sampling configurations. The retrieval uncertainty is linked with the instrument radiometric accuracy by analysing the impact of different levels of radiometric noise at the input.

The parameters retrieved in the inversion are used to drive two land-surface parameterization models, Biome-BGC and JULES. The effects of different configurations and of the radiometric noise on the NPP estimated are analysed.

The technique is applied to evaluate desirable sensor characteristics for driving models of boreal forest productivity. The results are discussed in view of the definition of future satellites and the selection of the best measurement configuration for accurate estimation of canopy characteristics.

Acknowledgments

I would like to thank first and foremost my supervisor, Peter North, without whose support, encouragement, expertise and patience this work would not have been possible. His optimism was always more than welcome. Also to my second supervisor, Mike Barnsley, for his wise guidance and advice at the critical moments.

I cannot thank enough to Raul, firstly for encouraging me to do this PhD but also for his unconditional support both when things went well and when they did not, for the conversations of hours on the telephone and for running to help me whenever I needed.

This thesis has also been possible thanks to many other contributions: Will's help, chat and company in the lab; Steve's hugs, meals and friendship; Pyrs' chats about life; Monica's weekends and unconditional friendship; supporting emails and visits from all the friends in Spain that made me feel I was not away; and all the people in the Geography Department, postgraduates and staff that made my days in Swansea lovely, I still think it does not rain so much there...

I also want to thank Pablo Zarco-Tejada for giving me the opportunity of spending three months in Cordoba and to everyone in the IAS (Berni, Guada, Oscar, Pilar, Marga, Sonia, Jolanda, Ausi, Imen...) for their warm welcome. They made me feel at home and made me wish to continue in a research career to work with people like them.

Finally, but most importantly, I have to thank my family for their constant support over all these years and for making me happy.

Other acknowledgments

This study has been funded by the National Physical Laboratory (NPL) and supported by NERC Climate and Land-Surface Systems Interaction Center (CLASSIC).

Biome-BGC version 4.1.1 was provided by the Numerical Terradynamic Simulation Group (NTSG) at the University of Montana.

BOREAS field data set was available on-line [http://www.daac.ornl.gov] from Oak Ridge National Laboratory Distributed Active Archive Center, Oak Ridge, Tennessee, U.S.A.

CASI images were provided by Pablo Zarco-Tejada, at the "Instituto de Agricultura Sostenible" (IAS), Cordoba, Spain.

A mis padres,

por enseñarme a vivir y compartirlo conmigo.

Acronyms and Abbreviations

AATSR Advanced Along-Track Scanning Radiometer

AGCM Atmospheric General Circulation Models

AMMA African Monsoon Multidisciplinary Analyses

AOT Aerosol Optical Thickness

APAR Absorbed Photosynthetic Active Radiation

ATSR-2 Along-Track Scanning Radiometer -2

AVHRR Advanced Very High Resolution Radiometer

BATS Biosphere-Atmosphere Transfer Scheme

BEPS Boreal Ecosystem Productivity Simulator

BETHY Biosphere Energy-Transfer Hydrology

BIOME-BGC BioGeochemical Cycles

BOREAS Boreal Ecosystems-Atmosphere Study

BRDF Bidirectional Reflectance Distribution Function

Cab Chlorophyll Content

CASA Carnegie-Ames Stanford Approach

CLASS Canadian Land Surface Scheme

DBH Diameter at Breast Height

DGVM Dynamic Global Vegetation Models

DN Digital Number

ECV Essential Climate Variables

EMIC Earth Models of Intermediate Complexity

ENVISAT ENVIronmental SATelite

ERS European Remote Sensing Satellites

ESA European Space Agency

ETM Enhanced Thematic Mapper

EOS Earth Observing System

fAPAR Fraction of Absorbed Photosynthetic Active Radiation

FC Fractional Cover

FIFE First ISLSCP Field Experiment

GCM Global Climate Model

GCOS Global Climate Observing System

GEWEX Global Energy and Water Cycle Experiment

GIS Geographic Information System

GPP Gross Primary Productivity

HAPEX Hydrological-Atmospheric Pilot Experiment

IFOV Instantaneous Field of View

IGBP International Geosphere-Biosphere Program

IGOS-P Integrated Global Observing Strategy Partnership

IPCC Intergovernmental Panel on Climate Change

ISLSCP International Satellite Land Surface Climatology Project

JULES Joint UK Land Environment Simulator

LAD Leaf Angle Distribution

LAI Leaf Area Index

LBA Large-Scale Biosphere-Atmosphere Experiment in Amazonia

LoTEC Local Terrestrail Ecosystem Carbon

LSP Land Surface Parameterisation

LUE Light Use Efficiency

LUT Look Up Table

NCE Net Carbon Exchange

NEP Net Ecosystem Productivity

NIR Near Infrared

NPP Net Primary Productivity

MERIS Medium-Resolution Imaging Spectrometer

MISR Multiple Multi-angle Imaging SpectroRadiometer

MODIS MODerate-Resolution Imaging Spectrometer

NDVI Normalized Difference Vegetation Index

NOAA National Oceanic and Atmospheric Administration

OBS Old Black Spruce

OJP Old Jack Pine

PAR Photosynthetic Active Radiation

PFT Plant Functional Types

POES Polar-orbiting Operational Environmental Satellite

Proba Project for On-Board Autonomy

PVM Potential Vegetation Model

RMSE Root Mean Square Error

SiB Simple Biosphere

SPOT Satellite Pour l'Observation de la Terre

SVATS Soil-Vegetation-Atmosphere Transfer Schemes

SWIR Short Wave Infrared

SeaWiFS Sea-viewing Wide Field-of-View Sensor

TBM Terrestrial Biogeochemistry Model

TEM Terrestrial Ecosystem Model

TOAR Top of the Atmosphere Reflectance

TM Thematic Mapper

UNFCC United Nations Framework Convention on Climate Change

USGS United States Geological Survey

WCRP World Climate Research Programme

WMO World Meteorological Organization

YJP Young Jack Pine

Contents

List of Figures

List of Tables

Chapter 1

Context

This Chapter introduces the necessity to understand the Earth system in facing climate change, and the tools that are being used in this research area.

The main processes involved in the climate system and their interactions are briefly presented. These processes and their effects act at the global scale, although some areas are particularly sensitive to climate change. These hotspots will be briefly reviewed as one of them will be the focus of the rest of this work.

Parameters that can be quantitatively measured during long periods of time and hence used as indicators of climate change are listed. Although these indicators are useful in detecting changes, they do not provide any information about the cause of these changes. The synergy between climate models and satellite data provides an essential tool in the understanding of these processes being the motivation of the present study.

The final section presents the aim and objectives of the thesis and outlines the contents of each chapter.

1.1 The need to understand the Earth system

Strong evidence indicates that the Earth is changing due to anthropogenic activities. Our effect on the environment is driving a series of alterations in the Earth system whose magnitude and extent are not well understood yet. These alterations are referred to as global change which is forcing climate change. According to the Intergovernmental Panel on Climate Change (IPCC, 2001) the global climate warmed approximately 0.5°C on average in the 20th century. It is expected that this trend of increasing temperatures will continue throughout the 21st century, even if greenhouse gas emissions are reduced or stabilized (IPCC, 2001).

The main human influence on the climate system is occurring in terms of perturbation of the atmospheric composition (primarily fossil fuel burning) and land-use change. Human activities have dramatically increased carbon and aerosol concentrations in the atmosphere since the beginning of the Industrial Revolution, mid-18th century. The increased concentration of greenhouse gases in the atmosphere is expected to enhance the absorption and emission of infrared radiation while the effect of the increasing amount of aerosols on the radiative forcing is complex and not yet well known.

Land-use change refers to a change in the use or management of land including activities such as agriculture and irrigation, deforestation, reforestation, afforestation and also urbanisation or traffic. These changes alter the albedo and surface roughness as well as the interactions between the land and the atmosphere.

These changes are expected to affect significantly the Earth's climate over the next decades. The effect will be enhanced by feedback processes between Earth's systems with consequences difficult to predict and to quantify and, presently, the terrestrial domain component of the climate observing system remains the least well-developed component (WMO, 2004).

A sensitive monitoring of the Earth is fundamental to detect changes but, without a deep understanding of the processes involved, measures to mitigate them cannot be taken. An understanding of these processes and their controls is hence essential to predict the effects of the induced changes, reduce the damage and try to remediate what has been already done.

Two requirements are extracted from the above discussion: a means of monitoring the Earth at the global scale and a means of interpreting the observed changes. Both fields and their interaction are the subject of this thesis.

1.1.1 Land-surface and climate interactions

The climate system encompasses the atmosphere, the hydrosphere, the cryosphere, the pedosphere, the lithosphere and the biosphere. These components are connected via fluxes of energy, substances and momentum which carry feedbacks between them. It is now recognized that the land surface, and specifically vegetation, both respond to and influence climate and atmospheric processes across a wide range of spatial and temporal scales (e.g. Pielke et al., 1998; Foley et al., 2003). It is important to understand the links between vegetation and the terrestrial energy, water and carbon cycles, and how these might change due to eco-physiological responses to elevated carbon dioxide and changes in land use.

Land-surface and climate interactions can be interpreted in terms of biogeochemical and biogeophysical interactions. Biogeophysical interactions involve surface energy, moisture and momentum fluxes and are affected by changes in surface properties such as albedo, roughness, leaf area, etc. Biogeochemical interactions are associated with changes in terrestrial biomass and in the atmospheric chemical composition.

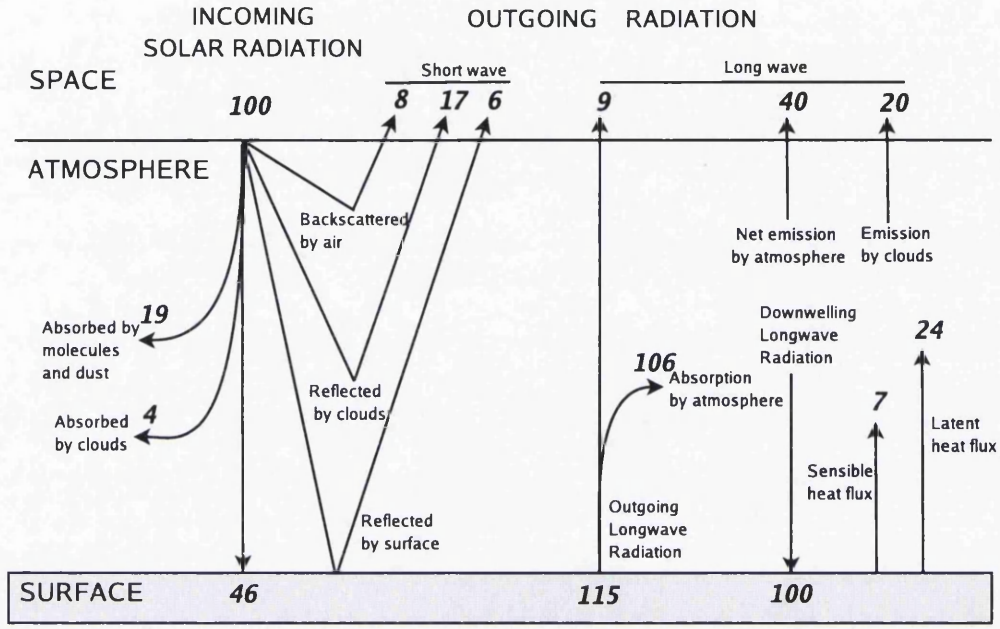

Figure 1.1: Earth's mean energy balance.
(Redrawn from Pitman, 2003)

Left hand side shows what happens with the incoming solar radiation and right hand side shows how atmosphere emits the outgoing infrared radiation. 46% of the incoming solar radiation is absorbed by the surface; that heat is returned to the atmosphere as sensible heat, latent heat (evapotranspiration) and thermal infrared radiation. Most of this radiation is absorbed by the atmosphere, which in turn emits radiation both up and down.

In terms of biogeophysical interactions, the amount of energy available to the climate is largely controlled by atmospheric processes. Each square meter of the Earth's surface outside the atmosphere receives an annual average of 342 Watts of solar radiation, 31% of which is immediately reflected back into space by clouds, by the atmosphere, and by the Earth's surface. The remaining 235 Wm^{-2} is partly absorbed by the atmosphere (23%) and by the surface (46%). This heat is returned to the atmosphere as infrared radiation, sensible and latent (evapotranspiration) heat (Pitman, 2003; IPCC, 2001, Chapter 1; Figure 1.1).

The terrestrial biosphere exerts a critical influence on the climate controlling the way that these units of energy are partitioned through its roughness, albedo and composition (e.g. Foley et al., 2003). Roughness is determined by both topography and vegetation and influences the atmosphere dynamically as wind blows over the land's surface. Soil

moisture and vegetation state determine the fraction of net radiation that is used for evapotranspiration and the rates of photosynthesis and respiration, hence influencing local air temperature and humidity (IPCC, 2001, Chapter 1). The energy budget is also affected in an indirect way by the biosphere through aerosols as spores, viruses, bacteria, pollen and other organic material that scatter incoming solar radiation.

Finally, the biosphere, both on land and in the oceans, affects the albedo (the amount of sunlight reflected back to the sky) of the Earth's surface. Large areas of continental forest have relatively low albedos (about 9 to 12% in boreal and tropical forests) compared to barren regions such as deserts (around 35% in the Sahara desert)(Sellers et al., 1997a). A higher albedo implies that more light is reflected with the consequent effect on the energy budget of the climate system.

In terms of biogeochemical interactions, changes in biomass affect the chemical composition of the atmosphere via changes in photosynthesis and respiration. In turn, changes in the chemical composition of the atmosphere influence plant physiology and thus biomass. These biogeochemical feedbacks act globally because of rapid global mixing of gaseous substances within the atmosphere. (IPCC, 2001, Chapter 1).

An important example of a biogeochemical feedback is the interaction between the atmospheric carbon dioxide (CO_2) concentration and the carbon uptake by the land surface and the oceans (IPCC, 2001, Chapter 3). In the last few years there has been a special interest in quantifying this flux of CO_2 into and out of the atmosphere to identify carbon sinks and sources (e.g. IPCC, 2001; Schimel et al., 2001). Given that the terrestrial and marine environments are currently absorbing about half of the carbon dioxide that is emitted by fossil-fuel combustion, knowledge of carbon exchange between the surface and the atmosphere is important. Mapping and monitoring carbon fluxes in different terrestrial environments is essential for understanding the relative contribution to the global carbon cycle and for forming mitigation strategies. Presently there are still considerable uncertainties in the magnitude of the sink in different regions and the contribution of different processes (Schimel et al., 2001), as well as the future effects of these feedbacks (Cox et al., 2000).

Understanding of these interactions is hence critical for assessing general patterns in vegetation as well as feedbacks between the biosphere and atmosphere and great effort is being made to understand and simulate climate-vegetation interactions (Pitman and Henderson-Sellers, 1998; IPCC, 2001; Foley et al., 2003). Research is mostly concentrated on 'hot spots' where the interaction is most significant and/or critical: boreal forests (e.g. Sellers et al., 1997b; Baldocchi et al., 2000), North and West Africa (e.g. Goutorbe et al., 1994; Petit et al., 2001), and Amazon forest (e.g. Costa and Foley,

2000; Chagnon and Bras, 2005). These specific biomes and their effect in the climate system are briefly presented next.

1.1.1.1 Ecological hotspots

Boreal forest

The boreal forest ecosystem encircles the Earth above 48°N and comprises about 21% of the forested land area (Sellers et al., 1997b).

The main influence of the boreal forest on the climate system is through its potential to sequester or release large volumes of carbon. Globally, more carbon is stored in forest soils than in forest vegetation and boreal forests are especially rich in soil carbon. It is estimated that boreal forests store 84% of the carbon as soil organic matter and 16% as living biomass (Dixon et al., 1994).

Climate predictions indicate that the greatest warming will occur at highest latitudes and this is expected to lead to changes in the carbon cycle enhancing ecosystem carbon gain by photosynthesis and carbon loss by respiration. These biogeochemical interactions are climatically important at long temporal scales, when terrestrial vegetation undergoes large geographic redistribution in response to climate change (Bonan et al., 1995; Baldocchi et al., 2000). Boreal forests also have a significant impact on the seasonal and annual climatology of much of the Northern Hemisphere by masking the high albedo of snow and through the partitioning of net radiation into sensible and latent heat (Sellers et al., 1997b).

Bonan et al., 1995 studied the boreal forest and tundra ecosystems and found that feedbacks exist that act to change the climate as a result of changes in the surface albedo between boreal forest and bare snow. Simulations showed that changes in vegetation cover could amplify global warming in high northern latitude regions, as the evergreen-dominated boreal forests of North America and Eurasia move northward, replacing treeless tundra (Levis et al., 1999). Evergreen forests are much darker than tundra causing a significant decrease in albedo.

Several studies on clarifying the complexity of interactions among environmental variables, vegetation distribution, carbon stocks and turnover, and water and energy exchange in high latitude regions (e.g. Chapin et al., 2000; McGuire et al., 2002; Williams et al., 2006), but there are still many uncertainties about the role of these ecosystems in the Earth system and further understanding on how these interactions influence carbon dynamics, water and energy exchange is required.

Tropical forests

Tropical forests are confined largely to three mayor regions between the latitudes of 10°N and 10°S - south and central America, Indo-Malaysian forests and central and western Africa- covering 7% of the terrestrial surface. These forest are the most ancient and biologically diverse ecosystems comprising an estimated 80% of the world's plant and animal species. Tropical forests contain around 41% global terrestrial biomass and carbon is partitioned more or less equally between vegetation and soil (Dixon et al., 1994).

Tropical forests are experiencing unprecedented rates of clearing and conversion as impoverished nations have converted their land for farming and grazing. This has effects in both atmospheric emissions and energy balance. This large-scale deforestation also has dramatic effects on mass and energy transfers between the land and the atmosphere (Chagnon and Bras, 2005). This is already affecting rain patterns in the Amazon and other parts of Brazil (e.g. Costa and Foley, 2000; Chen et al., 2002; Chagnon and Bras, 2005) but uncertainties in the projections of precipitation changes are still very high (Cox et al., 2000). The temperature effect due to deforestation is added to that of the greenhouse gases radiative forcing increasing the risk of forest fires.

Present studies aim to clarify the link between deforestation and precipitation in the Amazon and the Large-Scale Biosphere-Atmosphere Experiment in Amazonia (LBA) is contributing towards that goal (e.g. Silva Dias et al., 2002). It is hoped that this uncertainty in estimating likely regional climate changes for Amazonia will be improved substantially during this decade through the use of more complex climate models which take into account explicitly the regional climate and the two-way interaction between the biosphere and the atmosphere.

Savanna

Arid ecosystems cover more than 25% of the Earth's land surface (Asner et al., 2000). In subtropical deserts and semideserts vegetation does not completely cover the land surface and vegetation productivity is strictly limited by low water availability being highly dependent on precipitation and, hence, highly sensitive to climate variability.

One of the most studied areas in this biome is the Sahel, a tropical semi-arid region in the southern margin of the Sahara desert. The motivations for this interest are both the potential sensitivity of the area to climate change and the observed climate anomalies. The Sahel has experienced several drought periods in the past 500 years with the most persistent and severe drought starting in the 1960s.

Charney's hypothesis (Charney, 1975) pointed to a positive albedo-precipitation feedback as the cause of the Sahelian drought. The dryer the climate is, the scarcer is the vegetation and the greater is the fraction of bare soil increasing slightly the albedo and reducing the amount of net radiation absorbed by the surface. Removal of savanna vegetation produces a reduction in precipitation that, in turn, would lead to a decrease in vegetation cover and thus a further enhancement of the albedo.

Two large field campaigns have been conducted during the late 1980s (Sahelian Energy Balance Experiment, SEBEX, Wallace et al., 1991) and 1991-1992 (HAPEX-Sahel, Goutorbe et al., 1994, 1997) to improve the understanding of these mechanisms. HAPEX-Sahel provided the first observational evidence of the land surface influence on the regional rainfall in this area (Xue, 1997). Results showed that several factors, not only the land-use, are contributing to the drought and to the interannual variability in precipitation in the Sahel (Nicholson, 2000). Evidence has been found for a positive feedback between vegetation and rainfall at the monthly time scale, and for a land-surface memory operating at the annual time scale (Los et al., 2006), implying that land-use has an effect on the rainfall but not to the extent assumed by early studies (e.g. Xue, 1997). Global studies, based on general circulation models, presented evidence to suggest that the African rainfall variability is primarily driven by changes in remote sea surface temperatures, rather than by local properties of the land surface itself (Giannini et al., 2003) with a partial attribution of the recent recurrence of drought to the combined effects of aerosols and greenhouse gases (Held et al., 2005).

This shift in focus with regard to the causes of climate change (in this case African rainfall) from regional land use and land cover changes, to the global distribution of oceanic temperatures and anthropogenic emissions is a clear example of the necessity of a global approach to improve our understanding of the Earth system and to develop appropriate mitigation and adaptation strategies.

1.1.2 Monitoring Global Change

Global climate change is caused by an enormous number of factors including both human and natural variables. The monitoring of these changes involve the measurement of sensitive parameters that are directly affected.

Instrumental observations of land and ocean surface weather variables and sea surface temperature are available since the mid-19th century and ships' observations have been recently supplemented by data from dedicated buoys (IPCC, 2001, Ch.1). Presently, the Mauna Loa atmospheric CO_2 record is the most important data set in global change

science today, because of the length of time series. It is a measure of atmospheric chemistry, but the dynamics it follows are predominantly those of the land and ocean surface carbon exchanges of the biosphere and the anthropogenic load.

It must be pointed that any long observational record suffers from changes in instrumentation, measurement techniques, exposure and gaps due to political circumstances or wars. The Global Climate Observing System, established by the World Meteorological Organization, aims to implement and improve systematic observations and to improve the existing observational network (IPCC, 2001, Chapter 1).

As the multiple linkages between causes and impacts of climate change are not completely understood, specific indicators that allow us to detect and analyse these relationships have been defined (e.g. Erhard et al., 2002; DEFRA, 2003; Wake, 2005).

1.1.2.1 Indicators

Most frequently used indicators are temperature and precipitation. Global surface temperatures are affected by incoming sunlight, cloud cover, surface albedo and concentration of atmospheric components (such as greenhouse gases and other pollutants). Therefore temperature can be used to monitor changes in all these processes of the Earth's climate system. On the other hand, an increase in global surface temperatures will very likely lead to changes in precipitation and atmospheric moisture. Atmospheric water vapor is also a greenhouse gas affecting temperature, and climate change models suggest that a warming planet will likely experience increasing storm intensity and frequency (IPCC, 2001, Chapter 9).

Indicators relevant to the ocean are sea level and sea temperature (IPCC, 2001, Chapter 11). Sea level is affected by numerous factors on a range of timescales, from geological processes working over millions of years to the changing tides over the course of hours. It can be used as an indicator of changing climate. Factors such as changes in the size of ice sheets and glaciers, geological settling or uplift, thermal expansion, deposition of sediment, and thawing of permafrost are important. Sea temperature is also very relevant to climate change monitoring. Oceans circulation moves heat from the tropics to the polar regions at about the same rate as the atmosphere. The oceans are huge reservoirs of heat and thus have a strong influence on global and regional temperature. Because of their size, the oceans change temperature very slowly and can act as a heat sink or source, depending on the temperature of the air above it. Therefore, any change in sea surface temperature affects air temperature on a seasonal, annual, or multi-annual timeframe.

Other climate change indicators usually used include (e.g. Erhard et al., 2002; DEFRA, 2003; Wake, 2005): annual river discharge and frequency of low and high river flows which are related to changes in precipitation and temperature and to the timing of high spring flow; total winter snowfall and total days with snow on the ground, related to winter weather and temperature; lake ice-out (the day the majority of the lake ice is broken up in the spring) and ice-in (the day the majority of the lake first freezes over in the winter) indicator of local climate conditions.

Vegetation phenology

Indicators listed above refer to primary effects of temperature and precipitation changes on the Earth system. As evidence of climate change mounts, scientists have begun to search for signs of biological or ecological responses to this change. Plants are particularly useful to scientists as weather instruments and indicators of climate change because their phenological responses are driven by a combination of interactions amongst temperature, sunshine, rainfall, and humidity that is difficult to match by simple analysis of weather records (e.g. Myneni et al., 1997a, Nemani et al., 2003). Also changes in seasonal events in the life of plants and animals (e.g. flower bloom, spring arrival of migrating birds and insects, etc.) are potential bioindicators of climate change.

Phenology is the study of these seasonal biological events in the animal and plant world as influenced by the environment (Schwartz, 2003). Because vegetation phenology integrates the combined effects of biosphere-atmosphere interactions at seasonal (and longer) time scales, it provides a useful mechanism for studying and monitoring the effects of climate variability on ecosystem processes.

The length of the growing season, defined as the period between the last frost of spring and the first frost of winter, is a defining characteristic of an ecosystem and marks the period during which plants grow most successfully. As it is solely dependent on specific cold weather events, rather than monthly or annual averages, it has been widely used as a climate change indicator.

Efforts are being directed to identify key species, suitable for monitoring climate change. As an example, the European Phenology Network (EPN) (Van Vliet et al., 2003), a project funded by the European Commission in the context of the Fifth Framework Programme, aims to improve the monitoring of climate induced phenological changes throughout Europe.

Vegetation phenology is an emerging field of climate change science offering a means to monitor climate change at the global scale (e.g. Myneni et al., 1997a; Bogaert et al.,

2002; Coppin et al., 2004). Phenology also provides extra information that can be used in models to simulate Earth system processes as carbon fluxes and sequestration (e.g. Foody et al., 1996). Both the monitoring of phenological changes and the simulation of land surface processes are the focus of a great deal of research.

1.2 Modelling climate change

Observations alone are not sufficient to provide a global picture of the climate system. Climate models have been developed to enhance understanding of the climate system and to aid prediction of future climates. The climate system encompasses a wide variety of components and simplifications must be made to represent them in models. As a consequence, even the most sophisticated models remain very much simpler than the full climate system.

Global Climate Models, or General Circulation Models (GCMs) are based on theoretical climate science foundations and simulate the flows of energy and matter amongst the different components of the Earth system: atmosphere, hydrosphere, cryosphere, biosphere and the land surface. GCM are mainly used for studies on the decadal to century scale. For longer time-scale simulations of future and past climates Earth models of intermediate complexity (EMICs) are usually used instead. McGuffie and Henderson-Sellers, 2001 provides a comprehensive review of climate modelling.

Models of the various components of the climate system may be coupled to produce increasingly complex models. First simulations carried out with GCMs generally neglected the coupling between the climate and the biosphere. Vegetation distributions were considered static and atmospheric concentrations of CO_2 were based on results from simple carbon cycle models, ignoring the effects of climate change. Posterior inclusion of both an interactive carbon cycle and dynamic vegetation within GCMs showed a significant acceleration of CO_2 increase and climate change arising from the additional feedback loops (Cox et al., 2000). Presently, land surface importance on climate predictions is widely accepted and coupled in GCMs (e.g. Cox et al., 1999; Baldocchi et al., 2000; Arora, 2002).

Because of the high degree of interaction between land-surface and climate, a useful way to study and predict the outcome of feedback is to use submodels called Land Surface Parameterisations (LSPs) coupled to GCMs (e.g. Sellers et al., 1995; Cox et al., 1999). LSPs are models that simulate exchanges of energy, water and carbon between the atmosphere and the continents. The coupling of carbon-cycle process models with

regional climate databases can provide information on potential rates of biomass production and related rates of decomposition, while the coupling to GCM provides more realistic simulation of the Earth's system. Presently, fully coupled models of climate and terrestrial ecosystems are essential tools to explore the interactions between atmosphere, oceans, ice, and the terrestrial biosphere. A great deal of current research is being focused in the development of these models (Pitman, 2003) and in the combination of the observations and their temporal and spatial statistics with models (e.g. data assimilation, Williams et al., 2005)

1.3 Why remote sensing?

Many ecological studies and applications require extensive geographical data sets which are difficult to collect with field measurements. Satellite remote sensing, or Earth Observation, permits acquiring data rapidly and repeatedly over wide areas at several spatial resolutions. These measurements provide valuable data for both monitoring and modelling of global change. Remotely sensed data can be used from local to global scales in characterizing various ecological variables that are applicable in monitoring, for example, changes in land and vegetation cover, land use, vegetation structure, phenological cycles, natural disasters or biodiversity of habitats. It is also important to acknowledge the interactions between different parts of the biosphere, and obtaining simultaneous time-series data from the land-surface, oceans and atmosphere helps the assessment of many global environmental phenomena.

Remote sensing for monitoring

Satellite remote sensors offer major sources of consistent, continuous data for atmospheric, ocean, and land studies at a variety of spatial and temporal scales. Systematic global observations are essential components of long-term monitoring while frequent observations provide tools for the detection of changes at shorter time scales. The land sciences community has made extensive use of satellite image data for mapping land cover, estimating geophysical and biophysical characteristics of terrain features, and monitoring changes in land cover (e.g. Ehrlich et al., 1994; Loveland et al., 2000; Petit et al., 2001). Remote sensing has also proven to be an effective tool to detect phenological responses to climate change (e.g. Bogaert et al., 2002, Zhou et al., 2003). In terms of carbon-cycle processes, the integration of remote sensing and modelling produces spatially explicit information on carbon storage and flux.

Table 1.1: Essential climate variables identified by the GCOS and the contributing satellite data.

Climate Variable	Satellite Data
River Discharge	Laser/radar altimetry for river levels and flow rates.
Lake Level/Area	Proposed altimetry, high-resolution. Optical and radar and reprocessing of archived data.
Water Use (Area of Irrigated Land)	High/medium resolution optical/ radar systems.
Snow Cover	Moderate resolution optical for extent/duration of snow cover. Passive microwave for snow water equivalent.
Glaciers and Ice Caps	Visible and infrared high-resolution; Along track stereo optical imagery; Synthetic Aperture Radar. Satellite altimetry.
Permafrost and seasonallyfrozen ground	Satellite-derived variables (e.g., vegetation type and snow cover, water), plus skin temperature measurements.
Albedo	Geostationary Polar orbiters.
Land Cover	High/medium resolution optical/ radar systems.
fAPAR and LAI	Optical, multispectral and multiangular remote sensing.
Biomass	Low-frequency radar and laser altimetry.
Fire Disturbance	Optical remote sensing.

At the satellite level it is specially difficult to separate climate change effects from other disturbances such as urbanization, political changes or shifts in agricultural practices. To account for this, White et al., 2005 proposed the use of "phenoregions" for long-term monitoring of climate change effects. Each phenoregion comprises phenologically and climatically similar areas formed by a cluster of pixels whose spectrum is consistently dominated by annual cycles. This provides a quantitative method to identify regions with a maximal probability of displaying a climate response signal, on which phenological studies should be focused.

The Global Climate Observing System (GCOS) has identified Essential Climate Variables (ECV) that have a high impact on the requirements of the United Nations Framework Convention on Climate Change (UNFCCC) (GCOS, 2004). As an example of the potential of satellite instruments to monitor climate change, Table 1.1 shows the contributing satellite data to the ECVs correspondent to the terrestrial domain.

Remote sensing for ecological modelling

To improve our understanding of the Earth's system processes, ecological studies have traditionally focused on in-situ observations at individual sites. These observations must be applied across diverse scales through regional and global studies to provide insight to the global system. The use of models allows us to extrapolate physical processes, such as photosynthesis, respiration or evapotranspiration, that are measured at the leaf or canopy scales, to larger regions and temporal scales. Satellite remote sensing provides a key tool to extend these measurements by providing data at the appropriate resolutions (e.g. Sellers et al., 1995; Treitz and Howarth, 1999; Petit and Lambin, 2001; Nemani et al., 2003; Turner et al., 2003; Wulder et al., 2004; Turner et al., 2004). Earth observation information may also serve as an assessment tool for decision support (Rosenqvist et al., 2003; GCOS, 2004) and a source of data to test and improve models (e.g. Plummer, 2000; Williams et al., 2005). The most useful contributions of remote sensing technology to ecology are based on frequently repeated multispectral measurements covering very large areas providing information about ecosystem conditions, specially locations and types of environmental stresses.

In terms of carbon-cycle processes, approaches to understanding ecosystem carbon exchange are based in the use of in situ measurements (e.g. eddy covariance) and models that predict relative photosynthetic function in response to environmental conditions. Remote sensing is a key tool in both of these approaches providing consistent, regular large-scale measurements of the Earth's surface and allowing local measurements to be scaled up to wider regions.

Over the past three decades there has been a progressive evolution of remote sensing approaches for the collection of data (Boyd and Danson, 2005). The increasing availability of remote sensed data (e.g. Barnsley et al., 1997; Asner, 2000; Buermann et al., 2001; Asner et al., 2003) and the growing interest in quantifying terrestrial carbon flux (IPCC, 2001; WMO, 2004) have driven rapid progress in the integration of modelling and remote sensing (e.g. Sellers et al., 1997b; Chen et al., 1999b; Plummer, 2000; Dawson et al., 2003; Gerard, 2003). Great effort has been made on the development of algorithms and techniques to derive parameters from satellite retrieved data (e.g. Sellers et al., 1995; Roughgarden et al., 1991; Myneni et al., 1995; Dawson et al., 1999; Diner et al., 1999; Combal et al., 2002b; Chen et al., 2003). These remotely sensed data and the derived parameters provide valuable information that can be used in ecological models as inputs, as reference values to test and/or to validate estimations and in data assimilation (Plummer, 2000).

1.4 Aim and objectives

Previous paragraphs have introduced the importance of monitoring and understanding the Earth system. Global climate models, and specifically LSPs, help in the understanding of the system interactions and allow the simulation of future scenarios. These models require input data that can be provided by satellite remote sensing.

Satellite instruments offer a variety of capabilities that must be tailored to the specific application of the retrieved data. Typically, a consultation process is establish prior to the development of a new instrument in which the scientific community is consulted for their requirements (e.g. Sellers, 1993). This method of defining the requirements presents two problems. First, the requirements will be as dynamic as the research itself, which implies that by the time the instrument is developed and launched, the requirements might be well different from those initially formulated. This problem has a difficult solution although a major involvement of the scientific community during the development of the instrument could reduce the impact of this temporal gap.

The second problem refers to the way in which these requirements are expressed. The scientific community will formulate their requirements in terms of their tools, e.g. in terms of model parameter inputs, which does not relate straightforward to satellite capabilities. This second problem could be solved by the establishment of a framework for linking remote sensing capabilities to scientific requirements. This study focuses on the requirements of ecologists expressed in terms of LSPs parameters, which play a fundamental role in global climate models. In this area presently, no adequate framework exists. Despite isolated studies in various sub-disciplines (e.g. Plummer, 2000; Dawson et al., 2003) a comprehensive analysis is missed and appropriate methodologies that allow to link both communities are still required.

The aim of this study therefore is to establish a high-level framework for the development of future satellite sensors. The establishment of a sound methodological framework will extend the applicability of Earth observation to ecological models, which will finally result in better monitoring and predicting capabilities.

In order to achieve this goal the following issues will be addressed:

- ➢ Ecological requirements from the point of view of LSPs will be analysed to detect which parameters can be estimated by remote sensing.
- ➢ Satellite capabilities and methods to retrieve biophysical parameters will be reviewed in order to understand how ecology requirements can be met by satellite data.

➢ A methodology that permits us to link both ecological requirements and satellite specifications, will be developed.

The final aim of this work is to provide an operational methodology and to apply it to the analysis of optimal satellite capabilities for the estimation of LSPs inputs at the required accuracy.

The boreal forest will be used as test site in this study because it is an important biome in terms of the carbon budget and its structural complexity provides a good test for the methodology.

1.4.1 Thesis structure

Chapter 2 introduces ecological process models and remote sensing. Ecological process models are reviewed discussing their aim and the inputs typically required. Remote sensing information content is presented and the history of satellite missions related to land-surface studies is examined. Finally, past and present interactions between remote sensing and ecology communities are discussed highlighting weaknesses and extracting specific requirements for ecology from remote sensing data. Existent models and techniques that could potentially be used in the retrieval of biophysical parameters are introduced and reviewed in Chapter 3.

Chapter 4 discusses the data sets and models used in the study. A preliminary sensitivity analysis linking ecological model requirements to satellite specifications is presented in Chapter 5. A complete operational methodology to link both fields, remote sensing capabilities and ecological model requirements, is presented and applied in Chapter 6.

Finally, Chapter 7 summarises the work and draws out the main conclusions of the thesis. The directions in which future work should be focused are also discussed.

Chapter 2

Land surface modelling and Remote Sensing

The purpose of this chapter is to assess past, present and future interactions between land surface modelling and remote sensing.

Firstly, land surface models are reviewed analysing the different approaches used to simulate the processes involved. Then satellite remote sensing capabilities are introduced.

The history of Earth Observing satellites is examined analysing how the ecology community requirements have been met and identifying future trends and gaps in the planned missions. Interactions between both communities, ecologists and remote sensors, during the last few years are evaluated aiming to identify weaknesses in the communication process.

Relevant ecological parameters that can potentially be derived from remote sensing will be introduced next considering both meteorological and biophysical parameters. Requirements for these parameters are presented as well as the products provided by remote sensing.

The final section evaluates international programs aimed to improve the communication between both communitites, mainly through the definition of requirements and the validation of the products.

2.1 Land-surface Models

A wide range of land-surface models has been developed in the last years aimed to represent and improve our understanding of the interactions between the climate and

land surface on a global scale. These models are essential to predict and analyse the potential effects of human's activities and climate change on ecosystem functioning. They can be used off-line or isolated to study the land surface processes or integrated into GCMs providing a realistic boundary layer.

2.1.1 Types of land-surface models

Three broad types of land-surface models can be distinguished in respect to the representation of vegetation as described by Foley, 1995: soil-vegetation-atmosphere transfer schemes (SVATS), potential vegetation models (PVMs), and terrestrial biogeochemistry models (TBMs).

SVATS describe the surface energy, water and momentum balance and have been coupled to GCMs (General Circulation Model or Global Climate Models) to simulate the biophysical interactions between land surfaces and the atmosphere. The Simple Biosphere (SiB) of Sellers et al., 1986 was the first land-surface scheme that explicitly modeled plant physiology in a GCM. Other examples are BATS (Dickinson et al., 1993) and JULES (Essery et al., 2001; Best, 2005). For most SVATS, land cover is fixed, with seasonally-varying prescriptions of parameters such as reflectance, leaf area index or rooting depth. Some SVATS incorporate satellite data to characterise more realistically the seasonal dynamics in vegetation function (e.g. Sellers et al., 1994) and several simulate ecological processes such as primary productivity and plant respiration (e.g. Dickinson et al., 1993; Liu et al., 1997; Essery et al., 2001).

PVMs simulate distributions of vegetation as a function of climate without influences of anthropogenic or natural disturbance. Some include competition, varying combinations of plant functional types and physiological and ecological constraints on vegetation distributions. These models are useful in the simulation of vegetation distributions for the present climate as well as for past and future climates (Foley, 1995). The classical classification, the Holdridge Life Zone Model (Holdridge, 1967), classifies vegetation into ecological units while more recent approaches (Box, 1981) use unique combinations of plant functional types. Examples of PVMs are BIOME-I (Prentice et al., 1992) (later BIOME-3 was extended with NPP estimations and vegetation dynamics, Haxeltine and Prentice, 1996), MAPSS (Nellson, 1995) and the Terrestrial Vegetation Model (TVM, Leemans and van den Born, 1994).

Finally, TBMs, are process-based models developed with the principal goal of simulating NPP, typically using simple parameterizations of the surface energy and water balance. These models are useful to simulate the interacting dynamics of C and N.

The first to be applied globally was the Terrestrial Ecosystem Model (TEM, Melillo et al., 1993). Other examples include Forest-BGC (Running and Gower, 1991) and later BIOME-BGC (Running and Hunt, 1993) and BETHY (Knorr, 2000).

The work in this thesis focuses on land process models, SVATS and TBMs, that are referred as land surface parameterisations (LSPs).

2.1.2 Development of land surface parameterisations

LSPs have evolved from simple, unrealistic equations into more comprehensive and realistic representations of the global soil-vegetation-atmosphere transfer system over the last 30 years. Sellers et al., 1997a distinguish three generations of LSPs attending to the level of complexity

First-generation models, developed in the late 1960s and 1970s, used simple energy balance equations. These simple models represented exchanges of radiation, evapotranspiration and frictional deceleration of the lower atmosphere considering the vegetation a static layer between the soil and the atmosphere.

The second generation of models, developed in the early 1980s, were improved including vegetation interactions in the energy balance. These interactions comprise: radiation absorption, momentum transfer, biophysical control of evapotranspiration through stomatal conductance, precipitation interception, soil moisture availability and soil insulation. These models calculated water and energy budgets but they did not considered carbon fixation by vegetation.

The latest models, the third generation, provide a comprehensive description of energy exchange, evapotranspiration and carbon exchange by plants including modern theories of photosynthesis and plant water relations. CO_2 assimilation by vegetation is described in detail considering limiting effects of the enzyme Rubisco, the incident photosynthetic active radiation (PAR) and the photosynthetic efficiency of the leaf.

A wide range of LSPs is presently available, with different formulations for the processes simulated. The Project for the Intercomparison of Land-surface Parameterization Schemes (PILPS) was launched in 1992 to systematically analyse an array of land-surface schemes existing in GCMs (Henderson-Sellers et al., 1995, 1996). In the intercomparison the behaviours of participating land-surface schemes are diagnosed in controlled experiments implemented in four phases. The first two phases analyse the behaviour when driven in "off-line" by atmospheric forcings prescribed from GCM output (Phase 1) or from varied observational data sets (Phase 2). PILPS Phase 3 entails the diagnosis of land-surface schemes coupled to their "home" atmospheric host

models, while Phase 4 concerns the analysis of results from coupling different land-surface schemes to a common host. Results of the intercomparison show large discrepancies between the predictions made by the various models (Pitman and Henderson-Sellers, 1998), and it is not clear which formulations are better.

Present efforts are concentrated in the improvement of hydrology, soil respiration, and ecological responses. Other areas that are not being considered yet in LSPs are permafrost, the impact of frozen soils on infiltration and groundwater. Presently it is not well established how best to represent roots, root water uptake and the allocation of carbon for root growth in LSPs. This is important as increasing carbon assimilation may increase root growth, but increased temperature also increases root mortality.

Another problem facing present LSPs is the heterogeneity of the area represented. Climate models divide the Earth in grids within which calculations are made. Landscapes typically exhibit spatial heterogeneity in land cover at scales well below that of the grid cells. The heterogeneity in this grid implies that the nature of the interaction between the surface and the atmosphere varies greatly over that area as well as the parameters describing surface properties such as albedo, surface roughness, soil moisture and canopy structure. To deal with this heterogeneity and sub-grid-scale processes land surface models typically incorporate a number of "tiles" for the major vegetation types that are used to perform separate calculations for each group (e.g. JULES). This approach does not account for processes such as lateral fluxes between patches or edge effects. Other solution would be to use a finer climate model grid, but this would be computationally expensive.

LSPs represent the global distribution of plant functional types (PFTs) with identical seasonality profiles neglecting seasonal changes on vegetation and competition between PFTs. Studies have shown that this lack of detail can lead to big errors in climate simulations (e.g. Buermann et al., 2001; Bonan et al., 2002). To overcome these problems LSPs are usually coupled with Dynamic Global Vegetation Models (DGVMs). In a DGVM, plant biogeography is coupled with biogeochemical interactions to simultaneously simulate climate and ecosystem carbon and water cycles and the effects on PFTs distributions (Arora, 2002).

Phenology is already included in most DGVMs run off-line (uncoupled) from GCMs (Cramer et al., 2001) and present efforts are directed to couple DGVMs and GCMs (Foley et al., 1998; Levis et al., 1999). By coupling DGVM-GCM models phenologic processes as seasonal timing of land surface albedo and the timing and amount of litterfall are represented providing more realistic results. Some DGVMs such as IBIS (Foley et al., 1996) and Triffid (Cox, 2001) have been developed explicitly to be

coupled with GCM.

A great deal of research is directed towards the improvement of LSPs. Several intensive field campaigns have been designed to improve the understanding on the flows of matter and energy between the land surface and the atmosphere (e.g. FIFE Sellers et al., 1988, HAPEX-Sahel Goutorbe et al., 1994, 1997, BOREAS Sellers et al., 1997b and LBA Silva Dias et al., 2002). These projects provide fundamental data for the progress towards realistic and more accurate formulation of terrestrial biosphere models (e.g. Kimball et al., 1997a; Gamon et al., 2004).

2.1.3 LSPs Processes

The key land surface processes affecting the climate, and that must be included in LSPs, are the surface energy balance, the surface water balance and the carbon balance (Sellers et al., 1997a).

The net balance of the radiation absorbed by the land surface, *Rn*, is determined as:

$$R_n = S(1-\alpha) + L_w - \varepsilon\sigma T^4 \tag{2.1}$$

where S is insolation, α is the surface albedo, L_w is downward long-wave flux, ε is the surface emissivity, σ is the Stefan-Boltzmann constant and T is the land surface temperature (Sellers et al., 1997a). *Rn* comprises three heat flux terms: the ground heat flux, sensible heat flux and latent heat flux.

The surface water balance is the balancing of incoming and outgoing fluxes of water. A basic role of the land surface is to partition available water (precipitation or snow melt, P) between evaporation (E) and runoff (R):

$$P = E + R + \triangle S \tag{2.2}$$

where $\triangle S$ is the change in soil moisture storage.

Carbon balance is the balancing of carbon exchange between the land surface and the atmosphere. The amount of carbon sequestered by photosynthesis is called gross primary productivity (GPP). Part of this carbon is lost in growth and maintenance respiration called autotrophic respiration (R_A). Net primary productivity (NPP) is the difference between GPP and R_A and represents the final amount of carbon sequestered. NPP is a fundamental ecological variable in studies of terrestrial carbon cycle which is an important aspect of global climate change studies.

According to McGuire et al., 2001 the net carbon exchange (*NCE*) between the terrestrial biosphere and the atmosphere, including anthropogenic and non-anthropogenic disturbances, can be described by the equation:

$$NCE = R_H - NPP + E_{NAD} + E_{AD} + E_P \tag{2.3}$$

where R_H is heterotrophic respiration (i.e., decomposition), *NPP* is net primary production, E_{NAD} are emissions associated with non-anthropogenic disturbance, E_{AD} are emissions from anthropogenic disturbance, and E_P is the decomposition of products harvested from ecosystems for human use. A positive *NCE* indicates a terrestrial source of atmospheric CO_2 whereas a negative *NCE* indicates a terrestrial sink.

NPP and R_H account for the production and decomposition of organic matter in the terrestrial biosphere. The difference between NPP and R_H is the Net Ecosystem Productivity (NEP) and determines how much carbon is lost or gained by the ecosystem in the absence of disturbances such as harvest or fire.

The role of vegetation and NPP

Vegetation modifies the surface albedo, the energy partitioning between sensible and latent heat and the surface roughness length with the subsequent effect of the energy balance. Vegetation plays also a fundamental role in the water balance through the interception of precipitation and transpiration. Finally, the carbon exchange between the terrestrial biosphere and the atmosphere is highly dependant on the conversion of CO_2 into dry matter by vegetation.

Present LSPs simulate leaf evapotranspiration through semi-empirical models that explicitly considers stomatal conductance. Photosynthesis is also realistically represented with a biochemical description of CO_2 assimilation by chloroplasts, usually using the Farquhar's model (see Table 2.1).

The Farquhar's model describes the instantaneous leaf gross photosynthesis rate for C_3 plants as the minimum of two values, Rubisco-limited (W_c) and light-limited (W_j) gross photosynthesis rate in $\mu mol/m^2 s$:

$$W_c = V_m \frac{C_i - \Gamma}{C_i + K} \tag{2.4}$$

$$W_j = J \frac{C_i - \Gamma}{4.5C_i + 10.5\Gamma} \tag{2.5}$$

where V_m is the maximum carboxylation rate in $\mu mol/m^2s$; J is the radiation-dependent electron transport rate in $\mu mol/m^2s$; C_i is intercellular CO_2 concentration; $\Gamma$is temperature-dependent CO_2 compensation point without dark respiration; and K is a temperature-dependent function of enzyme kinetics. The units for C_i, Γ, K can be either in Pascal (Pa) or in ppmv (parts per million by volume). Posterior modifications of this model have been used for C3 plants (Collatz et al., 1991) and C4 plants (Collatz et al., 1992).

Farquhar's model was initially developed and validated for individual leaves and needs to be scaled up to plant canopy. Two methods have been proposed to integrate the Farquhar's model over the depth of a canopy: the Big-leaf methods and sunlit/shaded leaf methods.

Big-leaf models are the simplest methods used in photosynthesis, NPP and GPP calculations. These models are driven by remote sensing inputs of land cover types and/or leaf area index (LAI) or fAPAR. The LAI, in this case, is used to calculate the APAR and hence the mean PAR irradiance on leaves to drive the Farquhar leaf-level model for canopy-level photosynthesis calculations. Examples of models that use this big leaf approximation are SiB2, JULES (allows to choose other methods), BATS and BIOME-BGC.

Although the Big-leaf approximation has been shown to be successful for modelling evapotranspiration for plant canopies, it does not perform so well for photosynthesis because of the additional leaf internal control on carbon assimilation (Chen et al., 1999b). The response of leaf photosynthesis to light is nonlinear and sunlit leaves can be several degrees warmer than the shaded leaves with the consequent effect on stomatal conductance. Solutions include two or more layer models (e.g. BETHY considers three canopy layers) and sunlit/shaded distinction.

The preferable approach to scale from leaf to canopy is stratifying the canopy into sunlit and shaded leaf components. Examples of models that use this method are BEPS, CLASS and JULES.

Some models such as NASA-CASA, do not model photosynthesis explicitly and NPP is estimated by the Monteith equation (Monteith, 1977; Gower et al., 1999) in which daily NPP is derived from daily APAR and light use efficiency (LUE) as: NPP = LUE$\times$ APAR, where LUE is a measure of vegetation's ability to convert photosynthetically active radiation (PAR) to NPP (e.g. Dawson et al., 2003). APAR can be calculated as PAR$\times$fAPAR, where PAR is the incoming photosynthetic active radiation and fAPAR is the fraction of PAR absorbed by a vegetation canopy. NPP could then be easily calculated as: NPP=$\varepsilon \times$APAR, where ε is the conversion rate of APAR into NPP (i.e. the efficiency of conversion of PAR to dry matter). The advantages of this model are

its simplicity and the fact that fAPAR can be remotely sensed.

LSPs differ in the approach used in the carbon allocation. Some models do not simulate the dynamics of LAI so carbon allocation is not modelled (e.g. SiB2, TEM). Other models use fixed allocation fractions that may be determined by the vegetation type (e.g. CASA, Forest-BGC). A second option is to use plant allometric relationships and constraints (e.g. BATS, BIOME-BGC). Finally, the allocation pattern can be explicitly calculated in order to optimize growth or LAI (e.g. BETHY).

2.2 The utility of remote sensing

Remotely sensed images visually describe spatial landscape patterns: the location, areal extent, and changes over time of communities and ecosystems. Further application of remote sensing to ecology studies is provided by the establishment of linkages between environmental properties and radiative fluxes at different wavelengths. The first step in developing these connections is to consider the variables required by ecological models and the capabilities that remote sensing offers to fulfill those requirements.

2.2.1 Satellite capabilities relevant to land surface modelling

Most of the instruments placed into orbit for Earth observation have been passive sensors, imagers and sounders operating in the visible, infrared and microwave spectral regions.

Passive detection in the visible can only work when the sun's energy is available limiting visible light sensor observations on satellites from being used during a nighttime pass. Active sensors are devices providing their own energy source for illumination of the target, offering the capability to obtain measurements anytime, regardless of the time of day or season (Campbel, 2002).

Remote sensing instruments measure the signal that results from the scattering and the absorption of the electromagnetic radiation by an object. The received signal is a function of the size, shape and biochemical composition of the object (see Figure 2.1).

The Earth's atmosphere plays an important role as a filter for all incoming radiation, selectively controlling the passage towards the Earth's surface of the various components of solar radiation. The incoming radiation is either absorbed, transmitted or scattered

Table 2.1: Example of LSPs and their main characteristics

	Time Step	Spatial Scale	Canopy Structure	Biomass pools number	Sunlit/ shaded distinction	Leaf level C assim. approach	Soil layers	Soil water transport
BATS	5 min to 1 day	1 deg.	Big leaf	18	no	Transp. Monteith	3	3 layer diffusion
BEPS	1 day	stand to regional	Big leaf	4	yes	Farquhar photosynthesis	1	1 layer bucket
BETHY	1 hour/1 day	1 deg.	3 layers	25	no	Farquhar C3/ Collatz et al., 1992 C4	5	5 layers bucket
BIOME-BGC	1 day	Any	2 layers	4	yes	Farquhar photosynthesis	1	1 layer bucket
CLASS	30 min	regional	Big leaf	6	yes	Farquhar photosynthesis	3	3 layer diffusion
Ecosys	1 hour	patch-landscape	up to 15	8 tree/8 moss	yes	Farquhar photosynthesis	$\leq$ 15	Richard's equation
FORFLUX	1 hour/1 day	patch-landscape	N layers	3	yes	Farquhar photosynthesis	$\leq$ 20	Richard's equation
LoTEC	1 hor	10-100 m2	Big leaf	4	yes	Farquhar photosynthesis	$\leq$ 14	10 layer flow
NASA-CASA	1 day	1 deg.	n/a	3 tree/1 moss	no	NPP LUE Monteith	4	4 layer bucket
SiB2	30 min-day	1 deg/adjust.	Big leaf	9	no	Farquhar C3/ Collatz et al., 1992 C4	3	1 layer bucket
TEM	1 month	0.5 deg.	Big leaf	1 aggregated	no	*	1	1 layer bucket
JULES	30 min or more	patch-landscape	n layers	9 PFT	yes	C3: Collatz et al., 1991/C4: /Collatz et al., 1992	4	Richard's equation

BATS: Biosphere- Atmosphere Transfer Scheme (Dickinson et al., 1993), BEPS: Boreal Ecosystem Productivity Simulator (Liu et al., 1997), BETHY: Biosphere Energy-Transfer Hydrology (Knorr, 2000), BIOME-BGC (Running and Hunt, 1993), CLASS: Canadian Land Surface Scheme (Verseghy et al., 1993), Ecosys (Grant, 2001), FORFLUX (Nikolov and Zeller, 2003), LoTEC: Local Terrestrial Ecosystem Carbon (King et al., 1997), NASA-CASA: NASA Carnegie-Ames Stanford Approach (Potter, 1997; Potter et al., 2001), SiB2 : Simple Biosphere 2 (Sellers et al., 1996a), TEM: Terrestrial Ecosystem Model (McGuire et al., 2001), JULES: Joint UK Land Environment Simulator (Essery et al., 2001).

* scalar function of solar irradiance, air temperature and atm. CO2, moisture and N

Figure 2.1: Spectral reflectance curves for green vegetation and other land covers.

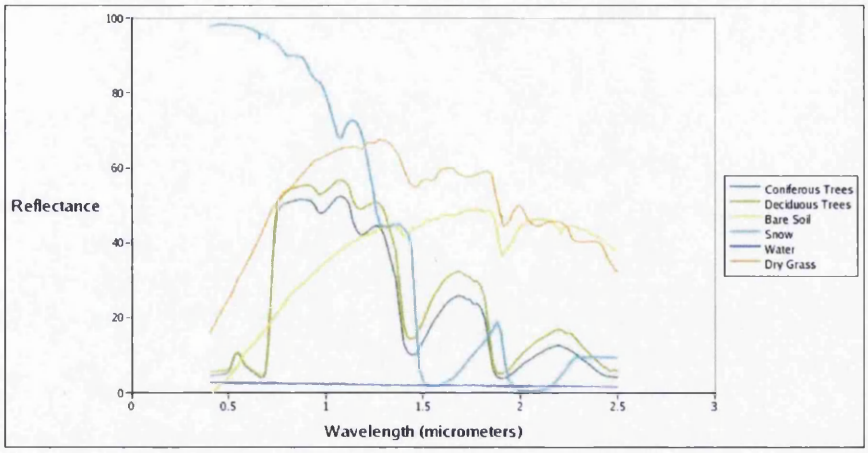

Spectral values reproduced from the ASTER Spectral Library through the courtesy of the Jet Propulsion Laboratory, California Institute of Technology, Pasadena, California. Copyright 1999, California Institute of Technology.

in all directions by atmospheric gases, vapors, and dust particles (aerosols). Spectral regions of high transmittance are referred to as atmospheric transmission bands or as atmospheric windows and are used to monitor land surface properties while emission/absorption lines are used to monitor the characteristics of the atmosphere. During the design of the instrument, channels are tailored to match the relevant regions according to the mission. (Lillesand et al., 2004, Chapter 5)

Other capabilities to consider are the resolution which includes spatial, spectral, temporal and radiometric resolution, the viewing angles and the calibration of the instrument.

2.2.1.1 Spatial, spectral, temporal and angular sampling

The different spatial, spectral, temporal and angular sampling resources will define the information retrieved by the instrument.

Spatial resolution

Spatial resolution refers to the size of the smallest object that can be distinguished in an image produced by remote sensing. Some instruments are designed to be capable of taking data at different spatial resolutions (e.g. MISR offers two modes). This allows measurent at higher resolutions only of selected targets as the data transmission rate at the maximum resolution could be excessive.

Spatial resolution is determined in large part by the Instantaneous Field of View (IFOV) defined as the angular cone of visibility of the sensor that determines the area seen

from a given altitude at a given time. The area viewed is equal to IFOV times the altitude. High resolution instruments offer more detail but usually a trade-off must be reached between coverage and detail as the volume of data could become unmanageable. (Lillesand et al., 2004)

Present satellites offer spatial resolutions ranging from 1-4 m (IKONOS) or 10-20 m (SPOT) to 7 km (POLDER). GCM can currently deal with 0.25° - 0.1° grids (25-30km - 10km grid) but the typical resolution is 1°-3° grids (100 - 300 km). LSPs scales range from 10 m to 100 km (Table 2.1).

Spectral resolution

Spectral resolution refers to the ability of a sensing system to distinguish between electromagnetic radiation of different wavelengths.

Spectral resolution is characterised by the full width at half-maximum (FWHM) response (the width of the bandpass defined as the wavelength interval recorded at 50% of the peak response). Depending on the number of bands sampled, sensors can be classified as multispectral or hyperspectral. The distinction between the two terms is a little blurred, but multispectral sensors generally collect from 3 to 12 bands (e.g. Enhanced Thematic Mapper Plus (ETM+) sensor on-board Landsat 7) and hyperspectral sensors often collect hundreds of bands (e.g. Airborne Imaging Spectrometer). Multispectral sensors generally collect wider wavelength bands as compared to hyperspectral sensors and they are denominated broadband and narrow-band sensors respectively.

There is a trade-off between spatial and spectral resolution in passive remote sensing. As these sensors use reflected energy from the sun, the amount of energy reflected at any particular point in time is fixed. Narrower wavelength bands reduce the amount of energy sampled and at some point there would not be enough energy to be detected unless the amount of ground being sampled increases (Pease, 1991; Lillesand et al., 2004).

Signal-to-noise ratio (SNR)

The SNR is a ratio of the magnitude of useful information (signal) to the magnitude of background noise. Background noise refers to both inherent instrument noise and unwanted signal arising from atmospheric effects. It indicates the precision required by a sensor to record details in the spectrum. SNR must be high enough to confidently distinguish the lowest signal of interest from spurious effects caused by electronic noise

or inherent fluctuations of the signal. The SNR is dependent on the detector sensitivity, the spectral bandwidth, and intensity of the light reflected or emitted from the surface being measured (Lillesand et al., 2004). SNR is appropriate to reflectance measurements, for thermal measurements Noise-Equivalent Temperature difference (NE deltaT) is used instead to measure the sensitivity of the instrument detectors (Pease, 1991). Both measures, SNR and NE deltaT, specify the minimum values above the background noise that the instrument detectors can discriminate as the signal coming from the target of interest.

Present passive instruments (e.g. MERIS, Verstraete et al., 1999; MODIS, Running et al., 1994; MISR, Diner et al., 2002) present a SNR of between 50 and 1500 depending on the spectral band.

Temporal resolution

Temporal resolution refers to the frequency of coverage, i.e. time between consecutive observations. The frequency of coverage for any particular site is usually equal to the repeat cycle, or the length of time that it takes for a satellite to view the entire Earth. However, some satellites have the ability to steer the sensors so that an area of interest can be viewed several times during a single repeat cycle. During the vegetation growing season, changes in the reflectance of Earth's surface can be observed on weekly time scales. Other applications will require even higher temporal frequencies (e.g. vegetation stress monitoring, hours to days) (Coppin et al., 2004). That is the reason why recent satellites have a wide viewing swath that allows them to view the entire Earth's surface in a small period of time (e.g. MODIS temporal resolution is 2 days and MERIS 3 days, Table 2.3).

Viewing angle

Traditional optical remote sensing systems provided single-view measurements of the Earth (e.g. Landsat series). Multiangle data can be obtained by composition of wide-field-of-view cross-track scanners data or by the quasi-simultaneous acquisition of measurements at more than one angle. Instruments with high swath width (e.g. MODIS, AVHRR) provide many off-nadir measurements of the land surface on each across-track scan line; over a sufficient period of time, ground locations will be observed from multiple view angles and with slightly different solar geometries. Other instruments - such as ATSR-2/AATSR (Stricker et al., 1995), CHRIS-Proba (Barnsley et al., 2004), POLDER (Deschamps et al., 1994) or MISR (Diner et al., 2002) - provide sequential

measurements at more than one angle by tilting the sensor in the along-track direction, targeting the same ground location within minutes and with similar solar geometries.

Over the past 15 years or so a variety of instruments with multi-angular observation capabilities have been launched. Their spatial resolutions vary from 20 m to 7 km, with 2 to 9 viewing angles, that measure the Earth's bi-directional reflectance field in a quasi-instantaneous manner, either over the entire globe or focused onto selected field sites (Table 2.3).

The Bidirectional Reflectance Distribution Function (BRDF) of earth surface materials contains information relating to their physical structure and composition that cannot be inferred from their spectral properties alone (Barnsley et al., 1997). The BRDF cannot be measured directly but it can be estimated using models of surface scattering in conjunction with reflectance data acquired at different viewing and illumination angles. Multiangular measurements provide valuable information to simulate the BRDF so images from different dates, taken under different illumination conditions and/or under different viewing geometries can be compared (Barnsley et al., 1997); this is fundamental to long-term monitoring and is also esential for the separability of different variables affecting the surface reflectance. Single view images do not contain enough information to decouple structural characteristics from biophysical parameters. Several studies have shown that multi-view angle optical measurements provide information on canopy structure distinct from which can be acquired through single-angle optical measurements (e.g. Barnsley et al., 1997; Diner et al., 1999; Asner, 2000; Chen et al., 2003) providing additional and unique data about the target attributes and structure.

On the other hand, some sun-view geometries are more useful than others as they provide more information. Sensors with multiple viewing angles are better equipped to obtain data at and around the 'hot spot' (the scattering in the solar direction and around it) and, consequently, have the potential to extract detailed information on the biophysical properties of earth surface materials.

The main problem with multiangular images is that a very accurate registration is required to make use of the data sets (Barnsley and Allison, 1996). Moreover multi-angle compositions made from instruments with high swath width such as MODIS provides images with a delay of several days hindering comparison.

2.2.1.2 Radiometric resolution and calibration

Radiometric resolution refers to the precision of the observation and defines the smallest radiance variation that the instrument can detect. It is not the same as accuracy. The

radiometric resolution describes the ability of the sensor to discriminate very slight differences in energy, while accuracy refers to how close is the detected value to the real value of reflected or emitted energy. Typically, radiometric resolution refers to the number of bits per pixel used to encode signal, in these terms, higher radiometric resolution means more data to store, transmit and process.

Radiometric calibration is used to assign a physical meaning to the digital number (DN) recorded by the sensor.

Absolute radiometric calibration refers to the calibration of the detector in reference to a well known source. For linear sensors absolute calibration is achieved by dividing the digital number (DN) output from the sensor by the value of a stable, spatially uniform radiance field at its entrance. Uncertainties are at best 3-5% and usually are highest in the extremes of the range (Dinguirard and Slater, 1999).

Relative calibration refers to the calibration of each sensor detector in relation to the others. It is achieved by normalising the output of different detectors to a given output so that they all give the same value when the sensor is irradiated with a stable, spatially uniform radiance field. Uncertainties are in the range of 0.1-0.5% measured as RMS variation in the output between sensors. Changes in the ratio between bands define stability of the sensors.

All instrument calibration involves generally extensive preflight calibration and repeated in-flight (or on-board) calibration. Sensor calibration involves usually comparing the detector of a particular spectral range against a known reference. On-board calibration employs on-board calibrators, space targets (as the sun, the moon, the stars, etc.), and/or ground targets as a known reference (Dinguirard and Slater, 1999).

On-board calibration is required to detect changes in the average output of sensors so they are not incorrectly interpreted as changes on the observed scene. Relative calibration is more accurate and it is usually used for short period calibrations (days). Absolute calibration is more stable so a combination of relative and absolute calibration is used for longer periods. On-board calibration uses an illumination device or well known terrestrial targets, the later is named vicarious calibration (Dinguirard and Slater, 1999).

Long-term monitoring requires stability in the measurements hence the calibration is a fundamental part in the design of an instrument.

2.2.2 Earth Observing Satellites

Land satellite data requirements are driven to a significant extent by the need for long-term monitoring of land surface parameters to determine surface condition and to detect change, as well as inputs to regional and global carbon, energy, and water process models (Sellers, 1993). In the last few years increasing interest on carbon monitoring and climate change have driven most scientific and research missions (GCOS, 2004, 2006). Operational missions provide long-term data ensuring that if a sensor fails it will be replaced by another. Research missions provide specific data but the continuity of the measurements if not warranted.

Two operational satellite programs have provided the longest record of land cover data: the Landsat (since 1972) and SPOT (Systèmé Probatoire d'Observation de la Terre, since 1981) series. These datasets are not continuous because of clouds. The NOAA (National Oceanic and Atmospheric Administration) satellite series with the AVHRR (Advanced Very High Resolution Radiometer) on-board, launched for meteorological purposes, have also provided long-term data very useful in global vegetation monitoring.

Table 2.2: Main optical missions monitoring land surface currently being flown

Mission / Agency	Launch / EOL date	Relevant Passive Instruments	Mission objective
Envisat (Environmental Satellite) ESA	01 Mar 02 /01 Mar 07	AATSR, MERIS	Physical oceanography, land surface, ice and snow, atmospheric chemistry, atmospheric dynamics/water and energy cycles
ERS-2 (European Remote Sensing satellite - 2) ESA	21 Apr 95 /31 Dec 05	ATSR/M, ATSR-2	Earth resources plus physical oceanography, ice and snow, land surface, meteorology, geodesy/gravity, environmental monitoring, atmospheric chemistry
Landsat-5 USGS	01 Mar 84 /31 Dec 09	MSS, TM	Earth resources, land surface, environmental monitoring, agriculture and forestry, disaster monitoring and assessment, ice and snow cover
Landsat-7 USGS	15 Apr 99/31 Dec 10	ETM+	
NMP EO-1 (New Millenium Program)/ NASA	21 Nov 00/30 Sep 05	ALI, Hyperion	Land surface, earth resources
POES /NOAA			Meteorology, agriculture and forestry, environmental monitoring, climatology,
NOAA-12	14 May 91/31 Dec 05	AVHRR/2	physical oceanography, volcanic
NOAA-14	30 Dec 94/31 Dec 05	AVHRR/2	eruption monitoring, ice and snow
NOAA-15	01 May 98/31 Dec 06	AVHRR/3	cover, space environment, solar flux
NOAA-16	21 Sep 00/31 Dec 06	AVHRR/3	analysis, search and rescue
NOAA-17	24 Jun 02/	AVHRR/3	
NOAA-18	20 May 05/	AVHRR/3	
SPOT-4 (Satellite Pour l'Observation de la Terre) CNES	24 Mar 98/31 Dec 05	VEGETATION	Cartography, land surface, agriculture and forestry, civil planning and mapping, digital terrain models, environmental monitoring
SPOT-5	04 May 02/04 May 07	VEGETATION	
Terra (formerly EOS AM-1) NASA	18 Dec 99/18 Dec 05	MISR, MODIS	Atmospheric dynamics/water and energy cycles, Atmospheric chemistry, Physical and radiative properties of clouds, airland exchanges of energy, carbon and water, vertical profiles of CO and methane vulcanology

Landsat Program

The Landsat Program represents the world's longest continuously acquired collection of space-based land remote sensing data. First Landsat satellite was launched in July 1972, initially called Earth Resources Technology Satellite (ERTS) and renamed Landsat at a later date. Landsat was the first satellite launched with the primary intent of providing long-term collection and continuity of Earth resources imagery.

Landsat-type observations fill an important niche between the highly repetitive but coarse spatial resolution observations from the NOAA AVHRR, NASA EOS MODIS, NASA SeaWiFS and French VEGETATION instruments and the ultra-high spatial resolution instruments such as IKONOS. Landsat provides systematic global coverage at a temporal resolution sufficient to capture seasonal variations (effective temporal resolution 16 days, reduced because of clouds) and at a spatial resolution of 30 m that allows the detection of changes on the Earth's land processes.

The Landsat satellites have always carried passive sensors capable of recording electromagnetic energy in the visible and infrared wavelengths. The Landsat MSS system evolved into the Thematic Mapper (TM) in 1982 and TM evolved into Enhanced Thematic Mapper (ETM) in 1999. Presently, the acquisition of Landsat 7 Enhanced Thematic Mapper Plus (ETM+) and Landsat 5 Thematic Mapper (TM) data continues.

SPOT Satellites

The SPOT Satellites were developed by a consortium of French, Swedish and Belgian companies. It is a system both operational and commercial and it has been in continuous operation since it was first launched on February 1986. Like the Landsat program, the SPOT series aims to provide long-term data continuity.

SPOT-1, -2 and -3 were launched in 1986, 1990 and 1993 respectively. The sensor payload consisted of two identical HRV (High Resolution Visible) sensors designed to operate in a panchromatic mode or multispectral mode supplying observations at a resolution of 10 and 20 metres respectively, in three spectral bands in the visible and the near infrared domain. SPOT-4 and -5 were launched in 1998 and 2001 and carry the two high resolution instruments named HRVIR (similar to HRV with an extra spectral band in the short wave infrared domain and a narrower bandwidth in the panchromatic mode) and a new low-resolution wide-coverage instrument, VEGETATION. Each HRV or HRVIR offers an oblique viewing capability, the viewing angle being adjustable through $\pm 27^{o}$ relative to the vertical. This off-nadir viewing enables the acquisition of stereoscopic imagery and provides a short revisit interval of 1 to 3

days. The VEGETATION system complements the HRVIR instruments by observing every day the whole Earth surface at a resolution of 1.15 km with a field of view of nearly 2250 km.

Due to the nature of the VIS-NIR data, extensive cloud cover can be problematic in obtaining good data in cloudy conditions. Taking into account the measurements which have to be discarded due to cloud coverage or bad atmospheric conditions, the system can provide one useful measurement every ten days allowing the observation and study of seasonal changes on a regional and global scale.

NOAA Series

The NOAA (National Oceanic and Atmospheric Administration) series satellites are meteorological platforms, with very low spatial resolution and high temporal resolution obtaining global information very frequently. It includes both geostationary and polar Operational Environmental Satellite, called GOES and POES.

NOAA POES series began with the TIROS-N satellite in 1978. The series from NOAA-6 (launched 1979) through NOAA-14 (launched 1994) carried the AVHRR (Advanced Very High Resolution Radiometer) sensor. The AVHRR flown aboard TIROS-N, NOAA-6, NOAA-8, and NOAA-10 had four channels, and the AVHRR aboard NOAA-7, NOAA-9, NOAA-11, NOAA-12 and NOAA-13 had five spectral channels (VIS, NIR, MIR and 2 in the Thermal IR). AVHRR in last series (NOAA-15 to 18) include an extra spectral channel in the SWIR. Presently six satellites are in operation, organized as primary morning (NOAA-17, launched 2002), primary afternoon (NOAA-18, launched 2005), secondary morning (NOAA-15, launched 1998), secondary afternoon (NOAA-16, launched 2000) and two morning standby (NOAA-12 and 14, launched 1991 and 1994). The NOAA satellites provide at least four image acquisitions per day for any location on the earth at 1 km resolution. Usually the afternoon satellites (NOAA-7, 9, 11, 14, 16 and 18) have been used for vegetation monitoring as illumination conditions are better at that time.

Data from AVHRR is free from NASA, as opposed to Landsat and SPOT satellites data, and is available daily. However, SPOT4-VEGETATION images provide better image positioning and better calibration than NOAA-AVHRR images.

Earth Observing System, EOS

The Earth Observing System (EOS) is the centerpiece of of NASA's Earth Science Enterprise (formerly Mission to Planet Earth, Wickland, 1991). It is a program of

multiple spacecraft and interdisciplinary science investigations to provide a 15 year data set of key parameters needed to understand global climate change. NASA has made a great effort to make data from this program widely available to the users data being free of charge.

Each mission in this program is dedicated to investigation of particular Earth system issues, including Terra (18 December 1999), Aqua (4 May 2002) and Aura (15 July 2004).

Terra, formerly known as EOS AM-1, carries a payload of five sensors that study interactions among Earth's atmosphere, land, oceans and radiant energy. Terra circles Earth in an orbit that descends across the equator at 10:30 a.m. when cloud cover is minimal (Sellers, 1993).

Aqua, formerly known as EOS PM-1, carries six instruments to gather information about water in land, sea and atmosphere and its orbit cross over the equator about 3 hours behind Terra.

Aura carries 4 instruments that provide observations of Earth's atmospheric ozone layer, air quality, and key climate parameters.

Aqua and Aura are destined to be part of a flotilla of satellites (A-Train) flying in formation in space, including Aqua, Aura, CloudSat (July 2005), Parasol (Polarization and Anisotropy of Reflectances for Atmospheric Science, carrying POLDER, 18 December 2004), Calipso (Cloud-Aerosol Lidar and Infrared Pathfinder Satellite Observation, July 2005) and OCO (Orbiting Carbon Observatory, 2008). The six satellites will cross the equator one at a time, a few minutes apart, at around 1.30 pm local time. The aim of the A-Train is to give a comprehensive picture of Earth weather and climate. The use of this set of less costly, less expensive, less complex satellites means that failure of one does not destroy an entire mission.

Terra payload includes a high spatial resolution instrument (Advanced Spaceborne Thermal Emission and Reflection Radiometer, ASTER), two broadband scanning radiometers (Clouds and the Earth's Radiant Energy System, CERES, including shortwave, long-wave and total channels), two moderate spatial resolution instruments (Multiangle Imaging Spectro-Radiometer, MISR and Moderate-resolution Imaging Spectroradiometer, MODIS) and a nadir sounding instrument (Measurement of Pollution in the Troposphere, MOPITT).

Aqua carries a CERES and a MODIS instruments also, toghether with three sounders (Atmospheric Infrared Sounder, AIRS, the Advanced Microwave Sounding Unit, AMSU-A and the Humidity Sounder for Brazil, HSB) and a microwave radiometer (Advanced Microwave Scanning Radiometer for EOS, AMSR-E).

The continuity of Terra and Aqua as well as AVHRR will be provided by NPOESS (National Polar Orbiting Environmental Satellite System) without an established date. NPOESS Preparatory Project (NPP) has been designed to function as a bridge between the NASA EOS program and NPOESS providing data continuity. NPOESS includes significant terrestrial remote sensing capabilities largely based on the experience of MODIS (Townshend and Justice, 2002) but does not include any multiangular instrument to give continuity to MISR measurements. NPOESS is an operational mission meaning that sustained observations will be collected and that a significant loss of observing capability will lead to a further instrument being placed in orbit.

European Space Agency (ESA) Missions

Two European Space Agency (ESA) remote sensing missions have also focused on Earth observation: ERS (European Remote Sensing Satellites) and ENVISAT (ENVIronmental SATellite).

ERS earth observation mission has been operating since 1991 when ERS-1 was launched (operated until March 2000). ERS-2 was launched in 1995 and has exceeded its nominal lifetime being still operational.

ENVISAT was designed to provide measurements of the atmosphere, ocean, land, and ice over a five year period and was launched in March 2002. The ENVISAT payload is aimed to ensure the continuity of the data measurements of the ERS satellites taking also into account the requirements related to the global study and monitoring of the environment. ENVISAT carries ten instruments including two moderate spatial resolution radiometers MERIS and AATSR (see table 2.3).

A third mission, designed as a technology demonstration mission, is the Project for On-Board Autonomy (Proba)(Barnsley et al., 2004). Proba started as a one-year mission and has provided data successfully ever since its launch on 22nd Oct 2001. Proba carries two instruments, a high resolution (20m) hyperspectral (up to 15 channels) instrument, CHRIS, and a black and white camera, HRC.

In 1999 ESA started to plan Earth observation beyond ENVISAT and launched the Living Planet Programme. Living Planet Programme focuses on the missions being defined, developed and operated in close cooperation with the science community. Two types of missions are considered: Earth Explorers for research and Earth Watches as prototype operational missions. So far, this approach has resulted in the selection six Earth Explorer missions with another six currently under assessment study. Two Earth Explorer satellites are scheduled for launch in 2007: GOCE (Gravity Field and

Steady-State Ocean Circulation Explorer) and SMOS (Soil Moisture and Ocean Salinity). Earth Watch includes the well-established meteorological missions with the European Organisation for the Exploitation of Meteorological Satellites (EUMETSAT) and also new missions focusing on the environment and civil security under GMES (Global Monitoring for Environment and Security) a joint initiative between the European Commission and ESA, currently being defined. It must be noted that, to the date, no mission has been proposed carrying a passive sensor that would ensure continuity of MERIS data. As in the case of NASA, future ESA missions will involve the use of smaller satellites on shorter, cheaper, focused missions.

Table 2.3: Current passive satellite instruments useful for terrestrial monitoring at moderate spatial resolution

Instrument	Mission	Spatial resolution	Swath	Temporal resolution	Spectral bands
AVHRR/3	NOAA-POES	1.1 km	2700 km	1 day	5 bands 0.58-12.50 μm (varying bandwidths)
SeaWiFs	Sea Star	1.1 km	1502 km	1 day	8 bands 0.40-0.89 μm
MODIS	Aqua, Terra	250 m (bands 1-2), 500 m (bands 3-7), 1 km (bands 8-36)	2330 km (cross track) by 10 km (along track at nadir)	1day	36 bands in range 0.4-14.4 μm
MISR	Terra	1.1 km (275 m on selected targets)	360 km	9 days	VIS: 0.44, 0.56, 0.67μm NIR: 0.86μm
MERIS	Envisat	Ocean: 1040m x 1200 m Land & coast: 260m x 300m	1150 km	3 days	VIS-NIR: 15 bands selectable across range: 0.4-1.05μm (bandwidth programmable between 0.0025 and 0.03μm)
AATSR	Envisat	1 km	500 km	3 days	VIS - NIR: 0.555, 0.659, 0.865μm SWIR: 1.6μm, MWIR: 3.7μm TIR: 10.85, 12μm
AATSR-2	ERS-2	1 km	500 km	3 days	VIS-SWIR: 0.65, 0.85, 1.27, and 1.6μm SWIR-TIR: 1.6, 3.7, 11 and 12μm Microwave: 23.8, 36.5GHz
VEGETATION	SPOT-4 SPOT-5	1.15km	2250 km	1day	VIS: 0.43- 0.47μm , 0.61-0.68μm, NIR: 0.78-0.89μm SWIR: 1.58-1.75μm
POLDER	PARASOL	6 x 7 km	2400 km	1 day	VIS: 0.443μm, 0.49μm, 0.565μm, 0.67μm, 0.763μm, 0.765μm, 0.865μm, 0.910μm, 1.020μm

Planned missions present serious gaps in terms of multispectral and multiangular sensors. As has just been pointed out, there is not planned instrument to provide continuity of MERIS data. Despite the scientific advances obtained with MISR instrument on Terra, currently there are not follow-on missions with similar observational characteristics. Moreover, AATSR visible and shortwave IR channels, on ENVISAT, may be deleted from future versions of the instrument. Another multiangular multispectral instrument proposed, the pointable SPECTRA instrument (Verhoef, 2003), was not selected for further development by ESA and the CARBON-3D mission concept (Hese et al., 2005), which offered a synergistic combination of passive multiangular and active lidar measurements of vegetation structure, was not selected for further development by DLR. In terms of long-term monitoring presently only NPP and NPOES are providing continuous datasets. ESA new missions are more exploratory missions, without any intention of continuity on measurements.

2.3 Remote sensing application to land surface

Satellite observations have demonstrated to be very useful on the retrieval of surface parameters (e.g.Chen and Cihlar, 1996; Knyazikhin et al., 1998a;Wulder, 1998; Asner et al. 2003).

The capabilities of remote sensing for ecological studies were extensively studied in the early nineties (e.g. Roughgarden et al., 1991, Sellers et al., 1995, Ustin et al., 1991). In this decade, land cover data at high spatial/low temporal resolution (e.g., Landsat) and fAPAR at high temporal/moderate spatial resolution (e.g., AVHRR) were widely used for environmental monitoring (e.g. Ehrlich et al., 1994), climate studies (e.g. Sellers et al., 1994), carbon stock estimations (e.g. Foody et al., 1996) and retrieval of biophysical parameters (e.g. Chen and Cihlar, 1996). However, remote sensing technology was not used to its fullest extent and it was realised that a bigger involvement of ecologists was required in order to provide insight and direction (Wickland, 1991).

A comprehensive assessment of required land cover parameters was developed at the International Satellite Land Surface Climatology Project (ISLSCP) meeting at Columbia, Maryland, in 1992 (Sellers et al., 1995). Results from this consultation showed that spatial and temporal resolution requirements ranged from 100 m to 100 km and from 6 hours to annually, respectively.

By the late 1990's, the development of land surface and ecosystem models increased the demand of global observations of parameters such as vegetation structure and chemistry, to be used as inputs in the models. These parameters cannot be obtained

via field measurements and are fundamental for the modelling of terrestrial ecosystem dynamics (including carbon cycling).

Several publications have reviewed the interaction between both communities (remote sensors and ecologists) and have pointed out the potential benefits that this would bring to both fields (Plummer, 2000, Turner et al., 2004). According to Plummer, 2000 the remote sensing community was putting much effort on deriving biophysical parameters but the needs of ecological process studies seemed not to be adequately taken into account, while ecological process studies were equally independent from remote sensing. This lack of communication between ecologists and remote sensors has been remarked by other authors (e.g. Asner, 1998). There seems to be a mismatch between the data wanted by ecologists and the data collected with remote sensing instruments (Wulder et al., 2004). However, it is not clear if this is a cultural perception more than a technological issue, as many researchers keep on using old methodologies which are based on past satellite specifications, e.g at a coarse resolution (Turner et al., 2003).

Present high spatial resolution instruments provide data at spatial scales fine enough to develop ecological studies at the landscape scale (e.g. Treitz and Howarth, 2000). Spatial resolution requirements are achievable until they are accompanied of demands of quick delivery and high temporal scale. While advances in technology are allowing always higher spatial resolution (e.g. 1m with the Panchromatic IKONOS sensor), the required delivery of the processed information ideally within 24h of the acquisition for real time data assimilation in NWP models, as well as the twice weekly revisit period seems much harder to achieve with satellite systems, except possibly with low resolution systems such as NOAA. Present moderate-resolution systems provide a spatial resolution between 1 and 250 metres with temporal re-visit time of 14-45 days (e.g. Landsat, SPOT HRV, EO-1). Coarse resolution sensors such as POLDER, NOAA/AVHRRR, VEGETATION, MODIS, MISR, MERIS etc., allow a more frequent coverage of the Earths surface (daily-weekly) but with spatial resolutions of 250 m - 1 km.

Advances in materials and optics have allowed the development of new instruments that can quantify biophysical properties more accurately than was possible before. Recent development of new sensors with moderate spatial but high spectral resolution (MODIS on Terra and Aqua, MERIS on Envisat), and the availability of multi-angle imaging capability (CHRIS-Proba, POLDER and MISR), have brought new perspectives and potential for land surface characterisation (bio-physical properties, biomass estimation, vegetation indices, land cover and cover change and possibly soil moisture).

Multi-directional and polarimetric instruments (such as MISR or POLDER) provide extra data about vegetation properties (Asner et al., 1998, Diner et al., 1999) and can potentially improve our understanding of atmospheric scattering and absorption (Kaufman et al., 1997; King et al., 1999; North et al., 1999) and solar-sensor geometry but these techniques are still underutilized for ecological applications (Chen et al., 2003). Hyperspectral data is also a promising tool to retrieve biophysical parameters (Treitz and Howarth, 1999; Ustin et al., 2004). New interferometric and polarimetric capabilities and LIDAR (e.g. ERS-1 and 2, ENVISAT) provide also new ways of retrieving information but they will not give continuity of previous data.

In terms of long-term monitoring, time series of satellite imagery have demonstrated to be useful to detect, map and monitor changes in ecosystems (Coppin et al., 2004). Numerous local scale studies have mapped and quantified land-cover change with fine resolution remote sensing data (e.g. Petit et al., 2001) but there are few such studies at the regional to global scales. Multisensor approaches are being used to create global datasets that permit longer-term studies and analyses at different scales by fusion of data from a range of sensors (Lambin and Linderman, 2006; Petit and Lambin, 2001). Monitoring by satellite sensors has also been combined with networks of in-situ observations to ensure long-term monitoring of terrestrial parameters (Running et al., 1999).

The implementation of the research requirements in terms of routine land cover monitoring include tasks such as validation procedures for land cover products (Teillet et al., 1997), automatisation of methods for operational implementation, assured continuity of satellite data in the future, and consensus on how land cover should be characterized (Defries and Townshend, 1999). Both communities should work together in this steps, and not only in the design stage through a requirements consultation.

Numerous studies have investigated the potential of specific instruments to extract biophysical variables (Bicheron and Leroy, 1999; North et al., 1999; Dawson, 2000; Huete et al., 2002; North, 2002b) from a general perspective but these studies are rarely linked to real ecological models or to the sensitivity of those models to errors in the retrieved parameters. This study aims to add one more step on the process of bringing together both communities, contributing to the definition of ecological requirements from remote sensing.

2.3.1 Relevant Ecological Parameters

A suite of land-surface variables, including land cover, leaf-area index (LAI), roughness length, and albedo, are required as inputs to the LSPs to characterize the state of

the land-surface-atmosphere system. Also meteorological inputs are required to drive LSPs including daily values of maximum and minimum air temperature, total solar radiation, mean humidity, and total precipitation. Continuous temporal and spatial datasets of these parameters are present requirements of LSPs from remote sensing.

It is important to consider the scale of simulation that will be used. Canopy processes present diurnal variations that in general follow predictable patterns. High temporal resolution models allow simulate explicitly these processes but they demand a lot of input data. Daily models, on the other hand, cannot simulate these detailed processes but they can be parameterised to simulate most of the daily variability. Low temporal resolution models allow improvement of the spatial resolution because of their moderate demand on computation and input data, with the subsequent reduction on spatial scaling errors. Either at coarse spatial resolution (2-5^o) or at moderate resolutions (1 Km and larger), satellite sensors offers a unique means to monitor the natural growing season variability at the required time scale.

2.3.1.1 Meteorological data

The key surface meteorological inputs required by ecological models are incident radiation, precipitation, humidity and air temperature. These measurements are normally obtained from permanent weather stations. Remote sensing can contribute to measurements of the surface climate, principally through estimation of incident radiation, cloud cover and precipitation.

The solar energy reaching the Earth's surface between the wavelengths 400nm and 700nm (photosynthetically active radiation, PAR) is the driver of plant photosynthesis and therefore regulates the rate of carbon fixed by terrestrial and aquatic plants. Incoming PAR is inferred by modelling the atmospheric radiative transfer process. This requires estimation of cloud cover and transmission, atmospheric state and surface albedo. PAR measurements have been routinely made using multispectral sensors and used to estimate global primary production (e.g. Prince and Goward, 1995).

Clouds influence the Earth's energy and hydrological cycles playing a critical role in climate. One of the largest uncertainties in global climate models is the representation of how clouds and aerosols influence the Earth's radiation budget at the surface, within the atmosphere and at the top of the atmosphere. First global estimates of shortwave (SW) and longwave (LW) radiative fluxes were made during the Earth Radiation Budget Experiment (ERBE) (Barkstrom, 1984). Errors in both SW and LW flux estimations were found to depend strongly on cloud properties. Multiangle imagery from sensors like MISR and CERES has improved dramatically the retrieval of clouds and

Table 2.5: Requirements for climate long-term monitoring (Ohring et al., 2004)

	Actual accuracy/stability	Required Accuracy	Required Stability
Albedo	AVHRR 5-10%/3-5% MODIS,MISR 3-5%/na	5%	1% per decade
Cloud Imagery (in units of cloud fraction between 0 and 1).	CERES and MODIS: 0.05/na	0.01	0.003 per decade
Downwelling LW radiation at the Earth surface	CERES:$\pm 3-5 W/m^2$/na	$\pm 1 W/m^2$	$\pm 0.2 W/m^2$per decade
Downwelling SW radiation at the Earth surface	CERES:$\pm 10 W/m^2$/na	$\pm 1 W/m^2$	$\pm 0.2 W/m^2$per decade
Downwelling solar radiation at TOA	CERES:$\pm 1 W/m^2$/na	$\pm 1 W/m^2$	$\pm 0.3 W/m^2$per decade
Outgoing LW radiation at TOA	CERES:$\pm 1 W/m^2$/na	$\pm 1 W/m^2$	$\pm 0.2 W/m^2$per decade

aerosols properties (Diner et al., 2005). Clouds and the Earth's Radiant Energy System (CERES, Wielicki et al., 1996) instruments on Terra are taking measurements of broadband shortwave, total, and window radiances since March 2000. CERES data used in combination with imager retrievals of cloud and aerosol data (e.g., from MODIS), and meteorological information from data assimilation models, and new algorithms have dramatically improved the accuracy of both SW and LW radiative fluxes compared to ERBE (Loeb et al., 2005). Multiangle imagery from MISR, which provides various looks with a small time difference, has made it possible to capture cloud properties such us cloud-top heights, the morphological structure of vertically developed clouds, and cloud advection velocities (Zong et al., 2002).

The National Institute of Standards and Technology (NIST), National Polar-orbiting Operational Environmental Satellite System- Integrated Program Office (NPOESS-IPO), National Oceanic and Atmospheric Administration (NOAA), and National Aeronautics and Space Administration (NASA) organized a workshop in 2002 (Ohring et al., 2004) to define absolute accuracies and long-term stabilities of global climate data sets that are needed to detect small changes associated with long-term global climate change from space. The report concluded that excellent absolute accuracy is vital for understanding the processes, while long-term stability of the datasets is crucial to ensure the detection of trends. Table 2.5 shows accuracy and stability requirements and present products for radiation parameters.

Precipitation is estimated by reference to cloud top parameters in optical wavelengths or through scattering of microwave radiation by water in the clouds. Global Precipitation Climatology Project (GPCP) was established by World Climate Research Pro-

gramme (WCRP) with the initial goal of producing global precipitation estimates for a number of years. The project has elaborated a one degree daily precipitation product for 1996 to present (Huffman et al., 2001) and a 2.5 degree monthly product from 1979 to present (Adler et al., 2003) from multi-satellite observations.

2.3.1.2 Land surface variables

The number and type of land surface parameters required by ecological models depends on the complexity of the model. Typically, spatial and temporal information on soil-moisture, roughness, texture, some measure of land cover or biome type, vegetation structural variables (LAI, cover fraction, height) and surface radiation variables such as surface albedo and the absorption of PAR are required. In the last years efforts have been channelled into the direct estimation of vegetation variables from remote sensing, rather than using mean values assigned to land cover classes. Soil physical and chemical properties, for example soil C and N, cannot be obtained by remote sensing (Sellers et al., 1995).

WMO has reviewed the requirements from its various programmes, in the framework of CEOS (Committee for Earth Observation Satellites), and also has coordinated the collection of requirements from other international programmes (WCRP, GCOS, GOOS, GTOS, IGBP, ICSU, UNEP). An Official CEOS/WMO Online Database containing the results of this consultation was released in 2000. Table 2.6 shows the requirements in terms of temporal and spatial resolution and accuracy extracted from it. The most relevant parameters are explained and discussed next.

Land cover

Land cover is the initial variable for parameterising ecological models. It provides a descriptive definition of the biome type present at a given location but it does not quantify the vegetation. Satellite data are used to provide information on land cover and the seasonal variation in leaf area for these models.

During the last decade, major results for land cover and vegetation monitoring have been obtained with optical coarse resolution sensors such as AVHRR on NOAA series and later with VEGETATION on SPOT-4 and 5. Annual sequences of NDVI (Normalized Difference Vegetation Index) over the globe have been calculated using AVHRR spectral channels 1 and 2. These data provided a 22-year satellite record of monthly changes in terrestrial vegetation at spatial resolutions of 1 km from a few individual years to 4 km, 8 km and coarser. Early climate and biogeochemical models used NDVI

Table 2.6: Requirements for land surface modelling. Only optimum values are shown.

	Source	Spatial Resolution	Temporal Resolution	Accuracy
Aerosol profile - Total column	GCOS, GTOS WMO IGBP	1 km 5 km, 50 km 100 km	24 h 0.25 h, 1 h 7 d	- 10%, 10% 10%
Albedo	Sellers et al., 1995	250 km	30 d, 1 d, diurnal cycle	±0.02
Cloud Imagery	GCOS, GTOS	1 km	3 h	-
Downwelling LW radiation at the Earth surface	GCOS, GTOS	25 km	3 h	±5W/m^2
Downwelling SW radiation at the Earth surface	GCOS, GTOS	25 km	24 h	±5W/m^2
Downwelling solar radiation at TOA	GCOS	-	3 h	±1W/m^2
Fire area/temperature	GCOS, GTOS IGBP UNEP	0.1 km 3 km 0.5 km	10 d 10 d 1 d	5 % / 50 K 5% / 200 K 5% /50 K
fAPAR	GCOS IGBP	0.1 km 0.03 km, 50 km	10 d 10 d	5% 5%
Land Cover	WMO GCOS, GTOS IGBP UNEP	10 m, 100 m 100 m 30m, 100m, 1km 1 m	0.02 y, 1 y 1 y 1 y 1 y	50 classes, 10 classes 50 classes 22, 22, 2 classes 20 classes
Land Surface Imagery	GCOS, GTOS WMO	1 m 10m	4 y 1d	- -
Land Surface Topography	GCOS, GTOS WMO IGBP	10m 100 m 10 m, 1 km	10 y 10 y 100 y	30 (vert) 1m (vert) 0.3m, 1m (vert)
LAI	GCOS, GTOS WMO	0.1 km 0.01 km, 10 km, 50 km	10 d 5 d,7 d,7 d	20% 5%
Outgoing LW Earth surface	GCOS, GTOS	25 km	3 h	±5W/m^2
Outgoing LW radiation at TOA	GCOS, GTOS WMO IGBP	50 km, 200 km 0.1 km, 10 km, 50 km 200 km	20 d, 3 h 1 h, 0.5 h, 1 h 6h	±5W/m^2 ±5W/m^2 ±10W/m^2
Ozone profile - Total column	GCOS, GTOS WMO	1 km 10 km, 20 km, 25 km, 50 km	24 h 0.5 h, 0.25 h, 6h ,1 h	- 5 DU (Dobson units)
PAR	Sellers et al 1995 WMO	250 km 5 km	30 d, 1 d, diurnal cycle 1 h	±10W/m^2 5 %
Snow cover	GCOS, GTOS WMO WCRP	1km, 100 km 0.1 km,1 km,5 km,15 km 1 km, 15 km	24 h 24 h, 120 h, 1h 12 h 24 h	5%, 10% 5%, 2%, 10%, 10% 10%
SW Earth surface bi-directional reflectance	Sellers et al 1994 WMO IGBP	250 km 25 km 100 km	30 d 24 h 7d	±10W/m^2 ±5W/m^2 1%
Vegetation Type	WMO IGBP UNEP	10 m, 50 m, 50 km 10 m, 100 m, 1 km 1 m	7d, 30 d, 7d 10 d, 1 y, 90 d 1 y	50, 30, 18 classes 2, 18, 18 classes 18 classes

Sources: ISLSCP Workshop Sellers et al., 1995; Global Climate Observing System (GCOS); World Meteorological Organization (WMO); Global Terrestrial Observing System (GTOS); International Geosphere-Biosphere Programme (IGBP); World Climate Research Programme (WCRP); United Nations Environmental Program (UNEP). CEOS/WMO database, Observational requirements (WMO, WCRP, GCOS, GOOS, GTOS, IGBP, ICSU, UNEP)

to calculate photosynthesis, the exchange of CO2 between the atmosphere and the land surface, land-surface evapotranspiration and the absorption and release of energy by the land surface. This data set was corrected for NDVI variations not related to actual vegetation change providing the first long term data set that can be used for computing the time series of other biophysical parameters(Los et al., 1994).

Land-cover change can be observed using satellite data but the accuracy is uncertain and different land-cover type characterization systems are used. Data sets characterizing global land cover are currently produced at resolutions of between 250m and 1km by several Space Agencies. So far, global land cover maps have been constructed using data from AVHRR (Loveland et al., 2000), SPOT-Vegetation (GLC-2000 at 1km spatial resolution, e.g. Bartalev et al., 2003 for Eurasia, containing 26 classes), and MODIS (Friedl et al., 2002, 17 classes). Global Landcover Classification for the year 2000 (GLC2000) project was carried out to provide accurate baseline land-cover information to the IPCC, the Convention to Combat Desertification, the Ramsar Convention and the Kyoto Protocol. It uses the FAO Land Cover Classification System. MODIS offers a Land Cover Product and a Land Cover Dynamics Product aimed to detect and quantify the intra-annual phenological dynamics of global vegetation cover and inter-annual changes in land cover type over time. The Land Cover classification product gives a primary classification based in the International Geosphere-Biosphere Programme (IGBP) scheme. Products are accompanied by assessments of its quality or confidence, the second most probable class label, percent and overall quality flags and an embedded land/water mask.

Future maps are also planned from MERIS, on-board ENVISAT, with data acquired over the full year 2005 at 300m spatial resolution (GLOBCOVER project). This product is intended to be available in January 2007.

The future National Polar Operational Environmental Satellite System (NPOESS) (which will provide the operational successor to the AVHRR with the Visible Infrared Imaging Radiometer Suite (VIIRS)) will produce also global land cover products in quarterly basis (Townshend and Justice, 2002).

Fractional cover

Fractional cover (FC) or canopy cover is defined as the percent of a fixed area covered by plant species or delimited by the vertical projection of its outermost perimeter. It includes dry and green vegetation (called Non-Photosynthetic Vegetation and Photosynthetic Vegetation respectively). Vegetation cover fraction affects surface albedo, i.e. the ratio of outgoing/incoming solar flux, so it is a fundamental parameter to define

the partitioning of flux between the ground and the canopy. It is also useful to detect disturbance such as fires or logging. The fractional cover retrieved by remote sensors has proven to be useful from biophysical and biogeochemical perspectives (Defries et al., 1999; Asner, 1998).

Leaf area index (LAI)

Leaf area index (LAI) represents the total leaf area of the canopy, ignoring the complexities of canopy geometry. LAI is closely related to many physical and biological processes related to vegetation dynamics such as photosynthesis, transpiration and evapotranspiration. LAI provides an ecophysiological measure of the photosynthetic and transpirational surface within a canopy, as well as a remote sensing measure of the leaf reflective surface within a canopy. Hence, LAI is a key variable in many models describing vegetation-atmosphere interactions, particularly with respect to the carbon and water cycles.

There are several definitions of LAI depending on the context in which it is used. According to Asner et al., 2003 the four most common definitions of LAI are :

1. Total LAI: based on the total outside area of the leaves, taking leaf shape into account, per unit area of horizontal land below the canopy
2. One-sided LAI: as half the total LAI, even if the two sides of the leaves are not symmetrical
3. Horizontally projected LAI: as the area of "shadow" that would be cast by each leaf in the canopy with a light source at infinite distance and perpendicular to it, summed up for all leaves in the canopy.
4. Inclined projected LAI (or "silhouette" LAI): representing the projected area of leaves while accounting for leaf inclinations.

Methods to estimate LAI in the field employ either direct or indirect techniques (Chen et al., 1997; Jonckheere et al., 2004). Direct methods includes destructive harvesting, litterfall collection or allometric estimations based on simple physical dimensions such as stem diameter at breast height. These methods are laborious and expensive.

Indirect methods use optical instruments and models providing quick and low-cost measurements over large areas. Full canopy structural definition requires leaf angle distribution (LAD), clumping, canopy height and macrostructure shape data. Commercially available instruments - such as the LICOR LAI-2000 (Li-Cor, Inc., Lincoln,

Nebraska), Sunfleck Ceptometer (Decagon Devices, Pullman, Washington) or hemispherical photography - measure LAI indirectly from the measurements of canopy gap fraction. This estimation assumes that foliage is randomly distributed in the canopy. Herbaceous canopies generally have simple structures with leaves more or less randomly distributed in space, but foliage in forests is organized in structures such as shoots, branches, tree crowns, and tree groups. Estimations made with this instruments must be corrected in some way for this complexity of canopy architecture.

Remote sensing allows to estimate LAI in an indirect way but full canopy structural definition is required: leaf angle distribution (LAD), clumping, canopy height and macrostructure shape data (Chen et al., 1997). Remote sensing is quite efficient on estimating LAI at values between 1 and 3. When the canopy cover is sparse, reflectance measurements are dominated by soil properties and the accuracy of the LAI is low. For LAI values exceeding 3 or 4, the measurements saturate. For this reason in some parts of the globe, such as in the humid tropics, LAI can only be measured by in situ methods. It must be considered that for high values of LAI, errors in the estimations become less important (e.g. between 5 and 8) as the productivity will be limited by the amount of incident light.

The Moderate Resolution Imaging Spectroradiometer (MODIS) LAI, for example, is a 1-km global data product updated once each eight-day period throughout the year. The Multi-angle Imaging Spectroradiometer (MISR) LAI has a spatial resolution of 1.1 km and also is updated every eight days. The MODIS LAI product is being derived mainly with the LUT method (explained in next chapter) and, for extreme conditions, the backup method based in vegetation indices. POLDER data have been used to estimate LAI by inverting a simple soil-vegetation reflectance model over limited regions (Bicheron and Leroy, 1999)

Globally validated growth cycle or LAI products available are derived from a variety of sensors and cover different periods: AVHRR (e.g. ECOCLIMAP), VEGETATION (CYCLOPES), ATSR-2/VEGETATION/AATSR (GLOBCARBON, Global Land Products for Carbon Model Assimilation) and MODIS/MISR from 2000.

Also global estimates of daily gross primary production (GPP) and annual net primary production (NPP) are now produced operationally at 1 km resolution from MODIS data (Turner et al., 2006). The product has an 8-day temporal resolution allowing the monitoring of seasonal and spatial patterns. A light use efficiency model is used to calculate GPP from daily PAR, fAPAR, LAI and meteorological data (minimum daily temperature and vapour pressure deficit). The NPP algorithm requires autotrophic respiration based on inputs of LAI and temperature, along with look-up table values

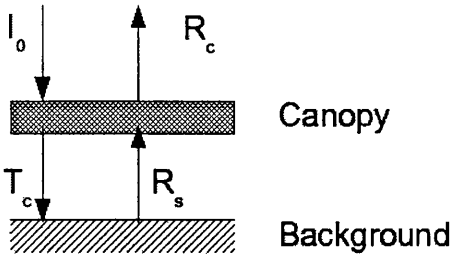

Figure 2.2: Scheme of radiation interaction with a vegetated surface, simplification for the estimation of fAPAR

for allometric constants and the base rate of respiration.

Fraction of Absorbed Photosynthetically Active Radiation (fAPAR)

The Fraction of Absorbed Photosynthetically Active Radiation (fAPAR) is the radiometric equivalent of the structural variable LAI. Not all incoming solar radiation is available for biomass production and photosynthesis. The portion of the electromagnetic radiation that is used for photosynthesis (400-700 nm) is called photosynthetically active radiation (PAR). fAPAR is defined as the fraction of incident PAR that is absorbed by the green leaves in the canopy. It excludes the fraction reflected back to the atmosphere and the fraction absorbed by the background (e.g. moss, soil, or understory in forest), but it includes the small fraction that is reflected by the background and absorbed by the green leaves on the way back to space.

fAPAR can be defined as a function of four radiation terms (Privette et al., 1996b):

$$fAPAR = \frac{I_0 - R_c - (T_c - R_s)}{I_0} \tag{2.6}$$

where I_0 is the incident radiation, R_c is the reflected radiation above the canopy, T_c is the radiation transmitted through the canopy and R_s is the radiation reflected by the soil-background (Figure 2.2).

fAPAR is an indicator of the state and productivity of vegetation and represents the fraction of the solar energy absorbed by vegetation during photosynthesis. Photosynthetic active radiation and LAI are often used to model evapotranspiration and plant productivity.

Spatially-detailed descriptions of fAPAR provide information about terrestrial carbon sinks, and can be of value in verifying the effectiveness of the Kyoto Protocol's implementation mechanisms.

fAPAR can be inferred from models describing the transfer of solar radiation in plant canopies, using remote sensing observations as constraints. Light absorption follows the seasonal changes of plant reflectance so fAPAR can be linearly related to the NDVI. It has been used in the estimation of primary production/photosynthetic activity, e.g. radiation interception, in crop models and in carbon studies.

As a first approximation NPP is proportional to the total amount of radiation absorbed by the plant canopy (APAR). Knowing incoming photosynthetic active radiation (PAR) APAR can be calculated as PAR$\times$fAPAR, and NPP can be calculated as NPP=$\varepsilon \times$APAR (Monteith, 1977). The conversion rate of APAR into NPP, ε, is species dependent so a land cover map is required to implement this method.

Daily recovery of fAPAR by satellite is possible but cloud and haze normally lead to fAPAR values that are multi-day averages. GTOS and GCOS require weekly to 10-day global fAPAR products at 250m-1km resolution (WMO, 2004).

It has been proposed that the availability of multi-angle remote sensing data could replace the traditional way of mapping NPP through fAPAR. NPP could be modelled instead by using canopy architectural parameters- such as LAI and clumping index- derived from multi-angle remote sensing (Chen et al., 2003). Some authors argue that LAI is preferable to fAPAR as LAI relates to standing biomass (e.g. evergreen forest) and this data can relate to NPP and to site water availability (e.g. Chen et al., 2003). LAI is a more physically-meaningful measure but presents the problem of saturation and sensitivity to clumping and to leaf optical properties.

LAI measured by satellites is inferred from reflectance, being tightly coupled to fAPAR, but this relationship varies with structure and must be defined through further definition of clumped leaf area and ground cover. Most LAI and fAPAR retrieval algorithms are based on inversion of radiative transfer models, which simulate radiation absorption and scattering in vegetation canopies (Myneni et al., 1995). Correlation with vegetation indices is also commonly used (Los et al., 1994, 2000). The algorithm being used to retrieve LAI and fAPAR from MODIS and MISR data is based on six distinct plant structural types (biomes) defined by Myneni et al., 1997b. This algorithm relies on a database describing the global distribution of these biomes to invoke different radiative transfer models. Application of the MODIS LAI product is limited by cloud cover, saturation in dense canopies and misclassification caused by using only 6 terrestrial biomes to represent all global vegetation structural types. In forested biomes (broad-leaf and needle-leaf forests), the MODIS product performs poorly under-predicting LAI values due to this problems (Myneni et al., 2002)

Chlorophyll content

Chlorophyll content (Cab) in vegetation can be used as an indicator of maximum photosynthetic capacity, leaf developmental stage, productivity and stress including nitrogen deficiencies (Ustin et al., 1998; Zarco-Tejada et al., 2004b). Estimation of leaf photosynthetic pigment content is one of the most frequently undertaken analyses in plant physiological studies. The distribution of chlorophyll within a vegetation canopy vary considerably in time and space making the estimation of canopy chlorophyll content, through destructive sampling, a labour intensive and expensive process. Consequently, methods are required which provide accurate, non-destructive and simple estimates of chlorophyll content and provide data at canopy scales, rather than for individual leaves.

Changes in leaf Cab produce large differences in leaf reflectance and transmittance spectra (Dawson et al., 1998), however, canopy reflectance is also strongly affected by other factors such as canopy architecture, Cab distribution into the canopy, leaf area index (LAI) and soil background (Dawson et al., 1999, 2003). Cab retrieval at canopy level is complicated and challenging. Several remote sensing techniques using reflectance in the red and near-infrared (NIR) spectral regions have been proposed to estimate Cab in leaves and canopies. Chlorophyll content is related positively to the point of maximum slope in vegetation reflectance spectra which occurs at wavelengths between 690-740 nm and is known as the "red edge". In stressed vegetation leaf chlorophyll content decreases, thereby changing the proportion of light-absorbing pigments and leading to less overall absorption (Zarco-Tejada et al., 2000). Loss of chlorophyll (chlorosis) increases reflectance across the visible and near-infrared spectrum and shifts the red edge toward shorter wavelengths, this effect is termed the "blue shift".

Several passive sensors cover the spectral range sensitive to Cab and have been used in the retrieval of chlorophyll content (e.g. Dawson, 2000; Zarco-Tejada et al., 2004b).

2.4 Evaluation of international programs

There is a strong international community request for the establishment of a strategy for integrated global observations and interaction amongst research fields. International programmes and partnerships are being created in order to improve both the quality and the availability of data. International Data Centres for some variables are functioning already and infrastructure to coordinate the collection of data for key in situ variables is being developed. Presently, Space Agencies provide observations for

some variables on a routine basis and improved mechanisms exist for international consensus (e.g. GTOS science panels and a Land Product Validation Group within the CEOS Working Group on Calibration and Validation (WGCV)).

The main projects are outlined here.

CEOS

The Committee on Earth Observation Satellite (CEOS) is an international coordinating organisation created in 1984 that comprises 25 Members (most of which are space agencies) and 20 associated organizations. It is recognized as the major international forum for the coordination of Earth observation satellite programs and for interaction of these programs with users of satellite data worldwide. Working Group on Calibration and Validation (WGCV, http://wgcv.ceos.org/) aimed to ensure long-term confidence in the accuracy and quality of Earth observation data and products. It comprises six groups, one of them is the Subgroup Land Product Validation (LPV) created in October of 2000. Its goal is to foster quantitative validation of higher-level global land products derived from remote sensing data and to relay results so they are relevant to users. On of its objectives is to work with users to define uncertainty objectives. It has launched LAI and albedo intercomparison studies (Morisette et al., 2006).

ESSP

The Earth System Science Partnership (ESSP, http://www.essp.org/) is a joint initiative that aims to undertake an integrated study of the Earth System by bringing together researchers from diverse fields. ESSP is particularly interested in human-driven changes and it comprises four global change programmes: International Geosphere-Biosphere Programme (IGBP, http://www.igbp.kva.se/), the International Human Dimensions Programme on Global Environmental Change (IHDP), the World Climate Research Programme (WCRP, http://www.wmo.ch/web/wcrp/), and DIVERSITAS, an international programme of biodiversity science. The International Council for Science (ICSU) is the common scientific sponsor of the four international global environmental change programmes.

IGBP, in collaboration with the United States Global Change Research Program, gave a first step in the involvement of ecologists in remote sensing missions with the launch of the Earth Science Enterprise (former Mission to Planet Earth, MTPE) in 1991 (Wickland, 1991). This is a NASA-initiated plan, that aims to provide the necessary instruments and data to fulfill scientific requirements. The goal was inherently ecological

and ecologists were called to play major roles in their formulation. However, ecologist community was not so involved (Wickland, 1991).

The Global Carbon Project [http://www.globalcarbonproject.org] is another program from the ESSP partnership. The scientific goals of the Global Carbon Project is to develop a comprehensive picture of the global carbon cycle through a research framework that integrates biogeochemical, biophysical and human components. The first stage was a 3-year consultation with the international research community (2000-2002) that ended in the formulation of the Science Framework and Implementation strategy (Canadell et al., 2003). This report does emphasize the improvement that satellite remote sensing has brought to the carbon cycle research and commits to provide information on the development and use of new research tools and approaches.

GCOS

The Global Climate Observing System (GCOS) was established in 1992 to ensure that the observations and information needed to address climate-related issues are obtained and made available to all potential users. It is co-sponsored by the World Meteorological Organization (WMO), the Intergovernmental Oceanographic Commission (IOC) of UNESCO, the United Nations Environment Programme (UNEP) and the International Council for Science (ICSU). GCOS is intended to be a long-term, user-driven operational system capable of providing the comprehensive observations required for monitoring the climate system, for detecting and attributing climate change, for assessing the impacts of climate variability and change, and for supporting research toward improved understanding, modelling and prediction of the climate system. It addresses the total climate system including physical, chemical and biological properties, and atmospheric, oceanic, hydrologic, cryospheric and terrestrial processes. The GCOS Implementation Plan (GCOS, 2004) identified Essential Climate Variables (ECVs) and their associated products. A posterior report contains specific satellite data requirements as well as recommendations on how to achieve them (GCOS, 2006).

GEOSS

Another important step towards an unified Earth observation approach was the creation of GEOSS (Global Earth Observation System of Systems, http://www.epa.gov/geoss/index.html) in 2004. GEOSS is an international framework to develop a 10-year (2004-2014) implementation plan to better understand the Earth system integrating data from thousands of instruments worldwide. The aim is to maximize the effectiveness of Earth

Observation by minimizing data gaps, building capacity and exchanging information as fully and quickly as possible.

GEWEX

The Global Energy and Water Cycle Experiment (GEWEX, http://www.gewex.org/) is a core project of the WCRP focused on the prediction of global and regional climate change. GEWEX has driven the formation of the Global Land-Atmosphere System Study (GLASS). GLASS includes the major efforts over the last decade that have done most to bring the land surface community together to understand why various LSPs perform differently: ALMA (Assistance for Land-surface Modelling activities), GLACE (Global Land-Atmosphere Coupling Experiment), PILPS(Project for Intercomparison of Land-surface Parameterisation Schemes, (Henderson-Sellers et al., 1995, 1996) and the Global Soil Wetness Project (GSWP) closely linked to the ISLSCP Initiative II (http://grads.iges.org/gswp/).

IGOS

Integrated Global Observing Strategy Partnership (IGOS) involves a number of partners, linking research, long-term monitoring and data producers and users. Its mission is to address how well user requirements are being met by the existing mix of observations, determine observation gaps and identify the resources to fill observation needs. The principle behind IGOS-P is to develop a strategy for coupling major Earth and space-based systems for global environmental observations of the land, oceans and atmosphere. The terrestrial theme of IGOS, the Integrated Global Observations for Land (IGOL), aims to provide a comprehensive picture of the present state of terrestrial ecosystems, and establish a framework for long-term monitoring of those ecosystems. The Integrated Global Carbon Observation (IGCO) Theme aims to develop a strategy for international global carbon observations. The IGCO report was approved by IGOS Partners in November 2003 and it is now in the implementation phase.

ISLSCP

International Satellite Land Surface Climatology Project (ISLSCP) was established in 1983 under the United Nation's Environmental Programme to promote the use of satellite data for the global land-surface data sets needed for climate studies.

ISLSCP Initiative I was a pilot project that collected global data at a 1 x 1 degree format for 1987-1988 (Sellers et al., 1995).The data was made available to the scientist

community through a CD-ROM published in 1995 and electronically via the NASA Goddard Space Flight Center (GSFC) Distributed Active Archive Center (DAAC). This dataset was aimed to support a range of uses such as weather forecast improvements, hydrological applications, macro-scale basin modeling, biogeochemical and carbon tracer models, global carbon flux model comparisons, general circulation models, model validation and comparison, algorithm development and education.

ISLSCP Initiative II was a second, more sophisticated collection of data including a 10-year core global data collection spanning the years 1987 to 1995 with improved spatial and temporal resolution (one-quarter to 1 degree).

2.5 Summary

LSPs require information on the temporal and spatial distribution of biophysical characteristics of ecosystems. Earth observation systems offer an unique source of such information providing remotely-sensed data at a wide range of scales and high frequency. To take advantage of all the benefits from these data it is fundamental to analyse how remote sensing can be combined effectively with models of ecosystem functioning. It is hence required to analyse the sensitivity of existing land-surface/climatic models to errors in satellite derived parameters and, based on this, define the priorities for satellite improvements.

Satellite missions aimed at monitoring the land surface have been reviewed as well as the advantages that they have brought to the research community. The design of future satellite missions should be tailored to meet the research community requirements. Three critical points must be considered in this: data information content, validation and continuity.

In terms of data information content, present tendency is towards multi or hyperspectral sensors. Recent technological advances have resulted in the development of smaller, more stable, better calibrated sensors which can measure higher spectral and spatial resolutions. In recent years, multiviewing sensor have proven to provide extra information about the canopy structure from which to extract biophysical parameters at an accuracy never available before. Nevertheless, there are serious gaps in planned missions for these type of sensors as there are no plans to provide continuity to present multiangular instruments (e.g. MISR instrument on Terra) and other candidate missions including mutiangular capabilities have not been selected for further development.

Validation is another critical point in the delivery of satellite data. Field data are only available sparsely. Collaboration between researchers in the field and those generating the products is needed to meet this challenge and presently several international groups are working to improve that collaboration.

Finally, the great advantage of satellite data is that they provide a long-term record of consistent measurements. This potential can only be achieved with the continuity of satellites to collect that data and store them in long-term datasets. To date, AVHRR, which was launched for meteorological applications and not for land cover applications, is the only source of continuous global data with a temporal coverage of more than a few years. Presently only NPP and NPOES are working to ensure the continuity of their datasets. Future sensors should ensure continuous long-term measurements and stability of the measurements to ensure the detection of trends but these requirements are usually threatened by changes in the programs and cuts in funding.

To cover these three fundamental points, the involvement of the scientific community should not cover only the initial consultation process but a continuous validation of procedures and algorithms, automatisation of methods for operational implementation and assured continuity of satellite data in the future.

Chapter 3

Estimation of parameters

This chapter reviews traditional and state-of-the-art approaches used in the estimation of biophysical parameters from remotely sensed data.

The first method presented is vegetation indices. Then physical based methods and their inversion are reviewed introducing the main radiation modelling approaches at the leaf, canopy and atmosphere levels.

Advantages and weaknesses of each of the methods are analysed. The aim is to present and discuss the available possibilities providing a background to the approach adopted in the next chapter.

3.1 Inference of biophysical parameters

To make use of radiative data collected by remote sensors, formal relations between the remotely sensed data and the variables of interest must be established. Two general types of approaches have been used to infer biophysical parameters (mainly LAI and fAPAR) from remote sensing data: empirical approaches and inversion of physical models (Asner, 1998).

Empirical approaches rely primarily on curve fitting or linear regression to correlate various measures of surface reflectance, including vegetation indices, to groundbased measurements. Empirical methods suffer from some limitations due to the lack of physics introduced in the retrieval technique and the small amount of radiometric information they can exploit, but have been widely used and have provided good estimations of several biophysical parameters from remote sensing data (e.g. Los et al., 1994, 2000).

Physical models attempt to model the relationship between canopy characteristics (leaf, canopy, and stand level biophysical characteristics such as LAI/fAPAR) and reflected radiation. Generally, these models are referred to as canopy reflectance models and are based on radiative transfer theory. These models also present some limitations such as the detail and/or fidelity with which the canopy can be represented and the computing time consumed.

3.2 Vegetation indexes

A vegetation index (VI) is a measurement computed from some spectral combination of remotely sensed data. It has been extensively demonstrated that canopy reflectance is strongly connected to canopy variables such as leaf area index (LAI) and leaf chlorophyll content through vegetation indexes (e.g. Verstraete and Pinty, 1996). Spectral channels are chosen in such a way that they reflect the contribution of vegetation depending on the spectral response of an area, minimising the contribution of other factors such as soil, lighting, atmosphere, etc. The red and near-infrared channels have been typically used because vegetation and soils display large differences in reflectance due to the strong chlorophyll absorption feature of green plants.

These approaches have applied various linear and nonlinear combinations of spectral bands, which maximize sensitivity of the index to LAI/fAPAR, while minimizing the sensitivity to unknown and undesired canopy characteristics (e.g., background reflectance).

The simple ratio (SR) index is one of the most commonly studied vegetation indices, and uses the NIR and VIS bands:

$$SR = NIR/VIS$$

Normalized difference vegetation index (NDVI) is one of the earliest indices that has been widely used. NDVI is based on the reflectance difference that green vegetation displays between the visible (VIS) and the near infrared (NIR) parts of the electromagnetic spectrum:

$$NDVI = (NIR - VIS)/(NIR + VIS)$$

The range of values obtained by the NDVI is between -1 and +1. Positive values correspond to vegetated zones while soil, clouds and snow present negative or close to 0 values.

NDVI and SR are most frequently used to derive LAI and fAPAR from space-borne

and airborne data (Chen and Cihlar, 1996). LAI is nonlinearly proportional to NDVI, while fAPAR is approximately linearly related to NDVI (Myneni et al., 1997b).

SR and NDVI are sensitive to both soil and atmospheric effects. Posterior indices have been based on the above described and aimed to reduce the effects of external factors (e.g. Huete, 1988; Verstraete and Pinty, 1996).

Most studies are based on vegetation indices related to canopy properties such as LAI, canopy cover, fAPAR and biomass computed from broadband spectral data (e.g. Los et al., 1994), although the advantage of hyperspectral data has been also recently shown (e.g. Gobron et al., 2000; Haboudane et al., 2002; Zarco-Tejada et al., 2004b). The estimation of biophysical parameters from vegetation index is specially hindered by the complexity of natural structures. Canopies with different LAI can have same vegetation index due to effects of clumping, cover type and BRDF differences. fAPAR relationship to vegetation indices is typically simpler, being linear with asymptote at LAI ~6, but this relationship is different for each cover type.

In general, no unique relationship between the parameter of interest and the vegetation index can be applied everywhere because the reflectances of plant canopies also depend on other factors, such as measurement geometry and spatial resolution. This makes the empirical relationships site- and sensor-specific and, therefore, unsuitable for application to large areas or in different seasons. In addition, soil background, as well as sun-view angular and atmospheric effects can have a big effect on the variation of vegetation indices for a same site at different dates (Asner et al., 1998; Verstraete et al., 1996).

Nevertheless, VI have been widely used, providing a valuable time series at the global scale (e.g. Los et al., 2000, 2005) as well as providing good monitoring tools at smaller scales (e.g. Haboudane et al., 2004; Zarco-Tejada et al., 2001, 2004b). Studies have shown that they can perform better than physical based approaches if the models do not approach the real scene at certain levels (North, 2002b). Hence VI are still essential tools in the analysis of not well known areas and especially at a global scale where a detailed modelling of the landscape would not be feasible.

Table 3.1 contains main vegetation indices currently used to estimate biochemical parameters (LAI, Chlorophyll and water content) with multispectral passive sensors.

Table 3.1: Vegetation indices for biochemical and LAI estimation calculated from multispectral and hyperspectral imagery (after Zarco-Tejada et al., 2005)

Structural, Chlorophyll and Water Indices

Normalized Difference Vegetation index (NDVI)	$NDVI = (R_{NIR} - R_{red})/(R_{NIR} + R_{red})$	Rouse et al., 1974
Modified Triangular Vegetation Index (MTVI1)	$MTVI1 = 1.2 \times [1.2 \times (R_{800} - R_{550}) - 2.5 \times (R_{670} - R_{550})]$	Haboudane et al., 2004
Modified Triangular Vegetation Index (MTVI2)	$MTVI2 = \frac{1.5 \times [1.2 \times (R_{800} - R_{550}) - 2.5 \times (R_{670} - R_{550})]}{\sqrt{(2 \times R_{800} + 1)^2 - (6 \times R_{800} - 5 \times \sqrt{R_{670}}) - 0.5}}$	Haboudane et al., 2004
Renormalized Difference Vegetation index (RDVI)	$RDVI = (R_{800} - R_{670})/\sqrt{(R_{800} + R_{670})}$	Roughgarden and Breon, 1995
Simple Ratio Index (SR)	$SR = R_{NIR}/R_{red}$	Jordan, 1969; Rouse et al., 1974
Modified Simple Ratio (MSR)	$MSR = \frac{R_{NIR}/R_{red} - 1}{(R_{NIR}/R_{red})^{0.5} + 1}$	Chen, 1996
Modified Chlorophyll Absorption in Reflectance Index (MCARI1)	$MACARI1 = 1.2 \times [2.5 \times (R_{800} - R_{670}) - 1.3 \times (R_{800} - R_{550})]$	Haboudane et al., 2004
Modified Chlorophyll Absorption in Reflectance Index (MCARI2)	$MACARI2 = \frac{1.5 \times [2.5 \times (R_{800} - R_{670}) - 1.3 \times (R_{800} - R_{550})]}{\sqrt{(2 \times R_{800} + 1)^2 - (6 \times R_{800} - 5 \times \sqrt{R_{680}}) - 0.5}}$	Haboudane et al., 2004
Soli-Adjusted Vegetation Index (SAVI)	$SAVI = [(R_{800} - R_{670})/(R_{800} - R_{670} + L)] \times (1 + L)\ [L \in (0, 1)]$	Huete, 1988; Qi et al., 1994
Improved SAVI with self-adjustment factor L (MSAVI)	$MSAVI = \frac{1}{2}[2 \times R_{800} + 1 - \sqrt{(2 \times R_{800} + 1)^2 - 8 \times (R_{800} - R_{670})}]$	Qi et al., 1994
Optimized Soli-Adjusted Vegetation Index (OSAVI)	$OSAVI = (1 + 0.16) \times (R_{800} - R_{670})/(R_{800} - R_{670} + 0.16)]$	Rondeaux et al., 1996
Modified Chlorophyll Absorption in Reflectance Index (MCARI)	$MCARI = [(R_{700} - R_{670}) - 0.2 \times (R_{700} - R_{550})] \times (R_{700}/R_{670})$	Daughtry et al., 2000
Transformed CARI (TCARI)	$TCARI = 3 \times [(R_{700} - R_{670}) - 0.2 \times (R_{700} - R_{550}) \times (R_{700}/R_{670})]$	Haboudane et al., 2002
Triangular Vegetation Index (TVI)	$TVI = 0.5 \times [120 \times (R_{750} - R_{550}) - 200 \times (R_{670} - R_{550})]$	Broge and Leblanc, 2000
Zarco-Tejada & Miller (ZTM)	$ZTM = R_{750}/R_{710})$	Zarco-Tejada et al., 2001
Normalized Difference Water Index (NDWI)	$NDWI = (R_{860} - R_{1240})/(R_{860} + R_{1240})$	Gao, 1996

3.3 Radiation modelling

Radiative data collected by remote sensors are not only controlled by the variables of interest but also by the state variables of the radiation transfer problem (Verstraete et al., 1996). Radiation transfer (RT) models provide the physical representation of this radiation transfer regime allowing to link the digital output to the desired physical quantity to meaningfully interpret remote sensing data. The approach is to simulate the satellite data and use the simulation to match observations. Used in this way, RT constitute an essential tool for the quantitative interpretation of remotely sensed data (Pinty et al., 2001).

Atmospheric radiative transfer codes are used to simulate the effect of the atmosphere on the measurement - absorption, scattering, adjacency, directional effects, etc... This permits us to detect if changes in the measurements are due to natural changes or to changes in the observation conditions. Once atmospherically corrected, the image must be interpreted as a function of the biophysical parameters involved in order to relate measurements and parameters.

Canopy radiative transfer models simulate the bidirectional reflectance distribution function (BRDF) of vegetation covers with differing leaf, soil and canopy characteristics. To account for different biochemical composition of the leaves- such as water and chlorophyll content - leaf reflectance models can be coupled to canopy reflectance models (e.g. Jacquemoud, 1993; Demarez and Gastellu-Etchegorry, 2000; Bacour et al., 2002; Combal et al., 2002a). Both types of models are introduced here.

3.3.1 Leaf Reflectance Models

These models simulate leaf reflectance, absorption and transmittance. The simplest ones consider the leaf as a single scattering and absorbing layer while the most complicated ones describe all the cells in detail (shape, size, position, and biochemical content).

Jacquemoud and Ustin, 2001 categorize computer-based leaf models into four classes, ordered in increasing complexity: plate models, N-flux models, stochastic and other radiative transfer models and ray tracing models. Amongst these, only radiative transfer models can be inverted by iterative methods.

Plate models represent the leaf as one or several absorbing plates. The index of refraction and the absorption coefficient of these plates defines the absorption and reflectance of the incident radiation. One example of plate model is PROSPECT (Jacquemoud and

Baret, 1990). PROSPECT is a leaf optical model that estimates leaf-level reflectance and transmittance from 400 nm to 2500 nm. Each leaf is considered as a stack of N absorbing plates with rough surfaces giving rise to scattering of light. These layers are separated by N-1 air spaces and are defined by their refractive index and absorption coefficient. The number of layers represents the scattering within the leaf. Absorption is calculated as the linear summation of the concentrations of the biochemicals (chlorophyll, water, dry water etc.) and the corresponding specific absorption coefficients. PROSPECT requires only three input parameters, the structure parameter N, the chlorophyll and water contents.

N-flux models consider the leaf as a block of diffusing and absorbing material. These models derive from the Kubelka-Munk theory of reflectance (Kubelka and Munk, 1931). Material diffusion and absorption is described by the correspondent coefficients and the final result is function of those and of the incident radiation.

Other models, such as the stochastic and ray tracing model require a detailed description of the internal leaf structure and the optical constants of leaf material. For example, LIBERTY (Leaf Incorporating Biochemistry Exhibiting Reflectance and Transmittance Yields, Dawson et al., 1998) approximates the cellular structure of leaves by spherical cells. The absorption is calculated as the linear summation of the individual absorptions of chlorophyll, water, cellulose, lignin and protein according to their content per unit of leaf area. LIBERTY was the first model specially designed to simulate the spectral response of both dried and fresh stacked pine needles.

3.3.2 Canopy reflectance models

Canopy reflectance models simulate the bidirectional reflectance distribution function (BRDF) of vegetation canopies. BRDF describes the radiation leaving the surface in a direction as a function of the characteristics of the incident radiation and of the surface itself. Surface reflectance is a function of the size, shape and distribution of objects on the surface and of the direction from which the surface is illuminated and viewed. In the specific case of vegetation canopies, this reflectance depends on the leaf optical properties, soil surface attributes, illumination conditions and viewing geometry (Jacquemoud et al., 1992; Myneni et al., 1995; Goel and Thompson, 2000).

Vegetation components such as leaves and stems are radiometrically characterised by their reflectance and transmittance. The reflectance of the canopy depends on the aggregation of individual scattering objects, described by structural properties such as the area density, angular and spatial distribution.

BRDF can be used to interpret remotely sensed observations and, if the model can be inverted (analytically or numerically), it can be used to estimate parameters from remotely sensed data.

Canopy reflectance models have followed empirical and physical approaches. Empirical models attempt to describe surface scattering by fitting some function to observed reflectance data (e.g. Walthall et al., 1985). The lack of physical meaning in the model parameters make them inadequate for use in the retrieval of biophysical parameters, although they are useful for correction and/or normalisation of directional effects in multiangular reflectance data (Roujean et al., 1992). Physical models are based on physical processes so their parameters are meaningful and their inversion can be used in the estimation of parameters. Three approaches have been followed in this type of models: turbid medium methods, geometric methods and scene simulation methods (Disney et al., 2000). The three approaches are based in the simulation or approximation of photon interaction with vegetation.

Turbid medium models

In the turbid medium approach, the canopy is approximated as one or more infinite layers forming a plane-parallel homogeneous scattering medium. These layers consist of randomly oriented infinitesimal scattering elements. The calculation of the radiation through the canopy is calculated by radiative transfer theory or Kubelka-Munk theory (Kubelka and Munk, 1931).

The location of any particular vegetation element is not specified and the canopy structure is described by statistical distributions. A major drawback of this method is that it does not consider the size of the scatterers within the canopy. A consequence of this is that mutual shadowing is not considered (Qin and Liang, 2000). Moreover, certain properties of the canopy reflected radiation are directly controlled by the size and orientation of the scattering objects, particularly the hot spot (the scattering in the solar direction and around it). A widely used model in this category is the SAIL model (Verhoef, 1984).

Turbid medium approximation is appropriate in dense canopy simulations with small vegetation but they fail to represent BRDF of forest canopies where canopies present a structured distribution.

Geometric methods

In these models the canopy is assumed to consist of geometrical objects of given shape and dimensions (spheroids, cones, cylinders etc.) and optical properties (reflectance, transmittance and absorptance) arranged on a surface. The geometry of the scene is calculated according to the size and density distribution of objects. The resulting areal proportions of sunlit and shadowed canopy and soil components are calculated under the assumption of parallel-ray geometry. The average reflectance of each scene pixel is calculated as a linear sum of the various areal proportions. Examples of these type of models are the works of Li and Strahler, 1992 and Chen and Leblanc, 1997.

A major drawback of these models is the assumption that all trees are of the same geometrical shape, as they cannot be used in mixed pixel analysis where different trees are present (Goel and Thompson, 2000). Also, they are difficult to relate to leaf spectra, diffuse light conditions and multiple scattering within crowns.

Scene simulation methods

Scene simulation models are computer models that simulate realistic 3D scenes and photon interactions. The major advantage of this explicit representation is that every object within a canopy can be represented to whatever level of detail is required. These models are usually coupled with leaf models to estimate biophysical parameters through model inversion (e.g. Dawson et al., 1999; Haboudane et al., 2004)

There are two methods for implementing scene simulation models, ray tracing and radiosity.

Ray tracing methods: Ray tracing methods are based on a sampling of photon trajectories within the scene. Rays (photons) are traced and their intersections calculated into a 3D scene. The application of an effective sampling scheme is fundamental and the Monte Carlo method offers a robust and simple solution to this problem (Disney et al., 2000). Realistic simulation of the bidirectional reflectance of any scene (represented as a collection of 3D objects) can be simulated by repeating the sampling process for every sample (pixel) in the viewing plane.

Ray tracing is computationally expensive compared with the methods above described. Each interaction between rays and canopy elements must be simulated. Rays interact (bounce) within the canopy until they either escape from the top of the canopy or the energy level associated with them reaches a minimum which has to be specified. Also a maximum number of scattering can be defined to reduce this calculation. In this context two main ray tracing schemes exist, a forward and a reverse mode. In the

forward mode the rays are traced from the light source and followed through all their interactions with the canopy until they reach the sensor position. This implies that a large number of photons will be scattered in other directions and will not be detected by the sensor. Conversely, the reverse mode trace the rays from the sensor to the illumination hemisphere which is a more computationally efficient. Examples of these models are Botanical Plant Modelling System (BPMS) (Lewis, 1999) and FLIGHT (North, 1996).

Radiosity methods: Radiosity models account for all energy emitted or reflected by every surface in a scene.The rate at which energy leaves a surface (the radiosity) is calculated as the sum of the rates at which the surface emits energy and reflects or transmits it from other surfaces. All light interactions in the scene must be calculated, independent of view, which makes these methods even more computationally expensive than ray tracing.

Hybrid models

Some approaches lie between the above exposed as for example hybrid models of turbid medium and geometric method that represent geometric objects with a turbid media of vegetation elements randomly distributed such as GeoSail (Huemmrich, 2001). Hybrid geometric optical-radiative transfer approaches have been applied for modelling albedo and directional reflectance of discontinuous canopies (e.g. FLIM Rosema et al., 1992; GORT Li et al., 1995; Ni et al., 1999). Also hybrid models of radiosity and ray tracing methods have been developed such as SPRINT (Spreading of Photons for Radiation INTerception) model (Goel and Thompson, 2000) and DART (Discrete Anisotropic Radiative Transfer) (Gastellu-Etchegorry et al., 1996).

3.3.3 Atmospheric Radiative Transfer Models

The atmosphere affects the propagation of electromagnetic radiation in its way from the Sun to the land surface and from the land surface to the satellite. These absorption and scattering effects of the atmospheric molecules and aerosols must be considered when analysing satellite data.

Radiative transfer theory describes the interaction of radiation with a scattering and absorbing media. Solution methods for radiative transfer problems have been extensively studied during the last century and among the solution methods in use today for atmospheric RT models are Discrete Ordinate methods (e.g. MODTRAN 4, Acharya et al.,

Figure 3.1:

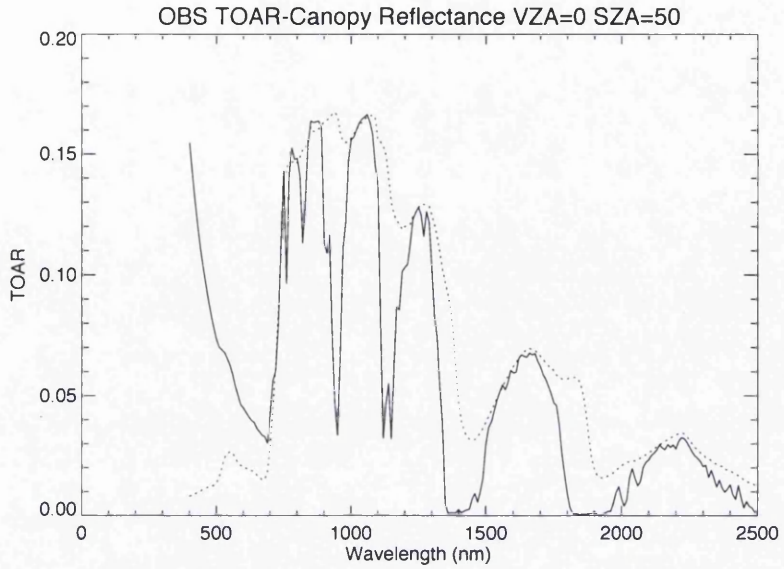

Figure 3.2: Spectrum of a boreal forest showing top of canopy reflectance (dotted line) and top of the atmosphere reflectance (continuous line).

1999) and the method of Successive Orders of Scattering (e.g. Second Simulation of Satellite Signal in Solar Spectrum, 6S, Vermote et al., 1997).

Atmospheric RT models calculate the transmission and emission of the atmosphere by using detailed scattering models including gas and aerosols. Some models calculate the atmospheric effect at wavelengths from the optical to the sub-millimetre (e.g. MODTRAN). Typically standard atmospheric models, based on common geographic locations, are used and there is the possibility of a user-defined atmospheric profile with any specified set of parameters. The reduction of sunlight intensity is called extinction and is represented through an extinction coefficient. The optical thickness (τ) is the characteristic atmospheric parameter that indicates the magnitude of absorption and scattering of the sunlight; τ corresponds to the integrated value of the extinction coefficient at each altitude by the atmospheric thickness.

Figure 3.2 shows the effect of the atmosphere on a canopy reflectance showing the reflectance at the top of the canopy and the reflectance at the top of the atmosphere for a clear atmosphere situation (aerosol optical thickness of 0.05).

A variety of radiative transfer models exist for simulation of radiances measured by satellite sensors. The most widely used in remote sensing applications are LOWTRAN (Kneizys et al., 1988), MODTRAN (Acharya et al., 1999), and 6S (Vermote et al., 1997). These models are well documented, reliable, and available to the scientific community. They are all medium or high spectral resolution band models and incor-

porate thorough treatments of gas absorption. LOWTRAN/MODTRAN include cloud models and are specially useful in the simulation of atmospheric effects in the whole electromagnetic spectrum. The 6S model does not include clouds and only covers the shortwave but is very flexible for clear sky satellite simulations.

3.3.4 Model inversion

The previous section discussed that radiative transfer models can simulate canopy reflectance as a function of canopy variables for any observational configuration. It has been extensively demonstrated that canopy reflectance is strongly connected to canopy variables such as leaf area index (LAI) and leaf chlorophyll content through vegetation indexes (e.g. Verstraete and Pinty, 1996). When used in the direct mode, these physical models determine the BRDF, or reflectance, as a function of the acquisition configuration and the soil and canopy structure and characteristics. The inverse problem involves determining certain variables, knowing the acquisition configuration and the BRDF measurements. Model inversion offers many advantages over the empirical techniques as it relies on fewer hypotheses and is based on fundamental physical theories.

The inversion can be performed by analytical methods if the model is linear. In this case the model or equation is rearranged to find the desired parameters. The searched variables are free parameters, or variables, and other parameters can be fixed to known values. Numerical methods allow the inversion of non-linear models. The general technique is the repeated run of the model to be inverted searching for the set of parameters that minimises the difference between the simulated and the observed reflectance. These iterative minimisation algorithms are typically based on a cost function.

These techniques present two problems: typically the problem is ill posed and so a single solution does not exist, and they are computationally too expensive to be used on an operational basis.

The inverse problem can be solved properly only if it is well posed. A problem is well posed if and only if its solution exists, is unique, and depends continuously on the data and the problem is ill posed if at least one of these statements does not hold. In remote sensing the inverse problem is by nature ill-posed for two reasons: the solution of the inverse problem is not necessarily unique, but a set of solutions could lead to similar match between the measured and the simulated reflectance values, and the measurement and model uncertainties may induce large variation in the solution of the inverse problem.

Combal et al., 2002b propose the use of prior information to solve the ill-posed problem and distinguish three different sources of prior information for remote sensing: (1) ancillary data measured on site or products provided by another sensor, (2) knowledge of the type of canopy architecture that defines the class of radiative transfer model to be used (turbid medium, geometric, or hybrid) and (3) knowledge of typical distribution of canopy biophysical variables used as input in radiative transfer models.

Significant efforts have been made to provide operational algorithms that allow us to apply numerical inversion. This is critical to be able to deal with the large datasets retrieved by remote sensing. Look up tables and neuronal networks are computationally efficient methods that allow us to do this inversion on a per pixel basis (Kimes et al., 2000) and hence to take full advantage of directional/spectral data from modern sensors (e.g., MODIS, MISR, POLDER, SeaWiFS).

Artificial neural networks (e.g. Weiss et al., 2002) are black boxes that learn adaptively from examples to approximate the input-output relationship of a model. Basically they map the function between the BRDF and the correspondent structural and optical parameters. A wide array of simulations must be created beforehand. These simulations are used to create training data for the ANN which consist in pairs of data containing the spectral reflectance and the true outputs (vegetation parameters). When there is a strong mathematical relationship between the inputs and the outputs of this training dataset, the ANN approximates it but the relationship is weak the results will be poor. A disadvantage of this approach is the lack of flexibility to work with variable directional/spectral data as the network should be trained again for each sampling case.

Look-up-tables (LUT)

A LUT is the most simple method to invert models. The principle of a LUT consists of generating a table of canopy variables by sampling the space of canopy realisation. Then a radiative transfer model is used to generate the corresponding table of reflectance values. Simulation are made for specific configurations representing the conditions of observations, i.e. wavelengths, view, and illumination geometry. To sample the variables, n values of each variable must be drawn with a distribution function specific to each variable. The space of model input variables must be sampled by drawing values within particular distribution functions. The modeled leaf, soil, and canopy properties leading to the successful minimization of the merit function are the retrieved parameters.

One advantage of LUT algorithms is that it uses a global search and thus is not sensitive to a local minimum. Moreover, the search is performed on pre-computed data, and it

can easily be parallelised.

LUT technique is used in this study as it permits a quick inversion of the models, as the calculations are done only once, and provides the flexibility required to test the different instrument configurations in terms of spectral and angular sampling. Several studies have demonstrated the potentials of using LUT to solve the inversion problem in remote sensing in the retrieval of vegetation parameters (e.g. Demarez and Gastellu-Etchegorry, 2000; Weiss et al., 2000; Combal et al., 2002b,a; Gascon et al., 2004)

Several considerations must be analysed when designing a LUT such as the dimension, the size (defined by number of samples) and the retrieval technique.

There is always a trade off between the size of the LUT and the accuracy of the retrieved parameters. Increasing the LUT size results in a better sampling but it will also require larger computer resources. A preliminary analysis is hence required to investigate the effect of the size of the LUT on the retrieval of canopy biophysical variables.

When searching the LUT it must be defined the number of possible solutions and the criteria of search.

The retrieval procedure typically considers that the target vegetation parameters have been found when the radiation values in the LUT agree with the measured radiation values within a prescribed accuracy. Several error functions have been proposed to calculate this:

Absolute error (Gascon et al., 2004):

$$\varepsilon^2 = \sum_{i=1}^{n} (\rho_i - \rho_{sim,i})^2 \tag{3.1}$$

Relative error (Gascon et al., 2004):

$$\varepsilon^2 = \sum_{i=1}^{n} \left(\frac{\rho_i - \rho_{sim,i}}{\rho_i}\right)^2 \tag{3.2}$$

Relative error with threshold (Gascon et al., 2004):

$$\varepsilon^2 = \sum_{i=1}^{n} \left(\frac{\rho_i - \rho_{sim,i}}{k_i}\right)^2 \tag{3.3}$$

Root Mean Square Error (Combal et al., 2002b):

$$RMSE = \sqrt{\frac{1}{n}\sum_{i=1}^{n} (R_i - R_{sim,i})^2} \tag{3.4}$$

where n is the number of measurements available; k_i is a predefined minimum ρ_i used to reduce the weight of reflectance values close to 0 in the cost function.

The cost functions are typically used to filter a preliminary set of candidates (Knyazikhin et al., 1998b; Weiss and Baret, 1999; Combal et al., 2002b). The final solution can be extracted from the candidates by taken a mean value (e.g. Weiss et al., 2000; Combal et al., 2002b), or interpolating among the retrieved values (e.g. Knyazikhin et al., 1998b). The maximum number of candidates accepted can be fixed beforehand (e.g. 10 in Combal et al., 2002b) or limited by the prior information used in the creation of the LUT (e.g. biome in Knyazikhin et al., 1998b).

The retrieval will be more accurate when the measurements provide more information about the target parameters so it is expected that multiple views, providing structural information, and multiple bands will improve it. It would be appropriate to give more weight to the most informative measurements (bands or viewing angles)(Verstraete et al., 1996; Privette et al., 1996a)

Hybrid solutions of indices and LUT have been proposed for the inversion. In these methods the inversion through a LUT is used in a first stage. If a solution within an acceptable tolerance value is not achieved, a solution based in vegetation indices is then applied. This is the method used in MODIS and MISR LAI/fAPAR algorithms (Knyazikhin et al., 1998b). These algorithm defines 6 cover types or biomes based on radiative transfer considerations: grasses & cereals, shrubs, broad leaf crops, savanna, broad leaf forest and needle forest. The method uses different relationships between the parameters and vegetation indices and make some assumptions within cover types (e.g., erectophile LAD for grasses/cereals or layered canopy for savanna). 1-D and 3D numerical radiative transfer models are used to forward-model for range of LAI resulting in look-up-table (LUT) of reflectances as function of both viewing and illumination angles and wavelength. The retrieval method aims to minimise RMSE as function of LAI between observations and appropriate models; if RMSE is small enough, fAPAR / LAI are retrieved from the table, if RMSE is high an empirical backup algorithm based on the NDVI is used.

3.4 Summary

Vegetation indices have been traditionally used to retrieve biophysical parameters from remote sensing data. These techniques do not have a physical basis and do not take full advantage of the multi spectral and multi angular data that the new generation of satellites provide. Nevertheless, they provide a valuable record for global scale time

series as well as efficient monitoring tools at regional scales. VIs also provide a unique medium for monitoring change at the global scale, and over poorly known areas where detailed modelling is not possible of feasible.

Techniques to estimate parameters from remote sensing are moving forwards to methods based on the physical properties of the observed targets. Canopy radiative transfer models and leaf reflectance models allow us to link the satellite data with the physical properties of the land surface. The inversion of these models is computationally expensive and presently great effort is being directed towards the development of operational inversion techniques that can be used on a per pixel bases. Nowadays, LUT and ANN constitute the most promising techniques and are being incorporated in the satellite products algorithms.

Chapter 4

Datasets and Methods

This chapter introduces the approach proposed to achieve the aim of this thesis: to link ecological models and satellite capabilities. The method here described is based in the creation of a sensor model that permits us to simulate satellite retrievals under different conditions and for different instrument capabilities. The next step in the study will be the definition and application of a retrieval technique to derive biophysical parameters from the simulated data. The retrieval technique will be explained in Chapter 6 where it is applied in an end-to-end study.

The strategy used to create the sensor model and the input parameters required at each stage of the analysis are depicted in this chapter. The study areas and datasets used are firstly presented. Then the methodology proposed is explained together with the models used. Two studies are included as a sensitivity analysis of the models. A comparative study between two leaf reflectance models is performed to justify the use of one of them. Also a study of the canopy model chosen is developed in order to check its capability to simulate BRDF in sparse vegetation landscapes.

The biophysical parameters analysed are reviewed outlining the considerations and/or assumptions made on any of them.

The final section comprises a compilation of meteorological and site specific parameterisations taken from different sources that will be used to run the LSPs.

4.1 Study Areas

The boreal forest is used as test site in this study because it is an important biome in terms of the carbon budget, albedo feedbacks and sensitivity to climate change. In addition, structural complexity provides a good test for the methodology. It represents

the most complex case of canopy modelling and inversion presenting several levels of clumping (shoots and branches) and crown mutual shadowing. Also, in this biome the ecological models are sensitive to vegetation parameters enabling a robust test of their uncertainty.

The required data were obtained from the BOREAS fieldcampaign.

4.1.1 BOREAS

The Boreal Ecosystem Atmospheric Study (BOREAS) was an international project developed in the northern boreal forests of Canada between 1993 and 1996 to understand the interactions of the boreal forest biome with the atmosphere (Sellers et al., 1997b; Gamon et al., 2004).

The main scientific goals on this project were to improve our understanding of the processes which govern the exchanges of energy, water, heat, carbon, and trace gases, and to develop and validate remote sensing algorithms for estimating parameters required to understand these processes at different scales.

The boreal forest is one of the Earth's largest ecosystems including coniferous and deciduous trees, upland forests, wetlands, lakes, many species of plants and animals. The general composition of boreal forests includes pure stands of deciduous broadleaved and conifer forests, mixed conifer/deciduous forests, pine/lichen and spruce/moss stands. The dominant genera include poplar (Populus), birch (Betula), willow (Salix), alder (Alnus), spruce (Picea), larch (Larix), pine (Pinus), fir (Abies) and hemlock (Tsuga) (Baldocchi et al., 2000).

In northerly latitudes of the boreal zone days are short (less than 8 h) during the winter and long (greater than 18 h) during the summer. Low solar elevation angles, relative to the tropical and temperate zones, cause midday values of incident energy to peak below 1000 Wm^{-2}during the summer growing season. Much of the boreal zone is south of the Arctic Circle (66N) so some sunlight is available to most boreal forest stands during the winter. At Prince Albert, Saskatchewan (53N), for example, the potential magnitude of mid-day solar radiation is on the order of 300 Wm^{-2} (Baldocchi et al., 2000).

Two study sites were chosen for the BOREAS experiment, The Southern Study Area (SSA) and The Northern Study Area (NSA), because they represent typical conditions of the northern and southern extremes of the boreal forest.

The Southern Study Area (SSA)

The Southern Study Area (SSA) is near Candle Lake, Saskatchewan and covers an area about 130 km wide by 90 km. This area was chosen for its sensitivity to moisture (Sellers et al., 1997b). The SSA is near the southern limit of the boreal forest and the transition to natural prairie grasslands and agricultural fields. The age of Forest stands in this region range between 50 and 100 years. Tree heights in mature stands range from 15 to 22 m, although there are stunted black spruce in bog areas. The vegetation cover is predominantly coniferous and classified as mixed boreal forest. In well drained and/or sandy soil the predominant species is jack pine (Pinus banksiana). Well drained glacial deposits present a mixture stands of trembling aspen (Populus tremuloides), balsam poplar (Populus balsamifera), and white spruce (Picea glauca). Finally, poorly drained sites support black spruce (Picea mariana) that are often covered with thick layers of sphagnum and feather moss.

The SSA has a mid-continental climate with average annual precipitation between 410 and 500 mm. Temperatures range from about 7°C to 24°C in the summer and from about -21°C to -4 °C in winter.

The Northern Study Area (NSA)

The Northern Study Area (NSA) is near Thompson, Manitoba and covers an area about 100 km wide by 80 km. Temperature is the major controlling factor in this area. The vegetation consists predominantly of black spruce, in stands of varying density, and some jack pine stands in the south and west portions of the region. Forest stands are generally mature, some being over 100 years old. Tree heights range up to 15 meters.

The NSA has a mid-continental climate. The average annual precipitation is between 410 and 500 mm. Temperatures range from about 5°C to 21°C in the summer and from about -26°C to -8 °C in the winter.

4.1.1.1 Field Campaigns

Three intensive field campaigns were held in 1994. BOREAS investigators got funding to return to the field for four campaigns in 1996 but the present study will use only data from the 1994 campaigns:

- IFC-1 : First Intensive Field Campaign: 24 May through 16 June 1994

- IFC-2 : Second Intensive Field Campaign: 19 July 1994 through 10 August 1994

- IFC-3 : Third Intensive Field Campaign: 30 August through 19 September 1994

The three summer campaigns aimed to characterize the development and functioning of the soil-vegetation-atmosphere system (radiation, energy, and gas exchange) during green-up (June), peak green (July-August), and beginning senescence (September). Whenever it has been possible, data from these dates has been used.

4.1.1.2 Data used

This study focuses on the SSA and analyses data collected during the 1994 fieldcampaign. Three coniferous sites are analysed, each characterised by a dominant species: Old Black Spruce *(Picea Mariana)*, Old Jack Pine *(Pinus Banksiana)* and Young Jack Pine *(Pinus Banksiana)*. The sites are referred as: OBS (Old Black Spruce), OJP (Old Jack Pine) and YJP (Young Jack Pine). Table 4.1 shows the location and main characteristics of each of the study sites.

Table 4.1: BOREAS Sites studied(Gower et al., 1997)

	OBS	OJP	YJP
Latitude	53.987 N	53.916 N	53.877 N
Longitude	105.122 W	104.692 W	104.647 W
Soil Type	Sandy loam/loam	Gray wooded to degraded black	Gray wooded to degraded black
Dominant species	Black spruce (Picea mariana)	Jack pine (Pinus banksiana)	Jack pine (Pinus banksiana)
Age years	115	65	25

Permafrost does not occur in the top 2 m of soil in any of the sites. The young (25-27 years) and old (60-65 years) jack pine stands are even-aged and were originated from wildfires and the soil is an excessively drained coarse sand. The black spruce stands occur in a 20-30 cm deep peat layer over a coarse-textured mineral soil.

Boreal forest presents special challenges with respect to understory effects on the above-canopy reflectance. The understory of these forests is usually composed of mixtures of lichens, moses and short herb species that are difficult to spectrally differentiate from the overstory. Miller et al., 1997 suggest that a seasonally independent understory reflectance can be used with small errors at the jack pine sites. OBS under-

story spectra shows large seasonal variations in the visible and near-infra red regions, this is probably due to the moss species dominance.

1994 was not a normal year in terms of meteorology in the BOREAS region. This year presented the longest frost-free period recorded at Prince Albert National Park (SSA); the frost-free period was of 150 days, notably longer than the previous record of 125 frost-free days in 1988. Also in this year the NSA experienced one of the driest years on record.

All data used in this study was downloaded from the BOREAS project website (http://www-eosdis.ornl.gov/BOREAS/bhs/BOREAS_Home.html). Data from four science groups are used: Airborne Fluxes and Meteorology (AFM) , Hydrology (HYD), Remote Sensing Science (RSS) and Terrestrial Ecology (TE). References are given at each parameter about its source.

4.2 Methods

It has been established in Chapter 2 that a method to link user requirements and satellite capabilities is required in order to better define future instruments. RT models provide satellite simulations under specific conditions that can be used to simulate the retrieval of biophysical parameters. Under these conditions we have complete control of the system allowing us to simulate any satellite instrument in terms of spectral bands, viewing angles and radiometric accuracy.

If a set of instrument configurations are simulated, estimated biophysical parameters with different levels of uncertainty can be retrieved. These biophysical parameters can then be used as inputs into LSPs. Running the LSPs with the real input parameters and then with the parameters retrieved from the satellite and comparing both results will permit to relate errors in the estimations of these models to the satellite configurations considered.

Two elements are required to implement this approach: a sensor model and a method to estimate biophysical parameters from the simulated data. This chapter introduces the sensor model while the estimation method will be described and applied in Chapter 6.

The method consists in the definition of a set of satellite configurations ($Configuration[i]$) each of which will provide a set of estimated biophysical parameters ($Parameters[i]$). These biophysical parameters will then be used to run the LSPs providing estimations ($LSPsEstimations[i]$). The sequence is hence:

$$Configuration[i] \Longrightarrow Parameters[i] \Longrightarrow LSPsEstimations[i]$$

so that we can establish a relationship between:

$$Configuration[i] \Leftrightarrow LSPsEstimations[i]$$

The next sections will discuss the technique chosen to simulate the instrument configuration as well as the coupling of the models involved.

4.2.1 Simulating satellite data

When simulating satellite data both surface and atmospheric effects on the radiation must be considered.

Canopy reflectance models can be used to simulate the reflected signal from the surface. Scene simulation methods can provide an explicit three dimensional representation of every object within the scene and leaf reflectance models allow the simulation of reflectance and transmittance of leaves with different biochemical properties (e.g. chlorophyll or water content). Hence, the coupling of leaf reflectance model with a canopy reflectance model allows us to simulate canopy reflectance for the whole range of possible parameters.

The atmosphere also affects the signal received by the sensor by absorbing or scattering the radiation. Atmospheric radiative transfer models simulate these effects using the ground reflectance as input and providing a Top of the Atmosphere Reflectance (TOAR) as the satellite would see it. These models must be parameterized with specific atmospheric data for the site.

In this study a leaf model is coupled with a hybrid geometric/radiative transfer bidirectional reflectance distribution function model and with an atmospheric radiative transfer model, 6S. The scheme in Figure 4.1 represents the coupling of these three models to simulate TOAR from specific site parameters.

4.2.1.1 Exploring satellite capabilities

The images created with the coupled models allow us to explore the angular and spectral capabilities of satellites in the retrieval of surface and atmospheric parameters.

The spectral analysis will focus on a few spectral bands. Studies have shown that hyperspectral instruments with hundreds of bands contain redundant information and

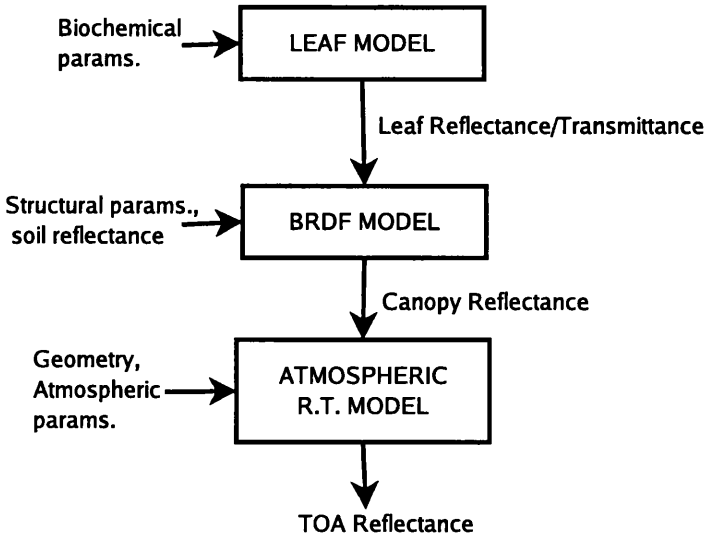

Figure 4.1: Models Coupled to simulate top of the atmosphere reflectance

typically a subset of these bands can be used to get at least 90% of the information (Thenkabail et al., 2004), in fact only a limited number of wavebands are required for canopy biophysical variable estimation (Weiss et al., 2000). The spectral bands to use in this study will be chosen from those that have proven to be useful in the retrieval of the variables analysed. This will be analysed by reviewing present satellite channels and wavelengths used in vegetation indices.

The benefits of multiangular remote sensing are also analysed by simulating the observed spectral reflectance values under different viewing geometries (Barnsley et al., 1997; Diner et al., 1999). Two advantages are expected from this: first, it offers the potential to retrieve information on atmospheric constituents due to the effect of the different atmospheric path lengths on the reflectance (North et al., 1999; North, 2002b,a; Grey et al., 2006); second, it should improve the retrieval of land-surface properties by accessing the structural information inherent in the BRDF (Barnsley et al., 1997; Chen et al., 2003; Diner et al., 2005). The number and value of viewing angles to use will be taken from a review of present instruments.

The effect of the radiometric accuracy of the sensor on the measurement of surface-leaving radiances will be considered through the addition of different levels of noise. In remote sensing, noise is produced by a number of factors, including thermal effects, sensor saturation, quantization errors and transmission errors. These types of noise are typically independent of the data and can be simulated by distorting the samples with different levels noise.

4.2.1.2 Retrieving biophysical parameters

The study focuses on key indicators of climate change that can potentially be estimated by hyperspectral remote sensing. Three key biophysical variables, leaf area index (LAI), the chlorophyll a+b content (Cab) and the fractional cover (FC) are considered in addition to one atmospheric parameter, aerosol optical thickness (τ). These parameters are used as inputs in the models and take values in site specific ranges. The TOAR resultant of these simulations will provide satellite data for the sensitivity analysis and the estimation of parameters from the instrument configurations considered.

The inversion of the models will provide estimations of the analysed parameters for each sample. These estimations will be used to drive the LSPs and estimate NPP. Inputs to the LSPs are daily climate data and key climate, vegetation, and site conditions. LAI will be used to drive the models and analyse the effects of the different levels of noise.

4.3 Models

This section presents the models chosen for each stage of the TOAR modelling. The main alternatives available are analysed and chosen models are selected in the basis of its suitability to represent the specific structural and biophysical characteristics of the sites considered.

4.3.1 Leaf reflectance models

There is some debate about the use of PROSPECT with coniferous leaves. For example, the developer of the model discusses another model (LIBERTY, Dawson et al., 1998) to needle simulation in his review Jacquemoud and Ustin, 2001. Some studies have shown that both models, LIBERTY and PROSPECT, are capable of accurately inverting simulated reflectances in the visible spectrum (Moorthy et al., 2003; Zarco-Tejada et al., 2004a). A small comparison between both models and field measurements for the three BOREAS sites studied was developed in order to decide which one to use.

Both models predict the reflectance and transmittance spectra of leaves in the visible and near infrared wavelengths (400 - 2500 nm) at 5 nm step.

In PROSPECT (Version 3.01, 5 May 1998) the leaf is considered as N layers, in which specific absorption coefficients and refractive index are known. PROSPECT requires four input parameters:

- Leaf structure parameter N: this parameter typically ranges between 1 and 2.5. The main effects of the leaf structure are found in the near infrared plateau.

- Chlorophylls a+b concentration (Cab in $\mu g/cm^2$): that affects the reflectance and transmittance in the visible (400-700 nm).

- Equivalent water thickness (Cw in cm or g/cm^2): this parameter takes into account light absorption by leaf water content in the middle infrared (1100-2500 nm).

- Dry matter content (Cm, g/cm^2): this characteristic is responsible of light absorption between 800 and 2500 nm.

The LIBERTY model (Leaf Incorporating Biochemistry Exhibiting Reflectance and Transmittance Yields) was specifically designed for conifer needles. Radiative transfer theory for determining the optical properties of powders is used to simulate the optical properties of individual conifer needles whose small sive makes the measurement tricky. LIBERTY requires the following input parameters: cell diameter, intercellular air space, leaf thickness, baseline and albino absorption, and chlorophyll, water, lignin-cellulose and nitrogen content.

4.3.1.1 LIBERTY and PROSPECT comparison

Available input parameters were used to run the models. For those parameters that change during the season (Cab, Cw and Cm) a best fit estimation was used. The best fit was found minimizing the error over the whole spectrum between measured and simulated reflectance and transmittance. Final inputs used in both models are showed in Tables 4.3 and 4.5.

Table 4.3: LIBERTY parameters for BOREAS SSA coniferous forest

Parameter	Value	Comments
Average Cell Diameter(μm)	40	Typical value
Intercellular Air Space (arbitrary)	0.028	Dawson et al., 1999
Leaf Thickness (arbitrary)	1.6	Typical value
Baseline absorption (arbitrary)	0.0006	Typical value
Albino absorption (arbitrary)	2	Typical value
Chlorophyl content (mg/m^2)	OBS: 292, 193.9, 295.6 OJP: 270.7, 131, 242.7 YJP: 218.9, 190, 290.3	Values for each field campaign IFC1/IFC2/IFC3 Middleton et al., 1997b
Water content (g/m^2)	55.6-103.3-165	Dawson et al., 1999 Min,Mean and Max values
Lignin and cellulose content (g/m^2)	53.3-63.4-73.6	Dawson et al., 1999 Min,Mean and Max values
Nitrogen content (g/m^2)	1	Typical value

Data from Dawson et al., 1999 refers to Jack Pine but, according to results showed in Middleton et al., 1997b, the three species (OJP, YJP and OBS) present similar values being the seasonal changes more important than interspecies variations. It is, therefore, possible to extend these values to Old Black Spruce needles.

LIBERTY reflectances and transmittances were compared with field data for IFC1,IFC2 and IFC3. Water content and lignin cellulose content values were varied in the range and the values that minimised Reflectance_RMSE+Transmittance_RMSE were chosen. These values happened to be the same for the the two Jack Pine species: Water content=55.6 g/m^{2} and Lignin-cellulose content=63.4 g/m^{2}. For Old Black Spruce The water content value that minimizes the error is Cw=103.3 g/m^{2}

PROSPECT parameters (Cab, Cw, Cm and N) were fitted to the leaf reflectance and transmittance data (in the range 400-1000nm) (Middleton et al., 1997a) for each tree species separately. Ranges used in the fitting analysis as well as the source and the final result are indicated in Table4.5.

Table 4.5: PROSPECT Parameters for BOREAS sites

Parameter	Range	Source	OBS	OJP	YJP
N	2-3	Bicheron and Leroy, 1999	2	2.6	2.6
Cab ($\mu g/cm^2$)	IFC1 IFC2 IFC3	Middleton et al., 1997b	29 19.39 29.56	27.07 13.10 24.27	21.89 19 29.03
Cw (cm)	0.005-0.04	Jacquemoud et al., 1996	0.04	0.01	0.03
Cm (g/m^2)	0.002-0.2	Model range	0.028	0.012	0.012

RMSE between the model results (leaf reflectance and transmittance) and field data were calculated for each of the three field campaigns. Table 4.6 shows final results of the comparative study:

LIBERTY presented a total mean RMSE (calculated as the mean for the three sites and the three field campaigns) of 0.097 for reflectance and 0.088 for transmittance, compared to 0.038 and 0.022 obtained with PROSPECT.

The analysis is performed in the visible as available field data (reflectance and transmittance) only covered the range 400-1000nm. PROSPECT has proved to simulate leaf reflectance and transmission well in the visible spectrum before (Moorthy et al., 2003). Two bands of the study are out of this range (1240nm and 1600). Values obtained with PROSPECT in these two bands agreed with values modeled by LIBERTY. Similar good results with PROSPECT have been reported by Kuusk and Nilson (2000). Based on these results, PROSPECT was chosen to simulate leaf reflectances in the rest of the study.

Table 4.6: Comparative analysis PROSPECT-LIBERTY

		LIBERTY		PROSPECT	
		Reflect. RMSE	Transmit. RMSE	Reflect. RMSE	Transmit. RMSE
IFC1	OBS	0.063	0.084	0.022	0.016
	OJP	0.145	0.089	0.024	0.014
	YJP	0.1315	0.073	0.041	0.028
IFC2	OBS	0.037	0.086	0.026	0.029
	OJP	0.107	0.104	0.061	0.030
	YJP	0.113	0.089	0.061	0.030
IFC3	OBS	0.037	0.072	0.034	0.020
	OJP	0.118	0.097	0.040	0.019
	YJP	0.119	0.094	0.032	0.015
Total Mean RMSE		0.097	0.088	0.038	0.022

4.3.2 Canopy Reflectance Models

Only a canopy model with a physical basis will serve our purposes so that biophysical parameters can be inferred from its inversion.

A range of physical canopy reflectance models exist, from simple turbid-medium models to complex three-dimensional scene models. Coniferous forest offers a challenging structure so ideally a detailed three dimensional model should be used.

Finally, the computational efficiency must be considered as we will need to run the model many times. Scene simulation models produce realistic 3D scenes and photon interactions. Ray-tracing methods allow the sampling of photon trajectories and their intersections within the scene. The Monte Carlo method offers a robust and simple solution to this sampling scheme (Disney et al., 2000). In forward mode, rays are traced from the light source and followed through each of their interactions with the canopy until they reach the sensor position. This tends to be inefficient because a large number of photons are scattered in directions other than that of the sensor but in reverse mode, rays are traced from the sensor to the illumination hemisphere, which is more efficient in computational terms.

Taking these considerations into account, an hybrid 3-D radiative transfer/geometric

optic model using Monte Carlo ray-tracing, was chosen, the Forest Light (FLIGHT, North, 1996). FLIGHT has been used previously in the representation of coniferous forests (Dawson et al., 1999) and has performed well in the RAMI exercises (Pinty et al., 2001, 2006) presenting a good compromise between realistic 3D representation and accuracy, and computational costs.

4.3.2.1 FLIGHT

The FLIGHT model represents canopy as geometric shapes using cones and/or ellipsoids to represent crowns. The interactions within crowns are estimated as probabilistic functions of interactions between traced rays and canopy elements defined by LAI, FC and leaf angle distribution (LAD) function. LAD function describes the frequency distribution of leaf at different inclinations. The model permits to chose a range of LAD ranging from planophile (mostly horizontal leaves) to erectophile (mostly vertical leaves).

FLIGHT permits us to consider two sources of illumination, direct light from the sun as well as diffuse light from the environment. The combination of these two incident radiations provides a realistic representation of real illumination conditions and is important in scaling canopy processes such as photosynthesis and conductance, as the responses of canopy to diffuse and direct solar radiation are different (Gu et al., 2002). The geometry of the scene must be specified by the solar and viewing zenith/azimuth angles; the atmospheric optical thickness must be given also as an input parameter and is used to estimate the percentage diffuse light.

The model can be run in forward and reverse modes. Forward mode simulates the rays from the source (sun) forwards, generating outputs at all possible viewing directions. The reverse mode simulates rays from the viewer backwards, this derives in a reduction of calculations, and, therefore, of time. One of the parameters to define is the number of ray paths simulated (or photons fired) which defines the accuracy of the model as well as the running time. Errors are in the order of $1/sqrt(n)$ were n is the number of ray paths traced. A higher n will provide a higher accuracy but also will require more time to run. A value of 250,000 ray paths was chosen for this study which corresponds to an error of 0.002 and a running time of around 2 minutes depending on the complexity of the scene. This value provides accuracy enough to test the effect of radiometric noise at levels ranging from 0.005 absolute value while the execution time is not too long allowing us to create the required LUT in a reasonable time.

Input parameters representing the canopy structure and spectral characteristics were taken from the field data.

4.3.2.2 FLIGHT evaluation

An analysis was made to test the ability of FLIGHT to simulate real scenes in a sparse canopy landscape. The aim of this experiment is to test FLIGHT in a realistic scenario, as this model will be a central piece of the rest of this work. The biome used in this experiment is vastly different from the boreal forest used throughout this thesis, however it provides a good test of the capability of the model to simulate scene reflectance in sparsely vegetated areas. The sites used are olive orchards that share the common characteristic of the sparseness of the vegetation with the coniferous forests used in this thesis. In these conditions the global reflectance of the scene is highly influenced by soil making the canopy signal difficult to separate. Shadows and mutual shadowing between canopies is also an issue in the representation and interpretation of these landscapes. The results of this experiment are intended to provide an instructive comparison of the model with real data, facilitating the testing of the model's ability to represent the highlighted issues.

FLIGHT allows for the simulation of detailed scenes by defining the specific locations and characteristics of each tree within the scene. This capability can be used to simulate scenes similar to the ones obtained with an instrument allowing comparison of reflectance values between both scenes, simulated and measured.

An olive orchard situated in Southern Spain was used as test site. Airborne CASI images and other field data such as leaf spectral properties were obtained from a field campaign developed in 2003 by the Institute for Sustainable Agriculture (IAS), Spanish National Research Council (CSIC).

Test site

The field data used correspond to three sites of olive orchard (*Olea europaea* L.) comprising groves of irrigated and non-irrigated crops located in Seville, Southern Spain. Denomination and coordinates of the sites are given in Table 4.7.

Table 4.7: Test sites

Denomination	Crop	Latitude	Longitude
Cañaveralejo	Irrigated olive orchard	4° 51' 58" W	37° 19' 26"
Tobalico	Non-irrigated olive orchard	4° 52' 32" W	37° 18' 41"
Aguilillas	Irrigated olive orchard	5° 2' 37" W	37° 15' 56"

Compact Airborne Spectrographic Imager (CASI) hyperspectral imagery and leaf optical properties were provided by the Institute for Sustainable Agriculture (IAS), Spanish National Research Council (CSIC). Table 4.8 shows the origin of each of the input data required to run FLIGHT.

Table 4.8: FLIGHT input parameters

Parameter	Source
Individual tree coordinates (x,y)	Measured over CASI images
Leaf Reflectance/Transmittance	Mean values from field data
Crown radius	Measured over CASI images
Soil reflectance	Extracted from CASI images
Ilumination/viewing geometry	Extracted from CASI data

The analysed sites are partially vegetated areas with distinct crowns, as the coniferous forests analysed in this thesis. Shadows and mutual shadowing between canopies play a fundamental role both in the radiation received by each canopy (hence in the production) and in the radiation recorded by the sensor. It is hence very important that the canopy model represents these effects. As an example of the capability of FLIGHT to achieve this representation, figure 4.2 shows the images created by FLIGHT for three different solar zenith angles.

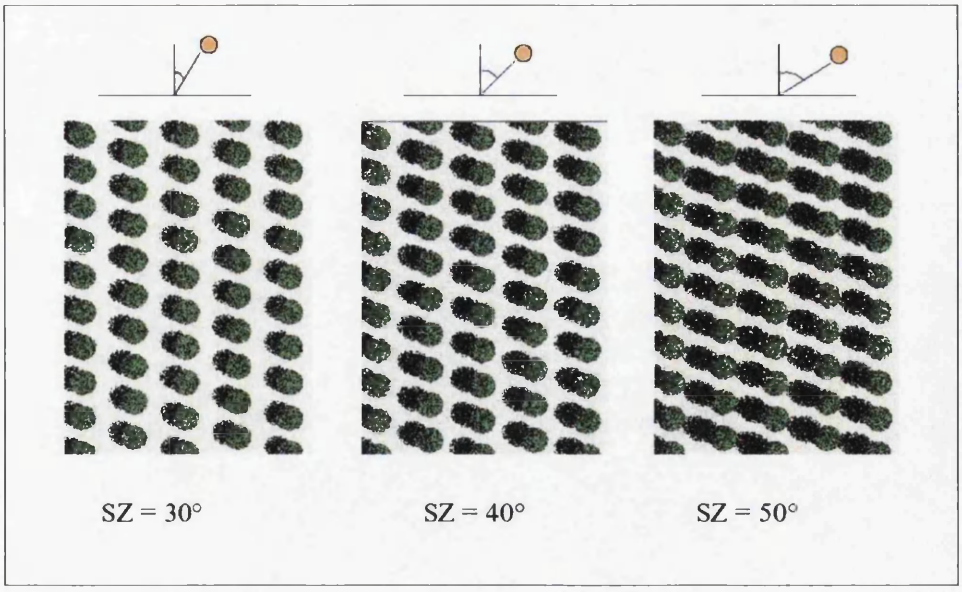

Figure 4.2: Simulated images at three different solar zenith angles, nadir view and 45 relative azimuth.

CASI data

CASI data from 2003 in spatial mode was used. In July 2003 the Compact Airborne Spectrographic Imager (CASI) sensor was flown over Spain in collaborative research with York University (Canada) and the Spanish aerospace institute (Instituto Nacional de Tecnica Aeroespacial, INTA). CASI spatial mode was used to get the imagery with 1 m spatial resolution and 8 user-selected spectral bands placed in the spectrum to enable the calculation of specific narrow-band indices sensitive to pigment concentration (bands were centered at 490, 550, 670, 700, 750, 762, 775 and 800 nm with full-width at half maximum (FWHM) ranging between 7 and 12 nm). The band situated at 762 was discarded in this study as it presented high levels of noise.

The data was provided calibrated and atmospherically corrected. The 12-bit radiometric resolution data collected by CASI were processed to at-sensor radiance using calibration coefficients derived in the laboratory by the Earth Observations Laboratory (EOL), York University, Canada. Aerosol optical depth data at 340, 380, 440, 500, 670, 870, and 1020 nm were collected using a Micro-Tops II sunphotometer (Solar Light Co., Philadelphia, PA, USA) in the study area at the time of data acquisition to derive aerosol optical depth at 550 nm. Atmospheric correction was applied to CASI imagery using CAM5S atmospheric correction model (O'Neil et al., 1997). Reflectance data were georeferenced using GPS data collected onboard the aircraft. Soil reflectance spectra were used to perform a flat-field correction that compensated for residual effects on derived surface reflectance estimations in atmospheric water and oxygen absorption spectral regions.

Table 4.9 shows the seven bands used.

Table 4.9: CASI spectral bands used (spatial mode)

Channel	Band center (nm)
1	490.74
2	550.62
3	670.35
4	700.71
5	750.19
6	775.00
7	799.86

A subset of trees presenting uniform spatial distribution was chosen to measure the plantation pattern. Figures 4.3, 4.4 and 4.5 show the chosen areas for each site, the sun/sensor geometry at which the images were collected and structural data extracted from the images.

Geometry		Data obtained from the image	
Solar Zenith Angle	39	Mean crown radius	2 m
Viewing Zenith Angle	0	Vert. distance between trees	5.5 m
Relative Azimuth	67	Hor. distance between trees[1]	7.5 m

[1]Only in this case, horizontal distance was measured as distance between rows and not between trees. Vertical distance is distance between trees in the same row.

Figure 4.3: CASI image: Cañaveralejo

Geometry		Data obtained from the image	
Solar Zenith Angle	43	Mean crown radius	3.5 m
Viewing Zenith Angle	0	Vert. distance between trees	9 m
Relative Azimuth	81	Hor. distance between trees	10 m

Figure 4.4: CASI image: Tobalico

Geometry		Data obtained from the image	
Solar Zenith Angle	45	Mean crown radius	2 m
Viewing Zenith Angle	0	Vert. distance between trees	8 m
Relative Azimuth	83	Hor. distance between trees	7.5 m

Figure 4.5: CASI image: Aguilillas

FLIGHT images

Simulations of the three areas were created with the structural parameters presented in Figures 4.3, 4.4 and 4.5. A typical LAI value for olive orchards of 1.0 (Zarco-Tejada pers. comm.) and planophile leaf angle distribution were used.

Soil reflectance values were taken from each of the images by identifying pure soil pixels. Leaf reflectance/transmittance values were available from lab measurements taken on the date in which the images were collected. These reflectance and transmittance values (400-2500 nm) were obtained using a full-range spectroradiometer (Analytical Spectral Devices, Inc., Boulder, Colorado) and an integrating sphere (LI-1800, LI-COR Inc., Lincoln, Nebraska). The ASD spectrometer acquired measurements at 1.4-nm intervals in the visible and near-infrared (NIR) and at 2.0-nm increments in the shortwave infrared (IR) (SWIR) region. Each reflectance and transmittance spectrum represented the mean of 100 individual spectral measurements. A typical spectrum was calculated as mean value of the measurements available.

The number of ray paths was fixed at 250,000, the same value that will be used in the rest of this thesis.

FLIGHT model generates an image output file with one value per pixel and per band representing the reflectance. This file can be easily converted to an ENVI loadable format. In this study, FLIGHT output images were converted to Band Interleaved by Pixel Format (BIP) in order to compare them with the CASI images.

Spectral reflectances between the CASI images and the FLIGHT simulation were compared both at crown and at scene levels by selecting regions of interest on the images and extracting the reflectance values.

Results

Modelled data was compared to observed images at the crown level and at the scene level. The crown level comparison was based in pure tree pixels collected from the images while the scene level comparison was made in aggregated pixels including canopy, soil and shadows.

Figures 4.6, 4.7 and 4.8 show the CASI images and FLIGHT simulated images. Overall shapes and shadows are very similar. Differences in the colors displayed are due to the scaling that ENVI does on the palette used to adapt them to the range of values represented. To compare spectra from both images, results from the regions of interest created both at crown and at scene level are represented in the graphs and in the tables

of Figures 4.9, 4.10 and 4.11. RMSE between the observed and the simulated data are reported both at crown level and at the scene level. The same scenes were simulated with LAI values different from the real value: 0.5, 2.0 and 3.0; results from these simulations showed a higher RMSE between the simulated and the CASI spectra in all cases (4.12).

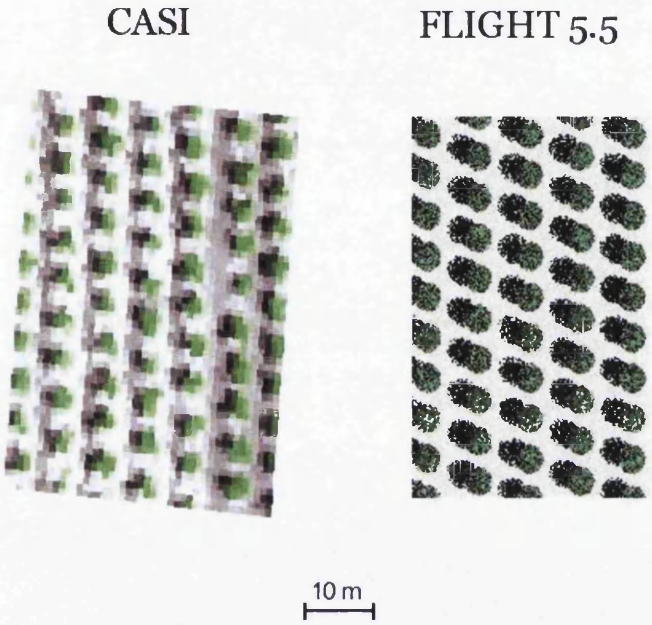

Figure 4.6: Observed and simulated images for Cañaveralejo site

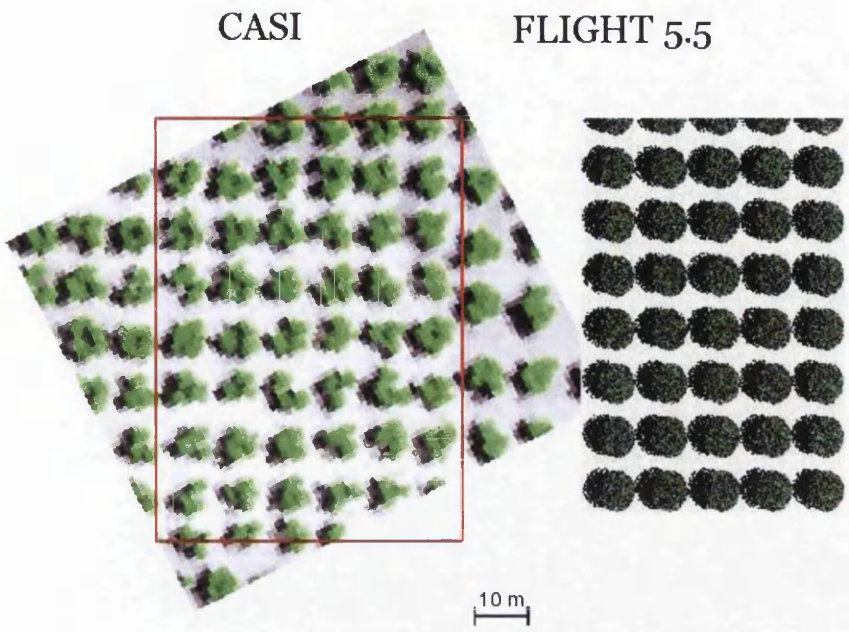

Figure 4.7: Observed and simulated images for Tobalico site

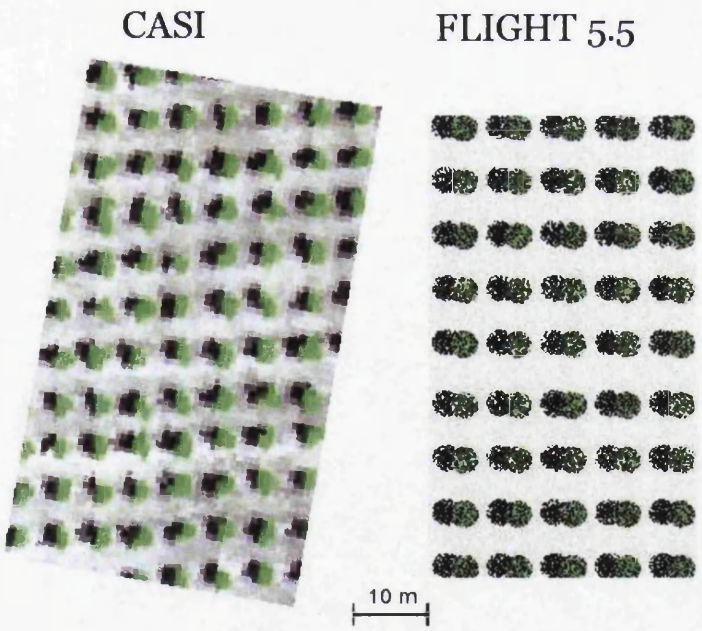

Figure 4.8: Observed and simulated images for Aguilillas site

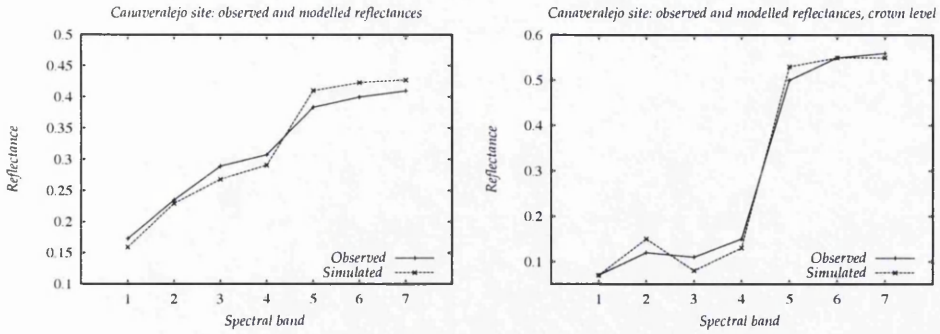

	Aggegated pixels	Crown level
RMSE	0.018	0.021

Figure 4.9: Results Cañaveralejo

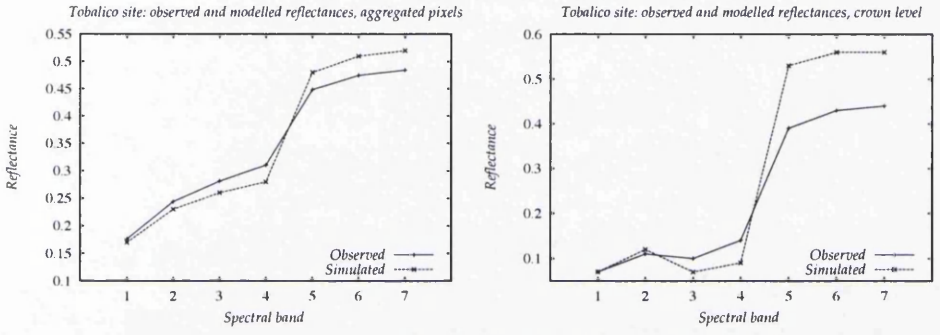

	Aggegated pixels	Crown level
RMSE	0.031	0.073

Figure 4.10: Results Tobalico

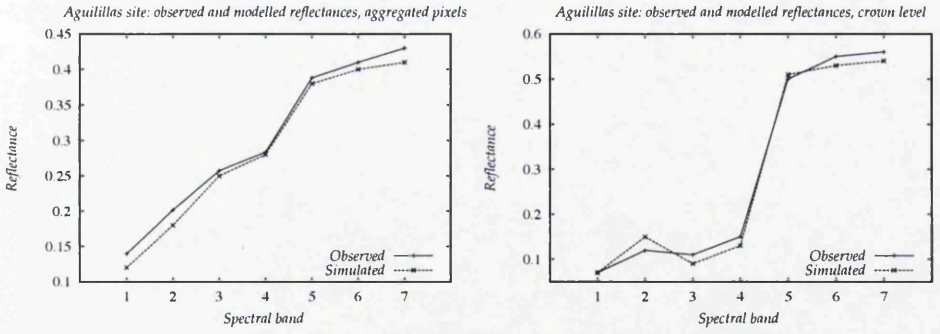

	Aggegated pixels	Crown level
RMSE	0.014	0.019

Figure 4.11: Results Aguilillas

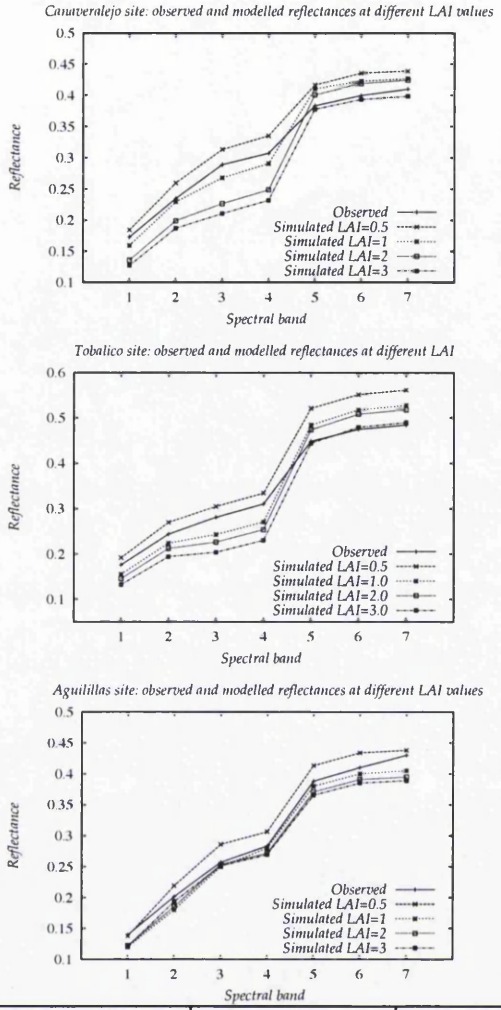

LAI	Cañaveralejo RMSE	Tobalico RMSE	Aguilillas RMSE
0.5	0.027	0.052	0.020
1	0.018	0.031	0.014
2	0.039	0.040	0.019
3	0.048	0.049	0.022

Figure 4.12: Results for different LAI values for the three sites

Small differences in aggregated pixels could be explained by inaccuracies when choosing the regions of interest used. FLIGHT simulates crowns as spheres while real olive orchards present an irregular shape, this makes difficult to select regions of interest with an equal percentage of each component (soil, tree and shadow) in both images to compare (observed and modelled).

Other sources of error are errors in the input parameters and errors of the model itself.

FLIGHT errors are of the order of 0.002, likely much smaller than those introduced for the assumptions made in the input parameters such as the leaf spectral values calculated as mean field values.

The high error observed at the crown level at Tobalico could be due to the use of a generic olive leaf spectrum, which seems to work well in the other two sites (both irrigated) while it might not be representative of non-irrigated olive orchards. The objective of this test was accomplished as the results showed the capability of the model to simulate the scenes, so no further investigation was made regarding the non-irrigated site simulation.

The overall conclusion of this experiment is that FLIGHT can simulate adequately sparsely vegetated areas at an accuracy good enough to be compared with airborne images. Structural representation of the canopies, assessed by the overall shape and position of trees and shadows, presents also a high degree of fidelity. It can be concluded also that the errors introduced by the Monte Carlo approximation became negligible when compared to errors introduced by assumptions in the input parameters.

4.3.3 Atmospheric Radiative Transfer Models

MODTRAN (MODerate resolution atmospheric TRANsmittance and radiance code) and 6S (Second Simulation of Satellite Signal in the Solar Spectrum) are the most widely used radiative transfer models in remote sensing.

As mentioned in previous chapter, MODTRAN provides precise evaluation of the radiative transfer in the whole electromagnetic spectrum, while 6S covers only the solar spectrum. Other advantages of MODTRAN over 6S are the consideration of clouds and of absorption between two consecutive scattering effects leading to precise evaluation of the RT in bands with strong gaseous absorption. The disadvantage is the computing cost with 6S being much quicker to run than MODTRAN.

The present study will focus on the solar spectrum, wavelengths presenting strong gaseous absorption will be excluded as this feature make them unsuitable for the retrieval of vegetation parameters. Also clouds do not need to be considered as we are dealing with own created images. These reasons and the fact that the model will have to be run many times, make 6S the most suitable candidate to simulate atmospheric effects presenting the advantage of lower time consumption while the disadvantages will not have mayor impact in the results.

4.3.3.1 Second Simulation of Satellite Signal in the Solar Spectrum (6S)

6S code has been developed by the Laboratoire d'Optique Atmospherique at the Universite de Lille and it is written in FORTRAN77 (Vermote et al., 1997). 6S uses the method of Sucessive Orders of Scattering which calculates the diffuse radiance associated with photons scattered once, twice, three times, and so on.

The model calculates the signal at the top of the atmosphere as the sum of four components: (1) photons directly transmitted from the sun to the target and directly reflected back to the sensor, (2) photons scattered by the atmosphere then reflected by the target and directly transmitted to the sensor, (3) photons directly transmitted to the target but scattered by the atmosphere on their way to the sensor and (4) photons having at least two interactions with the atmosphere and one with the target.

The absorption is computed using statistical band models by dividing the solar spectrum into intervals of $10cm^{-1}$ using HITRAN (high-resolution transmission molecular absorption database). Moreover, 6S provides a complete treatment of the scattering processes, although gaseous absorption is decoupled from the scattering process, as it has been mentioned before. Aerosol and aerosol-rayleigh coupled system are solved using the Successive Orders of Scattering method.

The code can be used in the forwards mode to estimate the effect of the atmosphere on the surface reflectance, or in the reverse mode to derive the surface reflectance from the top-of-the-atmosphere reflectance.

Inputs are specified at an input file and include zenith and azimuth angles of the sun and satellite, atmospheric and aerosol models, spectral conditions and ground reflectance.

6S permits us to use an atmospheric model defined by the user or one of the six standard atmospheric models (Tropical, Mid-latitude Summer, Mid-latitude Winter, Sub-arctic Summer, Sub-arctic Winter and the U.S. Standard 62). These models compute the gaseous absorption and the Rayleigh scattering with a spectral resolution of 2.5 nm.

The optical scattering parameters for the aerosols are computed using pre-defined aerosol models (specified in the World Meteorological Organization report): Continental, Maritime, Urban, Desert, Biomass and the Stratospheric model, or a model defined by the user model based on a mixture of 4 basic components (dust-like, oceanic, water-soluble and soot).

Spectral bands can be chosen from the ones included in the code for different instruments or defined by the user. Ground reflectance can also be defined by the user, or by a standard spectral reflectance defined in the code.

For the surface contributions, both Lambertian and non-Lambertian surfaces are considered. In the first case, the value of the surface reflectance must be provided by the user or chosen from the pre-defined typical spectra. In the second case, the angular distribution of the surface reflectance can be given by multiangular in-situ measurements or estimated by parametric model.

The main limitation of 6S is the inaccuracy in strong gaseous absorption bands but, its particular mathematical formulation makes it rapid yet accurate enough and specially suitable in those applications where a great number of simulations is needed.

4.3.3.2 Coupling the models

FLIGHT can use directly PROSPECT reflectance/transmittance outputs as input so the coupling between these two models is straightforward.

The coupling between FLIGHT and 6S was made by feeding the reflectance values calculated by FLIGHT into 6S. This had to be repeated once for each simulated band as FLIGHT provides outputs at several wavelengths while 6S calculates only one band at a time. The maximum and minimum wavelengths required as input in 6S were calculated as the wavelength used in FLIGHT $\pm 5nm$ providing a bandwidth of $10nm$.

A program in C was created that run the models sequentially taking the output from one of them and preparing the input for the next one.

4.3.4 Land surface parameterisations

Chapter 2 made clear the wide range of LSPS presently available. In order to make this study as representative a possible two models were chosen as illustrative of medium and high complexity LSPs, namely BIOME BGC and JULES. Other reasons for selecting those and no others were their availability, documentation (White et al., 2000; Best, 2005) and previous application in similar ecosystems (Kimball et al., 1997b; Alton et al., 2006). These models are briefly introduced and further details about the inputs will be given later.

4.3.4.1 BIOME-BGC

The BIOME-BGC (BioGeochemical Cycles) model (Running and Gower, 1991; White et al., 2000) is a multi-biome generalization of FOREST-BGC (Running and Gower, 1991), a model originally developed to simulate a forest stand development through

a life cycle.The model requires daily climate data and the definition of several key climate, vegetation, and site conditions to estimate fluxes of carbon, nitrogen, and water through ecosystems. Allometric relationships are used to initialize plant and soil carbon (C) and nitrogen (N) pools based on the leaf pools of these elements.

BIOME-BGC is written in C with no specific hardware requirements. Version used was 4.1.1, 5 July 2000.

The fundamental drivers of Biome-BGC are daily surface weather data. The model also requires a description of the site vegetation ecophysiology and site specific physical characteristics. The parameters estimates are daily fluxes of carbon, nitrogen and water between the atmosphere, plant state variables and litter and soil state variables.

BIOME-BGC predicts projected LAI as a function of the amount of leaf carbon and of the canopy average specific leaf area (SLA, defined as the projected area per unit of leaf carbon mass, averaged over the canopy). Both are inputs provided by the user, SLA does not change over time while leaf carbon is one the vegetation state variables that the model updates everyday according to the estimated fluxes.

Photosynthesis is calculated by a modified form of the Farquhar model, regulated by canopy conductance, leaf maintenance respiration and daily meteorological conditions (air pressure, air temperature and solar irradiance). Transpiration and evaporation are calculated using a modified Penman-Monteith approach, as function of air temperature, humidity and solar irradiance. Both maximum photosynthesis and maximum transpiration rates are regulated by the canopy conductance to water vapor.

BGC represents the canopy as a single homogeneous layer in the sense that all units of leaf area in the canopy are represented using a single, canopy-averaged conductance. Complete horizontal homogeneity is assumed within that unit area over which all fluxes and storage are quantified. This assumption is generally not valid at subdaily (e.g., hourly) time-steps because the reduction of irradiance at lower vertical layers of the canopy reduces conductances at the bottom of the canopy. The sunlit shaded distinction is based in a ratio between specific leaf area for leaves in the shaded canopy fraction and specific leaf area for leaves in the sunlit canopy fraction specified by the user in the input file.

In BIOME-BGC most simulated ecosystem activity occurs at a daily time step (e.g. soil water balance, photosynthesis, allocation, litterfall, and C and N dynamics in the litter and soil) driven by daily values for maximum and minimum temperatures, precipitation, solar radiation, and air humidity. Phenological timing is determined once a year and for evergreen vegetation, current climatic conditions determine the beginning and end of the growing season.

4.3.4.2 JULES

The Joint UK Land Exchange System (JULES, Best, 2005) is a land surface scheme initially based on the Met Office Surface Exchange Scheme (MOSES). The last version of MOSES was the MOSES 2.2 (Essery et al., 2001) which is used in the Unified Model or off-line. The off-line version was the basis for JULES with the intention to make it available to the research community so they can test and improve the model.

JULES uses a tiled land-surface scheme with 9 surface types: broadleaf trees, needle-leaf trees, C3 (temperate) grass, C4 (tropical) grass, shrubs, urban, inland water, bare soil and ice. Each tile has different surface properties and the surface energy and water balances are aggregated across the tiles in a gridbox. The grid box mean values of the fluxes to the atmosphere are calculated as the area-weighted means of the fluxes from the tiles.

The model considers a variable number of soil layers (four by default) for both temperature and moisture.

The influence of atmospheric variables as temperature, humidity and radiation are explicitly parameterised on the stomatal resistance of vegetation. Evaporation from transpiring vegetation is defined by a canopy conductance parameter, gc, calculated by a photosynthesis model depending on temperature, humidity deficit, incident radiation, soil moisture availability and vegetation type. The photosynthesis model is based on the Farquhar's model for C3 plants and in further improvements of this model (Cox, 2001), as explained in Sellers et al. (1996b), for C4 plants. LAI is the main driver of the NPP calculations. Photosynthesis and leaf conductance are calculated at the leaf level and then extrapolated to the canopy by means of the LAI. Plant respiration is calculated from nitrogen and carbon content and both parameters are dependent of LAI.

4.3.5 Biophysical parameters analysed

Aerosol optical thickness and fractional cover were fed directly into the LSPs. LAI and fAPAR required some considerations before using them.

- **LAI**

The definition used in this thesis is one half of the total green leaf area per unit of ground surface area. Some considerations must be taken into account when applying

this definition. When studying radiation interception by leave we need to use one half of the total radiation intercepting area per unit of ground surface, while when studying photosynthesis we are interested in the total green leaf as shaded leaves are also involved in the process (Chen and Cihlar, 1995).

Indirect methods assume that foliage is randomless distributed in the canopy. Estimations made with these instruments must be corrected in some way to account for the complexity of canopy architecture. A correction factor termed "clumping index" (Ω) has been proposed to quantify the effect of this nonrandom spatial distribution of foliage (Chen et al., 1997). This non-randomness corrected LAI is usually referred as "effective LAI". By knowing the clumping index, real LAI can be calculated as:

$$LAI_{Real} = \frac{LAI_{Effective}}{\Omega}$$

The use of a clumping index is critical in any photosynthesis models and it must be taken into consideration specially in sunlit/shaded leaf models as its value greatly modifies the amounts of sunlit and shaded leaves (Chen et al., 1999b).

This correction is particularly critical in conifer forest stands where the effective LAI is considerably smaller than LAI (usually 50%) measured by instruments because leaves are grouped together in tree crowns, branches, shoots, and so on.

FLIGHT does not consider clumping so effective LAI values were used to get appropriate representation of light interactions. Also LSPs are based on radiation interception and do not consider clumping correction. For this reason, Effective LAI was used to run FLIGHT and LSPs.

Soil reflectance

Soil reflectance is one of the most sensitive parameters in canopy reflectance models (Fang et al., 2002). This effect is more important at lower values of LAI while for LAI values higher than 3, in homogeneous canopies, the importance of the soil background decreases (Bicheron and Leroy, 1999). Soil reflectance inputs for the models can be collected from field measurements or extracted from a soil spectral library. Other approaches calculate soil reflectances at each wavelength as multiples of a defined soil parameter (Kimes et al., 2002). Generally, using field-measured soil reflectance is the most accurate approach if the data are available (Fang and Liang, 2004). Reflectances from a soil spectral library or empirically calculated may not represent real conditions in the field. The approach used in this study was the use of soil reflectances available from field measurements, specifically understory reflectances.

fAPAR

fAPAR is the fraction of photosynthetically active radiation (fPAR) absorbed by the canopy between 400 and 700 nm. This can be represented as (Privette et al., 1996b):

$$fAPAR = \int_{400}^{700} F_{a,\lambda} W_\lambda d_\lambda \tag{4.1}$$

where $F_{a,\lambda}$ is the fraction of radiant energy absorbed by the canopy at wavelength λ and W_λ is the fraction of fPAR energy incident at at wavelength λ. These terms can be calculated for specific bands: $F_{a,\lambda}$ can be calculated with FLIGHT and W_λ with 6S. The total fAPAR can then be calculated as the sum of all the bands covering the 400-700nm range.

When bands are not contiguous, a method can be used to artificially extend the bandwidths such that all the photosynthetic active frequencies are represented (Privette et al., 1996b). To do this the fraction of energy incident at each band is used to weight the correspondent broader band. The fAPAR is estimated then by summing the spectral products of fAPAR at each band times the weight:

$$fAPAR = \sum_{i=1}^{n} F_{a,i} W_i \tag{4.2}$$

where $F_{a,i}$ is the mean fraction of radiant energy absorbed by the canopy at band i, calculated from FLIGHT 5.5, and W_i are the weights determined from 6S.

Weights estimation

6S gives irradiance in terms of energy, it is watts per square meter (W m^{-2}). Time (seconds) is contained within the term watt: 1 W = 1 joule (J)s^{-1}. Photon counts are usually used instead of energy units since photosynthetic rates are essentially independent of the energies of the absorbed photons. In this case, units are expressed in moles per square meter per second ($mol/m^2 s$), where "moles" refers to the number of photons (1 mol of light = 6.02×10^{23} photons, Avogadro's number). This measure is called photon irradiance.

On the other hand, the energy of a photon depends on its frequency, as expressed by Planck's law:

$$E = \frac{hc}{\lambda} \tag{4.3}$$

where c is the speed of light ($3 \times 108m/s$), h is Planck's constant ($6.63 \times 10^{34}Js$), and λ is the wavelength of light, usually expressed in nm ($1nm = 10^{-9}m$). We can solve for the $h\lambda$ part of the equation, and we obtain $1,988 \times 10^{-16}$, and write this equation as:

$$E = \frac{1,988 * 10^{-16}J}{\lambda} \tag{4.4}$$

where λ is expressed in nanometers.

N is the Avogadro's number, then the conversion is as follows:

$$\frac{I}{EN} = \frac{mol}{m^2 s} \tag{4.5}$$

And I' the irradiance in terms of photon counts:

$$I' = \frac{I}{EN} = \frac{mol}{m^2 s} \tag{4.6}$$

To calculate weights these values are :

$$W_i = \frac{I'_i}{\sum_{i=1}^{n} I'_i} = \frac{\frac{I_i}{EN}}{\sum_{i=1}^{n} \frac{I_i}{EN}} = \frac{I'_i * \lambda_i}{\sum_{i=1}^{n} I'_i * \lambda_i} \tag{4.7}$$

A preliminary study was made to test this technique. Weights were calculated to be compared with those obtained by Privette et al., 1996b. The same three bands were used. Privette et al., 1996b considered Solar Zenith angle in the range 22-56 degrees, so weights were obtained for SZ values of 30°, 40° and 50° and the average weight was calculated. Table 4.10 shows results of the comparison study.

Table 4.10: Comparison with Privette et al. 1996 results, "estimated" column shows average values for SZ= 30°,40° and 50°

Band	Limits (nm)	Average Weight Privette et al., 1996b	Average Weight Estimated
1	400-520	0.345	0.346
2	520-615	0.342	0.361
3	615-700	0.313	0.293

The method was adapted to be used with those bands used in the present study that correspond to the the photosynthetically active radiation (400- 700nm).

4.4 Running the LSPs

The BIOME-BGC model was used in the sensitivity analysis and in the final methodology (Chapters 5 and 6) while JULES is only used in the final methodology (Chapter 6). Inputs and considerations for both models are presented here.

4.4.1 BIOME-BGC

BIOME-BGC requires two input files: daily meteorological data and initialization data. The model generates an output file of daily estimates of site carbon balance characteristics. The initialization file provides site-specific information about stand morphology, soil type, and soil condition. BIOME-BGC simulates biogeochemical and hydrologic processes across multiple biomes based on the logic that differences in process rates between biomes are primarily a function of climate and general life-form characteristics. The carbon balance portion of BIOME-BGC utilizes daily meteorological data in conjunction with general stand and soil information to predict net photosynthesis, growth, maintenance, and heterotrophic respiration at a daily time-step. BIOME-BGC is general in the sense that the surface is represented by singular, homogeneous canopy and soil layers.

4.4.1.1 Meteorological data

BIOME-BGC requires daily meteorological data. The input file must contain nine values for each day; these are shown in Table 4.11

Meteorological data files were generated using the MTCLIM version 4.3 program (Numerical Terradynamic Simulation Group School of Forestry, University of Montana). MTCLIM is a weather simulation model designed especially for application in mountainous terrain. This code allows to simulate all the required parameters using observations of temperature and precipitation. Moreover, given input data from one location, MTCLIM allow to generate weather information for another location with potentially different elevation, slope and aspect from the input location.

The MTCLIM code and documentation is available from the Numerical Terradynamic Simulation Group School of Forestry website (www.forestry.umt.edu/ntsg).

Required input data for MTCLIM are daily observations of maximum and minimum temperature, and daily total precipitation. These data was available from BOREAS (Kimball et al., 1997b) for the OBS and OJP sites. These datasets contain daily meteorological data derived from approximate 15 minute measurements obtained from SRC

mesonet and flux tower sites for 1994. Information from OJP was used to calculate YJP meteorological data with MTCLIM assuming that OJP site was at an heigh of 579 m and YJP at 533 m.

Table 4.11: Daily meteorological data required by Biome BGC

Parameter	Description	Units	Source
Year	the numerical year, repeated for each yearday	-	n/a
Day	numerical day of the year (1-365)	days	n/a
Tmax	the daily maximum temperature	degrees Celsius	Field data[1]
Tmin	the daily minimum temperature	degrees Celsius	Field data[1]
Tday	average daytime temperature (sunrise to sunset)	degrees Celsius	MTCLIM[2]
prcp	daily precipitation	centimeters	Field data[1]
VPD	daylight average vapor pressure deficit	Pa	MTCLIM[2]
srad	daylight average shortwave radiant flux density	Wm^{-2}	MTCLIM[2]
daylen	daylength (sunrise to sunset, seconds)	seconds	MTCLIM[2]

[1]Field data taken from BOREAS RSS-08 BIOME-BGC MODEL SIMULATIONS AT TOWER FLUX SITES IN 1994

[2]Data generated with MTCLIM 4.3 weather simulation model

4.4.1.2 Initialisation data

Two initialisation files were required apart from the one with meteorological data: the initialization file (denoted file.ini) and the ecophysiological constants file (denoted file.epc).

The initialisation file provides general information about the simulation such as description of the physical characteristics of the site, a description of the time-frame for the simulation, the names of all the other required input files, the names for output files that will be generated, and lists of variables to store in the output files.

The ecophysiological constants file contains the ecophysiological description of the vegetation at the site. It includes parameters such as leaf C:N ratio, maximum stomatal conductance, fire and non-fire mortality frequencies, and allocation ratios.

The initialization data files were created with information obtained from the BOREAS experiment with Biome BGC (Kimball et al., 1997b) (data available on the BOREAS site, not on the paper itself). This experiment used a previous version of BIOME BGC, which required less input parameters. Parameters not used in that study were

obtained from a data set specifically containing documented input parameters of major natural temperate biomes in the United States for use with the BIOME-BGC Terrestrial Ecosystem Model (White et al., 2000). In some cases initialisation parameters were not in any of the two sources but were estimated from the data available. Tables 4.12 and 4.13 show the parameters used and the source (only the most relevant parameters are shown).

4.4.2 JULES

JULES requires two input text files, a file with meteorological driving data and a run control file. The model produces one dump file. The model time step is defined by the meteorological data, with a minimum value of 30 minutes which is the time step used in this study.

4.4.2.1 Meteorological data

Meteorological data was obtained from BOREAS AFM-07 Saskatchewan Research Council (SRC) Surface Meteorological and Radiation Data. The data set comprises Suite A (meteorological and energy balance measurements) and Suite B (diffuse solar and longwave measurements) components. Suite A measurements were taken at each of 10 sites, and Suite B measurements were made at 5 of the Suite A sites. These data was collected from December 1993 until December 1996. Table 4.14 shows parameters used from these field data sets and the conversions made to fit them to the units required by the model.

4.4.2.2 Initialisation data

Initialisation parameters were taken from the field data if available, if not default or standard values were used as shown in Table 4.16. JULES NPP is highly sensitive to soil parameters. The field data divided the soil into a higher number of layers than the four used by default in JULES (6 for OBS and YJP sites and 14 for OJP site, see Appendix II). Increasing the number of soil layers to match those reported by the field measurements made the model very unstable. JULES is designed to work best for the default soil-layer configuration so it is recommended to keep those values (E. Blynth pers. communication). Field measurements were therefore interpolated to match the default four layers used in JULES. Final values used are showed in Table 4.16 and original field data is in Appendix II.

The fixed concentration of atmospheric $CO_2$was calculated as the mean value of field data values of ambient CO_2 concentration (BOREAS TE-04 Gas Exchange Data from Boreal Tree Species). Values abnormally low (< 100) were filtered, before calculating the mean. Field data units are mixing ratio (micromoles of CO_2/total air molecules), and JULES requires mass mixing ratio so the molecules were converted into mass (multiplying by 44 gC/mole) and then divided by total mass of air (approximated as 28.8 g/mole). Results are shown in Table 4.18.

Table 4.18: Values of fixed concentration of $CO_2$for each site

Site	Field data (mixing ratio, ppm)	Calculated mass mixing ratio, ppm by mass
SOBS	352.492	538.529
SOJP	367.41	561.32
SYJP	370.774	578.512

ppm: parts per million

Hydraulic conductivity at saturation was calculated from BOREAS Soil Hydraulic Properties: HYD01. JULES units are kg/m^2s; assuming a density of 1000 , this rate is equivalent to the rate expressed in mm/s. Field data units were m/day, so values were converted to mm/s multiplying by 1000/(24*60*60). Results are shown on Table 4.19.

Table 4.19: Hydraulic conductivity at saturation for each site

Site	Field data (m/day)	Calculated (kg/m^2s)
OBS	0.79	0.009
OJP	1.46	0.0169
YJP	1.86	0.0215

4.5 Summary

A methodology has been presented to examine the impact of various satellite-sensor properties on the estimation of biophysical parameters and their effect on LSPs. A well-characterized scene is required, which is simulated by coupling three numerical models, namely: a model of leaf spectral reflectance, PROSPECT; a model of vegetation canopy reflectance, FLIGHT; and an atmospheric radiative-transfer model, 6S. The scene simulations produced using these models provide the spectral and angular

reflectance samples employed in the biophysical property retrieval. The values estimated are subsequently used to drive the two LSPs used in this study are BIOME-BGC and JULES.

The test site is a boreal forest, which represents an important biome in terms of the global carbon budget. Moreover, models are typically sensitive to a range of surface properties for this biome type, enabling a robust evaluation of their uncertainty. This biome type is also structurally complex, providing a challenging test of the proposed method. A study of FLIGHT has been performed in order to check its capability to simulate BRDF in sparse vegetation landscapes. The results showed good agreement with airborne data concluding that simulations are realistic and can be used to characterise sparsely vegetated areas.

The study focuses on the estimation of five surface biophysical properties: fractional cover, fAPAR, effective LAI, leaf chlorophyll content and AOT, all of which can be estimated by means of satellite remote sensing.

Meteorological and site specific parameterisations used to drive BIOME-BGC and JULES have been presented.

Table 4.12: BiomeBGC input parameters ini file

Parameter	OBS	OJP	YJP	Comments
number of meteorological data years	1	1	1	-
number of simulation years	2	2	2	-
first simulation year	1994	1994	1994	-
constant atmospheric CO2 concentration (ppm)	294.842	294.842	294.842	-
effective soil depth(m)	0.5	0.5	0.5	(a)
sand percentage by volume in rock-free soil (%)	75.0	93.0	92.0	(a)
silt percentage by volume in rock-free soil (%)	20.0	4.0	5	(a)
clay percentage by volume in rock-free soil (%)	5.0	3.0	3.0	(a)
site elevation (m)	569.0	579.0	533.0	(b)
site latitude (degrees)	53.987	53.916	53.877	(b)
site shortwave albedo	0.1	0.1	0.1	(b)
wet+dry atmospheric deposition of N (kgN/m2/yr)	0.0001	0.0001	0.0001	(c)
symbiotic+asymbiotic fixation of N (kgN/m2/yr)	0.00008	0.00008	0.00008	(c)
water stored in snowpack (kg/m2)	7.0	7.0	7.0	(d)
initial soil water as a proportion of saturation	0.5	0.2	0.2	(e)
first-year maximum leaf carbon (kgC/m2)	0.427	0.267	0.267	(b)
first-year maximum stem carbon (kgC/m2)	0.12	0.15	0.15	(b)
coarse woody debris carbon (kgC/m2)	0.03	0.037	0.037	(b)
litter carbon, labile pool (kgC/m2)	0.1792	0.1984	0.1984	(f)
litter carbon, unshielded cellulose pool (kgC/m2)	0.1232	0.1364	0.1364	(f)
litter carbon, shielded cellulose pool (kgC/m2)	0.1232	0.1364	0.1364	(f)
litter carbon, lignin pool (kgC/m2)	0.1344	0.1488	0.1488	(f)
soil carbon, fast microbial recycling pool (kgC/m2)	0.01	0.01	0.01	(g)
soil carbon, medium microbial recycling pool (kgC/m2)	0.05	0.05	0.05	(g)
soil carbon, slow microbial recycling pool (kgC/m2)	1.14	0.3	0.3	(g)
soil carbon, recalcitrant SOM soil carbon, recalcitrant SOM (slowest	7.5	1.04	1.04	(g)
litter nitrogen, labile pool (kgN/m2)	0.073	0.048	0.064	(h)
soil nitrogen, mineral pool (kgN/m2	0.6	0.28	0.31	(h)

(a) Calculated as mean values in the first 0.5m of soil from BOREAS field data RSS08. (b) Field data, BOREAS RSS08. (c) Typical value. (d) Calculated from 144mm of snow. (e) Field data, BOREAS HYD01. (f) RSS08: calculated as litter carbon*correspondent fraction. (h) Calculated from TE01(See Appendix). (g) Total soil C was available from RSS08, this amount was distributed among the 4 pools using stabilisation values after 5 years spin-up running of the model.

Table 4.13: BiomeBGC input parameters, ecophysiological constants file

Parameter	OBS	OJP/YJP	Comments
transfer growth period as fraction of growing season	0.3	0.3	RSS08
litterfall as fraction of growing season	0.3	0.3	RSS08
annual leaf and fine root turnover fraction	0.25	0.25	White et al., 2000
annual live wood turnover fraction	0.70	0.70	White et al., 2000
annual whole-plant mortality fraction	0.005	0.005	White et al., 2000
annual fire mortality fraction	0.005	0.005	White et al., 2000
Allocation: new fine root C : new leaf C	1.0	1.0	White et al., 2000
Allocation: new stem C : new leaf C	2.00	2.22	White et al., 2000
Allocation: new live wood C : new total wood C	0.1	0.059	White et al., 2000
Allocation: new croot C : new stem C	0.29	0.29	White et al., 2000
Allocation: current growth proportion	0.5	0.5	White et al., 2000
C:N of leaves(kgC/kgN)	41.3	40.3	White et al., 2000
C:N of leaf litter, after retranslocation(kgC/kgN)	50.5	103.0	White et al., 2000
C:N of fine roots (kgC/kgN)	59.2	59.2	White et al., 2000
C:N of live wood(kgC/kgN)	59.2	59.2	White et al., 2000
C:N of dead wood(kgC/kgN)	730.0	660.0	White et al., 2000
leaf litter labile proportion	0.31	0.31	White et al., 2000
leaf litter cellulose proportion	0.45	0.45	White et al., 2000
leaf litter lignin proportion	0.24	0.24	White et al., 2000
fine root labile proportion	0.24	0.24	White et al., 2000
fine root cellulose proportion	0.42	0.42	White et al., 2000
fine root lignin proportion	0.34	0.34	White et al., 2000
dead wood cellulose proportion	0.725	0.72	White et al., 2000
dead wood lignin proportion	0.275	0.28	White et al., 2000
canopy water interception coefficient (1/LAI/d)	0.1	0.1	RSS08
canopy light extinction coefficient	0.5	0.5	RSS08
all-sided to projected leaf area ratio	2.2	2.2	RSS08
canopy average specific leaf area (m2/kgC)	9.76	8.2	White et al., 2000
ratio of shaded SLA:sunlit SLA	2.00	2.00	RSS08
fraction of leaf N in Rubisco	0.07	0.07	RSS08
maximum stomatal conductance (m/s)	0.001	0.001	RSS08
cuticular conductance (m/s)	0.00001	0.00001	RSS08
boundary layer conductance (m/s)	0.0008	0.0008	RSS08
leaf water potential: start of conductance reduction (MPa)	-0.6	-0.5	White et al., 2000
leaf water potential: complete conductance reduction (MPa)	-2.8	-1.7	White et al., 2000
vapor pressure deficit: start of conductance reduction (Pa)	1000.0	1000.0	RSS08
vapor pressure deficit: complete conductance reduction (Pa)	4000.0	4000.0	RSS08

Table 4.14: Meteorological Data sources and calculations (Γ represents field data)

Model Parameter	BOREAS Source[a]	Field Units	JULES Units	Conversion
Downward Solar Radiation	AMS_A_94[b]	W/m^2, 15 mins avg	W/m^2, 30 mins avg	$\frac{\Gamma_{1\,15min}+\Gamma_{2\,15min}}{2}$
Downward Longwave Radiation	AMS_B_94[c]	W/m^2	W/m^2	$\frac{\Gamma_{1\,15min}+\Gamma_{2\,15min}}{2}$
Rainfall rate[d]	AMS_A_94[b]	mm/15min	kg/m^{2}s	$\frac{\Gamma_{1\,15min}+\Gamma_{2\,15min}}{30\times60}$
Snowfall rate[e]	AMS_A_94[b]	mm/15min	kg/m^{2}s	$\frac{\Gamma_{1\,15min}+\Gamma_{2\,15min}}{30\times60}$
Temperature[f]	AMS_A_94[b]	Degrees Celsius	Kelvin	Γ +273
Southerly wind speed	AMS_A_94[b]	m/s	m/s	$\frac{\Gamma_{1\,15min}+\Gamma_{2\,15min}}{2}$
Easterly Wind Speed	AMS_A_94[b]	Westerly m/s	m/s	$\frac{\Gamma_{1\,15min}+\Gamma_{2\,15min}}{2}$
Surface Pressure	AMS_A_94[b]	kiloPascals	Pa	$\frac{1000*(\Gamma_{1\,15min}+\Gamma_{2\,15min})}{2}$
Specific humidity	AMS_A_94[b]	Relative Humidity (%)	Kg/Kg	Conversion[g]

[a]Data in this table was extracted from BOREAS AFM-07 SRC Surface Meteorological and Radiation Data.
[b]AMS_A_94 dataset corresponds to Suite A stations, equipped to measure basic meteorological and radiation parameters. The Suite A radiation sensors measured shortwave and net radiation, PAR, and longwave radiation.
[c]AMS_B_94 dataset corresponds to Suite B stations. Suite B sensors consist of a diffuse shortwave radiation sensor and a pyrgeometer measuring incoming and outgoing longwave radiation.
[d]kg/m^2s is equivalent to mm/s
[e]Accumulated precipitation at temp < 0°C was considered snow
[f]Temperature was measured as average of within canopy temperature.
[g]Specific humidity of air at air temperature is given by
$q_a = \frac{0.62e_a}{p-0.38e_a}$
where p is atmospheric pressure (mb) and e_a is the vapor pressure of water that can be calculated from air temperature (T_a) and relative humidity (r_h) as:
$e_a = 0.01 \times r_h 10\text{^}\frac{0.7859+0.03477T_a}{1.0+0.00412T_a}$

Table 4.16: JULES initialisation data

Model parameter	OBS	OJP	YJP	Comments
ntiles,can_model	9,3	9,3	9,3	9 tiles, rad. canopy model with heat capacity
rad_type	1	1	1	Downward solar and Longwave radiation
can_rad_mod, ilayers	3,10	3,10	3,10	Veg. canopy rad. model 3, 10 layers
l_spec_albedo	T	T	T	Spectral albedo
l_phenol,l_triffid,l_trif_eq	F,F,F	F,F,F	F,F,F	No phenol,TRIFFID or Equilibrium models
l_vg_soil,l_point_data	T,T	T,T	T,T	Van Genuchten soil hydraulic model model, Driving data are point data
l_cosz,l_julian,l_360	T,F,F	T,F,F	T,F,F	SZ cosine calculated, month-day format, 365 days year
iyear,ijulian,imonth,iday	1994,-1,1,1	1994,-1,1,1	1994,-1,1,1	year, julian day,month and day at start of run
UTC_secs_init	-50400	-50400	-50400	Time of day(secs) at start[1] (00:00)
latitude,longitude	53.99,105.122	53.91,104.692	53.87,104.65	Latitude, Longitude
timestep,nsteps	1800.0, 17520	1800.0, 17520	1800.0, 17520	Time step 30 min=met data
phenol_period,triffid_period	1,1	1,1	1,1	Not used
print_step	48	48	48	Print every time step: 48 for daily
co2_mmr	5.38529e-04	5.6132e-04	5.81738e-04	CO2 mass mixed ratio (see calculation)
sm_levels	4	4	4	Number of soil layers: typical value
dzsoil(1:sm_levels)	0.1, 0.25, 0.65, 2.0	0.1, 0.25, 0.65, 2.0	0.1, 0.25, 0.65, 2.0	Thickness of each soil layer: typical values
zsmc,zst	1.0,1.0	1.0,1.0	1.0,1.0	Depth of soil (for moisture, for temperature): sum of soil layers
meteorological d.file	File	File	File	Calculated with MTCLIM
readTimeStamp,read2Wind	F,T	F,T	F,T	Use double wind component (east/north wind speed)
z1_uv, z1_tq	20,20	20,20	20,20	Height of measurements
frac(1:ntype)	0, 1.0, 0, 0, 0, 0, 0, 0, 0	0, 1.0, 0, 0, 0, 0, 0, 0, 0, 0	0, 1.0, 0, 0, 0, 0, 0, 0, 0	Fraction of each cover type: BT, NT, C3G, C4G, Shr, Urb, Wat, Soil, Ice. Only Neddle trees.
canopy(1:ntiles)	9*0.0	9*0.0	9*0.0	Water held in canopy kg/m2
cs	8.7	1.4	1.4	Initial soil C (kg/m^2), Kimball et al., 1997b
gs	0	0	0	Initial surface conductance(m/s)
rgrain(1:ntiles)	9*50.0	9*50.0	9*50.0	Ini. grain size of snow(mm) typ. value
stheta(1:sm_levels)	0.7, 0.5, 0.5, 0.5	0.3, 0.2, 0.2, 0.2	0.3, 0.2, 0.2, 0.2	Soil water content for each layer(0-1) as % of sat. Estimated initial conditions.
snow_tile(1:ntiles)	9*7	9*7	9*7	[2]Snow amount for each tile (kg/m^2)
snow_grnd	7.0	7.0	7.0	[2]Snow amount on the ground (kg/m^2)
t_soil(1:sm_levels)	248.4,267.22,267.85,269.58	248.4,267.22,267.85,269.58	248.4,267.22,267.85,269.58	Temp. of each soil layer: field data (AMS_A)
tstar_tile(1:ntiles)	9*248.4	9*248.4	9*248.4	Temp. of each tile (=surface temp)
canht_ft(1:npft)	0,8.9,0,0,0	0,14.2,0,0,0	0,4.5,0,0,0	Canopy height(Leblanc et al., 1999)
lai(1:npft)	0, XX, 0, 0, 0	0, XX, 0, 0, 0	0, XX, 0, 0, 0	LAI: changed on running
b (1:sm_levels)	4*3.57	4*1.78	4*2.63	N fitting parameter of the van Genuchten (HYD1[3])
sathh (1:sm_levels)	4*0.294	4*0.128	4*0.145	ALPHA fitting parameter of the van Genuchten (HYD1[3])
satcon (1:sm_levels)	0.00914	0.0169	0.0215	Hydraulic conductivity at saturation (kg/m^2s) (Calculated from HYD1)[3]
smvcst (1:sm_levels)	0.51, 0.17, 0.083, 0.09	0.4, 0.239, 0.095, 0.128	0.32, 0.23, 0.098, 0.064	Volumetric soil moisture content at saturation: field data Calculated from HYD1)[3]
smvccl (1:sm_levels)	0.15, 0.056, 0.021, 0.03	0.0468, 0.0294, 0.0118, 0.0125	0.0715, 0.0487, 0.0219, 0.0137	Volumetric soil moisture content, critical p. From Moisture at -33kPa Calculated from HYD1,)[3]
smvcwt (1:sm_levels)	0.05, 0.022, 0.013, 0.012	0.0255, 0.0157, 0.0081, 0.0074	0.037, 0.0213, 0.0127, 0.0089	Volumetric soil moisture content, wilting p. From Moisture at -1500kPa Calculated from HYD1)[3]
hcap (1:sm_levels)	1.5e6	1.8e6	1.8e6	Dry heat capacity: Typical values
hcon (1:sm_levels)	0.33	0.35	0.35	Dry thermal conductivity: Typical values
albsoil	0.1	0.1	0.1	Soil albedo (Kimbal 1997)

[1]Start time was midnight 1 Jan 1994, 7 hours of difference to UTC.[2]Assuming snow water content= 5%, 144mm of snow.[3] Data collected by Richard Cuenca, Shaun Kelly, and David Stangel as part of the HYD-1 investigation of the BOREAS Project. See Appendix for calculations. Typical values were calculated assuming that OBS soil is a sandy loam soil and YJP and OJP are sand soils (HYD1).

Chapter 5

Sensitivity analysis of spectral and directional capabilities

This chapter presents a sensitivity analysis of simulated TOARs to spectral and directional capabilities for a set of biophysical parameters.

The parameters considered are the key indicators previously selected: leaf area index (LAI), fraction of absorbed of photosynthetically active radiation (fAPAR), chlorophyll a+b content (Cab), fractional cover (FC) and aerosol optical thickness (AOT). Accuracy requirements defined from the ecological model BIOME-BGC, and extracted from the literature for each of the parameters are used to establish the minimum sensitivity required from the instrument.

The sensitivity of TOARs to the parameters is analysed over different spectral and directional sampling configurations. A preliminary test is made to demonstrate the major information content of the principal plane, comparing the variance of the signal in this plane to that obtained at other planes in which satellite data can be collected.

The aim of this study is to identify the most beneficial geometries as well as the spectral bands containing maximum information. Results of this study will be used for the final study presented in Chapter 6.

5.1 Methodology

Typically, TOARs retrieved by satellite sensors are used to estimate biophysical parameters that can be later used to drive ecological models (e.g. Ehrlich et al., 1994; Knyazikhin et al., 1998b; Dawson, 2000). The method presented here follows these

steps in reverse order, starting from the definition of the accuracy requirements at the model output to constrain the uncertainty of the input parameters and, finally, the sensitivity of the instrument.

The NPP estimated by the BIOME-BGC model is used as the starting point for this process. Figure 5.1 presents the method used to link the NPP accuracy requirements with satellite instrument specifications.

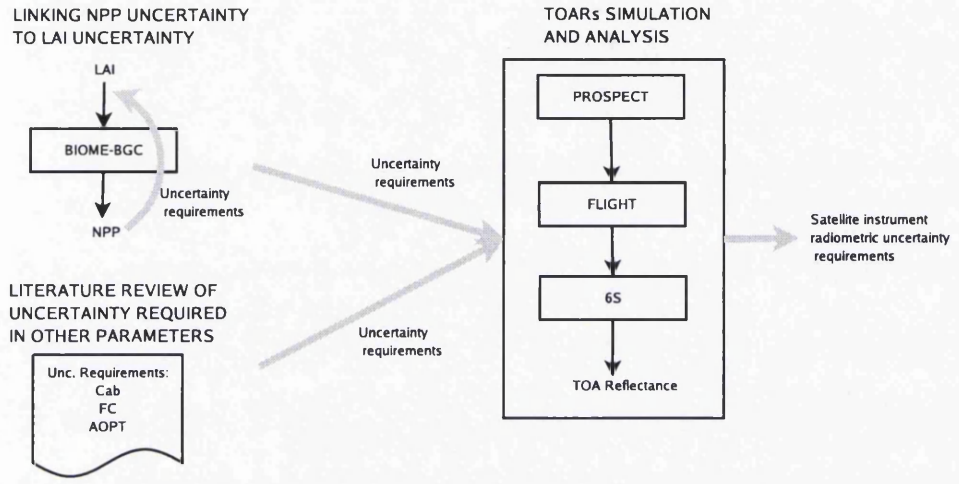

Figure 5.1: Methodology proposed to link biophysical uncertainty requirements to instrument radiometric specifications.

Accuracy requirements are defined by the requirements at the output of the model and by the literature. LAI constrains the maximum rate of carbon uptake in BIOME-BGC so that a relationship between NPP and LAI can be established. fAPAR is linked to LAI in the model so it cannot be studied independently. The other parameters considered in the study - Cab, FC and AOT - are not used as inputs in BIOME-BGC but strongly affect the accuracy at which LAI can be retrieved. These parameters are also included in the simulation to account for the interaction effect.

NPP accuracy requirements are related to input LAI by variations over a base case LAI value. The base case is calculated as the mean of the field data values for each site. This base case value is distorted in a range between $\pm 50\%$ at steps of 10% and the resultant values are used to drive BIOME-BGC. The results provide an estimation of the relationship between errors on estimated NPP and errors on LAI inputs so that LAI accuracy requirements can be defined based in NPP especifications.

Base case values are also established for Cab, FC and AOT based on *in situ* data. A factorial experiment is then performed in which all the parameters are perturbed by a certain percentage, based on the requirements previously established, in order to detect both individual and interaction effects on TOAR.

A merit-of-change value is used to represent the difference between the TOAR for the base-case (all the input parameters with their base-case value) and for each perturbation at each wavelength. This merit value is calculated as:

$$M = |\rho_{base} - \rho_{dist}| \tag{5.1}$$

where ρ_{base} is the TOAR for the base case and ρ_{dist} is the TOAR for the distorted case (one or more input parameters distorted) for a given sun-sensor-target geometry and for an specific wavelength. The resulting merit value corresponds to the radiometric accuracy that the instrument should have at that wavelength to be able to detect changes on the parameters greater or equal to the perturbation value used.

The sun sensor geometry strongly affects the signal received by the sensor (Barnsley et al., 1997). Ideally we would like to work with the geometry that provides more information. The first step is to define which plane of the viewer-sensor geometry contains more information in order to limit our study to it. The information content of each spectral and directional sampling case is analysed in terms of the variability of the merit-of-change function. A preliminary analysis of the standard deviation of this function is made in different planes defined by the viewer-sensor geometry. The coupled models (PROSPECT, FLIGHT and 6S) are used to simulate TOARs in three possible plains defined by the relative azimuth angles: principal plane (0° and 180°), cross plane (90°), and transversal plane (45° and 135°). The aim is to confirm that the principal plane is the optimal plane for the retrieval of the parameters (Privette et al., 1996b).

The merit-of-change function is then calculated for the whole optical spectrum (400nm-2500nm) only in the principal plane. Results are used to choose the most relevant wavelengths for further analysis.

Finally, the merit-of-change function is used to asses the information content of different sun-sensor geometries, only in the principal plane and for the subset of wavelengths selected in the previous stage.

5.2 Input data

Input parameters used for each of the models and their sources are presented in Table 5.1. Values for the biophysical parameters analysed correspond to the base case.

Table 5.1: Site parameters and sources

		OBS	OJP	YJP	Source
PROSPECT	N	2.64	2.53	2.08	Bicheron and Leroy, 1999
	Cab (μg/cm2)	46.5	55.7	39.4	Bicheron and Leroy, 1999
FLIGHT	Crown Closure(%)	42	31	43	Leblanc et al., 1999
	Crown Radius (m)	0.45	1.3	0.85	Leblanc et al., 1999
	Crown center to top dist. (m)	9	7.2	4	Leblanc et al., 1999
	Min height to first branch (m)	0.49	6.9	0.49	Leblanc et al., 1999[1]
	Max height to first branch (m)	0.51	7.1	0.51	Leblanc et al., 1999[1]
	LAI	5.6	2.4	2.8	Gower et al., 1997
	DBH (m)	0.07	0.13	0.03	Gower et al., 1997
6S	Atmospheric model	Subarctic summer			Correspondant to the simulated latitude
	Aerosol model	Biomass			Grey et al., 2006

[1]Leblanc et al., 1999 gives mean height to first branch, maximum and minimum are calculated as mean$\pm 0.1m$

5.2.1 Input parameter ranges

The uncertainty of the input parameters is simulated through the distortion of the base cases. The maximum uncertainty acceptable for each input parameter is used to define the percentage of distortion for each case.

NPP requirements can be defined based on the estimate of anthropogenic effect. Global terrestrial NPP has been estimated at about 60 PgC/yr and the average value of global emissions from fossil fuel burning and cement production in the 1990s was 6.3 ± 0.4 PgC/yr (IPCC, 2001). Therefore, we define a useful estimate of NPP to be within an uncertainty of at most 10%.

One of the systematic observations needed to reduce uncertainty in direct and indirect radiative forcing are satellite measurements of aerosol optical thickness. It has been

suggested that a value of 10% for aerosol optical thickness accuracy over the land is needed (Mishchenko et al., 2004).

About 10 to 30% of the current total anthropogenic emissions of CO_2 are estimated to be caused by land-use change; fraction of cover measurements provide some information on this change. No requirement was found on the literature and as a change in fraction cover of less than 10% is difficult to verify both by field or remote sensing measurements (Asner, 1998) this value was used in the study.

No references were found in the literature either to optimal values of chlorophyll content estimation. However it has proved to be of great importance in the estimation of NPP (Dawson et al., 2003). For a particular LAI, different values of foliar chlorophyll content lead to different remotely-sensed estimates of fAPAR, while the actual canopy fAPAR value remains relatively constant. In the study by Dawson et al., 2003 uncertainties of 47% were obtained in the estimation of fAPAR for Cab values ranging between $\pm 1 std.dev.$ of the mean value. An accuracy value of 10% is used in this study as useful in the estimation of chlorophyll content.

Based on these requirements, each parameter is perturbed by a value equal to the accuracy required on the estimation ($\pm$10%). The spectral range between 400nm and 2500nm is sampled every 10nm giving a total 211 bands. Solar and viewing zenith angles are sampled at intervals of 10°. Ranges sampled are presented in Table 5.3.

Table 5.3: Range of parameters used in the generation of spectra

Parameter	Values
Solar zenith angle	30°... 70° at 10° intervals
View zenith angle	0°... 80° at 10° intervals
Relative azimuth angle	0°, 180° (Pcpal. plane)
Wavelengths	400-2500nm (every 10nm, 211 channels)
LAI	$\pm$10%
Cab	$\pm$10%
FC	$\pm$10%
AOT	$\pm$10%

5.3 Results

5.3.1 Azimuthal sampling analysis

Standard deviation of the TOARs simulated is represented at each wavelength (Figure 5.2). Results conclude that major variability occurs in the principal plane, specially in the visual and NIR spectrum where differences are up to 15% higher than in the cross plane and 20% higher than in the transversal plane.

5.3.2 BIOME-BGC Sensitivity analysis

BIOME-BGC was driven with the base-case LAI for each site and the resultant NPP was considered the real value. Errors on NPP estimations were hence calculated as the difference between the output of the base case and the output with the distorted LAI. The percentage of error on the estimated NPP is represented against the percentage of distortion of the input LAI in Figure 5.3. Results show similar patterns in the three cases. Absolute values were used in the NPP axis to emphasize the major error induced at lower values of LAI.

It is clear that the larger the LAI, the less sensitive the results are to errors in LAI estimation. At larger LAI the fraction of sunlit leaves decreases and that of shaded leaves increases, reducing the sensitiyity of canopy photosynthesis. This effect was particularly clear in the case of the OBS (LAI = 5.6) where an error of 50% on the estimation of LAI corresponds to an error of 20% in the NPP predicted by the model. The relationship can be approximated by a linear function so that to achieve the 10% accuracy proposed for the NPP, a mean value of LAI error of 10% was estimated.

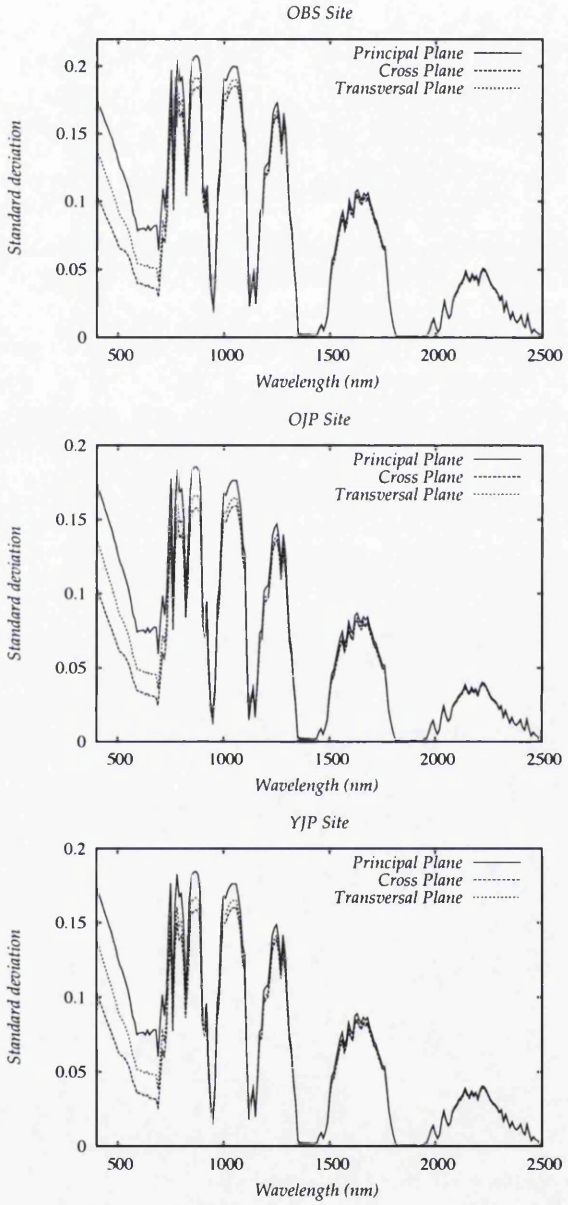

Figure 5.2: Standard deviation of the TOA reflectances at each site in the principal, cross and transversal planes.

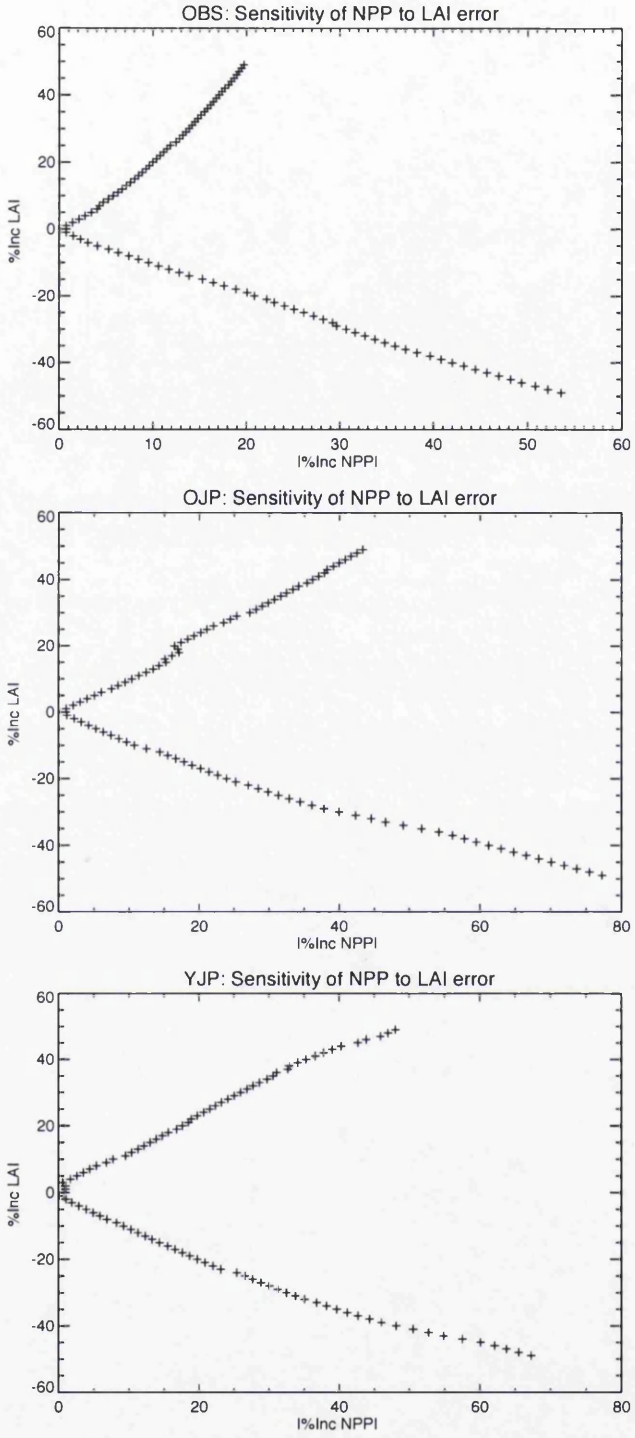

Figure 5.3: Sensitivity of NPP estimation to error in LAI for three forest sites (NPP is presented in absolute value)

5.3.3 Radiometric requirements analysis

The merit function was calculated for each case simulated and represented against wavelength (Figure 5.4).

As was expected, water absorption bands (around 940nm, 1100nm, 1450nm, 1950nm and 2500nm) and carbon dioxide absorption bands (1400nm, 1600nm and 2000nm) strongly affected the top of the atmosphere reflectance reducing the sensitivity to land surface signal to the point of making the reflectances of the different cases indistinct. Excluding those absorption bands, it can be noted from Figure 5.4 that the smaller spectral variability occurs both at the lowest and at the highest wavelengths of the spectrum. At low wavelengths the signal is highly affected by Raleigh scattering (caused by molecules much smaller in diameter than the wavelength of the light). In fact, TOAR registered at 440nm was almost completely due to the atmosphere effect (top of the canopy values around 0.8% produced a TOA reflectance around 15%). The shortwave infrared (SWIR) bands are sensitive to leaf water content, but this parameter was constant during the simulation which could explain the low variations obtained. 15 bands were extracted from these 211. At each part of the spectrum (VIS, NIR and SW) the wavelengths presenting higher merit function values were chosen. The final set of channels used is presented in Table 5.4.

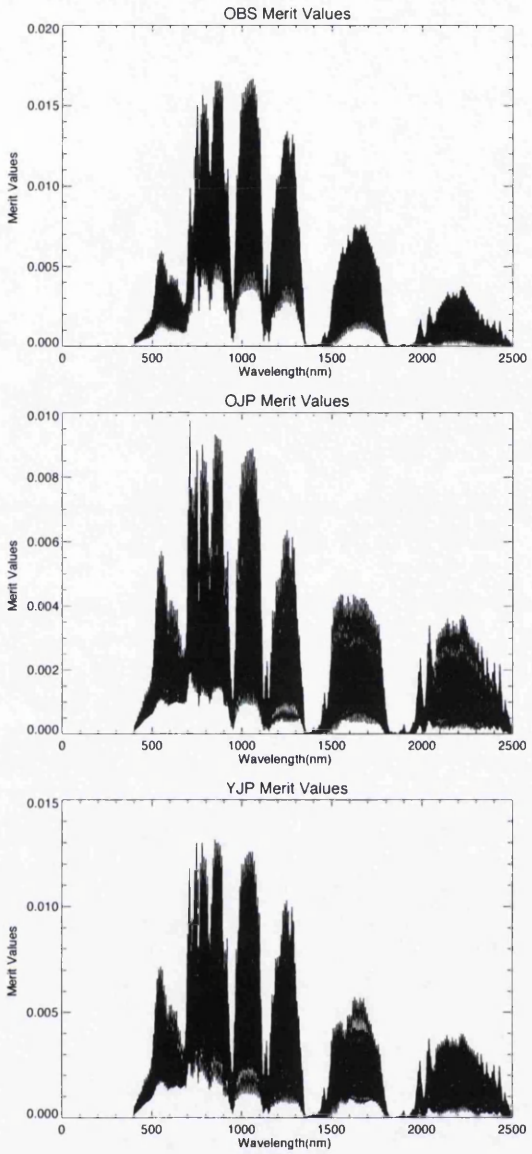

Figure 5.4: Merit-of-change values at each site in the full spectrum (400nm-2500nm) for all the cases simulated in the factorial experiment. The merit function gives the instrument sensitivity required to detect 10% change in the biophysical parameters.The over plotting of all the cases gives an impression of the range of variability at different wavelengths.

The reflectance variability was higher in the near infrared (NIR, 700-1300nm) due to the leaf effects as have been reported in previous studies (e.g. Asner, 1998). To distinguish the simulated reflectances in this region of the spectrum, i.e. to detect a 10% change in the parameters, minimum absolute radiometric accuracy requirement ranges between 0.001 for the OJP site and 0.004 for the OBS site.

The aerosol effect was very small as the base case aerosol optical thickness value used corresponds to very clear sky (0.05). Comparison of TOA reflectance at different view-

Table 5.4: Set of bands used

Band ID	Wavelength (nm)	Spectrum	Sensitivity Level [a]
1	440	VIS	14
2	500	VIS	20
3	560	VIS	34
4	630	VIS	28
5	690	VIS	25
6	700	VIS	40
7	740	NIR	59
8	790	NIR	64
9	830	NIR	53
10	870	NIR	70
11	1035	NIR	66
12	1200	NIR	38
13	1250	NIR	48
14	1650	SWIR	26
15	2100	SWIR	14
16	2250	SWIR	14

[a]Sensitivity Level represents the Mean merit function value for the three sites, multiplied by 10.000 to get an integer.

ing angles did not show clear differences that could be related to the aerosol content as would be expected because of the different atmospheric path lengths. Mean merit-of-change values for each of the forests studied are shown in Figure 5.4.

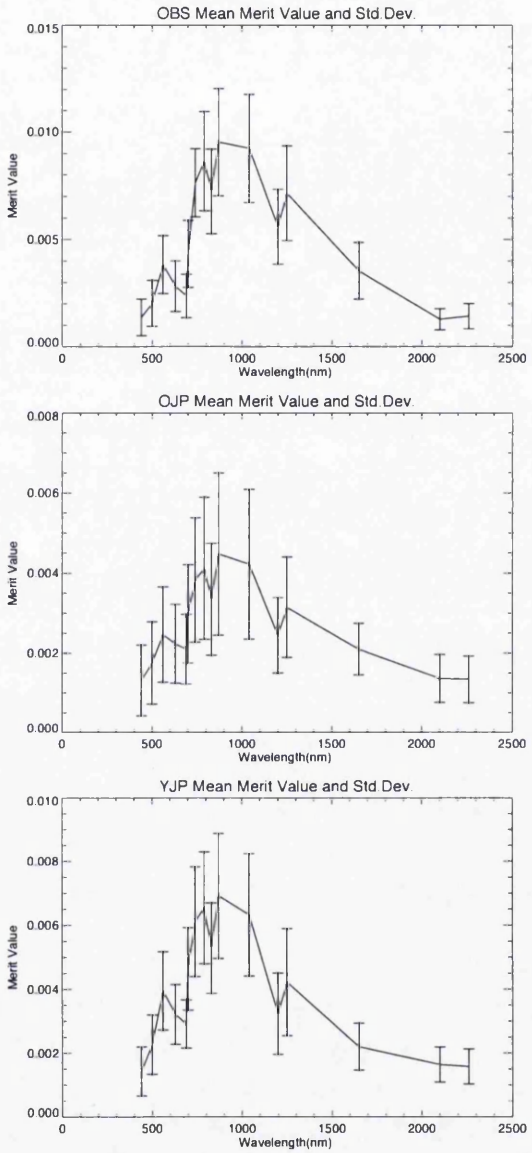

Figure 5.5: Mean merit-of-change values at each site at for the 16 wave bands choosen. Error bars show $\pm\sigma$ due to different solar zenith angles.

The graph shape is similar for the three cases and resembles slightly the spectral reflectance curve of the TOA reflectance. OJP presents the lowest value which implies that a higher accuracy will be required on the measurements in order to distinguish between cases. This is due to the sparser distribution of trees in this site, presenting also the lower LAI of the sites studied. As result, understory, composed of mixtures of lichens, mosses and short herbs, has a strong effect on the signal smoothen-

ing TOAR effects due to the analysed parameters. In general the NIR region and the green peak (560 nm) presented the highest values which means that less radiometric accuracy is required to detect changes at those wavelengths. OJP site requires mean absolute radiometric accuracy of approximately 0.0045 ± 0.002 at 870 nm while values of 0.0069 ± 0.002 and 0.0095 ± 0.0025 were obtained for the YJP and OBS sites respectively. The green peak requires radiometric accuracies of 0.0038 ± 0.0013 for YJP and OBS. The spectral difference is smaller at the OJP site with a mean value of 0.0025 ± 0.0012.

5.3.4 Optimal directional sampling

When comparing merit-of-change values for each view zenith angle, (Fig. 5.6) nadir view and near the hot-spot (sun behind the sensor) directions present the highest sensitivities. In the visible wavelengths the nadir view attained improved estimates with requirements of 0.0011 ± 0.001 at 550nm while other viewing angles sensitivity was lower by a factor of ten. Figure 5.5 corresponds to variations of the parameters in the ranges analysed while Figure 5.6 shows the specific case of LAI error between 0% and 50%.

The best retrieval was obtained at viewing angles around the hot-spot in the near infrared with values up to 0.0116 ± 0.002 at 870nm for the OBS compared to values of 0.0052 ± 0.002 at nadir for the same wavelength. Thus, directional sampling in the principal plane and near the hot spot and at nadir directions appeared to be optimal for biophysical variable estimation.

5.3.4.1 AOT analysis

The sites analysed presented clear atmospheres during the field campaigns so low values of AOT have been used in the study. The effects of higher AOT values and of errors on their estimation are analysed here for one of the sites (OBS).

The effect of errors on AOT estimation is analysed by relating them to the shortwave irradiance derived by the atmospheric radiative transfer model. 6S model provides estimations of solar, diffuse and environmental irradiance for specific surface albedo. Shortwave irradiance (between 400 and 4000nm) is calculated as the sum of these three components assuming an albedo of 0.1, for AOT values ranging between 0.05 (clear atmosphere) up to 0.8 (hazy atmosphere). Irradiance errors are then calculated as deviations from the base case (AOT=0.05). Daily irradiance values used in the meteorological input data file are distorted in a percentage according to these errors

Figure 5.6: Merit-of-change values for the OBS site at each wavelength, SZA=30°

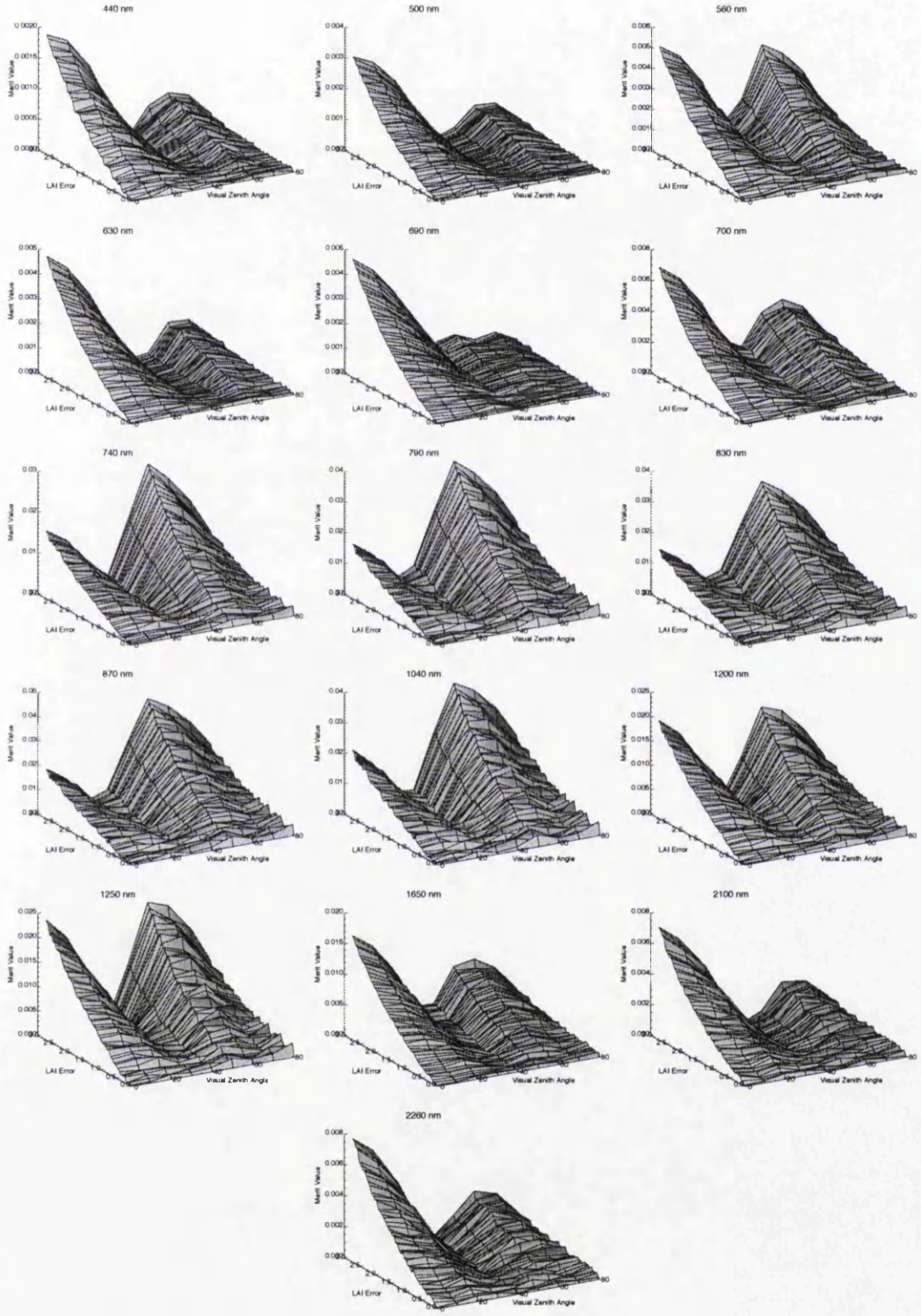

x axis: Variation in visual zenith angle 0°-80° in the backscattering direction

y axis: LAI error between 0 and 50%

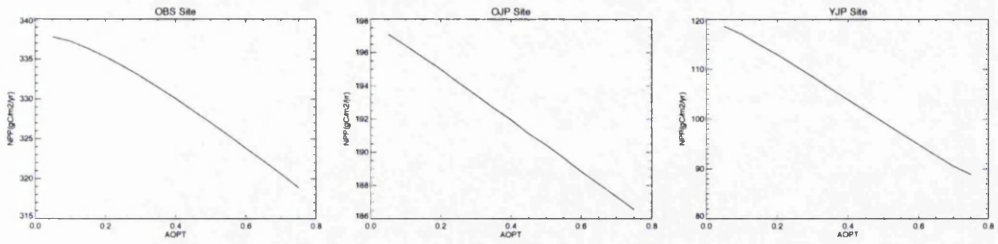

Figure 5.7: AOT-NPP dependence on the three sites

and used to run BIOME-BGC. This allows us to analyse the effect of errors on the estimation of AOT on the NPP retrieved. BIOME-BGC original code was used in this analysis (i.e. without the modification used in Chapter 6 and presented in Appendix A).

The three cases analysed present very similar behaviour. All show a decrease on the NPP at higher AOT. A high value of AOT represents less direct light transmission so less radiation reaches the surface. Nevertheless, studies have shown that light use efficiency increases with diffuse light (Alton et al., 2005), a phenomenon not considered in BIOME-BGC. The results, therefore, are representative of the sensitivity of the model to the errors on AOT estimations but not of the real effect of an increase in aerosols on NPP.

Table 5.5: RMSE of the NPP estimated by BIOME-BGC under the AOPT error assumptions (calculated from the base case: AOPT=0.05)

	RMSE		
AOPT	OBS	OJP	YJP
0.1	0.71	0.79	1.80
0.15	1.83	1.62	4.50
0.2	3.10	2.46	6.80
0.25	4.55	3.36	9.23
0.3	6.10	4.22	11.66
0.35	7.78	5.07	14.24
0.4	9.49	5.88	16.82
0.45	11.32	6.81	19.42
0.5	13.12	7.58	21.98
0.55	14.92	8.40	24.54
0.6	16.79	9.25	27.04
0.65	18.58	10.14	29.43
0.7	20.43	10.95	31.74
0.75	22.33	11.77	33.14

Analysing the RMSE in reference to the base case (AOT=0.05) YJP site is the most sensitive with RMSE ranging between 1.8 and 33.14 (Table 5.5).

5.4 Conclusion

It has been demonstrated that the principal plane provides most information. The results also show that some view angles (nadir view and near the hot-spot direction) are more sensitive to changes in biophysical parameters. The radiometric accuracy can be reduced by an order of magnitude compared with other sun-sensor geometries. As was expected NIR showed higher spectral variability in vegetated areas. NIR showed the lowest requirements in terms of radiometric accuracy with values ranging between 0.0045 ± 0.002 and 0.0095 ± 0.0025 at 870nm. These wavelengths are optimal for the retrieval of biophysical parameters according to the result obtained. Clear sky condi-

tions were used and as a consequence the effects of atmospheric scattering by aerosols was not significant at the different sun-sensor geometries.

This methodology allowed us to analyse satellite instrument requirements in terms of radiometric accuracy and satellite-sun geometry. Results in terms of spectral and angular sampling will be used in next chapter for the analysis of different satellite configurations.

Chapter 6

Retrieval of biophysical parameters and NPP estimation by different satellite configurations

The aim of this chapter is to develop and apply a methodology to relate the requirements of ecological models with satellite capabilities by analysing specific instrument configurations.

Biophysical parameters are estimated using a look-up-table approach and considering different sets of viewing angles, spectral channels and radiometric noise.

6.1 Methodology

The methodology used in this study was introduced in Chapters 3 and 4. The basic idea is to simulate the estimation of parameters from well known scenes under different satellite instrument configurations and use them to run the ecological models.

The LUT technique is used in this study beause it permits a quick inversion of the models, as the calculations are done only once, and provides the flexibility required to test the different instrument configurations in terms of spectral and angular sampling.

The LUT is implemented in three stages. Firstly, the parameters space of canopy is sampled for several sun-sensor geometries. The ranges and density of sampling are defined at this point. Secondly, for each combination of canopy parameters, top of the atmosphere reflectances are computed and stored in the LUT. This is achieved by coupling the three models (PROSPECT, FLIGHT and 6S). Finally, the LUT is used to

retrieve the set of parameters correspondent to a series of test data. The test data used are observed TOARs, created with the same arrangement of coupled models as the LUT but with randomly sampled input parameters. These test TOARs are distorted by different levels of Gaussian noise resembling the radiometric noise that affects remote sensing instruments.

The retrieved parameters are then used as inputs in the ecological models. The accuracy of both the retrieved parameters and the NPP estimated by the models are analysed, allowing us to relate the radiometric noise at the instrument to the accuracy of the ecological models estimations. Also the relative performance of each of the instrument configurations is reviewed. The study analyses four instrument configurations corresponding to a high and a low number of viewing angles and spectral channels. Figure 6.1 shows an schematic representation of this methodology.

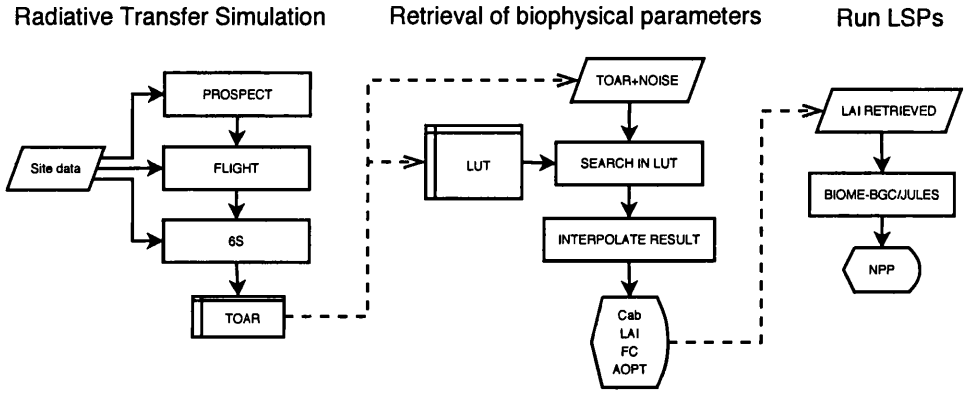

Top-of-the-atmosphere reflectances (TOARs) are simulated by coupling a leaf reflectance model, a canopy reflectance model and an atmospheric radiative transfer model. These TOARs are used to populate a LUT and to create the samples from which we want to retrieve the parameters. Biophysical parameters are retrieved from "noisy samples" by means of the LUT. LAI retrieved are used to drive the ecological models analysing the effects of the different levels of noise on the NPP estimated. This process is repeated for each of the instrument configurations analysed.

Figure 6.1: Diagram of the methodology

6.2 Spectral and directional sampling

Present satellites offer a range of angular and spectral capabilities targeted at different applications. The aim here is to compare single viewing, multiviewing and varying multispectral capabilities, so a minimum and a maximum number of each (viewing angles and spectral channels) will be analysed.

As the visible and near infrared range provides the bulk of information on canopy and leaf reflectance properties, two channels located at those wavelengths are considered

as the minimum requirements for the retrieval of biophysical parameters.

For the maximum case, wavelengths used by present satellites monitoring vegetation properties and by vegetation indices that have proven to be useful on the retrieval of biophysical parameters were considered, as well as bands specifically useful in the retrieval of aerosols. In the previous chapter, a set of 16 bands that showed the maximum sensitivity to the parameters analysed was derived. To make this study less site specific and more related to real present satellites, those bands were used only as a reference and the final set was chosen from wavelengths presently used in real instruments. The instruments analysed are: MISR, AATSR, MODIS, MERIS, POLDER, CHRIS, VEGETATION and AVHRR (Table 6.1).

The final set includes seven bands distributed in the visible spectrum covering chlorophyll absorption (440, 460, 620 and 670nm) and vegetation pigments reflectance (490nm and 550nm), two bands around the red edge (700 and 800nm), 4 in the near-infrared (840, 860, 870 and 900nm) and two more in the shortwave-infrared (1240 and 1600nm).

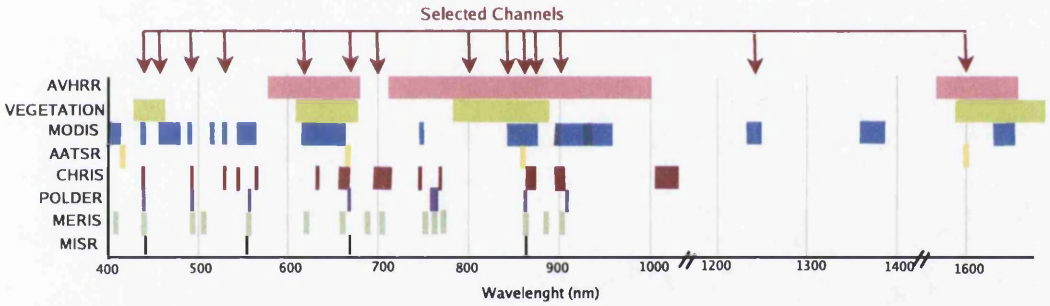

Figure 6.2: Selected channels compared to present satellite channels

Spectral channels used for more than one instrument were crossed with bands used in vegetation indices for the estimation of vegetation parameters (Table 6.3) and with the bands retrieved in Chapter 5. The result was the set of 14 channels presented in Figure 6.2 and described in Table 6.3.

Table 6.1: Present satellite channels

Bands	Description	MISR	AATSR	MODIS	MERIS	POLDER	CHRIS	VEGET	AVHRR
410	Water colour			*	*				
420	Atm. scattering			*					
430								*	
440	Chlor. ab. max.			*	*	*	*	*	
450								*	
460	Soil-Vegetation			*				*	
470	differences			*				*	
480	Water colour			*					
490	Chlor. and org. pigments				*	*	*		
510	Suspended sediments				*				
520	Water Colour			*					
530							*		
540		*		*					
550	Green vegetation		*	*			*		
560	Chlor. absorp. min.	*		*	*	*			
570							*		
580									*
590									*
600	Mapping vegetation								*
610								*	*
620	Vegetation Chlorp abs.			*	*			*	*
630	Land cover Transforms			*			*	*	*
640	Cloud/edge det. mask			*				*	*
650				*				*	*
660	Sediments, atmosphere			*	*		*	*	*
670	Chlorophyl fluorescence	*	*	*	*	*	*	*	*
680								*	*
690							*		
700	Fluo. ref, atm. corrections				*		*		
710							*		
720									*
730									*
740	Aerosol properties			*			*		*
750	Vegetation, cloud				*				*
760	Oxygen abs. R-branch				*	*			*
770	Atmosphere corrections				*				*
780							*		*
790								*	*
800	Mapping vegetation							*	*
810								*	*
820								*	*
830								*	*
840	Cloud/veg./water/edge			*				*	*
850	detection			*				*	*
860	Vegetation Chlorp. abs.	*		*	*	*		*	*
870	(Aerosol & atmop. prop.)		*	*			*	*	*
880	Atmospheric corrections				*			*	*
890	W.vapour/atmosp. props			*			*	*	*
900	W.vapour/atmosp. props			*	*		*		*
910	W vapour/atmosp. prop			*		*			*
920	W vapour/atmosp. prop			*					*
930	W vapour/atmosp. prop			*					*
940	W vapour/atmosp. prop			*					*
950	W vapour/atmosp. prop			*					*
960-1010									*
1020							*		
1050									*
1060									*
1230				*					
1240	Leaf and canopy prop			*					
1250				*					
1360-1390	Cirrus cloud mask			*					
1600	Leaf w cont (850nm)		*						
1630-1650	Snow/clouds			*				*	
2105-2155	Land/cloud properties			*					

Table 6.3: Selected Bands

Band	Wavelength(nm)	Spectrum	Utilitity	Instruments Covered	Indices Covered
1	440	VIS blue	Chlorophyll absorption maximum	MODIS, MERIS, POLDER, CHRIS, VEGETATION	
2	460	VIS blue	Soil/vegetation difference	MODIS, VEGETATION	
3	490	VIS blue	Vegetation pigments	MODIS, POLDER, CHRIS	
4	550	VIS green	Chlorophyll reflectance	MISR, MODIS, MERIS, POLDER	$MTVI_{1,2}$, $MCARI_{1,2}$, MCARI, TCARI, TVI
5	620	VIS red	Vegetation Chlorophyll absorption	MODIS, MERIS, VEGETATION,AVHRR	
6	670[a]	VIS red	Vegetation Chlorophyll absorption	MISR, AATSR, MODIS, MERIS, POLDER, CHRIS, VEGETATION,AVHRR	NDVI, SR, MSR, $MTVI_{1,2}$, RDVI, $MCARI_{1,2}$, SAVI, MSAVI, OSAVI, MCARI, TCARI
7	700	VIS red	Atm. correction, red edge	MERIS, CHRIS	MCARI, TCARI
8	800	NIR	Structural indices	VEGETATION, AVHRR	$MTVI_{1,2}$, RDVI, $MCARI_{1,2}$, SAVI, MSAVI, OSAVI
9	840	NIR	Cloud, vegetation and water edges detection	MODIS, VEGETATION,AVHRR	
10	860	NIR	Vegetation chlorophyll absorption	MISR, MODIS, MERIS, POLDER, VEGETATION,AVHRR	NDWI
11	870[a]	NIR	Aerosol / atmospheric properties	AATSR, MODIS, CHRIS, VEGETATION,AVHRR	NDVI, SR, MSR,
12	900	NIR	Water vapour absorption, vegetation	MODIS, MERIS, CHRIS, AVHRR	
13	1240	SW	Leaf and canopy properties	MODIS	NDWI
14	1600	SW	Leaf water content	AATSR,VEGETATION, AVHRR	

[a]Bands used in 2 bands analysis

The definition of the angular sampling capabilities was also based on existent instruments. Most recent multiview instruments, displayed on Table 6.4), were considered

and the one presenting the maximum number of viewing angles (MISR, Diner et al., 2002) was chosen for the multiview case. The case of one single view was taken as being each of the MISR angles used in isolation. Another option would have been to use the nadir view but this view is not the optimal for the type of landscape analysed here and the results would have been misleading. The chosen option covers instruments with a wide field of view and pointable instruments.

Table 6.4: Most recent multiview satellite instruments

Sensor	Angular Resolution	Multiviewing Sampling Method	Optical Bands
AVHRR	±55	Temporal compilation of across-track	1 VIS, 1 NIR
POLDER	±42	Temporal compilation and very wide fore/afterwards FOV	4 VIS, 4 NIR
MODIS	±55	Temporal compilation of across-track	20 full SW spectrum
MISR	$0, \pm 26.1, \pm 45.6, \pm 60, \pm 70.5$	9 fixed cameras	3 VIS, 1 NIR
CHRIS	$0, \pm 36, \pm 55$	Tilting on along or cross-track directions	up to 62

6.3 LUT

The LUT approach requires construction of a set of precalculated spectral-directional reflectances as a function of the key canopy biophysical properties analysed (Weiss et al., 2000; Combal et al., 2002a). In this section the implementation of the LUT is explained. For simplicity the implementation is divided in three stages: sampling scheme, LUT and test data creation and retrieval technique.

Creation of the LUT

A code in C was created to generate LUTs for any site and for the instrument configuration (viewing angles and spectral channels) and sun-sensor geometries required. The code prepares the input files for the three models used in the simulation of TOAR (PROSPECT, FLIGHT and 6S), calls the models and saves the output TOAR together with the parameters that generated that output. The time to run will be function of the

number of cases simulated times the time of running each of the coupled models. To simplify the process PROSPECT was run offline and leaf reflectance and transmittance values for each Cab value considered were saved to be accesed on execution.

The LUT created has five dimensions correspondent to the five parameters that can potentially be retrieved: Cab, FC, LAI, fAPAR and AOT.

When accessing the LUT for the retrieval of parameters, it is read in memory as a three dimensional matrix indexed by solar zenith angle (SZA), view zenith angle (VZA) and relative azimuth (RA). Each component of this matrix contains a list of stored data with the next structure:

```
struct sample_list {
struct sample_list *next;
float TOAR[NBANDS];
float Cab;
float FC;
float LAI;
float fAPAR;
float AOT;
} ;
```

When accessing the LUT with one viewing zenith angle, one pointer goes through the list that corresponds to the correspondent geometry (SZA, VZA and RA). When accessing the LUT with the 9 viewing angles, 9 pointers go through the lists that correspond to the input SZA and RA. In fact, as only principal plane was simulated, RA is only relevant to define the sign of VZA (RA=0 for VZA>0 and RA=180 for VZA<0).

6.3.1 LUT sampling scheme

The sampling of the data in the LUT will highly affect the accuracy of the retrievals. The objective here is to get an operational LUT sparse enough to allow quick access but dense enough also to provide accurate retrievals.

The ranges in which the parameters are sampled are taken from the field data in order to cover realistic values. Sampling points should be positioned along these ranges to maximise the variability in the parameter space captured in the final LUT. For some parameters, as in the case of LAI, a regular sampling will result in an oversampling of lower values as the reflectance varies rapidly at those values and typically a transformation is applied to linearise the function (Fig. 6.3). This is achieved by applying the

transformation F to each variable x such that the sensitivity of the reflectance to the transformed variable is constant, i.e. :

$$\frac{dr}{dF(x)} = k \tag{6.1}$$

Hence, two points must be taken into account when defining the sampling technique to use: the distribution function of the parameters, to guarantee a uniform sampling, and the number of samples, to guarantee an adequate density of samples.

It must be defined which solar and sensor geometries will be included in the LUT. For the present study solar zenith was sampled regularly in the range presented during the field campaigns which corresponds to the range 40 to 70 degrees. MISR's view zenith angles were chosen to analyse the advantages of multiview capability. Only the principal plane was analysed as it presents the maximum variability as was shown in Chapter 5. This is an ideal situation, in real life relative azimuth depends on the satellite and sun relative positions, but it provides a good reference to analyse the advantages of the different capabilities analysed. Table 6.5 shows the simulated geometries.

Table 6.5: Geometries included in the LUT

Parameter	Angles (degrees)	Comments
Solar Zenith	40, 50, 60, 70	Based on latitude
View Zenith	+/-70.5, +/-60, +/-45.6, +/-26.1, 0	MISR viewing angles
Relative Azimuth	0, 180	Principal Plane

6.3.1.1 Input parameters

Leaf reflectance: PROSPECT input data

Leaf reflectances and transmittances with different levels of chlorophyll content were simulated to populate the LUT. Model parameters fitted in the comparison study presented in Chapter 4 (Cw, Cm and N) were used to parameterise the model.

Chlorophyll content range to be used in the sampling to create the LUT was defined according to field data as shown in Table 6.6.

Canopy reflectance: FLIGHT input data

Main inputs required by FLIGHT are leaf and soil reflectances and structural data.

Leaf reflectances were simulated with PROSPECT. Soil reflectances were taken from the field data. Understory reflectance (Miller et al., 1998) data was used so all materials under the canopy were taken into account. Structural data includes LAI, fraction cover and tree structural characteristics. Stands were simulated as cones. FLIGHT parameters used and their source are displayed in Table 6.6.

Table 6.6: Leaf, stand and atmospheric data for the three sites

	OBS	OJP	YJP	Source
e/c	c	c	c	
Exy (m)	0.45	1.3	0.85	Leblanc et al., 1999
Ez (m)	9	7.2	4	Leblanc et al., 1999
Min_HT (m)	0.49	6.9	0.49	Leblanc et al., 1999
Max_HT (m)	0.51	7.1	0.51	Leblanc et al., 1999
DBH (m)	0.071	0.129	0.032	Gower et al., 1997
Leaf size (m)	0.01	0.01	0.01	Estimation
LAD[1]	[0.15, 0.20, 0.18, 0.15, 0.13, 0.09, 0.05, 0.03, 0.02]			FLIGHT default for coniferous
$LAI_{\text{effective}}$ range	1.03-3.79	0.98-2.04	0.51-2.0	Chen and Cihlar, 1998
C_{ab} range	10.0-32.8	10.7-51.3	10.4-47.9	Middleton et al., 1997b
FC range	25-45	25-45	25-45	Chen and Cihlar, 1996Chen et al., 1999a
Daily fAPAR range	0.77-0.85	0.63-0.72	0.68-0.77	Chen and Cihlar, 1998
AOPT range	0.05-0.15	0.05-0.15	0.05-0.15	Walthall and Loechel, 1999

[1] Measured as angle between normal to leaves and vertical, each value represents the fraction of leaves lying within 10 degree bins from 0 to 90

Leaf angle distribution (LAD) was taken from the default value recommended in the code for spruce. The angle is measured as angle between normal to leaves and vertical and each value represents the fraction of leaves lying within 10 degree bins from 0 to 90.

Effective LAI was used in the canopy radiation model. We need a value that represents

effects on light interaction with the canopy; as the model does not consider clumping within the canopy, effective LAI must be used. The range of values for effective LAI was defined considering maximum and minimum values observed during the three field campaigns (Chen and Cihlar, 1998). Ranges of fAPAR where also extracted from the field measurements in order to check that results were consistent (Chen and Cihlar, 1998).

Fractional cover represents the percentage of area covered by the crowns. Crown closure, defined as the percentage of ground covered by a vertical projection of the outermost perimeter of the crowns in a stand, was used as fraction cover. Two sources were considered to define the sampling range: Chen and Cihlar, 1996 give crown closure for the IFC1 in late spring and Chen et al., 1999a that gives crown closure values estimated from CASI.

The number of photon trajectories in FLIGHT defines the accuracy of the image. A value of 250000 photons was used in a compromise between precision (errors in reflectance values in the order of 0.002 in absolute value, approximately 2% error) and computational cost (mean time of execution 30 secs. per sample).

Atmospheric radiative transfer: 6S inputs

6S model simulates the atmospheric effects on the reflectance. Ground reflectance values at each band obtained from the FLIGHT simulation were used as inputs.

A clear atmosphere was considered based on the results measured during the field campaign (Walthall and Loechel, 1999), so aerosol optical thickness values between 0.05 and 0.15 were used. Subarctic summer atmospheric model and biomass aerosol model were used for the simulation (Grey et al., 2006).

6.3.1.2 Number of samples for the LUT

There is always a trade off between the size of the LUT and the accuracy of the retrieval of parameters. Increasing the LUT size results in a better sampling but it will also require larger computer resources. A preliminary analysis was made to investigate the effect of the size of the LUT on the retrieval of canopy biophysical variables.

The transformation functions proposed by Combal et al., 2002b were used to set the density of probability proportional to the sensitivity of the reflectance to the variable considered. The objective is to provide better sample domains where the reflectance is more sensitive to the considered variable avoiding oversampling of those areas in

which the reflectance does not change so much. Fractional cover shows a linear reflectance output but in the case of LAI and Cab transformations should be applied. Transformations used are showed in Table 6.7 .

Table 6.7: Transformations applied to the parameters in the sampling

Parameter	Transformation
LAI	$exp^{-LAI/2}$
C_{ab}	$exp^{-Cab/100}$
FC	FC
AOPT	AOPT

Figure 6.3 shows the result of the transformation on LAI reflectance for one of the sites. After the transformation, the relationship between TOAR and LAI is linear, this implies that a regular sampling in the horizontal axis will lead to a regular sampling in the vertical axis.

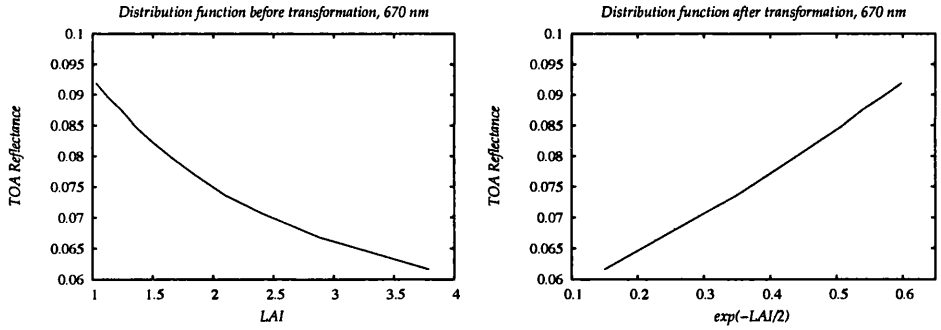

Figure 6.3: Relationship between the top of the atmosphere reflectance and LAI before and after transformation (data from OBS site)

Number of samples

A preliminary study was made with 21 samples of each parameter (FC, Cab and LAI). For AOT only a maximum and a minimum values were considered; those were 0.05 and 0.15 respectively.

TOARs were calculated for a constant AOT value of 0.05 and for 21 sampling points for each of the input parameters. Then subsamples of 11, 6 and 3 sampling points were considered. These correspond to 1, 3 and 9 unsampled values between each pair of sampled values respectively when compared to the 21 samples case. For each case, TOARs were calculated for the unsampled values laying between the sampled

ones as an interpolation and compared to the correspondent modelled values. Both the sampling and the interpolation took into consideration the distribution functions previously defined for each variable.

The experiment was run with a SZA of 40 for all viewing angles considered in the study in the principal plane. One parameter was changed at a time, while the others were kept at default values taken from the mean field values. RMSE was calculated between the simulated spectra and the spectra calculated as interpolation between the two contiguous samples. Sampling values and results of this study are presented in Table 6.8.

Table 6.8: Sampling-interpolation analysis results

		OBS		OJP		YJP	
Parameter	NS	Range	RMSE	Range	RMSE	Range	RMSE
Cab	11	10-32.8	0.0008	10.7-51.3	0.0001	10.4-47.9	0.0002
	6		0.0015		0.0002		0.0004
	3		0.0018		0.0011		0.0015
LAI	11	1.03-3.79	0.0007	0.98-2.04	0.0005	0.51-2	0.0007
	6		0.0010		0.0005		0.0006
	3		0.0030		0.0009		0.0020
FC	11	25-45	0.0009	25-45	0.0011	25-45	0.0009
	6		0.0010		0.0014		0.0009
	3		0.0019		0.0023		0.0018
Default values		Cab=24 FC=42 LAI=2.04		Cab=24 FC=31 LAI=1.77		Cab=24 FC=43 LAI=1.55	

Data collected from field data results BOREAS RSS-07 LAI, Gap Fraction, and fAPAR Data

A value of 6 samples was chosen for almost all the cases. This value provides notably better results that 3 samples while 11 does not seem to improve the estimations a great deal. Only in the case of LAI for the OBS site 11 samples were used, this denser sampling was required as this site presents a wider range of LAI variation.

The result of coupling the models and simulating spectrums for the chosen number of samples was a LUT of 28,512 simulations for the OBS site (~5.5 Mb) and 15,552 simulations for each of the jack pine sites (~3Mb each). Finally it must be pointed that,

while LAI, Cab and FC were directly included in the LUT as input values, fAPAR was calculated using the technique explained in the Methodology chapter (after Privette et al., 1996a) and included later in the LUT.

These LUTs are notably smaller than the ones used in similar studies (e.g. Weiss et al., 2000 used a LUT with 280,000 entries) but the space the canopy realisation is much smaller (e.g. LAI range was between 0 and 8 in Weiss et al., 2000) and they are not generic but site specific tables.

6.3.2 LUT and test data creation

The LUT was created by running the set of coupled models (PROSPECT, FLIGHT and 6S). For each combination of input parameters TOAR was calculated and saved together with the input parameters that generated the spectrum. These values form the LUT that will be used in the inversion for the retrieval of parameters.

The same process was applied to create the test data. A set of TOARs, representing remotely sensed values, was created to be used as input in the inversion. 200 input test data (each at 9 viewing angles) were created by randomly sampling the simulated range for each parameter at each site. These values will be the test data to be searched for in the LUT, i.e. to estimate biophysical parameters correspondent to those spectrums.

Both the LUT and the samples, were created for the case of maximum number of bands and maximum number of viewing angles. During the analysis, only the correspondent subset will be used to analyse each of the configurations considered.

The structure of these subsets for each of the configurations will be as follows:

- 1 viewing angle and 2 bands:

$$R_{sample} = \begin{pmatrix} r_{\lambda_{RED}} & r_{\lambda_{NIR}} \end{pmatrix} \tag{6.2}$$

- 1 viewing angle and 14 bands:

$$R_{sample} = \begin{pmatrix} r_{\lambda_1} & r_{\lambda_2} & \cdots & r_{\lambda_{14}} \end{pmatrix} \tag{6.3}$$

- 9 viewing angles and 2 bands:

$$R_{sample} = \begin{pmatrix} r_{\lambda_{RED}}(\Omega_1) & r_{\lambda_{NIR}}(\Omega_1) \\ r_{\lambda_{RED}}(\Omega_2) & r_{\lambda_{NIR}}(\Omega_2) \\ \vdots & \vdots \\ r_{\lambda_{RED}}(\Omega_9) & r_{\lambda_{NIR}}(\Omega_9) \end{pmatrix} \tag{6.4}$$

- 9 viewing angle and 14 bands:

$$R_{sample} = \begin{pmatrix} r_{\lambda_1}(\Omega_1) & r_{\lambda_2}(\Omega_1) & \cdots & r_{\lambda_{14}}(\Omega_1) \\ r_{\lambda_1}(\Omega_2) & r_{\lambda_2}(\Omega_2) & \cdots & r_{\lambda_{14}}(\Omega_2) \\ \vdots & \vdots & \ddots & \vdots \\ r_{\lambda_1}(\Omega_9) & r_{\lambda_2}(\Omega_9) & \cdots & r_{\lambda_{14}}(\Omega_9) \end{pmatrix} \tag{6.5}$$

where $r_{\lambda_i}(\Omega_j)$ represents the top of the atmosphere reflectances at the band i and the viewing angle j.

Noise model

In remote sensing imagery, noise degrades the interpretability of the data. Noise can be produced by numerous factors including thermal effects, sensor saturation, quantisation errors and transmission errors. This noise is typically independent of the data, and is generally additive in nature so it can be generally represented as a normally distributed (Gaussian), zero-mean random process with a probability density function given by

$$f(x) = \frac{1}{\sigma_n\sqrt{2\pi}} e^{-x^2/2\sigma_n^2} \tag{6.6}$$

where σ_n is the standard deviation of the noise process.

The effect of additive noise (an) on a reflectance value R, can hence be modelled as the summation of the true signal, S, with the noise: $R = S + an$.

The Box-Muller algorithm generates this Gaussian noise (also called white noise) simulating an unit normal random variable via a transformation of two independent random variables that are uniformly distributed over [0,1]. The Polar Method is a simpli-

fication of the Box-Muller equation by applying some trigonometry (Ross, 1984) so that the final equation is:

$$x = \sqrt{-2 \times log(S)/S} \times V1 \tag{6.7}$$

where S is a random number generated as:

$U1 = rand()$

$U2 = rand()$

$V1 = 2 \times U1 - 1$

$V2 = 2 \times U2 - 1$

$S = V1 \times V1 + V2 \times V2$

The noise is finally calculated as:

$$Noise = \sigma_n \times x \tag{6.8}$$

Different levels of Gaussian noise, ranging between 0.0 and 0.1 at steps of 0.005, were added to the reflectances of the test data. The level of noise is characterised by a $2\sigma_n$ distribution (i.e. for a level of 0.005, $2\sigma_n = 0.005$) so that 95% of the errors introduced are within the required range. The resultant reflectances were used to retrieve the parameters from the LUT.

6.3.3 LUT retrieval

The retrieval of parameters from the LUT is defined by the number of candidates to be retrieved and by the criteria of search used.

The retrieval procedure typically considers that the target vegetation parameters have been found when the radiation values in the LUT agree with the measured radiation values within a prescribed accuracy. The functions typically used to achieve this have been introduced in the methodology Chapter. The retrieval method applied in this study is the RMSE computed using the differences between the modelled and measured reflectances at each band and at each viewing angle. This RMSE is used to retrieve a set of candidate solutions. A maximum of 10 candidates is allowed, being the LUT entrances with minimum RMSEs.

Absolute RMSE is calculated as:

$$RMSE = \sqrt{\frac{1}{n}\sum_{i=1}^{n}(\rho_{LUT,i} - \rho_{Inpu,i})^2} \tag{6.9}$$

where n is the number of bands times the number of viewing angles considered in each case.

Absolute RMSE is used instead of relative RMSE as the Gaussian noise is additive and using relative errors will mask the additive effect of the noise.

The minimum RMSE retrieved would correspond to the optimal result if the exact set of parameters used in the test data would had been used in the creation of the LUT. This is not the case, as test data were randomly generated, and the optimal result must be in the neighbourhood of this minimum.

The final result is calculated as an interpolation of the best candidates. A previous filtering of the results is made to eliminate outsiders. Candidates with a RMSE less than a percentage of the minimum RMSE are discarded, i.e. a candidate i is discarded if:

$$RMSE_i \leq MinRMSE + (\alpha \times MinRMSE) \tag{6.10}$$

where α represents the percentage of deviation from the *MinRMSE* accepted.

α is proportional to the instrument radiometric *Noise* considered at each case, with a minimum value of 10%:

$$\alpha = 0.1 + Noise$$

The final result for each estimated parameter is calculated as a weighted average between the selected candidates. The weights applied are calculated as:

$$W_i = \left(1 - \frac{RMSE_i}{\sum RMSE}\right)/(n-1) \tag{6.11}$$

where n is the number of candidates used in the interpolation and i varies from 1 to n.

With this technique we ensure that at least one value will be retrieved, the one with minimum RMSE. It also permits to consider up to 10 possible candidates among which to interpolate discarding those with RMSE too far away from the minimum.

6.4 Biophysical parameters estimation

The performance of the four satellite configurations covering the maximum and minimum number of viewing angles and spectral bands are analysed at each site, that is: 9 views 14 bands (9v/14b), 9 views 2 bands (9v/2b), 1 view 14 bands (1v/14b), 1 view 2 bands (1v/2b). Absolute errors between the original input and the retrieved parameter are calculated for each sample at each level of noise. Figures 6.4, 6.6, 6.5 and 6.7 show the final results for each parameter at each of the sites. In these figures the radiometric noise added to the input data is represented against the absolute error on the estimation calculated as the average of the errors obtained.

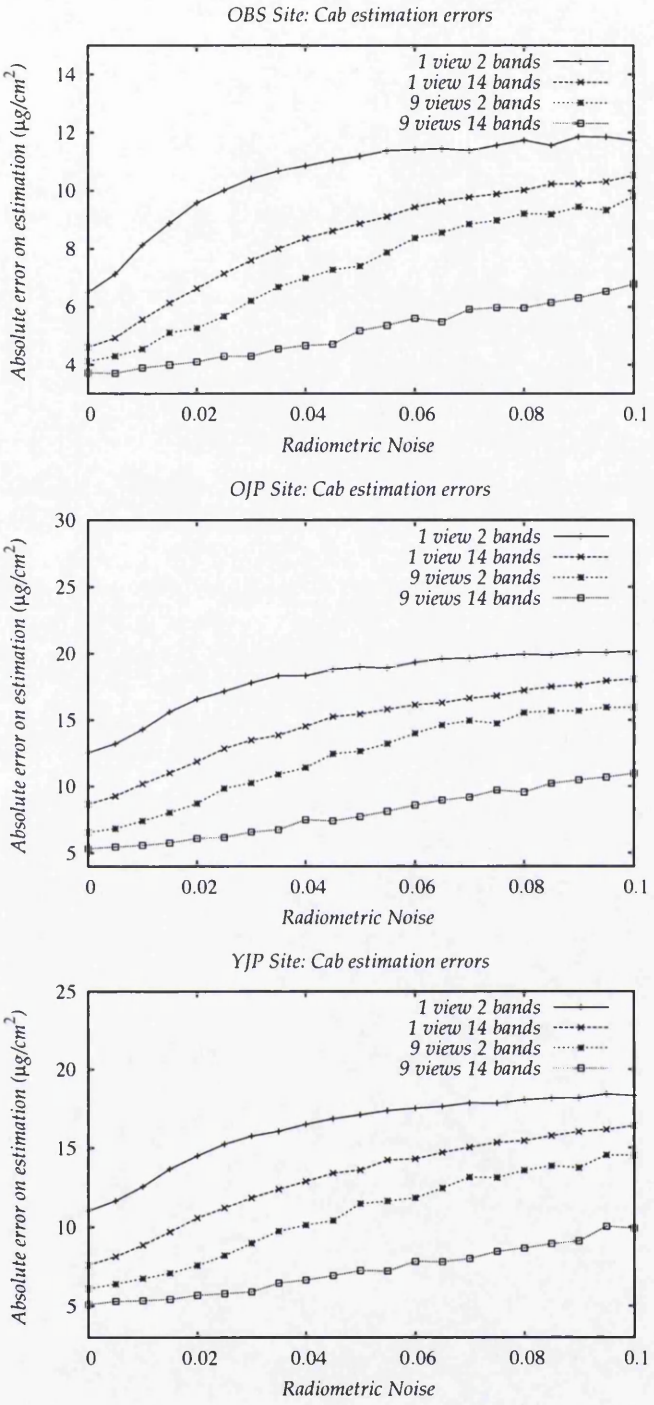

Figure 6.4: Cab estimations OBS, OJP and YJP sites

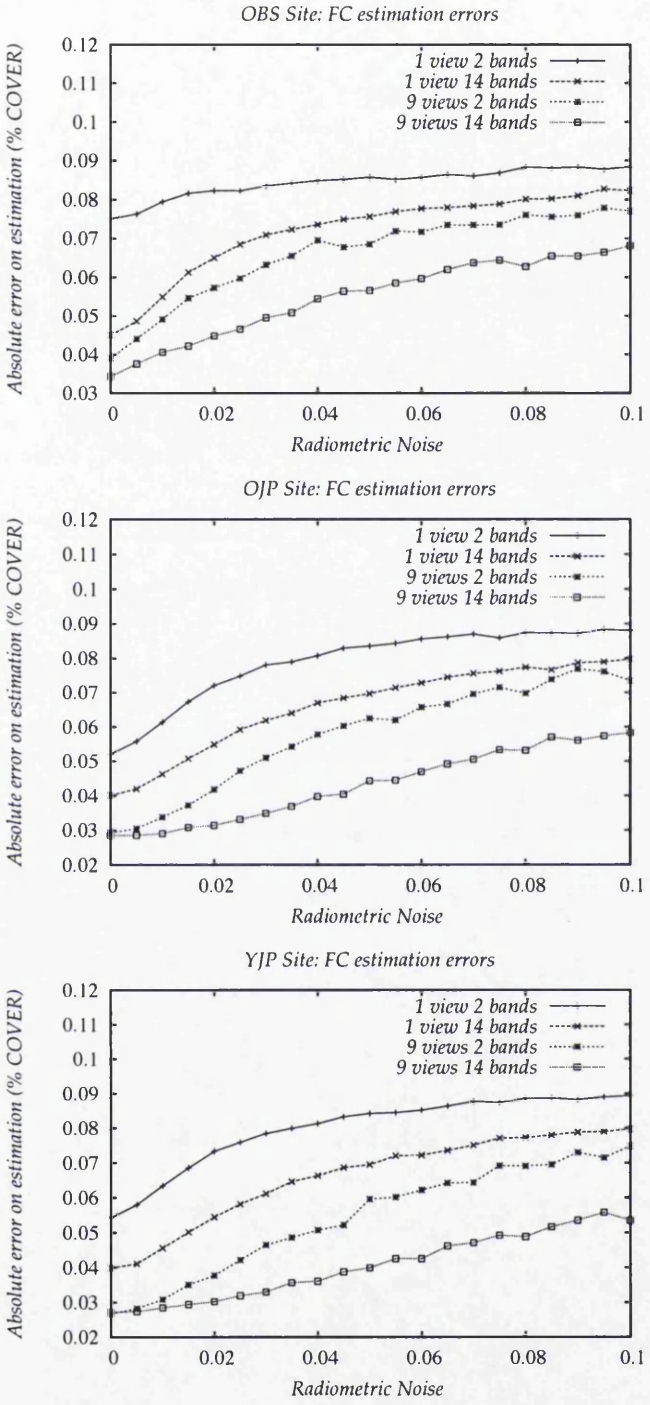

Figure 6.5: FC estimations OBS, OJP and YJP sites

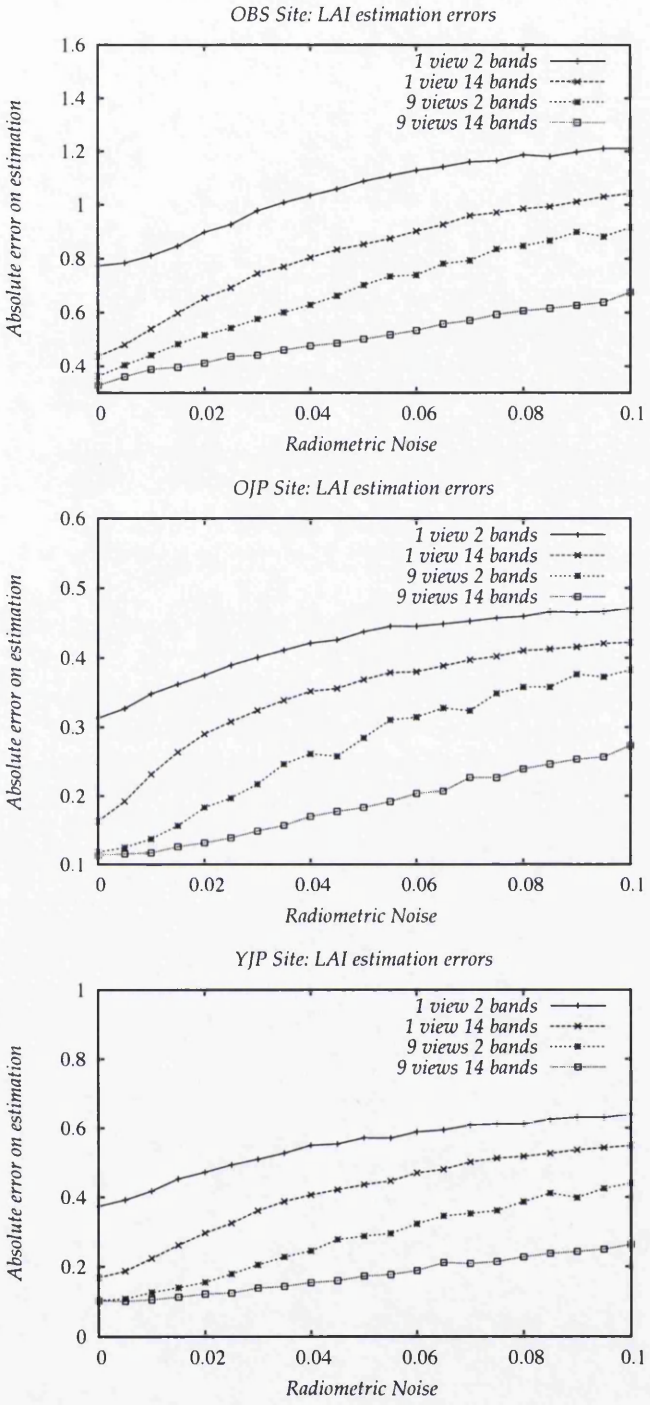

Figure 6.6: LAI estimations OBS, OJP and YJP sites

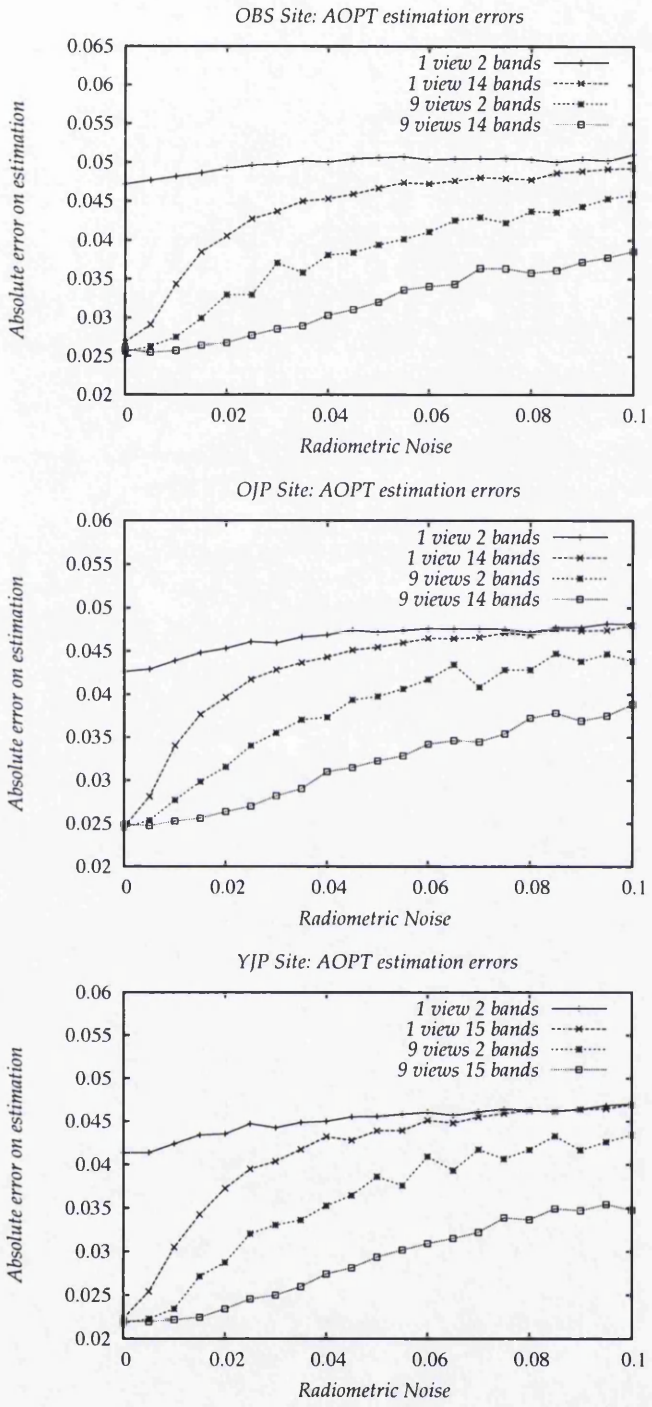

Figure 6.7: AOPT estimations OBS, OJP and YJP sites

The results show a non-zero intercept at zero noise level. Different combinations of input parameters produce very close spectra leading to the retrieval of several candidates (e.g. Fig. 6.8) and, hence, to the errors observed. In addition, there is an intrinsic error introduced in the simulation by the Monte Carlo simulation. Since Monte Carlo methods are stochastic, and simulations contain statistical fluctuations inversely pro-

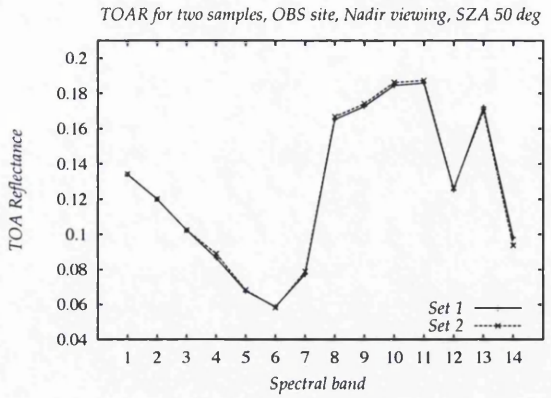

	Cab	FC	LAI	AOPT
Set 1	23.5	0.4	1.66	0.05
Set 2	32.8	0.35	1.36	0.05

Figure 6.8: Example of two sets of input parameters producing close spectrums

portional to the square of the root of the number of photon trajectories considered. In this study these fluctuations are in the range of ± 0.002 which implies a relative error between 1% up to a 10% on reflectance depending on the band.

The behaviour of the retrieval shows a smooth, linear increase in errors with noise.

The better performance of the multiview configuration is clear in all the cases. The minimum instrument configuration, with one single view and 2 bands, results in the worst outcome in all cases but is specially incapable of detecting AOT, which indirectly affected the estimations of the other parameters.

With one viewing angle and 14 bands the retrieval of Cab and FC is close to the one obtained with multiple viewing angles at the lowest noise (0.005) but the error increases rapidly at higher levels of noise.

Retrievals obtained with 9 viewing angles provide double the accuracy in the estimations than the respective configurations (2 and 14 bands) with one viewing angle. In these cases the noise has a low effect, specially in the retrieval of LAI, showing the utility of this capability in the retrieval of canopy structural information.

Atmospheric effect

The atmospheric effect on the retrieval was analysed by studying each solar zenith angle separately (Table and Figures 6.9 and 6.10). Results are consistent at low levels

of noise showing that best retrievals are obtained when the sun is higher (solar zenith angle value lower) as the atmospheric effect is smaller due to the shorter path-lengths. At higher levels of noise the behaviour is very irregular. The threshold for this irregularity was lower in the AOT retrieval. The two AOT values considered correspond to very clear atmospheres so it is likely that, at certain levels of noise, the effect of the disturbance is higher than the effect of the AOT on the final signal.

Table 6.10: Effect of solar zenith angle on the retrieval of parameters. Absolute and relative RMSE of the retrieved parameters are showed for each solar zenith angle for the case of 9 viewing angles and 14 bands and a noise of 0.01. Values shown are mean values for the three sites.

	RMSE	40°	50°	60°	70°
Cab	Abs.RMSE	3.57	4.22	5.00	6.95
	Rel.RMSE	0.12	0.15	0.18	0.27
FC	Abs.RMSE	0.02	0.026	0.034	0.051
	Rel.RMSE	0.05	0.07	0.09	0.15
LAI	Abs.RMSE	0.15	0.18	0.20	0.27
	Rel.RMSE	0.07	0.08	0.09	0.13
fAPAR	Abs.RMSE	0.015	0.016	0.018	0.025
	Rel.RMSE	0.03	0.04	0.04	0.05
AOPT	Abs.RMSE	0.02	0.023	0.026	0.028
	Rel.RMSE	0.21	0.24	0.27	0.29

Noise effect

The relative effect of the noise on the distorted TOARs was analysed to relate the results to SNR especifications. The lowest values of TOAR for each band and for each site were taken as representative of the worst case as the final signal will comprise a higher percentage of noise. The relative noise was calculated as percentage of the signal for each site. The results for a noise of 0.01 in absolute value are shown in Fig. 6.11, for other levels of noise results are proportional.

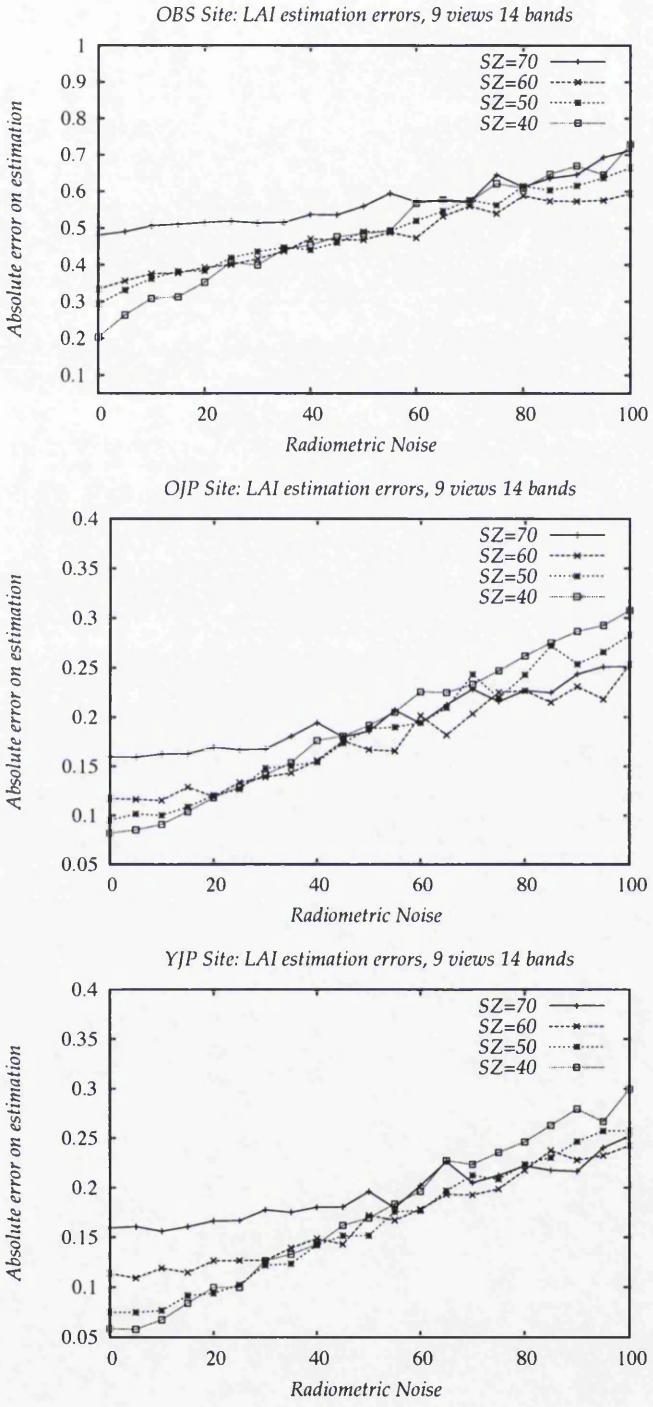

Figure 6.9: LAI estimations with all viewing zenith angles and all bands at each Solar Zenith angle

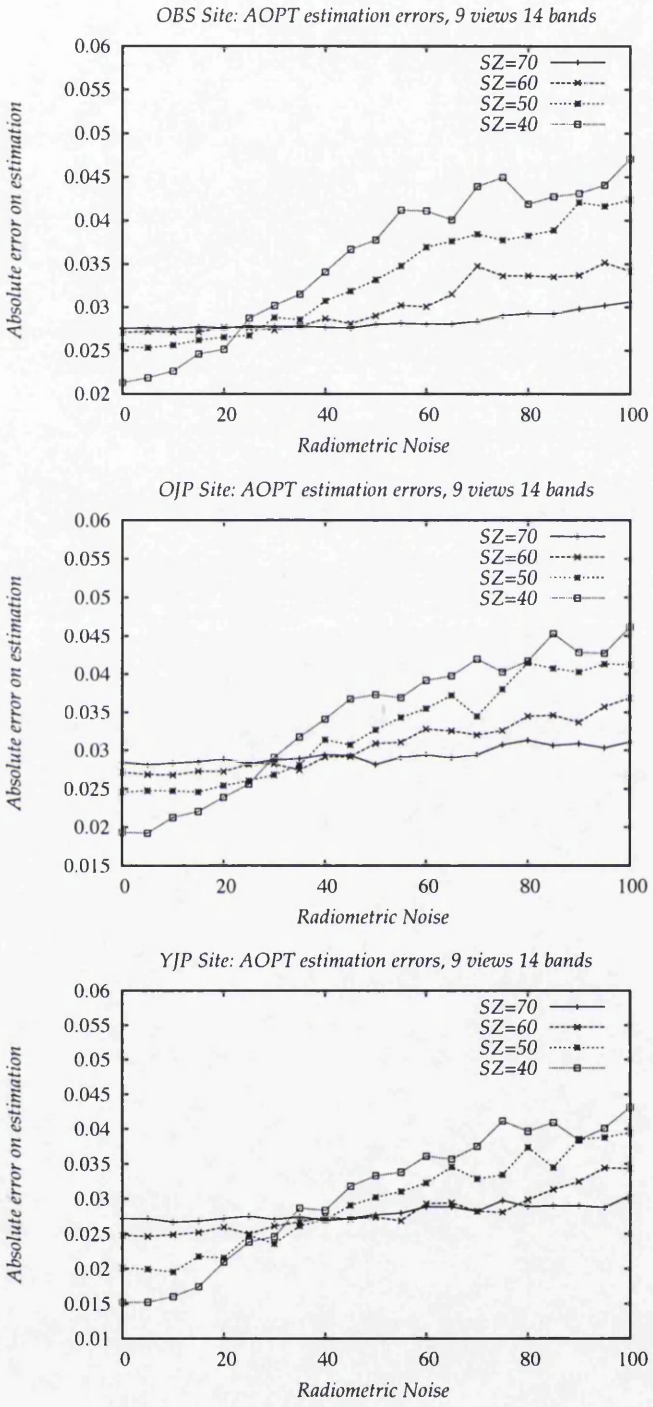

Figure 6.10: AOT estimations with all viewing zenith angle and all bands at each Solar Zenith angle

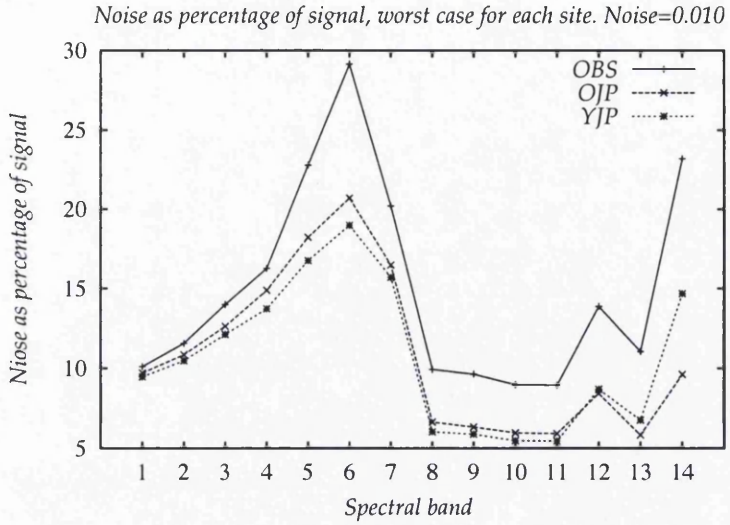

Figure 6.11: Percentage of noise at each channel for an absolute noise of 0.010

The OBS site presents a denser canopy and lower reflectance values. This is explained by the complex structure of the coniferous forest in which light radiation gets trapped. The denser the canopy, the higher is this effect. This implies that the additive noise introduced was a higher percentage of the signal in this site than in the other two cases. As a consequence, the denser the canopy, the better SNR will be required in the retrieval of parameters from the remotely sensed data.

The levels of noise analysed were quite high when related to present satellite instruments. For example, MODIS SNR requirements in the visual spectrum are between 100 and 200 and the performance of the instrument is between 100 and 250 (Guenther et al., 2002). This implies that the instrument noise is between 1% and 2,5% of the retrieved signal. For a dark signal, e.g. a reflectance of 0.02, the absolute value of this noise would range between 0.0002 and 0.0005. The method here used to simulate reflectances has an uncertainty higher than those values (uncertainty of 0.002 introduced by the Monte Carlo simulation) so it cannot be used at such low levels. To simulate the satellite data with an uncertainty of 0.0002, 25 million samples would be required in the Monte Carlo simulation what would take about 30 minutes to run for each case. It is expected that the tendency will be the same at lower levels of noise, but with the data here used no further conclusions can be extracted. Figure 6.12 shows the result of the analysis for a range of noise between 0 and 0.02 at steps of 0.001 (being 0.002 the uncertainty introduced by the Monte Carlo simulation on the modelled data). It can be seen that the tendency is the same. Lower noises cannot be analysed with our LUT as the data uncertainty would be higher than the noise analysed.

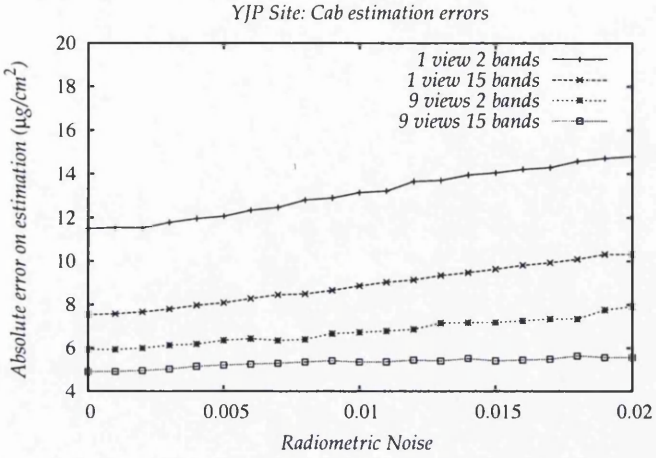

Figure 6.12: Cab estimations, YJP site. Case with low levels of noise

6.5 NPP estimation

From the estimated parameters (Cab, FC, AOT and LAI) the only parameter that can be used as input in the LSPs analysed is LAI.

Both LSPs used in this study use LAI as main driver of vegetation related processes. In JULES, LAI is an input parameter but that is not the case in BIOME-BGC so minor modifications were made to the code to force it to use the estimated LAI.

In BIOME-BGC, LAI is internally calculated. The routine "radtrans.c" was modified to use LAI from an input file instead of this calculation (code modifications are showed in Appendix A). LAI is later used in the model to estimate sun and shade fractions, fAPAR and specific leaf area for sun and shade canopy fractions, these calculations remained the same.

The output analysed from both models was the annual NPP.

6.5.1 Parameterising the LSPs

Typically, ecological models are run, or "spun up", for two or three years and the output of the last year is recorded (e.g. Kimball et al., 1997a). This allows the model to settle down when some of the input parameters are not well known but also when the internal calculations are not very stable.

To check the stabilisation of the models in the second year, they were spun up for 3 years for a repeating pattern of weather data. The BIOME-BGC original code was used in the stabilisation analysis (without the forced input LAI from file). Meteorological

input data for the year 1994 was used. BIOME-BGC estimated daily values were recorded. For JULES, the 30 min step values (gC/m2/sec) were added to obtain daily values comparable to BIOME-BGC outputs.

Graphs 6.13 and 6.14 show daily NPP estimations during these three years simulation. It can be seen that in the second year both models are stabilised. Therefore, only two years were used taking the annual NPP from the second year. Figure 6.14 shows a strong decline in the NPP estimated by JULES for the OJP site before the end of the growing season. This is due to a decrease of soil moisture content and similar results have been reported in previous studies on this site (Kimball et al., 1997a).

Other estimated parameters were also check for stabilisation, those are gross primary productivity (GPP), plant respiration and heterotrophic (soil) respiration, represented in Figures 6.15 and 6.16. GPP and heterotrophic graphs show that the heterotrophic respiration was the main cause of the initial instability in the BIOME-BGC model, showing the complexity of modelling the soil hydrology of this landscapes. Also heterotrophic respiration was the main difference between the two models, being much higher in BIOME-BGC.

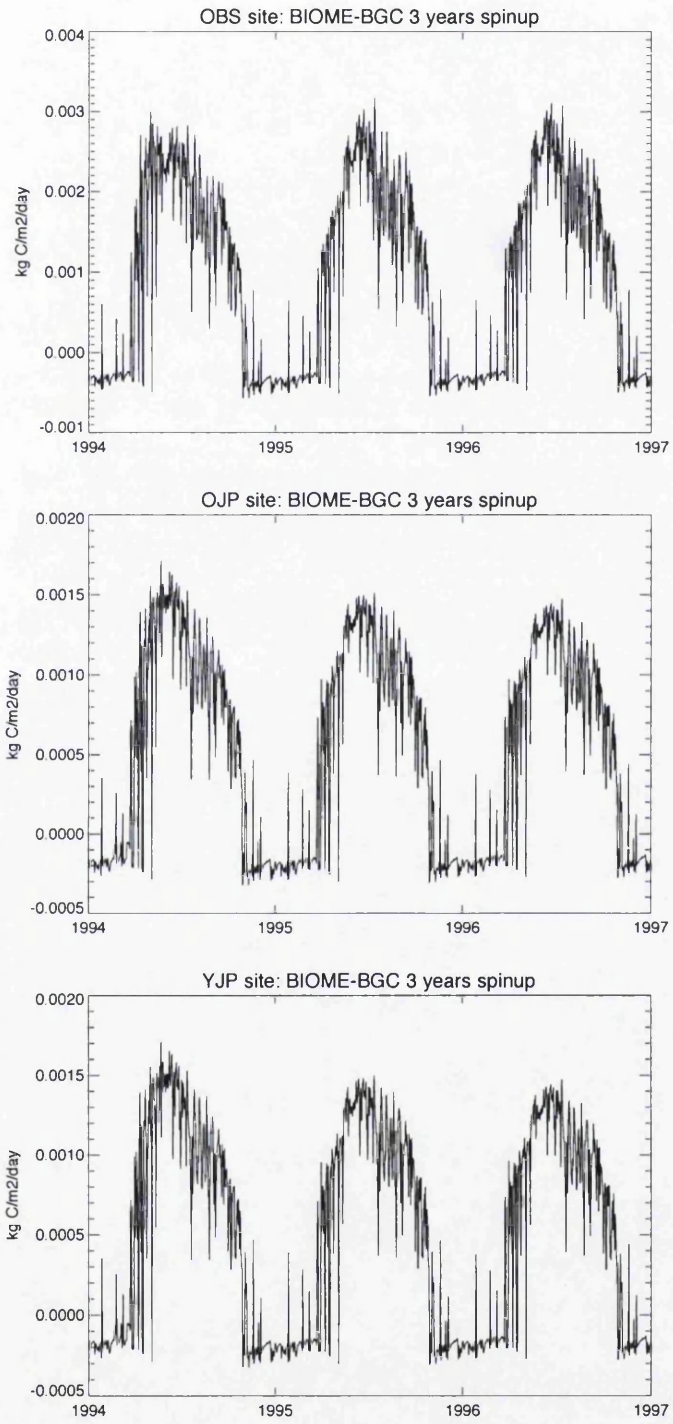

Figure 6.13: NPP simulated by BIOME-BGC in the 3 years spin up

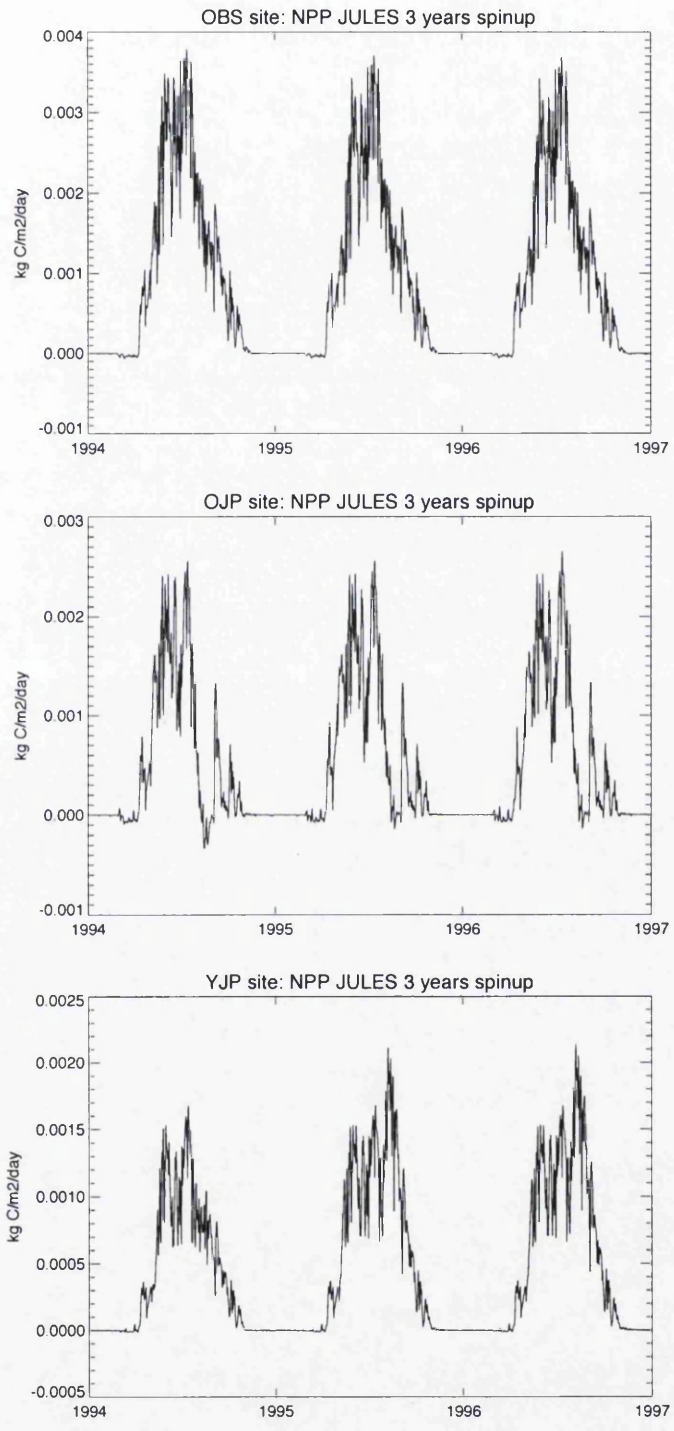

Figure 6.14: NPP simulated by JULES in the 3 years spin up

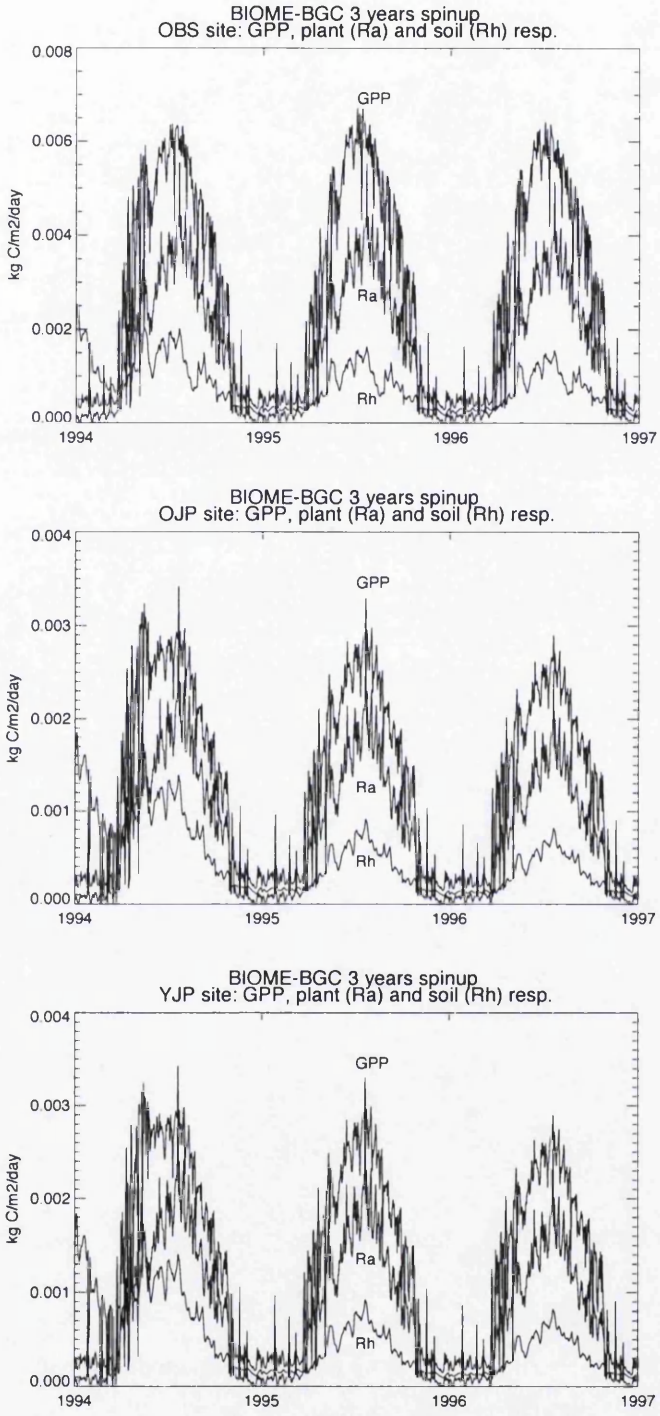

Figure 6.15: GPP, soil and plant respiration simulated by BIOME-BGC in the 3 years spin up

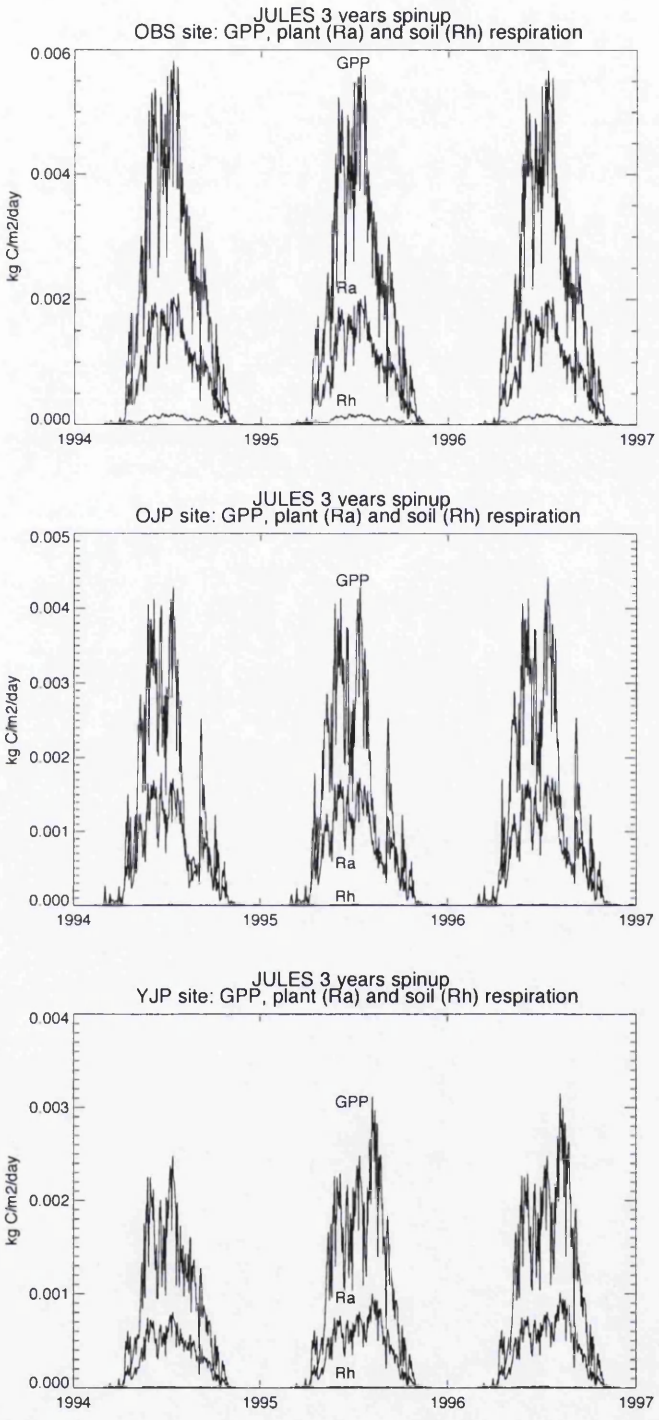

Figure 6.16: GPP, plant and soil respiration simulated by JULES in the 3 years spin up

Results obtained from the models were compared with those reported in the literature for the same sites. To do this, average effective LAI values were taken from LAI-2000 measurements (Table 6.11). These values have been corrected by increasing them

in a 15% to account for the underestimation detected in LAI-2000 measurements as explained in Chen et al., 1997. Results were in the range of the NPP reported by field estimations and by other modelling studies (Table 6.11). No published results were found for the YJP site but the productivity is expected to be lower than that of the OJP as trees are younger and in a growing stage, which was consistent with the results obtained.

Table 6.11: Mean effective LAI and estimated NPP

	OBS	OJP	YJP	Source
Effective LAI	2.3	1.7	1.5	Chen et al., 1997
Literature field data NPP (gC/m2y)	266	226	-	Gower et al., 1997
Literature modelled NPP (gC/m2y)	170	110	-	Kimball et al., 1997b
BIOME-BGC NPP (gC/m2y)	209	181	160	
JULES NPP (gC/m2y)	203	180	178	

6.5.2 Sensitivity analysis results

Effective LAI values estimated with the LUT inversion were used to drive the BIOME-BGC and JULES models.

Effective LAI is used instead of LAI corrected for clumping effects (Chen et al., 1997) in both models. BIOME-BGC uses projected LAI in the internal calculations which was assumed to be equivalent to effective LAI. JULES uses radiation interception to estimate productivity, as there is no consideration of clumping index within this calculation, effective LAI was considered more appropriate.

Annual NPP estimated by the models is recorded and errors are analysed in terms of mean absolute error between the NPP obtained with the real LAI value and the one obtained with the LAI estimated from the satellite retrieval simulation. The process is repeated for each site and for the four hypothetical instrument configurations and results are represented against noise (see Figures 6.17 and 6.18). The tendency is similar to the observed in the graphs of the biophysical parameters with multiview capability providing the better results, even with only two spectral bands.

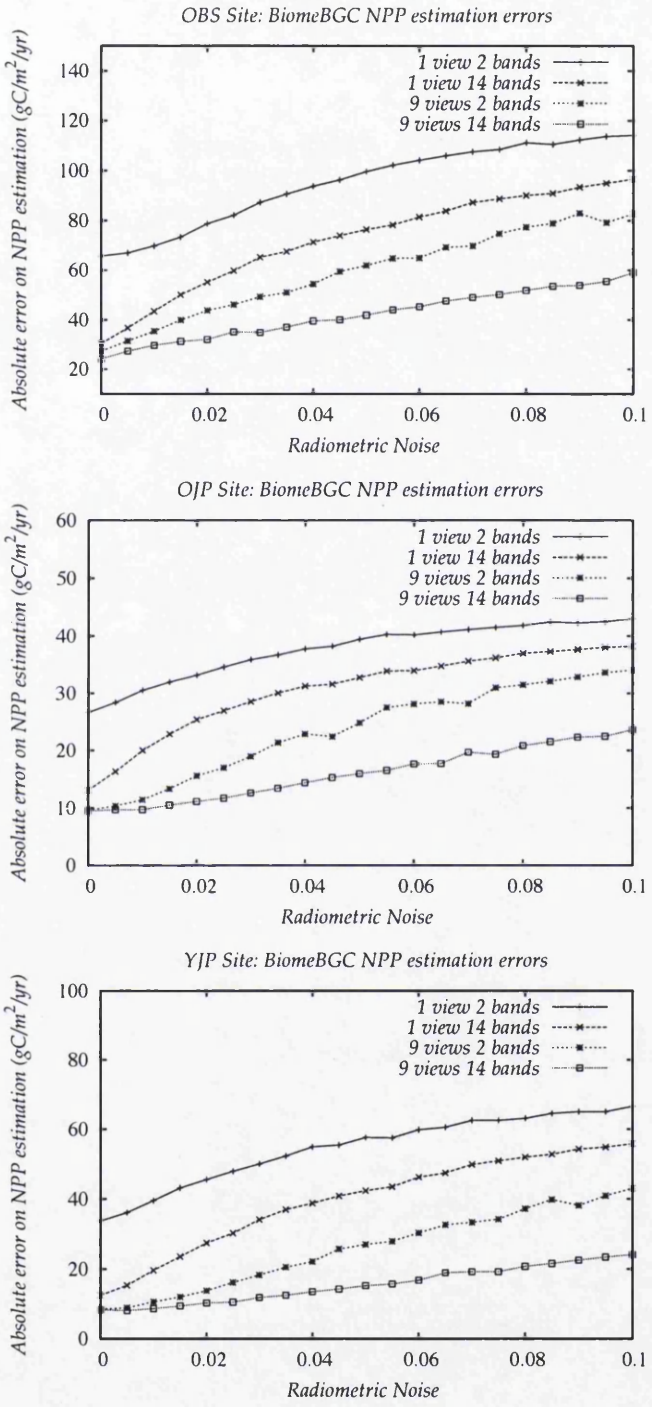

Figure 6.17: BIOME-BGC NPP errors vs instrument noise at each site

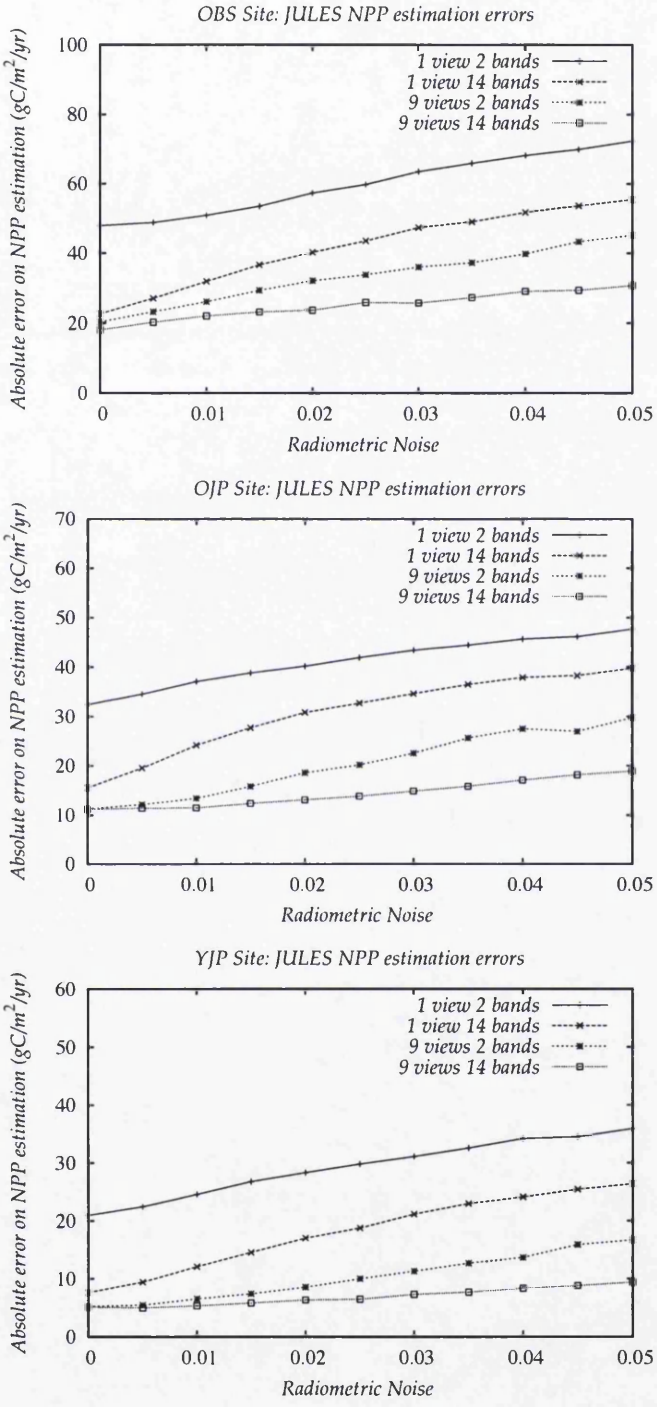

Figure 6.18: JULES NPP errors vs instrument noise at each site

6.6 Discussion

The better performance of the multiview configuration is clear in all the cases.

In the retrieval of biophysical parameters, the minimum instrument configuration, with one single view and 2 bands, develops worst in all cases but is specially incapable of detecting AOPT, which indirectly affected the estimations of the other parameters.

With one viewing angle and 14 bands the retrieval of Cab and FC is close to the one obtained with multiple viewing angles at the lowest noise (0.005) but the error increases rapidly at higher levels of noise.

Retrievals obtained with 9 viewing angles provide double accuracy in the estimations compared with the respective configurations (2 and 14 bands) with one viewing angle. In these cases the noise has a low effect, specially in the retrieval of LAI, showing the utility of this capability in the retrieval of canopy structural information.

When analysing the NPP estimated by the models, the configuration with 9 views and 14 bands also performed better at all levels of noise and no magnification of the errors was detected. The second best results were obtained with 9 views and only two bands. At a radiometric noise of 0.01, with the 1v/14b configuration, errors on NPP estimated range between 19.6 gC/m^2y (YJP site with BIOME-BGC) and 43.5 gC/m^2y (OBS site with BIOME-BGC). The 9v/14b configuration improves those figures between a 31% and a 56% with errors ranging from 8.6 gC/m^2y (YJP site with BIOME-BGC) to 29.7 gC/m^2y (OBS site with BIOME-BGC). Doubling the radiometric accuracy from 0.02 to 0.01 produces improvements of around 10%, 25%, 20%, and 15% for each of the configurations, 1v/2b, 1v/14b, 9v/2b and 9v/14b respectively. Increasing the number of bands from 2 to 14 produces improvements between 30% and 50% at noise levels under 0.015 for one single view. In the case of 9 viewing angles, at the same noise level (i.e. under 0.015), the improvement obtained by the higher spectral sampling is only 10%-20%.

JULES showed to be less sensitive to effective LAI inputs, and hence to errors on it, than BIOME-BGC. As an example, for a level of noise of 0.01 and the highest information configuration (9v/14b) NPP errors derived from JULES were 18, 6.9 and 3.8 gC/m^2y, while for Biome-BGC were 29.7, 9.7 and 7.8 gC/m^2y for OBS, OJP and YJP respectively.

The results show a clear advantage of the multiple angular sampling against the other sensor configurations analysed. The sites studied are coniferous forest. These forests present a complicated vertical structure in which the viewing angle is likely to be highly important. Single angle observations (e.g. at nadir) are not able to capture

the effects of the structure of the canopy so that measurements such as these can be highly misleading. Multiple viewing observations provide critical information required to better characterise the biophysical parameters of this structural complex landscapes which explains the better retrieval results obtained in this study. A caveat is that there may be further errors in using MVA data not modelled, principally registration errors, hindering the use of these data.

6.7 Summary

In this Chapter a method has been presented that links satellite instrument capabilities with ecological models.

Three coupled models - PROSPECT, FLIGHT and 6S - have been inverted using a simple technique based on look-up tables (LUTs). This LUT was used to estimate canopy biophysical variables from remotely-sensed data observed at the top of the atmosphere in several viewing directions and spectral wavebands within the visible and near-infrared domains. Four different directional and spectral configurations have been investigated. The retrieval uncertainty was linked with the instrument radiometric accuracy by analysing the impact of different levels of radiometric noise at the input. The effective LAI values retrieved in the inversion were used to drive two land-surface parameterisation models, Biome-BGC and JULES. Finally, the effects of the different configurations and of the radiometric noise on the NPP estimated were analysed.

The results show that multiangular information improves dramatically the accuracy of the estimations, even when only two spectral channels are used. Satellite data obtained at multiple views provides structural data critical to characterise the biophysical parameters of the coniferous sites analysed. A denser spectral sampling (from 2 to 14 channels) also improves the error of the estimations (up to 50% for one single viewing angle). This improvement is lower in the case of multiple viewing angles (10-20%). Radiometric accuracy does not show such a large relative effect on the retrieval with only a 10%-25% improvement obtained by doubling the radiometric accuracy of the instrument from 0.02 to 0.01.

The inclusion of multiangular capabilities in future satellite instruments targeted at monitoring the vegetation would improve the retrieval of vegetation information allowing us to detect the intrinsic structural characteristics of the canopies. Spectral information and radiometric accuracy are not so critical if multiple viewing is available but the relative cost of each of these capabilities should also be considered when designing the instrument.

Chapter 7

Discussion and conclusion

This final chapter discusses the main outcomes of each chapter looking at the implications for satellite development and ecological models.

Future research directions are proposed both in terms of overcoming limitations of the methodology used and in terms of extending the applicability to wider studies.

Finally, the last section, summarises the most important points of this work.

7.1 Summary of the thesis

Any attempt at quantifying the nature, extent and dynamics of the processes controlling the Earth system must rely on both an accurate understanding of the mechanisms involved and a set of tools to monitor continuously and repetitively the Earth's surface.

The importance of ecological processes in global change has been justified in **Chapter 1**. Ecological models are fundamental tools to quantify and understand the processes involved allowing us to extrapolate physical processes measured at the leaf or canopy scales, to larger regions and temporal scales. These models require critical input data, both at regional and global scales, that only satellite instruments can provide at the required frequency.

Chapter 2 reviewed the requirements of ecology from satellite sensors in terms of parameters, resolution and uncertainty. Satellite missions launched to fulfill those requirements as well as international programs aimed to define requirements and to make the data widely available have also been examined. The involvement of the research community in the design of future instruments was demonstrated to be fundamental. That comprises not only the specification of requirements at the design stage but also

a major involvement once the instrument is operational so that their changing requirements can be met as much as possible by the provided products. In terms of data information content, present tendency is towards multi or hyperspectral sensors. In recent years, multiviewing sensor have proven to provide extra information about the canopy structure from which to extract biophysical parameters at an accuracy never available before. Nevertheless, there is no planned sensor to provide continuity to the MISR instrument on Terra; other candidate missions including mutiangular capabilities have not been selected for further development. Continuous long-term measurements are also threatened by changes in the NPOES program and there are gaps in other planned missions such as ESA passive sensors after ENVISAT and in the continuity of MISR instrument.

Present methods used in the retrieval of biophysical parameter were reviewed in **Chapter 3**. Vegetation indices have been traditionally used to retrieve biophysical parameters from remote sensing data. Techniques to estimate parameters from remote sensing are moving forwards to methods based on the physical properties of the observed targets and nowadays, LUT and ANN constitute the most promising techniques and are being incorporated in the satellite products algorithms.

Chapter 4 presented the selected study area, the boreal forest biome for its importance in the carbon cycle and its challenging structural characteristics. The methodology proposed to link ecological models requirements and satellite instrument capabilities was also presented in this chapter.

A preliminary sensitivity analysis, in **Chapter 5**, has shown the advantages of sampling in the princial plane and near the hot spot for the retrieval of biophysical parameters and the effect of the uncertainties on those in the output of one of the LSPs analysed. The principal plane showed to provide most information which agrees with previous studies. The results also showed that some view angles (nadir view and near the hot-spot direction) are more sensitive to changes in biophysical parameters; in fact the radiometric accuracy required can be reduced by an order of magnitude compared with other sun-sensor geometries. Also in agreement with previous studies, wavelengths located in the NIR exhibit optimal characteristics for the retrieval of biophysical parameters according to the result obtained.

Finally, in **Chapter 6**, a complete methodology is proposed and applied that allows us to link four different instrument configurations to the errors at the output of the two LSP models. Results showed that multiple viewing angles provide extra information of the canopy structure improving dramatically the retrieval of biophysical parameters from the instrument data. The effect on the retrieved data on the LSPs analysed showed

a consistent dependence on the errors on the estimated parameters. Some instrument configurations lead to errors of up to a 50% in the NPP estimated by the models at low levels of noise (0.005). The extra information provided by the multiple viewing configuration reduced those errors to a 10-20%. It also showed a smoother behavior in the rate of increase of NPP errors with increased noise. The limitations of the method in terms of uncertainty have been pointed out, but the results are representative of the relative performance of each of the instrument configurations.

7.1.1 Implications for satellite development

The use of satellite data to derive biophysical parameters has progressed significantly over the last few decades. Sensor instrument technology has been improved providing data with finer spatial resolutions. Also improved methods for deriving parameters have been developed. Presently the tendency on passive sensors is towards hyperspectral sensors, in some cases with multiviewing capabilities. There is no doubt that the more information you have the better but most information will be redundant and the amount of data could became unmanageable. In most cases the final application will require only data from a few relevant bands. On the other hand, multiviewing data is providing additional information allowing to retrieve parameters with an accuracy not possible before. Based on the results of this study, the inclusion of multiple view angle capabilities in future satellite-sensors targeted at monitoring Earth's surface is likely to improve significantly the retrieval of information on surface biophysical properties and, in particular, the intrinsic structural characteristics of vegetation canopies. Spectral information and radiometric accuracy are less critical if a multiple view angle capability is available, but the relative cost of each must also be considered when designing instruments. Future satellites should continue on this line of improvement as it seems that an end line has been reached in terms of spectral resolution.

Also efforts should be targeted to the development algorithms that could make full used of this information. It is widely accepted now that vegetation indices, widely used for the retrieval of vegetation parameters, provide limited information. They are site specific requiring prior calibration and are not physically based, nor accounting for bidirectional effects. Physically-based bidirectional reflectance models permit us to retrieve these parameters decoupling structural and biophysical effects. BRDF can be estimated using models of surface scattering in conjunction with reflectance data acquired at different viewing and illumination angles. Retrieving BRDF in this way will allow us to compare images from different dates taken at different illumination conditions and/or under different viewing geometries ensuring long-term applicabil-

ity of the retrieved data. This is another strong reason to incorporate multiviewing capabilities in future instruments.

The main original contribution of this study is the development of an end-to-end methodology that allows us to link the satellite configurations with the effects of the retrieved parameters on the ecological models. This or similar procedures should be incorporated in the definition and assessment of future satellite instruments.

This study was restricted to passive sensors in the visual and NIR domains. LIDAR has arisen in the last few years as a promising technology that could potentially be used in the retrieval of above-ground biomass (e.g. Patenaude et al., 2004; Lefsky et al., 2005; Andersen et al., 2005), being considered to work synergistically with multiviewing remote sensing for future missions (Hese et al., 2005). This and other technologies would provide extra information that can be used both to assimilate into the models as well as to validate the estimations obtained from them. Future missions are now being planned which are significantly driven by research requirements and applying the lessons learned during the last three decades of remote sensing. There is an inclination towards small, flexible missions (such us the ESA Sentinels and the A-Train satellites) in which less costly, less expensive, less complex satellites are used and the failure of one does not kill an entire mission. Nevertheless worrying gaps have been identified in multispectral and multiangular instruments. The combination of a set of instruments providing different land-surface characteristics is important to characterise the requirements for future missions and ideally all the available technologies should be considered.

7.1.2 Implications for ecological models

Presently main requirements of ecological models from remote sensing are reliable estimations of biophysical parameters. Ecological models are increasingly using satellite derived parameters such as fAPAR, LAI and NDVI (e.g. NASA-CASA model Potter et al., 2003). Models should continue in this line, incorporating satellite products and also using satellite data in their validations.

Products must be available at a time scale between days and weeks to make them useful for this community. Uncertainty of the products should be assessed, but in some cases it is difficult to know which data to use as ground truth to compare with, as in the case of LAI.

The analysed models were highly sensitive to soil parameters and, in some cases, not very stable. This exposes that there is still a lot to improve in the parameterisations

used. Satellite data can contribute a great deal in providing both driving and validating data that will help in the understanding of these processes.

The work here presented has been limited to the boreal forest biome. Each biome presents intrinsic challenges both in terms of remote sensing and of radiative transfer and ecological modelling. Other relevant biomes, such us the tropical forest, should be also investigated to asses the specific requirements of those ecosystems from remote sensing.

Finally, in terms of use of the retrieved parameters in the LSPs, the applicability was restricted to one parameter, LAI, and only used as input to the models. This reveals the lack of capability of present models to incorporate satellite derived data. Further modifications of the models to permit the use of other biophysical parameters as inputs was out of the scope of this study. However, future developments in these models could open that possibility. Other prospects of using the satellite derived parameters include the data assimilation into the models and the comparison of model estimations (e.g. NPP or GPP) with satellite products. To this respect it would be interesting to asses the effects of the uncertainties in the satellite retrieved parameters linking them with the performance of the data assimilation techniques presently used in ecological models (e.g. Williams et al., 2005).

7.1.3 Future research

In terms of the methodology used in this thesis, the LUT approach can be improved in several ways, but further analysis will be required. It would be appropriate to give more weight to the most informative measurements (bands or viewing angles)(Verstraete et al., 1996; Privette et al., 1996a) but as several parameters were retrieved at a time the weighting to use was not straightforward. A different approach could be to retrieve the parameters in different stages so that the appropriate weights for each parameter can be used.

Absolute RMSE was used in the comparison between observed and LUT reflectances. As the additive noise was absolute in value, and not weighting was considered, relative RMSE gave worst retrievals in the preliminary tests and that is why it was discarded. Relative RMSE would allow us to emphasize on bands or directions that have the largest absolute reflectance values. These bands would present higher signal to noise ratios (noise being smaller in reference to the received signal). The effects of the noise could hence be reduced by applying an adequate weighting improving the overall performance of the method. Nevertheless, final results in terms of relative performance

of each of the instrument configurations should not be different from the ones obtained as the same method was applied to all of them.

The same methodology could be extended to the analysis of the combination of multi-angular and LiDAR data which would be expected to improve drastically the capability of deriving structural and biophysical parameters.

7.2 Conclusion

Diagnosis and prediction of climatic, environmental, and ecological changes in the Earth's system has proven to be an enormously challenging task. The synergistic use of all the technologies available is fundamental to approach the study of the processes involved.

Remote sensing has been providing global measurements for a few decades already, and future satellites should be designed to ensure the continuity and improvement of those data. Long term monitoring must be guaranteed but also technological advances must be incorporated into the new instruments to fully take advantage of the available capabilities. This study has developed a methodology to allow a quantitative analysis of how improvements in satellite technology are related to improvements in ecological modelling, with a focus on the stability of long-term dataset generation.

An analysis of potential satellite configurations clearly concluded that an instrument with multiple viewing capabilities would dramatically improve the retrieval of biophysical parameters and, as a consequence, the accuracy on the estimations made by the models that use those parameters. The inclusion of multiple view-angle capabilities is additionally likely to constrain the retrieval of information on the intrinsic structural characteristics of vegetation canopies. Nevertheless there is a clear gap in the planned missions for instruments incorporating such capability.

LSPs are continuously evolving as the physics underlying the simulated processes are better understood. This thesis established that there is currently a gap between the capabilities of existing and planned sensors and the ability of models to utilise parameters, for example leaf chlorophyll, which may be derived. It is important that both modelling and EO communities work together in the development of new techniques to estimate and apply parameters.

The involvement of the scientific community in the development of satellite instruments should cover not only the initial consultation process but the continuous validation of procedures, algorithms and products and the definition of future plans to

assure continuity of satellite data. In this context, several international organisations have arisen in the last few years aimed to improve the communication between both communities (e.g. CEOSS, ESSP, GCOS).

Increasingly, satellite missions should be tailored for the target research communities, and designed to provide the required data at the required accuracy, as well as stimulate model development to efficiently assimilate satellite data. This thesis offers a protoype for this process.

Appendix A

BIOME-BGC modifications

A.1 Modifications to the radtrans.c routine

In BIOME-BGC model LAI is internally calculated. The routine "radtrans.c" was modified to use LAI from an input file instead of this calculation. LAI is later used in the model to estimate sun and shade fractions, and specific leaf area for sun and shade canopy fractions, these calculations remained the same. Modifications are indicated with a comment "APB".

```
/*
radtrans.c
calculate leaf area index, sun and shade fractions, and specific
leaf area for sun and shade canopy fractions, then calculate
canopy radiation interception and transmission
Modification APB (Ana Prieto-Blanco):
LAI is read from file LAI.data instead of being calculated
*-*-*-*-*-*-*-*-*-*-*-*-*-*-*-*-*-*-*-*-*-*-*-*-*-*-*-*-*-*-*-*-*
Biome-BGC version 4.1.1
Copyright 2000, Peter E. Thornton
Numerical Terradynamics Simulation Group (NTSG)
School of Forestry, University of Montana
Missoula, MT 59812
*-*-*-*-*-*-*-*-*-*-*-*-*-*-*-*-*-*-*-*-*-*-*-*-*-*-*-*-*-*-*-*-*
*/
#include <stdio.h>
#include <stdlib.h>
#include <string.h>
#include <math.h>
#include <malloc.h>
#include "bgc_struct.h"
#include "bgc_func.h"
#include "bgc_constants.h"
int radtrans(const cstate_struct* cs, const epconst_struct* epc,
```

```
metvar_struct* metv, epvar_struct* epv, double albedo)
{
/* calculate the projected leaf area and SLA for sun and shade fractions
and the canopy transmission and absorption of shortwave radiation
based on the Beer's Law assumption of radiation attenuation as a
function of projected LAI.
*/
char filename[70]; /* APB new variable*/
int ok=1;
double proj_lai, aLAI; /* APB new variables*/
double albedo_sw, albedo_par;
double sw,par;
double swabs, swtrans;
double parabs;
double k;
double k_sw, k_par;
double swabs_plaisun, swabs_plaishade;
double swabs_per_plaisun, swabs_per_plaishade;
double parabs_plaisun, parabs_plaishade;
double parabs_per_plaisun, parabs_per_plaishade;
FILE *fLAI; /* APB new variable*/
/* The following equations estimate the albedo and extinction
coefficients for the shortwave and PAR spectra from the values given for the
entire shortwave range (from Jones, H.G., 1992.  Plants and Microclimate,
2nd Edition.  Cambridge University Press.  pp.  30-38.)  These conversions
are approximated from the information given in Jones.
*/
/* Modified APB: Reads LAI from an input file */
sprintf(filename,"/geog/home/research/aprieto/bin/BiomeBGC/unixbgc411/LAI.data");
fLAI=fopen(filename,"rb");
if (fLAI!=NULL)
{ fscanf(fLAI,"%lf",&aLAI);
fclose(fLAI);
}
if (cs->leafc > 0.0)
{
/* Calculate whole-canopy projected and all-sided LAI */
/*epv->proj_lai = cs->leafc * epc->avg_proj_sla;*/
/* Modified APB: uses LAI read from file instead of internal calculation */
epv->proj_lai = aLAI;
epv->all_lai = epv->proj_lai * epc->lai_ratio;
/* Calculate projected LAI for sunlit and shaded canopy portions */
epv->plaisun = 1.0 - exp(-epv->proj_lai);
epv->plaishade = epv->proj_lai - epv->plaisun;
if (epv->plaishade < 0.0)
{
printf("FATAL ERROR: Negative plaishade\n");
printf("LAI of shaded canopy = %lf\n",epv->plaishade);
ok=0;
}
/* calculate the projected specific leaf area for sunlit and
```

```
shaded canopy fractions */
epv->sun_proj_sla = (epv->plaisun + (epv->plaishade/epc->sla_ratio)) /
cs->leafc;
epv->shade_proj_sla = epv->sun_proj_sla * epc->sla_ratio;
}
else if (cs->leafc == 0.0)
{
epv->all_lai = 0.0;
epv->proj_lai = 0.0;
epv->plaisun = 0.0;
epv->plaishade = 0.0;
epv->sun_proj_sla = 0.0;
epv->shade_proj_sla = 0.0;
}
else
{
printf("FATAL ERROR: Negative leaf carbon pool\n");
printf("leafc = %.7e\n",cs->leafc);
ok=0;
}
k = epc->ext_coef;
proj_lai = epv->proj_lai;
/* calculate total shortwave absorbed */
k_sw = k;
albedo_sw = albedo;
sw = metv->swavgfd * (1.0 - albedo_sw);
swabs = sw * (1.0 - exp(-k_sw*proj_lai));
swtrans = sw - swabs;
/* calculate PAR absorbed */
k_par = k * 1.0;
albedo_par = albedo/3.0;
par = metv->par * (1.0 - albedo_par);
parabs = par * (1.0 - exp(-k_par*proj_lai));
/* calculate the total shortwave absorbed by the sunlit and
shaded canopy fractions */
swabs_plaisun = k_sw * sw * epv->plaisun;
swabs_plaishade = swabs - swabs_plaisun;
if (swabs_plaishade < 0.0)
{
printf("FATAL ERROR: negative swabs_plaishade (%lf)\n",swabs_plaishade);
ok=0;
}
/* convert this to the shortwave absorbed per unit LAI in the sunlit and
shaded canopy fractions */
if (proj_lai > 0.0)
{
swabs_per_plaisun = swabs_plaisun/epv->plaisun;
swabs_per_plaishade = swabs_plaishade/epv->plaishade;
}
else
```

```
{
swabs_per_plaisun = swabs_per_plaishade = 0.0;
}
/* calculate the total PAR absorbed by the sunlit and
shaded canopy fractions */
parabs_plaisun = k_par * par * epv->plaisun;
parabs_plaishade = parabs - parabs_plaisun;
if (parabs_plaishade < 0.0)
{
printf("FATAL ERROR: negative parabs_plaishade (%lf)\n",parabs_plaishade);
ok=0;
}
/* convert this to the PAR absorbed per unit LAI in the sunlit and
shaded canopy fractions */
if (proj_lai > 0.0)
{
parabs_per_plaisun = parabs_plaisun/epv->plaisun;
parabs_per_plaishade = parabs_plaishade/epv->plaishade;
}
else
{
parabs_per_plaisun = parabs_per_plaishade = 0.0;
}
/* assign structure values */
metv->swabs = swabs;
metv->swtrans = swtrans;
metv->swabs_per_plaisun = swabs_per_plaisun;
metv->swabs_per_plaishade = swabs_per_plaishade;
/* calculate PPFD: assumes an average energy for PAR photon (EPAR, umol/J)
unit conversion:  W/m2 --> umol/m2/s.  */
metv->ppfd_per_plaisun = parabs_per_plaisun * EPAR;
metv->ppfd_per_plaishade = parabs_per_plaishade * EPAR;
metv->parabs = parabs;
return (!ok);
}
```

Appendix B

Soil parameters

B.1 Soil Hydraulic Properties

These data was collected by Richard Cuenca, Shaun Kelly, and David Stangel as part of the HYD-1 investigation of the BOREAS Project (Kelly and Cuenca, 1998). The soil hydraulic properties were measured on a scale ranging from 5 to 20 cm. Values represent mean values for the area.

Table B.1: Field data

	OBS	OJP	YJP	Transformation	OBS	OJP	YJP
Saturated hydraulic conductivity of the soil, m/day	.79	1.46	1.86	to kg/m^{2}s	0.00914	0.0169	0.0215
N fitting parameter of the van Genuchten function	1.28	1.56	1.38	1/(N-1)	3.57	1.78	2.63
ALPHA fitting parameter of the van Genuchten function	3.4	7.8	6.9	1/a	0.294	0.128	0.145
Saturated volumetric water content of the soil (m^3H_2O/m^3soil)	.51	.4	.32	Variable with depth[a]	0.51 0.17 0.08 0.09	0.4 0.3 0.32 0.2	0.32 0.23 0.098 0.064
Bulk density of the soil (Kg/m^3)	1390	1450	1190	Used to estimate N content (Kg/m^2)as: %N*Bulk density	0.6	0.28	0.31
Soil texture	Sandy Loam	Sand	Sand				

[a]Values collected in the field were for the first 20 cm of soils. These values were used for the first layer, other layer values were calculated assuming a % decrease in the same amount as the %Water content at 10kPa, as this is the amount of water when the soil is in equilibrium state.

B.2 Soil Lab Data

These data set was collected by Terrestrial Ecology (TE)-01 team to provide a set of soil properties for BOREAS investigators in the SSA (Anderson, 2000). The soil samples were collected at sets of soil pits in the vicinity of the flux towers in the BOREAS SSA. The collected soil samples were analysed in a lab. Only one pit was taken for the OBS site, 3 for the YJP and 4 for the OJP. A representative pit of each was chosen for this study. Parameters used are shown in next table.

Table B.2: Pit from OBS site

Horizon	Depth (m)	Structure Description	%sand	%silt	%clay	%Water content at 10kPa	%Water content at 33kPa	%Water content at 1500kPa	Bulk density (kg/M3)
moss	-.15,-.1	living moss							
LFH	-.1,0	weakly decomposed litter							4% more than OJP Gower 97
Ae	0,0.02	single grain	75.56	19.96	4.47	21.84	16.64	5.64	1250
AB	0.02,0.05	single grain	72.79	21.42	5.77	21.33	14.82	4.86	1520
Bt	0.05,0.17	moderate medium subangular blocky	64.6	28.7	6.68	18.31	14.78	4.95	1660
Bfj	0.17,0.42	moderate fine blocky	95.98	1.9	2.1	2.22	2.03	1.19	-
Ck	0.42,0.6	amorphous	94.99	2.95	2.04	3.36	2.2	1.31	-
Ck	0.6,0.72	amorphous	96.06	2.8	1.13	3.53	3.01	1.18	-

Table B.3: Pit from OJP site

Horizon	Depth (m)	Structure Description	%sand	%silt	%clay	%Water content at 10kPa	%Water content at 33kPa	%Water content at 1500kPa	Bulk density (kg/M3)
LFH	-0.03,0	weakly decomposed roots (charcoal)							320
Ae	0,0.02	single grain	93.98	3.15	2.85	8.5	6.23	3.26	1250
AB	0.02,0.05	single grain	92.43	4.89	2.67	5.88	4.6	2.9	1470
Bm	0.05,0.25	single grain	91.25	5.28	3.45	5.04	4.1	2.06	1570
C1	0.25,0.85	single grain	97.22	1.59	1.17	1.41	1.19	0.84	1470
C2	0.85,1.0	single grain	97.69	1.18	1.11	1.52	1.13	0.72	-
C3	1.0,1.5	single grain	97.69	1.05	1.25	1.66	1.17	0.78	-
Ck	1.5,1.9	single grain	97.07	1.13	1.78	2.51	1.97	1.32	-
IICk	1.9,2.52	single grain	98.41	.77	.81	1.62	1.0	0.43	-
IICk	2.5,3.0	single grain	98.02	.99	.97	2.05	1.04	0.59	-

Table B.4: Pit from YJP site

Horizon	Depth (m)	Structure Description	%sand	%silt	%clay	%Water content at 10kPa	%Water content at 33kPa	%Water content at 1500kPa	Bulk density (kg/M3)
LFH	-1,0	weakly decomposed litter (charcoal)							730
Ahej	0,0.08	single grain	91.06	6.29	2.64	11.26	7.72	4.09	1280
Bm	0.08,0.35	single grain	90.15	6.29	3.55	7.82	4.87	2.13	1590
C1	0.35,0.5	single grain	95.25	2.5	2.24	2.37	1.81	1.15	1600
ICk	0.5,0.7	single grain	96.01	2.68	1.29	1.52	1.11	.92	1580
IICk	0.7,1.5	single grain	96.82	.61	2.55	1.94	1.17	.87	-
IIICk	1.5,2.2	single grain	95.06	3.01	1.92	2.29	1.56	.9	-

%Water content at 10kPa was used as Water content at field capacity

%Water content at 33kPa was used as Water content at the critical point

%Water content at 1500kPa was used as Water content at the wilting point

Litter N content was calculated from bulk density of the litter layer times leaf N content. Results: OBS=0.073, OJP=0.048, YJP=0.064.

References

Acharya, P. K., Berk, A., Anderson, G. P., Larsen, N. F. Tsay, S. C., and Stamnes, K. H. (1999), MODTRAN4: Multiple Scattering and Bi-Directional Reflectance Distribution Function (BRDF) Upgrades to MODTRAN. *Society of Photo-Optical Instrumentation Engineers(SPIE) Proceedings,Optical Spectroscopic Techniques and Instrumentation for Atmospheric and Space Research III* 3756:354–362.

Adler, R. F., Huffman, G. J., Chang, A., Ferraro, R., Xie, P., Janowiak, J., Rudolf, B., Schneider, U., Curtis, S., Bolvin, D., Gruber, A., Susskind, J., and Arkin, P. (2003), The version 2 Global Precipitation Climatology Project (GPCP) monthly precipitation analysis (1979-present). *Journal of Hydrometeorology* 4:1147–1167.

Alton, P., Mercado, L., and North, P. (2006), A sensitivity analysis of forest biomes using the land-surface scheme JULES: biophysical parameters; the representation of canopy photosynthesis, stomatal conductance and canopy architecture; and uncertainties in meteorological driving data. *Global Biogeochemical Cycles* submitted.

Alton, P. B., North, P., Kaduk, J., and Los, S. (2005), Radiative transfer modelling of direct and diffuse sunlight in a Siberian pine forest. *Journal of Geophysical Research* 110:D23209.

Andersen, H. E., McGaughey, R. J., and Reutebuch, S. E. (2005), Estimating forest canopy fuel parameters using LIDAR data. *Remote Sensing of Environment* 94:441–449.

Anderson, D. W. (2000), BOREAS TE-01 SSA Soil Lab Data. Data set., Available online [http://www.daac.ornl.gov] from Oak Ridge National Laboratory Distributed Active Archive Center, Oak Ridge, Tennessee, U.S.A.

Arora, V. (2002), Modeling vegetation as a dynamic component in soil-vegetation-atmosphere transfer schemes and hydrological models. *Reviews of Geophysics* 40.

Asner, G. P. (1998), Biophysical and biochemical sources of variability in canopy reflectance. *Remote Sensing of Environment* 63:234–253.

Asner, G. P. (2000), Contributions of multi-view angle remote sensing to land-surface and biogeochemical research. *Remote Sensing Reviews* 18:137–162.

Asner, G. P., Braswell, B. H., Schimel, D. S., and Wessman, C. A. (1998), Ecological research needs from multi-angle remotely sensed data. *Remote Sensing of Environment* 63:155–165.

Asner, G. P., Scurlock, J. M. O., and Hicke, J. A. (2003), Global synthesis of leaf area index observations: implications for ecological and remote sensing studies. *GLOBAL ECOL BIOGEOGR* 12:191–205.

Asner, G. P., Wessman, C. A., Bateson, C. A., and Privette, J. L. (2000), Impact of tissue, canopy, and landscape factors on the hyperspectral reflectance variability of arid ecosystems. *Remote Sensing of Environment* 74:69–84.

Bacour, C., Jacquemoud, S., Leroy, M., Hauteceur, O., Weiss, M., Prevot, L., Bruguier, N., and Chauki, H. (2002), Reliability of the estimation of vegetation characteristics by inversion of three canopy reflectance models on airborne POLDER data. *Agronomie* 22:555–565.

Baldocchi, D., Kelliher, F. M., Black, T. A., and Jarvis, P. (2000), Climate and vegetation controls on boreal zone energy exchange. *Global Change Biology* 6:69–83.

Barkstrom, B. R. (1984), The Earth Radiation Budget Experiment (ERBE). *Bulletin of the American Meteorological Society* 65:1170–1186.

Barnsley, M. J. and Allison, D. (1996), Effect of Image-to-Image Mis-Registration on Multiple View Angle (MVA) Data Sets. *Remote Sensing : Science and Industry, Proceedings of the 22nd Annual Conference of the Remote Sensing Society* .

Barnsley, M. J., Allison, D., and Lewis, P. (1997), On the information content of multiple view angle (MVA) images. *International Journal of Remote Sensing* 18:1937–1960.

Barnsley, M. J., Settle, J. J., Cutter, M., Lobb, D., and Teston, F. (2004), The PROBA/CHRIS mission: a low-cost smallsat for hyperspectral, multi-angle, observations of the Earth surface and atmosphere. *IEEE Trans. Geosci. Remote Sens.* 42:1512–1520.

Bartalev, S. A., Belward, A. S., Erchov, D. V., and Isaev, A. S. (2003), A new SPOT4-VEGETATION derived land cover map of Northern Eurasia. *International Journal of Remote Sensing* 24:1977–1982.

Best, M. (2005), JULES Technical Documentation, *Technical report*, Hadley Centre, Met Office.

Bicheron, P. and Leroy, M. (1999), A Method of biophysical parameter retrieval at global scale by inversion of a vegetation reflectance model. *Remote Sensing of Environment* :251–266.

Bogaert, J., Zhou, L., Tucker, C. J., Myneni, R. B., and Ceulemans, R. (2002), Evidence for a persistent and extensive greening trend in Eurasia inferred from satellite vegetation index data. *Journal of Geophysical Research* 107.

Bonan, G. B., Chapin, F., and Thompson, S. L. (1995), Boreal forest and tundra ecosystems as components of the climate system. *Climatic Change* 29:145–167.

Bonan, G. B., Levis, S., Kergoat, L., and Oleson, K. W. (2002), Landscapes as patches of plant functional types: an integrating concept for climate and ecosystem models. *Global Biogeochemical Cycles* 16:1021.

Box, E. (1981), *Macroclimate and Plant Forms: An Introduction to Predictive Modeling in Phytogeography*, The Hague ; Boston : Dr. W. Junk.

Boyd, D. and Danson, F. M. (2005), Satellite remote sensing of forest resources: three decades of research development. *Progress in Physical Geography* 29:1–26.

Broge, N. H. and Leblanc, E. (2000), Comparing prediction power and stability of broadband and hyperspectral vegetation indices for estimation of green leaf area index and canopy chlorophyll density. *Remote Sensing of Environemnt* 76:156–172.

Buermann, W., Dong, J., Zeng, X., Myneni, R. B., and Dickinson, R. E. (2001), Evaluation of the utility of satellite-based vegetation leaf area index data for climate simulation. *Journal of Climate* 14:3536–3550.

Campbel, J. B. (2002), *Introduction to remote sensing, Third edition*, Taylor and Francis ; London and New York.

Canadell, J., Dickson, R., Hibbard, K., Raupach, M., and Young, O. (2003), Science framework and Implementation, *Global Carbon Project Report No. 1 1*, Global Carbon Project.

Chagnon, F. J. F. and Bras, R. L. (2005), Contemporary climate change in the Amazon. *Geophys. Res. Lett.* L13703, doi:10.1029/2005GL022722.

Chapin, F. S., Mcguire, A. D.and Randerson, J., Pielke, R., Baldocchi, D., Hobbie, S. E., Roulet, N., Eugster, W., Kasischke, E., Rastetter, E. B., and Zimov, S. A., R. S. W. (2000), Arctic and boreal ecosystems of western North America as components of the climate system. *Global Change Biology* 6:211–223.

Charney, J. G. (1975), Dinamics of deserts and drought in the Sahel. *Quarterly Journal of the Royal Meteorological Society* 101:193–202.

Chen, J., Carlson, B. E., and Del Genio, A. D. (2002), Evidence for strengthening of the tropical general circulation in the 1990s. *Science* :838–841.

Chen, J. M. (1996), Evaluation of vegetation indices and modified simple ratio for boreal applications. *Canadian Journal of Remote Sensing* 22:229–242.

Chen, J. M. and Cihlar, J. (1995), Plant canopy gap size analysis theory for improving optical measurements of leaf area index. *Applied Optics* 34:6211–6222.

Chen, J. M. and Cihlar, J. (1996), Retrieving leaf area index of boreal conifer forests using landsat TM images. *Remote Sensing of Environment* :153–162.

Chen, J. M. and Cihlar, J. (1998), BOREAS RSS-07 LAI, Gap Fraction, and fPAR Data. Data set., Available on-line [http://www.daac.ornl.gov] from Oak Ridge National Laboratory Distributed Active Archive Center, Oak Ridge, Tennessee, U.S.A.

Chen, J. M. and Leblanc, S. G. (1997), A four-scale bidirectional reflectance model based on canopy architecture. *IEEE Transactions in Geoscience and Remote Sensing* 35:1316–1337.

Chen, J. M., Leblanc, S. G., Miller, J. R., Freemantle, S. E., Loechel, C. L., Walthall, K. A., Innanen, H., and White, P. (1999), Compact Airborne Spectrographic Imager (CASI) used for Mapping Biophysical Parameters of Boreal Forests. *Journal of Geophysical Research-Atmosphere* 102:27.945–27.948.

Chen, J. M., Liu, J., Cihlar, J., and Goulden, M. L. (1999), Daily canopy photosynthesis model through temporal and spatial scaling for remote sensing applications. *Ecological Modelling* :99–119.

Chen, J. M., Liu, J., Leblanc, S. G., Lacaze, R., and Roujean, J. L. (2003), Multi-angular optical remote sensing for assessing vegetation structure and carbon absorption. *Remote Sensing of Environment* 84:516–525.

Chen, J. M., Rich, P. M., Gower, S. T., Norman, J. M., and Plummer, S. (1997), Leaf area index of boreal forests: theory, techniques, and measurements. *Journal of Geophysical Research* :29429–29443.

Collatz, G. J., Ball, J. T., Grivet, C., and Berry, J. A. (1991), Physiological and environmental regulation of stomatal conductance, photosynthesis and transpiration: a model that includes a laminar boundary layer. *Agricultural and Forest Meteorology* 54:107–136.

Collatz, G. J., Ribas-Carbo, M., and Berry, J. A. (1992), Coupled photosynthesis-stomatal conductance model for leaves. *Aust. J. Plant Physiol.* 19:519–538.

Combal, B., Baret, F., and Weiss, M. (2002), Improving canopy variables estimation from remote sensing data by exploiting ancillary information. Case study on sugar beet canopies. *Agronomie* 22:205–215.

Combal, B., Baret, F., Weiss, M., Trubuil, A., Mace, D., Pragnere, A., Myneni, R., Knyazikhin, Y., and Wang, L. (2002), Retrieval of canopy biophysical variables from bidirectional reflectance. Using prior information to solve the ill-posed inverse problem. *Remote Sensing of Environment* 84:1–15.

Coppin, P., Jonckheere, I., Nackaerts, K., Muys, B., and Lambin, E. (2004), Digital change detection methods in ecosystem monitoring: a review. *International Journal of Remote Sensing* 25:1565–1596.

Costa, M. H. and Foley, J. A. (2000), Combined effects of deforestation and doubled atmospheric CO2 concentrations on the climate of Amazonia. *Journal of Climate* 13:18–34.

Cox, P. M. (2001), Description of the TRIFFID dynamic global vegetation model, *Technical note, 24.*, Hadley Centre, Bracknell, UK.

Cox, P. M., Betts, R. A., Bunton, C. B., Essery, R. L. H., Rowntree, P. R., and Smith, J. (1999), The impact of new land surface physics on the GCM simulation of climate and climate sensitivity. *Climate Dynamics* :183–203.

Cox, P. M., Betts, R. A., Jones, C. D., Spall, S. A., and Totterdell, I. J. (2000), Acceleration of global warming due to carboncycle feedbacks in a coupled climate model. *Nature* :184–187.

Cramer, W., Bondeau, A., Woodward, F. I., Prentice, I. C., Betts, R. A., Brovkin, V., Cox, P. M., Fisher, V., Foley, J. A., Friend, A. D., Kucharik, C., Lomas, M. R.,

Ramankutty, N., Sitch, S., Smith, B., White, A., and Young-Molling, C. (2001), Global response of terrestrial ecosystem structure and function to CO2 and climate change: results from six dynamic global vegetation models. *Global Change Biology* :357–373.

Daughtry, C. S. T., Walthall, C. L., Kim, M. S., Brown de Colstoun, E., and McMurtrey III, J. E. (2000), Estimating corn leaf chlorophyll concentration from leaf and canopy reflectance. *Remote Sensing of Environment* :229–239.

Dawson, T. P. (2000), The potential for estimating chlorophyll content from a vegetation canopy using the Medium Resolution Imaging Spectrometer (MERIS). *International Journal of Remote Sensing* 21:2043–2051.

Dawson, T. P., Curran, P. J., North, P. R. J., and Plummer, S. E. (1999), The Propagation of Foliar Biochemical Absorption Features in Forest Canopy Reflectance. *Remote Sensing of Environment* 67:147–159.

Dawson, T. P., Curran, P. J., and Plummer, S. E. (1998), LIBERTY - Modelling the effects of leaf biochemical concentration on reflectance spectra. *Remote Sensing of Environment* :50–60.

Dawson, T. P., North, P. R. J., Plummer, S. E., and Curran, P. J. (2003), Forest ecosystem chlorophyll content: implications for remotely sensed estimates of net primary productivity. *International Journal of Remote Sensing* 24:611–617.

DEFRA (2003), Review of UK Climate Change Indicators, *Technical Report GA01048*, Department for Environment Food and Rural Affairs.

Defries, R. S., Field, C. B., Fung, I., Collatz, G. J., Bounoua, L., and Townshend, J. R. G. (1999), Combining satellite data and biogeochemical models to estimate global effects of human-induced land cover change on carbon emissions and primary productivity. *Global Biogeochemical Cycles* 13:803–815.

Defries, R. S. and Townshend, J. R. G. (1999), Global land cover characterization from satellite data: from research to operational implementation? *Global Ecology and Biogeography* 8:367–379.

Demarez, V. and Gastellu-Etchegorry, J. P. (2000), A modeling approach for studying forest chlorophyll content. *Remote Sensing of Environment* 71:226–238.

Deschamps, P. Y., Breon, F. M., Leroy, M., Podaire, A., Seze, G., and Bricaud, A. (1994), POLDER mission: Instrument characteristics and scientific objectives. *IEEE Trans. Geosci.* 32:598–615.

Dickinson, R. E., Henderson-Sellers, A., and Kennedy, P. J. (1993), Biosphere Atmosphere Transfer Scheme (BATS) Version le as Coupled to the NCAR Community Climate Model, *Ncar technical note*, NCAR, 72 pp.

Diner, D. J., Asner, G. P., Davies, R., Knyazikhin, Y., Muller, J. P., Nolin, A. W., Pinty, B., Schaaf, C. B., and Stroeve, J. (1999), New directions in Earth observing: scientific application of multi-angle remote sensing. *Bulletin of the American Meteorological Society* 80:2209– 2228.

Diner, D. J., Beckert, J. C., Bothwell, G. W., and Rodriguez, J. I. (2002), Performance of the MISR instrument during its first 20 months in Earth orbit. *IEEE Trans. Geosci. Remote Sens.c* 40:1449–1466.

Diner, D. J., Braswell, B. H., Davies, R., Gobron, N., Hu, J., Jin, Y., Kahn, R. A., Knyazikhin, Y., Loeb, N., Muller, J.-P., Nolin, A., Pinty, B., Schaaf, C. B. Seiz, G., and Stroeve, J. (2005), The value of multiangle measurements for retrieving structurally and radiatively consistent properties of clouds, aerosols, and surfaces. *Remote Sensing of Environment* 97:495–518.

Dinguirard, M. and Slater, P. (1999), Calibration of Space-Multispectral Imaging Sensors; A Review. *Remote Sensing of Environment* 68:194–205.

Disney, M. I., Lewis, P., and North, P. (2000), Monte Carlo methods in optical canopy reflectance modelling. *Remote Sensing Reviews* 18:163–196.

Dixon, R. K., Brown, S., Houghton, R. A.and Solomon, A. M., Trexler, M. C., and Wisniewski, J. (1994), Carbon pools and flux of global forest ecosystems. *Science* 263:185–190.

Ehrlich, D., Estes, J. E., and Singh, A. (1994), Applications of NOAA AVHRR 1-km data for environmental monitoring. *International Journal of Remote Sensing* 15:145–161.

Erhard, M., Minnen, J., and Voigt, T. (2002), Proposed set of Climate Change State and Impact Indicators in Europe - ETC/ACC Technical Report, Final Version., *Technical report*, European Topic Centre on Air and Climate Change (ETC/ACC).

Essery, R. L. H., Best, M. J., and Cox, P. M. (2001), MOSES 2.2 Technical Documentation., *Technical note, 30.*, Hadley Centre, Bracknell, UK.

Fang, H. and Liang, S. (2004), A hybrid inversion method for mapping leaf area index from MODIS data: experiments and application to broadleaf and needleleaf canopies. *Remote Sensing of Environment* 94:405–424.

Fang, H., Liang, S., and Kuusk, A. (2002), Retrieving leaf area index using a genetic algorithm with a canopy radiative transfer model. *Remote Sensing of Environment* 85:257–270.

Foley, J. A. (1995), Numerical models of the terrestrial biosphere. *Journal of Biogeography* 2:837–842.

Foley, J. A., Costa, M. H., Delire, C., Ramankutty, N., and Snyder, P. (2003), Green surprise? How terrestrial ecosystems could affect earth's climate. *Frontiers in Ecology and the Environment* 1:38–44.

Foley, J. A., Levis, S., Prentice, I. C., Pollard, D., and Thompson, S. L. (1998), Coupling dynamic models of climate and vegetation. *Global Change Biology* 4:561–579.

Foley, J. A., Prentice, I. C., Ramankutty, N., Levis, S., Pollard, D., Sitch, S., and Haxeltine, A. (1996), An integrated biosphere model of land surface processes, terrestrial carbon balance, and vegetation dynamics. *Global Biogeochemical Cycles* 10:603–628.

Foody, G. M., Palubinskas, G., Lucas, R. M., Curran, P. J., and Honzak, M. (1996), Identifying Terrestrial Carbon Sinks: Classification of Successional Stages in Regenerating Tropical Forest from Landsat TM Data. *Remote Sensing of Environment* 55:205–216.

Friedl, M. A., McIver, D. K., Hodges, J. C. F., Zhang, X. Y., Muchoney, D., Strahler, A. H., Woodcock, C. E., Gopal, S., Schneider, A., Cooper, A., Baccini, A., and Gao, F.and Schaaf, C. (2002), Global land cover mapping from MODIS: algorithms and early results. *Remote Sensing of Environment* 83:287–302.

Gamon, J., Huemmrich, K., Peddle, D., Chen, J., Fuentes, D., Hall, F., Kimball, J., Goetz, S., Gu, J., Mcdonald, K., Miller, J., Moghaddam, M., Rahman, A., Roujean, J.-L., Smith, E., Walthall, C. L., Zarco-Tejada, P., Hu, B., Fernandex, R., and Cihlar, J. (2004), Remote Sensing in Boreas: Lessons Learned. *Remote Sensing of Environment* 89:139–162.

Gao, B. C. (1996), NDWI - a normalized difference water index for remote sensing of vegetation liquid water from space. *Remote Sensing of Environment* 58:257–266.

Gascon, F., Gastellu-Etchegorry, J. P., Lefevre-Fonollosa, M.-J., and Dufrene, E. (2004), Retrieval of forest biophysical variables by inverting a 3-D radiative transfer

model and using high and very high resolution imagery. *International Journal of Remote Sensing* 25:5601–5616.

Gastellu-Etchegorry, J. P., Demarez, V., Pinel, V., and Zagolski, F. (1996), Modelling radiation transfer in heterogeneous 3D vegetation canopies. *Remote Sensing of Environment* 58:131–156.

GCOS (2004), Implementation plan for the global observing system for climate in support of the UNFCCC., *Technical report*, World Meteorological Organization WMO/TD No. 1219.

GCOS (2006), Systematic Observation Requirements for Satellite-Based Products for Climate., *Technical report*, World Meteorological Organization WMO/TD No. 1338.

Gerard, F. (2003), Single angle, dual angle and multi-temporal viewing: assessing through modelling the implications for forest structure variable extraction. *International Journal of Remote Sensing* 24:1317 – 1334.

Giannini, A., Saravanan, R., and Chang, P. (2003), Oceanic forcing of Sahel rainfall on interannual to interdecadal time scales. *International Journal of Remote Sensing* 302:1027–1030.

Gobron, N., Pinty, B., Verstraete, M. M., and Widlowski, J. L. (2000), Advanced vegetation indices optimized for up-coming sensors: Design, performance, and applications. *IEEE Transactions on Geoscience and Remote Sensing* 38:2489–2505.

Goel, N. S. and Thompson, R. L. (2000), A snapshot of canopy reflectance models, and a universal model for the radiation regime. *Remote Sensing Reviews* 18:197–225.

Goutorbe, J., Lebel, T., Tinga, A., Bessemoulin, P., Brouwer, J., Dolman, A. J., Engman, E. T., Gash, J. H. C., Hoepffner, M., Kabat, P., Kerr, Y. H., Monteny, B., Prince, S., Said, F., Sellers, P., and Wallace, J. S. (1994), HAPEX-Sahel: a large-scale study of land-atmosphere interactions in the semi-arid tropics. *Annales Geophysicae* 12:53–64.

Goutorbe, J. P., Lebel, T., Dolman, A. J., Gash, J. H. C., Kabat, P., Kerr, Y. H., Monteny, B., Prince, S., Stricker, J. N. M., Tinga, A., and Wallace, J. S. (1997), An overview of HAPEX-Sahel: A study in climate and desertification. *Journal of Hydrology* 189:4–17.

Gower, S. T., Kucharik, C. J., and Norman, J. M. (1999), Direct and indirect estimation of leaf area index, fAPAR, and net primary production of terrestrial ecosystems. *Remote Sensing of Environment* 70:29–51.

Gower, S. T., Vogel, J. G., Norman, J. M., Kucharik, C. J., Steele, S. J., and Stow, T. K. (1997), Carbon distribution and aboveground net primary production in aspen, jack pine, and black spruce stands in Saskatchewan and Manitoba, Canada. *Journal of Geophysical Research-Atmospheres* 102:29029–29041.

Grant, R. F. (2001), *A review of the Canadian ecosystem model ecosys pp. 173-264 in: Modeling Carbon and Nitrogen Dynamics for Soil Management.*, CRC Press. Boca Raton, FL.

Grey, W. M. F., North, P. R. J., Los, S. O., and Mitchell, R. M. (2006), Aerosol optical depth and land surface reflectance from multi-angle AATSR measurements: Global validation and inter-sensor comparisons. *IEEE Transactions on Geoscience and Remote Sensing* 44:2184–2197.

Gu, L., Baldocchi, D., Verma, S., Black, T., Vesala, T., Falge, E., and Dowty, P. (2002), Advantage of diffuse radiation for terrestrial ecosystem productivity. *Journal of Geophysical Research* 107:4050–4073.

Guenther, B., Xiong, X., Salomonson, V. V., Barnes, W. L., and Young, J. (2002), On-orbit performance of the Earth Observing System Moderate Resolution Imaging Spectroradiometer first year of data. *Remote Sensing of Environment* 83:16–30.

Haboudane, D., Miller, J. R., Pattey, E., Zarco-Tejada, P. J., and Strachan, I. B. (2004), Hyperspectral vegetation indices and novel algorithms for predicting green LAI of crop canopies: Modeling and validation in the context of precision agriculture. *Remote Sensing of Environment* 90:337–352.

Haboudane, D., Miller, J. R., Tremblay, N., Zarco-Tejada, P. J., and Dextraze, L. (2002), Integration of hyperspectral vegetation indices for prediction of crop chlorophyll content for application to precision agriculture. *Remote Sensing of Environment* 81:416–426.

Haxeltine, A. and Prentice, I. C. (1996), An equilibrium terrestrial biosphere model based on ecophysiologicalconstraints, resource availability and competition among plant functionaltypes. *Global Biogeochemical Cycles* 10:693–709.

Held, I. M., Delworth, T. L., Lu, J., Findell, K. L., and Knutson, T. R. (2005), Simulation of Sahel drought in the 20th and 21st centuries. *Proc, Natl. Acad. Sci. U. S. A.* 102:17,891–17,896.

Henderson-Sellers, A., McGuffie, K., and Pitman, A. J. (1996), The Project for Intercomparison of Land-surface Parameterization Schemes (PILPS): 1992 to 1995. *Climate Dynamics* 12:849–859.

Henderson-Sellers, A., Pitman, A. J., Love, P. K., Irannejad, P., and Chen, T. H. (1995), The project for Intercomparison of land surface parameterisation schemes (PILPS) Phases 2 and 3. *Bulletin of the American Meteorological Society* 76:489–503.

Hese, S., Lucht, W., Schmullius, C., Barnsley, M., Dubayah, R., Knorr, D., Neumann, K., Riedel, T., and Schroter, K. (2005), Global biomass mapping for an improved understanding of the CO2 balance-the Earth observation mission Carbon-3D. *Remote Sensing of Environment* 94:94–104.

Holdridge, L. R. (1967), *Life zone ecology*, San Jose, Costa Rica.

Huemmrich, K. F. (2001), The GeoSail model: a simple addition to the SAIL model to describe discontinuous canopy reflectance. *Remote Sensing of Environment* 75:423–431.

Huete, A. R. (1988), A soil-adjusted vegetation index (SAVI). *Remote Sensing of Environment* 25:295–309.

Huete, A. R., Didan, K., Miura, T., Rodriguez, E. P., Gao, X., and Ferreira, L. G. (2002), Overview of the radiometric and biophysical performance of the MODIS vegetation indices. *Remote Sensing of Environment* 83:195–213.

Huffman, G. J., Adler, R. F., Morrissey, M., Bolvin, D. T., Curtis, S., Joyce, R., McGavock, B., and Susskind, J. (2001), Global Precipitation at One-Degree Daily Resolution from Multi-Satellite Observations. *Journal of Hydrometeorology* 2:36–50.

IPCC (2001), *Climate Change 2001: The Scientific Basis*, Cambridge University Press.

Jacquemoud, S. (1993), Inversion of the PROSPECT + SAIL Canopy Reflectance Model from AVIRIS Equivalent Spectra: Theoretical Study. *Remote Sensing of Environment* 44:281–292.

Jacquemoud, S. and Baret, F. (1990), PROSPECT: a model of leaf optical properties spectra. *Remote Sensing of Environment* 34:75–91.

Jacquemoud, S., Baret, F., and Hanocq, J. F. (1992), Modeling spectral and bidirectional soil reflectance. *Remote Sensing of Environment* 41:123–132.

Jacquemoud, S. and Ustin, S. L. (2001), Leaf Optical Properties: A State Of The Art, in *8th Int. Symp. Physical Measurements and Signatures in Remote Sensing*, pp. 223–232.

Jacquemoud, S., Ustin, S. L., Verdebout, J., Schmuck, G., Andreoli, G., and Hosgood, B. (1996), Estimating leaf biochemistry using the PROSPECT leaf optical properties model. *Remote Sensing of Environment* 56:194–202.

Jonckheere, I., Fleck, S., Nackaerts, K., Muys, B., Coppin, P., Weiss, M., and Baret, F. (2004), Review of methods for in situ leaf area index determination: Part I. Theories, sensors and hemispherical photography. *Agricultural and Forest Meteorology* 121:19–35.

Jordan, C. F. (1969), Derivation of leaf area index from quality of light on the forest floor. *Ecology* 50:663–666.

Kaufman, J., Tanre, D., Gordon, H. R., Nakajima, T., Lenoble, J., Grassl, H., Herman, B. M., King, D., and Teillet, P. M. (1997), Passive remote sensing of tropospheric aerosol and atmospheric correction for the aerosol effect. *Journal of Geophysical Research* 102:16815–16830.

Kelly, S. F. and Cuenca, R. H. (1998), BOREAS HYD-01 Soil Hydraulic Properties. Data set., Available on-line [http://www.daac.ornl.gov] from Oak Ridge National Laboratory Distributed Active Archive Center, Oak Ridge, Tennessee, U.S.A.

Kimball, J. ., Thornton, P. E., White, M. A., and Running, S. W. (1997), Simulating forest productivity and surface-atmosphere carbon exchange in the BOREAS study region. *Tree Physiology* 17:589–599.

Kimball, J. S., White, M. A., and Running, S. W. (1997), BIOME-BGC simulations of BOREAS stand hydrologic processes. *Journal of Geophysical Research* 102:29.043–29.051.

Kimes, D., Gastellu-Etchegorry, J., and Estève, P. (2002), Recovery of forest canopy characteristics through inversion of a complex 3D model. *Remote Sensing of Environment* 79:320–328.

Kimes, D. S., Knyazikhin, Y., Privette, J. L., Abuelgasim, A. A., and Gao, F. (2000), Inversion methods for physically-based models. *Remote Sensing Reviews* 18:381–439.

King, A. W., Post, W. M., and Wullschleger, S. D. (1997), The potential response of terrestrial carbon storage to changes in climate and atmospheric CO2. *Climate Changey* 35:199–227.

King, M. D., Kaufman, Y. J., Tanré, D., and Nakajima, T. (1999), Remote Sensing of Tropospheric Aerosols from Space: Past, Present, and Future. *Bulletin of the American Meteorological Society* 80:2229–2259.

Kneizys, F. X., Shettle, E. P., Abreu, L. W., Chetwynd, J. H., Anderson, G. P., Gallery, W. O., Selby, J. E. A., and Clough, S. A. (1988), Users Guide to LOWTRAN7, *Environmental research papers, no. 1010, afgl-tr-88-0177*, Air Force Geophysics Laboratory, Hanscom AFB, Massachusetts.

Knorr, W. (2000), Annual and interannual CO2 exchanges of the terrestrial biosphere: process-based simulations and uncertainties. *Global Ecology and Biogeography* 9:225–252.

Knyazikhin, Y., Martonchik, J. V., Diner, D. J., Myneni, R. B., Verstraete, M. M., Pinty, B., and Gobron, N. (1998), Estimation of vegetation canopy leaf area index and fraction of absorbed photosynthetically active radi-ation from atmosphere corrected MISR data. *Journal of Geophysics* 103:32239–32256.

Knyazikhin, Y., Martonchik, J. V., Myneni, R. B., Diner, D. J., and Running, S. (1998), Synergistic algorithm for estimating vegetation canopy leaf area index and fraction of absorbed photo-synthetically active radiation from MODIS and MISR data. *Journal of Geophysical Research* 103:32257–32276.

Kubelka, P. and Munk, F. (1931), Ein Beitrag zur Optik der Farbanstriche. *Zeits. f. techn. Physik* 12:593–601.

Kuusk, A. and Nilson, T. (2000), A Directional Multispectral Forest Reflectance Model. *Remote Sensing of Environment* 72:244–252.

Lambin, E. F. and Linderman, M. (2006), Time series of remote sensing data for land change science. *IEEE Transactions on Geoscience and Remote Sensing* 44:1926–1928.

Leblanc, S. G., Bicheron, P., Chen, J. M., Leroy, M., and Cihlar, J. (1999), Investigation of directional reflectance in boreal forests with an improved four-scale model and airborne POLDER data. *IEEE Transactions on Geoscience and Remote Sensing* 37:1396–1414.

Leemans, R. and van den Born, G. J. (1994), Determining the potential global distribution of natural vegetation, crops and agricultural productivity. *Water, Air and Soil Pollution* 76:133–161.

Lefsky, M. A., Harding, D. J., Keller, M., Cohen, W. B., Carabajal, C. C., Del Born Epirito-Santo, F., Hunter, M. O., and Oliveira Jr, R. (2005), Estimates of forest canopy height and aboveground biomass using ICESat. *Geophysical Research Letters* 32:1–4.

Levis, S., Foley, J. A., Brovkin, V., and Pollard, D. (1999), On the stability of the high-latitude climate-vegetation system in a coupled atmosphere-biosphere model. *Global Ecology and Biogeography* 8:489–500.

Lewis, P. (1999), Three-dimensional plant modelling for remote sensing simulation studies using the Botanical Plant Modelling System (BPMS). *Agronomie, Agriculture and Environment* 19:185–210.

Li, X. and Strahler, A. H. (1992), Geometrical-optical bidirectional reflectance modelling of the discrete crown vegetation canopy: effect of crown shape and mutual shadowing. *IEEE Transactions in Geoscience and Remote Sensing* 30:276–292.

Li, X., Strahler, A. H., and Woodcock, C. E. (1995), A hybrid geometric optical-radiative transfer approach for modelling albedo and directional reflectance of discontinuous canopies. *IEEE Transactions in Geoscience and Remote Sensing* 33:466–480.

Lillesand, T., Kiefer, R., and Chipman, J. (2004), *Remote sensing and image interpretation. Fifth edition*, Jonh Wiley and Sons.

Liu, J., Chen, J., Cihlar, J., and Park, J. (1997), A Process-Based Boreal Ecosystem Productivity Simulator Using Remote Sensing Inputs. *Remote Sensing of Environment* 62:158–175.

Loeb, N. G., Kato, S., Loukachine, K., and Manalo-Smith, N. (2005), Angular distribution models for top-of-atmosphere radiative flux estimation from the Clouds and the Earth's Radiant Energy System instrument on the Terra satellite. Part I: Methodology. *Journal of Atmospheric and Oceanic Technology* 22:338–351.

Los, S. O., Collatz, G. J., Sellers, P. J., Malstroom, C. M., Pollack, N. H., DeFries, R. S., Bounoua, L., Parris, M. T., Tucker, C. J., and Dazlich, D. A. (2000), A global 9-year biophysical land-surface data set from NOAA AVHRR data. *Journal of Hydrometeorology* 1:183–199.

Los, S. O., Justice, C. O., and Tucker, C. J. (1994), A global 1 by 1 degree NDVI data set for climate studies derived from the GIMMS continental NDVI data. *International Journal of Remote Sensing* 15:3493–3518.

Los, S. O., North, P. R. J., Grey, W. M. F., and Barnsley, M. J. (2005), A method to convert AVHRR Normalised Difference Vegetation Index time-series to a standard viewing and illumination geometry. *Remote Sensing of Environment* 99:400–411.

Los, S. O., Weedon, G. P., North, P. R. J., Kaduk, J. D., and Taylor, C. M. (2006), An observation-based estimate of the strength of rainfall-vegetation interactions in the Sahel. *Geophysical Research Letters* 33:L16402, doi:10.1029/2006GL027065.

Loveland, T. R., Reed, B. C., Brown, J. F., Ohlen, D. O., Zhu, Z., Yang, L., and Merchant, J. W. (2000), Development of a global land cover characteristics database and IGBP DISCover from 1 km AVHRR data. *International Journal of Remote Sensing* 21:1303–1330.

McGuffie, K. and Henderson-Sellers, A. (2001), Forty years of numerical climate modelling. *International Journal of Remote Sensing* 21:1067–1109.

McGuire, A. D., Sitch, S., Clein, J. S., Dargaville, R., Esser, G., Foley, J., Heimann, M., Joos, F., Kaplan, J., Kichlighter, D. W., Meier, R. A., Melillo, J. M., Moore, B., Prentice, I. C., Ramankutty, N., Reichenau, T., Schloss, A., Tian, H., Williams, L. J., and Wittenberg, U. (2001), Carbon balance of the terrestrial biosphere in the twentieth century: analyses of CO2, climate and land use effects with four processes-based ecosystem models. *Global Biogeochemical Cycles* 15:183–206.

McGuire, A. D., Wirth, C., Apps, M., Beringer, J., Clein, J., Epstein, H., Kicklighter, D. W., Bhatti, J., ChapinIII, F. S., deGroot, B., Efremov, D., Eugster, W., Fukuda, M., Gower, T., Hinzman, L., Huntley, B., Jia, G. J., Kasischke, E., Melillo, J., Romanovsky, V., Shvidenko, A., Vaganov, E., and Walker, D. (2002), Environmental variation, vegetation distribution, carbon dynamics and water/energy exchange at high latitudes. *Journal of Vegetation Science* 13:301–314.

Melillo, J. M., McGuire, A. D., Kicklighter, D. W., MooreIII, B., Vorosmarty, C. J., and Schloss, A. L. (1993), Global climate change and terrestrial net primary production. *Nature* 363:234–240.

Middleton, E. M., Chan, S. S., Rusin, R. J., and Mitchell, S. K. (1997), Optical properties of black spruce and jack pine needles at BOREAS sites in Saskatchewan, Canada. *Canadian Journal of Remote Sensing* 23:108–119.

Middleton, E. M., Sullivan, J. H., Bovard, B. D., DeLuca, A. J., Chan, S. S., and Cannon, T. A. (1997), Seasonal variability in foliar characteristics and physiology for boreal forest species at the five Saskatchewan tower sites during the 1994 boreal ecosystem-atmosphere study (BOREAS). *Journal of Geophysical Research* 102:28831–28844.

Miller, J., Peddle, D. R., and Freemantle, J. (1998), BOREAS RSS-19 1994 Seasonal Understory Reflectance Data. Data set., Available on-line [http://www.daac.ornl.gov] from Oak Ridge National Laboratory Distributed Active Archive Center, Oak Ridge, Tennessee, U.S.A.

Miller, J. R., White, H. P., Chen, J. M., Peddle, D. R., McDermid, G., Fournier, R. A., Shepherd, P., Rubinstein, I., Freemantle, J., Soffer, R., and LeDrew, E. (1997), Seasonal change in understory reflectance of boreal forests and influence on canopy vegetation indices. *Journal of Geophysical Research* 102:29475–29482.

Mishchenko, M. I., Cairns, B., Hansen, J. E., Travis, L. D., Burg, R., Kaufman, Y. J., Martins, J. V., and Shettle, E. P. (2004), Monitoring of aerosol forcing of climate from space: analysis of measurement requirements. *Journal of Quantitative Spectroscopy and Radiative Transfer* 88:149–161.

Monteith, J. L. (1977), Climate and efficiency of crop production in Britain. *Phil. Trans. R. Soc. London* 281:277–294.

Moorthy, I., Miller, J. R., Zarco-Tejada, P. J., and Noland, T. L. (2003), Needle Chlorophyll Content Estimation: A Comparative Study of PROSPECT and LIBERTY, in *International Geoscience and Remote Sensing Symposium, IGARSS'03*, volume 3, pp. 1676–1678.

Morisette, J. T., Baret, F., Privette, J. L., Myneni, R. B., Nickeson, J. E., Garrigues, S., Shabanov, N. V., Weiss, M., Fernandes, R. A., Leblanc, S. G., Kalacska, M., Sanchez-Azofeifa, G. A., Chubey, M., Rivard, B., Stenberg, P., Rautiainen, M., Voipio, P., Manninen, T., Pilant, A. N., Lewis, T. E., Iiames, J. S., Colombo, R., Meroni, M., Busetto, L., Cohen, W. B., Turner, D. P., Warner, E. D., Petersen, G. W., Seufert, G., and Cook, R. (2006), Validation of global moderate-resolution LAI products: a framework proposed within the CEOS land product validation subgroup. *IEEE Transactions on Geoscience and Remote Sensing* 44:1804– 1817.

Myneni, R. B., Hoffman, S., Knyazikhin, Y., Privette, J. L., Glassy, J., Tian, Y., Wang, Y., Song, X., Zhang, Y., Smith, G. R., Lotsch, A., Friedl, M., Morisette, J. T., Votava, P., Nemani, R. R., and Running, S. W. (2002), Global products of vegetation leaf

area and fraction absorbed PAR from year one of MODIS data. *Remote Sensing of Environment* 83:214–231.

Myneni, R. B., Keeling, C. D., Tucker, C. J., Asrar, G., and Nemani, R. R. (1997), Increased plant growth in the northern high latitudes from 1981-1991. *Nature* 386:698–702.

Myneni, R. B., Maggion, S., Iaquinta, J., Privette, J., Gobron, N., Pinty, B., Verstraete, M., Kimes, D., and Williams, D. (1995), Optical remote sensing of vegetation: modeling, caveats and algorithms. *Remote Sensing of Environment* 51:169–188.

Myneni, R. B., Nemani, R. R., and Running, S. (1997), Estimation of global leaf area index and absorbed PAR using radiative transfer models. *IEEE Transactions on Geoscience and Remote Sensing* 35:1380–1393.

Nellson, R. P. (1995), A model for predicting continental scale vegetation distribution and water balance. *Ecol. Appl.* 5:362–385.

Nemani, R. R., Keeling, C. D., Hashimoto, H., Jolly, W. M., Piper, S. C., Tucker, C. J., Myneni, R. B., and Running, S. (2003), Climate-driven increases in global terrestrial net primary production from 1982 to 1999. *Science* 300:1560–1563.

Ni, W. G., Li, X. W., Woodcock, C. E., Caetano, M. R., and Strahler, A. H. (1999), An analytical hybrid GORT model for bidirectional reflectance over discontinuous plant canopies. *IEEE Transactions on Geoscience and Remote Sensing* 37:987–999.

Nicholson, S. (2000), Land surface processes and Sahel climate Modeling. *Reviews of Geophysics* 38:117–140.

Nikolov, N. and Zeller, K. F. (2003), Modeling coupled interactions of carbon, water, and ozone exchange between terrestrial ecosystems and the atmosphere.I: Model description. *Environmental Pollution* 124:231–246.

North, P. R. J. (1996), Three-dimensional forest light interaction model using a Monte Carlo method. *IEEE Transactions on Geoscience and Remote Sensing* 34:946–956.

North, P. R. J. (2002), Estimation of aerosol opacity and land surface bidirectional reflectance from ATSR-2 dual-angle imagery: operational method and validation. *Journal of Geophysical Research* 107:No. 4149.

North, P. R. J. (2002), Estimation of fAPAR, LAI and vegetation fractional cover from ATSR-2 imagery. *Remote Sensing of Environment* 80:114–121.

North, P. R. J., Briggs, S. A., Plummer, S. E., and Settle, J. J. (1999), Retrieval of land surface bdirectional reflectance and aerosol opacity from ATSR-2 multiangle imagery. *IEEE Trans. Geosci. Remote Sensing* 37:526–537.

Ohring, G., Wielicki, B., Spencer, R., Emery, W., and Datla, R. (2004), Satellite instrument calibration for measuring global climate change., *Report from the nov 12-14, 2002 workshop*, NISTIR 7047.

O'Neil, N. T., Zagolski, F., Bergeron, M., Roger, A., Miller, J. R., and Freemantle, J. (1997), Atmospheric correction validation of CASI images acquired over the BOREAS southern study area. *Canadian Journal of Remote Sensing* 23:143–162.

Patenaude, G., Hill R. Milne, R., Gaveau, D., Briggs, B., and Dawson, T. (2004), Quantifying forest above ground carbon content using LiDAR remotesensing. *Remote Sensing of Environment* 93:368–380.

Pease, C. (1991), *Satellite imaging instruments*, Ellis Horwood Limited.

Petit, C. C. and Lambin, E. F. (2001), Integration of multi-source remote sensing data for land cover change detection. *International Journal of Geographical Information Science* 15:785–803.

Petit, C. C., Scudder, T., and Lambin, E. F. (2001), Quantifying processes of land-cover change by remote sensing: resettlement and rapid land-cover changes in south-eastern Zambia. *International Journal of Remote Sensing* 22:3435–3456.

Pielke, R., Avissar, R., Raupach, M., Dolman, A. J., Zeng, X. B., and Denning, A. S. (1998), Interactions between the atmosphere and terrestrial ecosystems: influence on weather and climate. *Global Change Biology* 4:461–475.

Pinty, B., Gobron, N., Widlowski, J.-L., Gerstl, A. A. W., Verstraete, M. M., Antunes, M., Bacour, C. Gascon, F., Gastellu, J.-P., Goel, N., Jacquemoud, S., North, P., Qin, W., and Thompson, R. (2001), Radiation Transfer Model Intercomparison (RAMI) exercise. *Journal of Geophysical Research* 106.

Pinty, B., Widlowski, J.-L., Taberner, M., Gobron, N., Verstraete, M. M., Disney, M., Gascon, F., Gastellu, J.-P., Jiang, L., Kuusk, A., Lewis, P., Li, X., Ni-Meister, W., Nilson, T., North, P., Qin, W., Su, L., Tang, S., Thompson, R., Verhoef, W., Wang, H., Wang, J., Yan, G., and Zang, H. (2006), Radiation Transfer Model Intercomparison (RAMI) exercise: Results from the second phase. *Journal of Geophysical Research* 109.

Pitman, A. J. (2003), The evolution of, and revolution in, land surface schemes designed for climate models. *International Journal of Climatology* 23:479–510.

Pitman, A. J. and Henderson-Sellers, A. (1998), Recent progress and results from the project for the intercomparison of land surface parameterization schemes. *Journal of Hydrology* :128–135.

Plummer, S. E. (2000), Perspectives on combining ecological process models and remotely sensed data. *Ecological Modelling* 129:169–186.

Potter, C., Klooster, S., Steinbach, M., Tan, P., Kumar, V., Shekhar, S., Nemani, R., and Myneni, R. (2003), Global teleconnections of climate to terrestrial carbon flux. *Journal of Geophysical Research* 108:4556.

Potter, C. S. (1997), An ecosystem simulation model for methane production and emission from wetlands. *Global Biogeochemical Cycles* 11:495–506.

Potter, C. S., Bubier, J., Crill, P., and LaFleur, P. (2001), Ecosystem modeling of methane and carbon dioxide fluxes for boreal forest sites. *Canadian Journal of Forestry Research* 31:208–223.

Prentice, I. C., Cramer, W., Harrison, S. P., Leemans, R., Monserud, R. A., and Solomon, A. M. (1992), A Global Biome Model Based on Plant Physiology and Dominance, Soil Properties and Climate. *Journal of Biogeography* 19:117–134.

Prince, S. D. and Goward, S. (1995), Global primary production: a remote sensing approach. *Journal of Biogeography* 22:815–835.

Privette, J. L., Emery, W. J., and Schimel, D. S. (1996), Inversion of a vegetation reflectance model with NOAA AVHRR data. *Remote Sensing of Environment* 58:187–200.

Privette, J. L., Myneni, R. B., Emery, W. J., and Hall, F. G. (1996), Optimal sampling conditions for estimating grassland parameters via reflectance model inversions. *IEEE Transactions on Geoscience and Remote Sensing* 34:272–284.

Qi, J., Chehbouni, A., Huete, A. R., Keer, Y. H., and Sorooshian, S. (1994), A modified soil vegetation adjusted index. *Remote Sensing of Enviroment* 48:119–126.

Qin, W. and Liang, S. (2000), Plane-parallel canopy radiative transfer modelling: recent advances and future directions. *Remote Sensing Reviews* 18:281–305.

Rondeaux, G., Steven, M., and Baret, F. (1996), Optimization of soil-adjusted vegetation indices. *Remote Sensing of Environment* 55:95–107.

Rosema, A., Verhoef, W., Noorbergen, H., and Borgesius, J. J. (1992), A new forest light interaction model in support of forest monitoring. *Remote Sensing of Environment* 42:23–41.

Rosenqvist, A., Milne, A., Lucas, R., Imhoff, M. ., and Dobson, C. (2003), A review of remote sensing technology in support of the Kyoto Protocol. *Environmental Science and Policy* 6:441–455.

Ross, S. M., ed. (1984), *A First Course in Probability, 2nd Edition*, New York: Macmillan London: Collier Macmillan.

Roughgarden, J. and Breon, F. M. (1995), Estimating PAR absorbed by vegetation from bidirectional reflectance measurements. *Remote Sensing of Environment* 51:375–384.

Roughgarden, J., Running, S. W., and Matson, P. A. (1991), What Does Remote Sensing Do For Ecology? *Ecology* 72:1918–1922.

Roujean, J.-L., Leroy, M., and Deschamps, M. (1992), A bidirectional reflectance model of the Earth's surface for the correction of remote sensing data. *Journal of Geophysical Research* 97:20455–20468.

Rouse, J. W., Haas, R. H., Schell, J. A., Deering, D. W., and Harlan, J. C. (1974), Monitoring the vernal advancements and retrogradation of natural vegetation, *Technical report*, NASA/GSFC,Greenbelt, MD.

Running, S. W., Baldocchi, D. D., Turner, D. P., Gower, S. T., Bakwin, P. S., and Hibbard, K. A. (1999), A Global Terrestrial Monitoring Network Integrating Tower Fluxes, Flask Sampling, Ecosystem Modeling and EOS Satellite Data. *Remote Sensing of Environment* 70:108–127.

Running, S. W. and Gower, S. T. (1991), FOREST-BGC, a general model of forest ecosystem processes for regional applications. II.Dynamic carbon allocation and nitrogen budgets. *Tree Physiology* 9:147–160.

Running, S. W. and Hunt, E. R. (1993), *Generalization of a forest ecosystem process model for other biomes, BIOME-BGC, and an application for global-scale models. In:Scaling Physiological Processes: Leaf to Globe*, Academic Press, San Diego, CA.

Running, S. W., Justice, C. O., Salomonson, V., Hall, D., Barker, J., Kaufman, Y., Strahler, A., Huete, A., Muller, J.-P., Vanderbilt, V., Wan, Z., Teillet, P., and Carneggie, D. (1994), Terrestrial remote sensing science and algorithms planned for EOS/MODIS. *International Joutnal of Remote Sensing* 15:3587–3620.

Schimel, D. S., House, J. I., Hibbard, K. A., Bousquet, P., Ciais, P., Peylin, P., Braswell, B. H., Apps, M. J., Baker, D., Bondeau, A., Canadell, J., Churkina, G., Cramer, W., Denning, A. S., Field, C. B., Friedlingstein, P., Goodale, C., Heimann, M., Houghton, R. A., Melillo, J., MooreIII, B., Murdiyarso, D., Noble, I., Pacala, S. W., Prentice, I. C., Raupach, M. R., Rayner, P. J., Scholes, R. J., Steffen, W. L., and Wirth, C. (2001), Recent patterns and mechanisms of carbon exchange by terrestrial ecosystems. *Nature* 414:169–172.

Schwartz, M. D. (2003), *Phenology: An Integrative Environmental Science*, Kluwer Academic Publishers.

Sellers, P. J. Schimel, D. (1993), Remote sensing of the land biosphere and biogeochemistry in the EOS era: science priorities, methods and implementation. *Global and Planetary Change* 7:279–297.

Sellers, P., Hall, F. G., Asrar, G., Strebel, D. E., and Murphy, R. E. (1988), The 1st ISLSCP field experiment (FIFE). *Bulletin of the American Meteorological Society* 69:22–27.

Sellers, P., Mintz, Y., Sud, Y., and Dalcher, A. (1986), A Simple Biosphere (SiB) for use within General Circulation Models. *J. Atmos. Sci.* 43:505–531.

Sellers, P. J., Dickinson, R. E., Randall, D. A., Betts, A. K., Hall, F. G., Berry, J. A., Collatz, G. J., Denning, A. S., Mooney, H. A., Nobre, C. A., Sato, N., Field, C. B., and Henderson-Sellers, A. (1997), Modeling the Exchanges of Energy, Water, and Carbon Between Continents and the Atmosphere. *Science* 275:502–509.

Sellers, P. J., Hall, F., Kelly, R. D., Black, A., Baldocchi, D., Berry, J., Ryan, M., Ranson, K., Crill, P. M., Lettenmaier, D., Margolis, H., Cihlar, J., Newcomer, J., Fitzjarrald, D., Jarvis, P. G., Gower, S. T., Halliwell, D., Williams, D., Goodison, B., Wickland, D. E., and Guertin, F. E. (1997), BOREAS in 1997: Experiment Overview, Scientific Results and Future Directions. *Journal of Geophysical Research* 102:28,731–28,770.

Sellers, P. J., Los, S. O., Tucker, C. J., Justice, C. O., Dazlich, D. A., Collatz, G. J., and Randall, D. A. (1996), A revised land surface parameterization (SiB2) for at-

mospheric GCMs. Part II: The generation of global fields of terrestrial biophysical parameters from satellite data. *Journal of Climate* 9:706–737.

Sellers, P. J., Meeson, B. W., Hall, F. G., Asrar, G., Murphy, R. E., Schiffer, R. A., Bretherton, F. P., Dickinson, R. E., Ellingson, R. G., Field, C. B., Huemmrich, K. F., Justice, C. O., Melack, J. M., Roulet, N. T., Schimel, D. S., and Try, P. D. (1995), Remote sensing of the land surface for studies of global change: models-algorithms-experiments. *Remote Sensing od the Environment* 51:3–26.

Sellers, P. J., Randall, D. A., Collatz, G. J., Berry, J., Field, C., Dazlich, D. A., Zhang, C., and Bounoua, L. (1996), A revised land surface parameterization (SiB2) for atmospheric GCMs. Part 1: Model formulation. *Journal of Climate* 9:676–705.

Sellers, P. J., Tucker, C. J., Collatz, G. J., Los, S. O., Justice, C. O., Dazlich, D. A., and Randall, D. A. (1994), A global 1-deg by 1-deg NDVI data set for climate studies. Part 2. The generation of global fields of terrestrial biophysical parameters from the NDVI,. *International Journal of Remote Sensing* 15:3519–3545.

Silva Dias, M. A. F., Rutledge, S., Kabat, P., Silva Dias, P. L., Nobre, C., Fisch, G., Dolman, A. J., Zipser, E., Garstang, M., Manzi, A. O., Fuentes, J. D., Rocha, H. R., Marengo, J., Plana-Fattori, A., Sá, L. D. A., Alvalá, R. C. S., Andreae, M. O., Artaxo, P., Gielow, R., and Gatti, L. (2002), Cloud and rain processes in a biosphere-atmosphere interaction context in the Amazon Region. *Journal of Geophysical Research (Atmospheres)* 107:39–1,39–18.

Stricker, N. C. M., Hahne, A., Smith, D. L., and Delderfield, J. (1995), ATSR-2: The evolution in its design from ERS-1 to ERS-2. *ESA Bulletin* 83:32–37.

Teillet, P. M., Horler, D. N. H., and O'Neill, N. T. (1997), Calibration, Validation, and Quality Assurance in Remote Sensing: A New Paradigm. *Canadian Journal of Remote Sensing* 23:401–414, printed.

Thenkabail, P. S., Enclona, E. A., Ashton, M. S., and Van Der Meer, V. (2004), Accuracy Assessments of Hyperspectral Waveband Performance for Vegetation Analysis Applications. *Remote Sensing of Environment* 91:354–376.

Townshend, J. R. and Justice, C. (2002), Towards operational monitoring of terrestrial systems by moderate-resolution remote sensing. *Remote Sensing of Environment* 83:351–359.

Treitz, P. and Howarth, P. (2000), High Spatial Resolution Remote Sensing Data for Forest Ecosystem Classification: An Examination of Spatial Scale. *Remote Sensing of Environment* 72:268–289.

Treitz, P. M. and Howarth, P. J. (1999), Hyperspectral remote sensing for estimating biophysical parameters of forest ecosystems. *Progress in Physical Geography* 23:359–390.

Turner, D. P., Ritts, W. D., Cohen, W. B., Gower, S. T., Running, S. W., Zhao, M., Costa, M. H., Kirschbaum, A., Ham, J. M., Saleska, S. R., and Ahl, D. E. (2006), Evaluation of MODIS NPP and GPP products across multiple biomes. *Remote Sensing of Environment* 102:282–292.

Turner, D. P., V., O. S., and Kimball, J. S. (2004), Integrating remote sensing and ecosystem process models for landscape to regional scale analysis of the carbon cycle. *Bioscience* 54:573–584.

Turner, W., Spector, S., Gardiner, N., Fladeland, M., Sterling, E., and Steninger, M. (2003), Remote sensing for biodiversity science and conservation. *TRENDS in Ecology and Evolution* 18.

Ustin, S. L., Roberts, D. A., Gamon, J. A., Asner, G. P., and Green, R. O. (2004), Using Imaging Spectroscopy to Study Ecosystem Processes and Properties. *BioScience* 54:523–534.

Ustin, S. L., Smith, M. O., Jacquemoud, S., Verstraete, M. M., and Govaerts, Y. (1998), *Manual of Remote Sensing: Remote Sensing for the Earth Sciences Third Edition Volume 3*, New York Wiley.

Ustin, S. L., Wessman, C. A., Curtiss, B., Kasischke, E., Way, J., and Vanderbilt, V. C. (1991), Opportunities for Using the Eos Imaging Spectrometers and Synthetic Aperture Radar in Ecological Models. *Ecology* 72:1934–1945.

Van Vliet, A. J. H., Braun, P., Bruegger, R., Bruns, E., Clevers, J., Estreguil, C., Flechsig, M., de Groot, R. S., Grutters, M., Harrewijn, J., Jeanneret, F., Martens, P., Menne, B., Menzel, A., and Sparks, T. (2003), The European Phenology Network; Nature's Calendar on the move., *Technical report*, Wageningen University, Wageningen.

Verhoef, W., B. H. (2003), Remote sensing data assimilation using coupled radiative transfer models. *RPhysics and Chemistry of the Earth* 28:3–13.

Verhoef, W. (1984), Light scattering by leaf layers with applications to canopy reflectance modelling: the SAIL model. *Remote Sensing of the Environment* 16:125–141.

Vermote, E., Tanre, D., Deuze, J. L., Herman, M., and Morcrette, J. J. (1997), Second simulation of the satellite signal in the solar spectrum: An overview. *IEEE Trans. Geosci. Remote Sensing* 35:675–686.

Verseghy, D. L., McFarlane, N. A., and Lazare, M. (1993), CLASS - A Canadian land surface scheme for GCMS. II: Vegetation model and coupled runs. *International Journal of Climatology* 13:347–370.

Verstraete, M. M. and Pinty, B. (1996), Designing optimal spectral indexes for remote sensing applications. *IEEE Transactions on Geoscience and Remote Sensing* 34:1254–1265.

Verstraete, M. M., Pinty, B., and Curran, P. J. (1999), MERIS potential for land applications. *International Journal of Remote Sensing* 20:1747–1756.

Verstraete, M. M., Pinty, B., and Myneni, R. B. (1996), Potential and limitations of information extraction on the terrestrial biosphere from satellite remote sensing. *Remote Sensing of the Environment* 58:201–214.

Wake, C. M. (2005), Indicators of Climate Change in the Northeast 2005, *Technical report*, Clean Air-Cool Planet and The Climate Change Research Center, University of New Hampshire.

Wallace, J. S., Wright, I. R., Stewart, J. B., and Holwill, C. J. (1991), The Sahelian Energy Balance Experiment (SEBEX): Ground based measurements and their potential for spatial extrapolation using satellite data. *Advances in Space Research* 11:131–141.

Walthall, C. L. and Loechel, S. (1999), BOREAS RSS-03 Atmospheric Conditions from a Helicopter-Mounted Sunphotometer. Data set., Available on-line [http://www.daac.ornl.gov] from Oak Ridge National Laboratory Distributed Active Archive Center, Oak Ridge, Tennessee, U.S.A.

Walthall, C. L., Norman, J. M., Welles, J. M., Campbell, G., and Blad, B. (1985), Simple equation to approximate the bidirectional reflectance from vegetated canopies and bare soil surfaces. *Applied Optics* 24:383–387.

Weiss, M. and Baret, F. (1999), Investigation of a model inversion technique to estimate canopy biophysical variables from spectral and directional reflectance data. *Remote Sensing of Environment* 70:293–306.

Weiss, M., Baret, F., Leroy, M., Hautecoeur, O., Bacour, C., Prevot, L., and Bruguier, N. (2002), Validation of neural net techniques to estimate canopy biophysical variables from remote sensing data. *Agronomie* 22:547–553.

Weiss, M., Baret, F., Myneni, R., Pragnere, A., and Knyazikhin, Y. (2000), Evaluation of canopy biophysical variable retrieval performances from the accumulation of large swath satellite data. *Agronomie* 20:3–22.

White, M. A., Hoffman, F., Hargrove, W. W., and Nemani, R. R. (2005), A global framework for monitoring phenological responses to climate change. *Geophysical Research Letters* 32, l04705, doi:10.1029/2004GL021961.

White, M. A., Thornton, P. E., Running, S. W., and Nemani, R. R. (2000), Parameterization and Sensitivity Analysis of the BIOME-BGC Terrestrial Ecosystem Model: Net Primary Production Controls. *Earth Interactions* 4:1–85.

Wickland, D. E. (1991), Mission to Planet Earth: The Ecological Perspective. *Ecology* 72:1923–1933.

Wielicki, B. A., Barkstrom, B. R., Harrison, E. F., Lee-III, B. B., Louis Smith, G., and Cooper, J. E. (1996), Clouds and the Earth's radiant energy system (CERES); an earth observing system experiment. *Bull. Amer.Meteor. Soc.* 72:853–868.

Williams, M., Schwarz, P. A., Law, B. E., Irvine, J., and Kurpius, M. (2005), An improved analysis of forest carbon dynamics using data assimilation. *Global Change Biology* 11:89–105.

Williams, M., Street, L., Van Wijk, M. T., and Shaver, G. R. (2006), Identifying differences in carbon exchange among arctic ecosystem types. *Ecosystems* 9:288–304.

WMO (2004), Implementation plan for the global observing system for climate in support of the UNFCCC, *U.n. environment programme int.council, geneva, switzerland, gcos 92, wmo/td 1219*, WMO/TD.

Wulder, M. (1998), Optical remote-sensing techniques for the assessment of forest inventory and biophysical parameters. *Progress in Physical Geography* 22:449–476.

Wulder, M. A., Hall, R. J., Coops, N. C., and Franklin, S. E. (2004), High Spatial Resolution Remotely Sensed Data for Ecosystem Characterization. *BioScience* 54:511–521.

Xue, Y. (1997), Biosphere feedback on regional climate in tropical north Africa. *Quarterly Journal of the Royal Meteorological Society* 123:1483–1515.

Zarco-Tejada, P. J., Miller, J. R., Harron, J., Hu, B., Noland, T. L., Goel, N., Mohammed, G. H., and Sampson, P. H. (2004), Needle Chlorophyll content estimation through model inversion using hyperspectral data from Boreal Conifer Forest Canopies. *Remote Sensing of Environment* 89:189–199.

Zarco-Tejada, P. J., Miller, J. R., Mohammed, G. H., and Noland, T. L. (2000), Chlorophyll fluorescence effects on vegetation apparent reflectance: I Leaf-level measurements and model simulation. *Remote Sensing of Environment* 74:582–595.

Zarco-Tejada, P. J., Miller, J. R., Mohammed, G. H., Noland, T. L., and Sampson, P. H. (2001), Scaling-up and model inversion methods with narrow-band optical indices for chlorophyll content estimation in closed forest canopies with hyperspectral data. *IEEE Transactions on Geoscience and Remote Sensing* 39:1491–1507.

Zarco-Tejada, P. J., Miller, J. R., Morales, A., Berjón, A., and Agüera, J. (2004), Hyperspectral Indices and Model Simulation for Chlorophyll Estimation in Open-Canopy Tree Crops. *Remote Sensing of Environment* 90:463–476.

Zarco-Tejada, P. J., Ustin, S. L., and Whiting, M. L. (2005), Temporal and Spatial Relationships between Within-Field Yield Variability in Cotton and High-Spatial Hyperspectral Remote Sensing Imagery. *Agronomy Journal* 97:641–653.

Zhou, L., Kaufmann, R. K., Tian, Y., Myneni, R. B., and Tucker, C. J. (2003), Relation between interannual variations in satellite measures of northern forest greenness and climate between 1982 and 1999. *Journal of Geophysical Research* 108:4004.

Zong, J., Davies, R., Muller, J. P., and Diner, D. J. (2002), Photogrammetric retrieval of cloud advection and top height from the Multi-angle Imaging SpectroRadiometer (MISR). *Photogrammetric Engineering and Remote Sensing* 68:821–829.